Electro-Fenton Process and Related Electrochemical Technologies Based on Fenton's Reaction Chemistry

Enric Brillas,† Ignasi Sirés,† and Mehmet A. Oturan*,‡

Laboratori d'Electroquímica dels Materials i del Medi Ambient, Departament de Química Física, Facultat de Química, Universitat de Barcelona, Martí i Franquès 1-11, 08028 Barcelona, Spain and Université Paris-Est, Laboratoire Géomatériaux et Géologie de l'Ingénieur, 5 Bd Descartes, 77454 Marne-la-Vallée Cedex 2, France

Received April 4, 2009

Contents

1. Introduction

Water is essential for the subsistence of living beings. Although abundant on Earth, with a volume of about 1400 million km^3, almost 97% is constituted by saltwater from oceans or seas and less than 1% of freshwater is readily available for human uses. Unfortunately, water pollution remains a pervasive threat, with water quality being merely a concept reflecting the kind and quantity of contaminants contained within it.[1] It is well known[2–11] that large amounts of a high number of synthetic organic pollutants, including industrial chemicals, pesticides, dyes and pharmaceuticals and personal care products (PPCPs), are released daily into many types of wastewaters and enter into natural water

* To whom correspondence should be addressed. E-mail: Mehmet.Oturan@univ-paris-est.fr.
† Universitat de Barcelona.
‡ Université Paris-Est.

10.1021/cr900136g
Published on Web 10/19/2009

Enric Brillas was born in Barcelona, Spain, in 1951. He obtained his B.S. degree in Chemistry in 1974 and received Ph.D. degree in Chemistry in 1977 under the supervision of Professor J. M. Costa from the Universitat Autònoma de Barcelona. In 1980, he joined the Universitat de Barcelona as Associate Professor of Physical Chemistry. In 1982, he completed his studies in electrochemistry at the Università di Padova, Italy, with Professor E. Vianello in the field of organic electrochemistry. From 1987 to present, he has worked as Full Professor of Physical Chemistry at the Universitat de Barcelona. He was Headmaster of the Department of Physical Chemistry from 2000 to 2008. He was President of the electrochemistry group of the Real Sociedad Española de Química from 2004 to 2008. Currently, he is Director of the Laboratori d'Electroquímica dels Materials i del Medi Ambient at the Universitat de Barcelona. His research mainly focuses on organic electrochemistry, chemical kinetics, chemical catalysis and photocatalysis, electrocatalysis, and electrochemical treatment of organic pollutants. In the latter field, he has developed several electrochemical advanced oxidation processes such as electro-Fenton, photoelectro-Fenton, and peroxi-coagulation. In 1995, he received the international Chemviron Carbon Award for his initial research on electro-Fenton degradation of organics with a gas diffusion electrode. He has supervised the doctoral theses of 14 Ph.D. students. Since 2008, he has been Associate Editor of the journal *Chemosphere*. He has published 200 peer-reviewed papers, 4 books, and 8 book chapters and presented 125 contributions to scientific congresses.

Ignasi Sirés was born in Barcelona, Spain, in 1980. He obtained his B.S. degree in Chemistry in 2002 and Ph.D. degree in Chemistry with European's Mention in 2007, both from the Universitat de Barcelona. He has also conducted materials engineering studies at the Universitat de Barcelona and Universitat Politècnica de Catalunya. His thesis, carried out at the Laboratori d'Electroquímica dels Materials i del Medi Ambient within the team of Professor E. Brillas, was devoted to the development of electrochemical advanced oxidation processes for the treatment of pharmaceutical drugs in waters, focusing on direct anodic oxidation with BDD anodes and electro-Fenton and related electrochemical processes. He has undertaken predoctoral stays at the Ecole Nationale d'Ingénieurs de Sfax in Tunisia and the Université Paris-Est Marne-la-Vallée in France as well as postdoctoral stays at the Università degli Studi di Genova in Italy with Dr. M. Panizza and the Université Paris-Est Marne-la-Vallée with Professor M. A. Oturan, having worked as a contracted professor−researcher in 2007 and 2008. Dr. Sirés' scientific contributions are reflected in his 20 publications in ISI journals and participation as an invited lecturer at several international congresses. In 2008, he was awarded the Electrochimica Acta Travel Award for Young Electrochemists by the International Society of Electrochemistry. His research interests include environmental electrochemistry, electrochemical engineering, and the study of advanced nanostructured electrode materials aiming to develop novel and promising electrochemical technologies. Currently, he is pursuing postdoctoral work at the Electrochemical Engineering Laboratory of the School of Engineering Sciences at the University of Southampton in the United Kingdom under the supervision of Professor F. C. Walsh. In September 2009, he became a Lecturer at the Department of Physical Chemistry of the Universitat de Barcelona.

channels where they accumulate in the aquatic environment. This contamination arises from urban, industrial, and agricultural human activities and cannot be significantly reduced in conventional wastewater treatment plants because the vast majority of these compounds are persistent organic pollutants (POPs), owing to their high stability to sunlight irradiation and resistance to microbial attack and temperature. As a result, many POPs have been detected in low amounts, usually micrograms per liter, in rivers, lakes, oceans, and even drinking water all over the world. Although the carcinogenic, mutagenic, and bactericidal properties of most POPs remain unknown, there exists great concern for their removal from the aquatic environment to avoid the toxic consequences and potential hazardous health effects on living organisms, including human beings. Research on wastewater treatment is experiencing a new and definitive awakening, and current interest is focusing on the development of simple, safe, effective, and economical technologies for the total destruction of POPs before final disposal.

Several comprehensive and extensive surveys offer a wide revision on available ecofriendly techniques commonly used for wastewater remediation.[12−14] The simplest and cheapest methods are the so-called conventional treatments, which can be divided into two groups: (i) isolation/separation technologies based on physicochemical methods and (ii) transformation technologies dominated by both chemical and microbiological/enzymatic methods.

Traditional physicochemical treatments separate xenobiotics from the aqueous medium but without altering their chemical structure. These nondegradative techniques include adsorption onto inorganic and organic supports (usually with activated carbon), flocculation and sedimentation, flotation, distillation, extraction, air stripping, membrane processes (micro-, ultra-, and nanofiltration, reverse osmosis, and ion exchange), and coagulation with lime, aluminum, or iron salts.[13,14] In contrast, the transformation methods cause the cleavage of structural bonds, which induces the conversion of the initial pollutant into several intermediates. Among them, the most popular chemical methods for water disinfection are ozonation and chlorination. Bioremediation treatments are mainly based on activated sludge, trickling filters, or mixed and pure cultures under aerobic or anaerobic conditions and widely applied only as a final treatment or ultimate step before the release of the effluent from the treatment plant.[13] Incineration, plasma technology, solvated electron technology, and permeable reactive barriers are also utilized as alternative or complementary transformation processes for small volumes of highly concentrated pollutants.[14]

The inefficiency of conventional water treatments in destroying many toxic and biorecalcitrant organic pollutants has promoted the search for more potent methods. In this scenario, the electrochemical technology has received great attention for the prevention of pollution problems, as reported

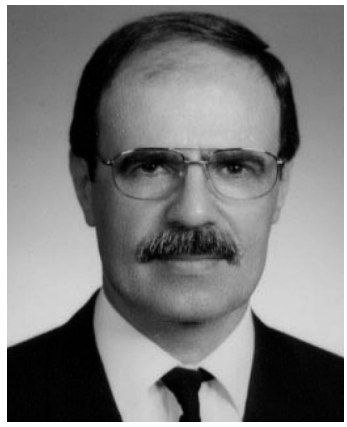

Mehmet A. Oturan was born in Tunceli, Turkey, in 1950. He obtained his B.S. degree in Chemical Engineering in 1973 and Ph.D. degree in Analytical Electrochemistry under the supervision of Professor A. Yildiz in 1979 at the Hacettepe University in Ankara before becoming Associate Professor at the same university. He undertook a postdoctoral stay in 1981 to complete his studies in electrochemistry at the Université Paris VII-Denis Diderot under Professor J. M. Savéant in the field of organic electrochemistry. From 1982 to 1989, he worked as contracted lecturer-researcher at the Université Paris VII-Denis Diderot. In 1989, he joined the newly formed Université de Marne-la-Vallée as Associate Professor. There he developed the electro-Fenton process in its "carbon-felt cathode" version. After obtaining his HDR degree (ability to supervise researchers) in 1999, he became Professor at the Université de Marne-la-Vallée (currently Université Paris-Est) in 2001. At present, he is Headmaster of the Department of Geomaterials at the IFSA (Institut Francilien des Sciences Appliquées), Director of the Laboratoire Géomatériaux et Environnement, leader of the Environmental Chemistry research group, head of the master Géo-Environnement, and Vice President of the French group of pesticides. His research activities mainly focus on the generation of radical species in a catalytic way by means of electrochemical, chemical, or photochemical techniques and its use in environmental chemistry including AOPs, chemical kinetics and mechanisms, and electrochemical engineering. He has been Associate Editor of the *Journal of Environment Engineering and Monitoring* since 2006. He has supervised 13 Ph.D. theses, published 100 peer-reviewed papers, 3 books and 6 book chapters, and presented 25 invited conferences and 130 communications to scientific congresses.

in several books and reviews.[15–19] Its main advantage is its environmental compatibility since the electron, the main reagent, is a clean reagent. Electrochemistry also offers other advantages such as versatility, high energy efficiency, amenability of automation, and safety because it operates at mild conditions. However, traditional treatments such as electrocoagulation, electroflotation, electroflocculation, electrochemical reduction, and electrochlorination, only partially remove POPs and/or produce undesirable and harmful byproducts.

Over the past decade, advanced oxidation processes (AOPs) have attracted increasing interest as promising powerful methods to efficiently removing POPs from water.[20–28] AOPs are environmentally friendly chemical, photochemical, or electrochemical methods sharing the common feature of the in-situ production of hydroxyl radical ($^{\bullet}OH$) as their main oxidizing agent. The most popular chemical AOP is the Fenton method, where a mixture of Fe^{2+} and H_2O_2 (Fenton's reagent) is used to degrade POPs.[22,23,25] The oxidation power of this technique can be notably improved by exposing the treated effluent to ultraviolet (UV) light (photo-Fenton method) or sunlight (solar photo-Fenton method).[23] Another way to obtain a high efficiency for decontamination consists of coupling the Fenton method with electrochemistry. Indeed, a large variety of electrochemical advanced oxidation processes (EAOPs) have also recently been developed.[26,27,29–31] EAOPs are mediated electrochemical treatments based on the destruction of POPs at the anode or using the Fenton's reagent partially or completely generated from electrode reactions. The former kind of EAOPs includes the so-called electrochemical degradation or anodic oxidation (AO) method,[29,30] which can also be performed with cathodic H_2O_2 generation (AO-H_2O_2).[31] Figure 1 presents a classification of EAOPs based on Fenton's reaction chemistry. The most popular technique among them is the electro-Fenton (EF) process, in which H_2O_2 is generated at the cathode with O_2 or air feeding while an iron catalyst (Fe^{2+}, Fe^{3+}, or iron oxides) is added to the effluent. Combined EF methods have also been reported for wastewater remediation. These include peroxi-coagulation (PC), photoelectro-Fenton (PEF), solar photoelectro-Fenton (SPEF), photoperoxi-coagulation (PPC), photoelectrochemical electro-Fenton (PEC-EF), sonoelectro-Fenton (SEF), and cathodic generation of Fe^{2+} as well as electrochemical and combined Fenton processes with H_2O_2 added to the solution or produced indirectly, including Fered−Fenton, electrochemical peroxidation (ECP), anodic Fenton treatment (AFT), photocombined methods, bio-ECP remediation, and plasma-assisted treatments. In these EAOPs, the ability for H_2O_2 electrogeneration at the cathode and its accumulation in the solution is evaluated from its current efficiency (CE), whereas parameters such as chemical oxygen demand (COD), total organic carbon (TOC), instantaneous current efficiency (ICE), and mineralization current efficiency (MCE) were usually employed to describe the degradation rate and degree of POPs. The kinetics of reactions involved has also been studied to determine their first-order rate constant (k_1) or second-order rate constant (k_2).

To our knowledge, few papers[26,27,31–33] and some book chapters[34] have summarized some data on the performance of EAOPs using Fenton's reagent for the degradation of several POPs. In this paper, we present a general and rigorous review on this topic, from the origins of Fenton's reaction chemistry for wastewater treatment to the current brand new devices developed until 2008. First, an overview of the peculiarities of AOPs, with special emphasis on the fundamentals and characteristics of Fenton and photo-Fenton methods, is described to design the framework in which related EAOPs are placed. The ability of different cathodes to electrogenerate H_2O_2 is also detailed to clarify the oxidation properties of the EF method and its combined processes. Fundamentals, experimental setups, and lab and pilot-plant experiments related to the major applications of these EAOPs to synthetic and real effluents are described and thoroughly discussed. Special attention is paid to EF systems given their preponderance and excellent results for wastewater remediation. The outlooks of all these emerging technologies for the upcoming future are finally envisaged.

2. Advanced Oxidation Processes (AOPs)

AOPs have been defined by Glaze et al.[20] as 'near ambient temperature and pressure water treatment processes which involve the generation of a very powerful oxidizing agent such as hydroxyl radical ($^{\bullet}OH$) in solution in sufficient quantity to effective water purification'. This concept has been further extrapolated to electrochemical systems generating heterogeneous $^{\bullet}OH$ on the anode surface under the application of high current density, as is the case for AO and AO-H_2O_2. AOPs are applied whenever conventional oxidation techniques are insufficient, when process kinetics

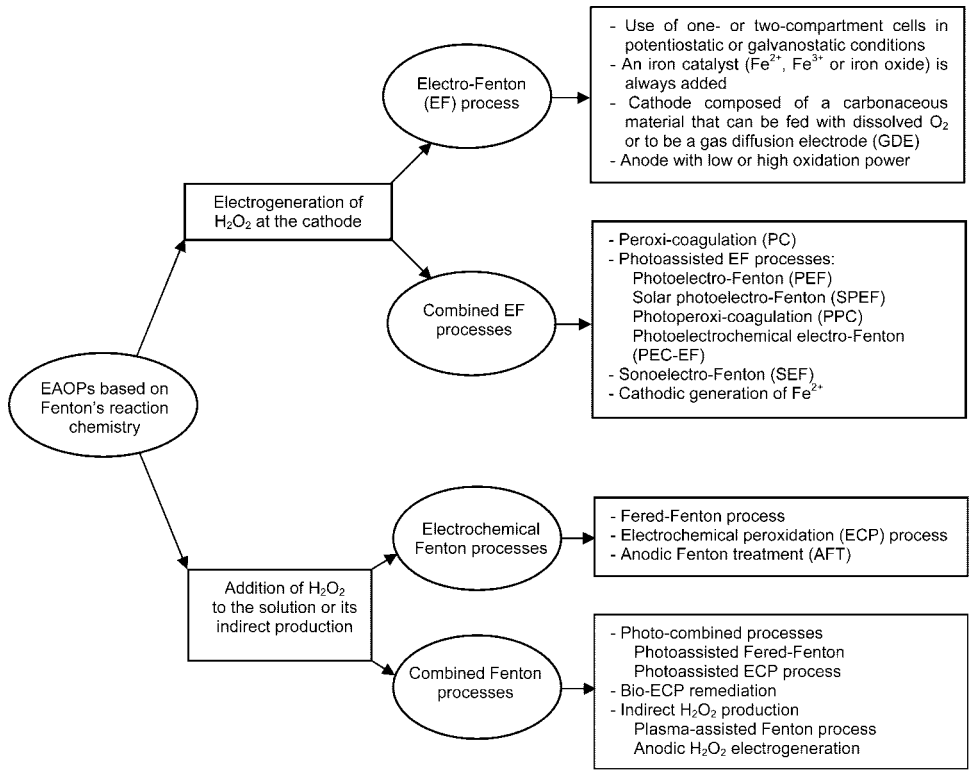

Figure 1. Classification of electrochemical advanced oxidation processes (EAOPs) based on Fenton's reaction chemistry used for the removal of organics from wastewaters. The different experimental variables for the most important electro-Fenton (EF) process are specified.

becomes very slow, or because contaminants are refractory to chemical oxidation in aqueous medium or partially oxidized yielding stable byproducts showing even greater toxicity than the starting pollutants. However, it must also be taken into consideration that the oxidation ability of most AOPs diminishes considerably when treating high organic matter contents (>5.0 g L^{-1}), thereby requiring the consumption of excessive amounts of expensive reactants that makes the treatment far less cost affordable.[35]

Key AOPs include heterogeneous and homogeneous photocatalysis based on near-UV or solar visible irradiation, AO, ozonation, Fenton's reagent, ultrasound, and wet oxidation (also called "hot AOPs"), while less conventional (and, consequently, less studied) but evolving processes include ionizing radiation with electron beams and γ-radiolysis, microwaves, pulsed plasma, UV/periodate, and ferrate reagent.[20–31,36,37] The most commonly applied AOPs for their practical usefulness and good performance are TiO_2/UV and solar photocatalysis,[38,39] O_3/UV,[40–42] H_2O_2/UV, and Fenton-based processes.[35,43] These processes generally involve interdisciplinary research and are widely investigated for the following reasons: (i) the diversity of technologies utilized, (ii) the high efficacy and effectiveness to treat low concentrations of organics, (iii) the large number of areas of potential application, and (iv) the use of harmless and easily degradable reagents.

Apart from the most common domain of wastewater treatment, AOPs are applied to groundwater treatment, soil and river sediments remediation,[44] municipal wastewater sludge conditioning, water disinfection, production of ultrapure water, volatile organic compounds (VOCs) treatment, and odor control.

2.1. Oxidizing Power and Reactivity of the Hydroxyl Radical

Traditionally, it is considered that AOPs include a large variety of degradation processes in which very oxidizing and unstable species such as $^{\bullet}$OH, whose mean lifetime is estimated as only a few nanoseconds in water,[45] has the predominant role. In fact, $^{\bullet}$OH is considered the most important free radical in chemistry and biology because of its multiple implications and applications.[13] This radical is generated in situ in the reaction medium and acts in a nonselective oxidation way onto organic compounds. Table 1 illustrates that $^{\bullet}$OH is the second strongest oxidizing agent after fluorine with a standard reduction potential of $E°(^{\bullet}OH/H_2O) = 2.8$ V/SHE. It destroys most organic and organometallic pollutants until total mineralization, i.e., conversion into CO_2, water, and inorganic ions. There are three possible attack modes of $^{\bullet}$OH onto organic molecules involving the following: (i) the dehydrogenation or abstraction of a hydrogen atom to form water, (ii) the hydroxylation or electrophilic addition to a nonsaturated bond, and (iii) electron transfer or redox reactions.

Some mechanistic studies have elucidated the particularities of these reactions.[46] The first mode is typical for alkanes and alcohols, showing k_2 values in the range 10^6-10^8 M^{-1} s^{-1}, whereas the second mode is given with aromatics with k_2 values as high as 10^8-10^{10} M^{-1} s^{-1}, as widely reported by Buxton et al.[47]

An interesting way of producing $^{\bullet}$OH is via hydrogen peroxide. This compound is a "green" chemical that leaves oxygen gas and water as byproducts. It is widely utilized, e.g., to bleach pulp, paper, and textiles, clean electronic

Table 1. Standard Reduction Potentials in Aqueous Medium of the Most Commonly Reported Oxidizing Agents for the Destruction of Organic Pollutants

oxidant	reduction reaction	$E°$/V vs SHE
fluorine	$F_{2(g)} + 2H^+ + 2e^- \rightarrow 2HF$	3.05[a]
	$F_{2(g)} + 2e^- \rightarrow 2F$	2.87[a]
hydroxyl radical	$^{\bullet}OH + H^+ + e^- \rightarrow H_2O$	2.80[b]
sulfate radical anion	$SO_4^{-\bullet} + e^- \rightarrow SO_4^{2-}$	2.60[c]
ferrate ion	$FeO_4^{2-} + 8H^+ + 3e^- \rightarrow Fe^{3+} + 4H_2O$	2.20[d]
ozone	$O_{3(g)} + 2H^+ + 2e^- \rightarrow O_{2(g)} + H_2O$	2.075[a]
peroxodisulfate ion	$S_2O_8^{2-} + 2e^- \rightarrow 2SO_4^{2-}$	2.01[b]
hydrogen peroxide	$H_2O_2 + 2H^+ + 2e^- \rightarrow 2H_2O$	1.763[a]
permanganate ion (I)	$MnO_4^- + 4H^+ + 3e^- \rightarrow MnO_{2(s)} + 2H_2O$	1.67[e]
hydroperoxyl ion (I)	$HO_2^{\bullet} + 3H^+ + 3e^- \rightarrow 2H_2O$	1.65[a]
permanganate ion (II)	$MnO_4^- + 8H^+ + 5e^- \rightarrow Mn^{2+} + 4H_2O$	1.51[a]
hydroperoxyl ion (II)	$HO_2^{\bullet} + H^+ + e^- \rightarrow H_2O_2$	1.44[a]
dichromate ion	$Cr_2O_7^{2-} + 14H^+ + 6e^- \rightarrow 2Cr^{3+} + 7H_2O$	1.36[a]
chlorine	$Cl_{2(g)} + 2e^- \rightarrow 2Cl^-$	1.358[a]
manganese dioxide	$MnO_2 + 4H^+ + 2e^- \rightarrow Mn^{2+} + 2H_2O$	1.23[a]
oxygen	$O_{2(g)} + 4H^+ + 4e^- \rightarrow 2H_2O$	1.229[a]
bromine	$Br_{2(l)} + 2e^- \rightarrow 2Br^-$	1.065[a]

[a] Bard, A. J.; Parsons, R.; Jordan, J. *Standard Potentials in Aqueous Solutions*; Marcel Dekker Inc.: New York, 1985. [b] Latimer, W. M. *Oxidation potentials*, 2nd ed.; Prentice-Hall Inc.: Englewood Cliffs, NJ, 1952. [c] Eberson, L. *Electron Transfer Reactions in Organic Chemistry*; Springer: Berlin, Germany, 1987. [d] Arora, M. G. *Periodic table and periodic properties*; Anmol Pub. Pvt Ltd.: New Delhi, India, 1997. [e] Sharma, V. K. *Adv. Environ. Res.* **2002**, *6*, 143.

circuits, and delignify agricultural wastes as well as for disinfection in medical and industrial applications and as an oxidant in organic synthesis and wastewater treatment.[48] It was prepared for the first time in 1818 by Thénard[49] from a reaction between barium peroxide and nitric acid and was initially used for minimizing the disgusting odor in sewage treatment plants (STPs). The first industrial production of H_2O_2 was carried out in 1853 by the Consortium für Elektrochemische Industrie, when it was produced by anodic oxidation of sulfuric acid or bisulfates, followed by hydroly-

sis and distillation.[50] Later, in 1882, Traube obtained H_2O_2 by cathodic reduction of dissolved O_2 in aqueous NaOH.[51] At present, the most consolidated industrial procedure is based on the multistep catalytic oxidation of anthraquinone, the so-called "anthraquinone cyclic process" or "AO-process", developed by Riedl and Pfleiderer (BASF) between 1935 and 1945,[52] although in the pulp and paper industry another well-established process is the reduction of O_2 by carbon-polytetrafluoroethylene (carbon-PTFE) cathodes located in a trickle bed reactor, which was introduced by Dow Chemical and developed in association with Huron Technologies Inc.[50] Emerging approaches based on a clean technology that yields H_2O_2 directly from H_2 and O_2 have been recently reviewed by Campos-Martin et al.[53]

H_2O_2 alone is a weak oxidant with $E°(H_2O_2/H_2O) = 1.763$ V/SHE in acidic solution and $E°(H_2O_2/OH^-) = 0.88$ V/SHE in alkaline medium. It is only effective for attacking reduced sulfur compounds, cyanides, and certain organics such as aldehydes, formic acid, and some nitro-organic and sulfo-organic compounds.[48,54] Its oxidation power can be notably improved by combination with ozone, UV radiation, and transition-metal catalysts such as iron ions. The latter technology is the so-called Fenton's chemistry explained in the section below.

2.2. Fenton's Chemistry

Various review papers have focused on Fenton's reaction chemistry and, in most cases, include applications to water and soil treatment.[43,55–58] Among these reviews, the paper by Pignatello et al.[57] is worth highlighting because it presents the reactions involved in a clear and detailed manner. However, this paper limits the application of Fenton's reagent to the destruction of POPs when all reactants (H_2O_2 and iron ions) are added to the medium, which constitutes a different approach from the vast majority of EAOPs described in the present review, which are based on the electrogeneration and/or regeneration of such reactants at the electrodes of an electrolytic cell.

2.2.1. Origins

In 1876, Fenton's pioneering work pointed out the possible use of a mixture of H_2O_2 and Fe^{2+} to destroy tartaric acid.[59] Most people, however, consider that Fenton's chemistry began in 1894 when he published a deeper study on the strong promotion of the oxidation of this acid with such a reagent.[60] During the period 1901−1928, Manchot and co-workers[61] studied the stoichiometry of the reaction between H_2O_2 and Fe^{2+}. The extraordinary practical usefulness of Fenton's reagent for the oxidation of organic compounds was first assumed in the 1930s when Haber and Weiss[62,63] suggested a radical mechanism for the catalytic decomposition of H_2O_2 by iron salts. For this reason, the Fenton's reaction is sometimes called the Haber−Weiss reaction. Since then, mechanistic studies and valuable discussions about Fenton's reaction chemistry have been extensively reported by Merz,[64] Barb et al.,[65,66] Walling,[67] and Prousek,[68] and as a result, interest in such processes has been definitely renewed, even though widespread interest in Fenton's reagent as an application to oxidize toxic organics originally appeared in the mid-1960s.[69]

2.2.2. Fenton Process

The generally accepted mechanism of the Fenton process is initiated by the formation of hydroxyl radical in accordance with the classical Fenton's reaction, eq 1:[62,63,70–73]

$$Fe + H_2O_2 \rightarrow Fe^{3+} + {}^{\bullet}OH + OH^- \quad k_2 = 63\ M^{-1}\ s^{-1} \tag{1}$$

Since this reaction takes place in acidic medium, it can alternatively be written as:

$$Fe^{2+} + H_2O_2 + H^+ \rightarrow Fe^{3+} + H_2O + {}^{\bullet}OH \tag{2}$$

The generation of $^{\bullet}OH$ in the Fenton process has been very well defended by Walling[74] and confirmed using chemical probes or spectroscopic techniques such as spin trapping.[75] In addition, fundamental work on determining the rate constants involved in Fenton's chemistry was carried out by Rush and Bielski using pulse radiolysis.[76]

The technique becomes operative if the contaminated solution is at the optimum pH of 2.8−3.0, where it can be propagated by the catalytic behavior of the Fe^{3+}/Fe^{2+} couple. Interestingly, only a small catalytic amount of Fe^{2+} is required because this ion is regenerated from the so-called Fenton-like reaction 3 between Fe^{3+} and H_2O_2:[62,63]

$$Fe^{3+} + H_2O_2 \rightarrow Fe^{2+} + HO_2^{\bullet} + H^+ \tag{3}$$

Reaction 3 is associated with a two-step transformation in which the adduct $[Fe^{III}(HO_2)]^{2+}$ formed in the equilibrium reaction 4 is subsequently converted into Fe^{2+} and hydroperoxyl radical ($HO_2^{\bullet}$) following the first-order reaction 5:[77]

$$Fe^{3+} + H_2O_2 \leftrightarrows [Fe^{III}(HO_2)]^{2+} + H^+ \quad K = 3.1 \times 10^{-3} \tag{4}$$

$$[Fe^{III}(HO_2)]^{2+} \rightarrow Fe^{2+} + HO_2^{\bullet} \quad k_1 = 2.7 \times 10^{-3}\ s^{-1} \tag{5}$$

Generated $HO_2^{\bullet}$ exhibits such a low oxidization power compared with $^{\bullet}OH$ (see Table 1) that it is quite unreactive toward organic matter.[78] As can be observed, Fenton-like reaction 3 is much slower than Fenton's reaction 1. Fortunately, Fe^{2+} can be regenerated more rapidly by the reduction of Fe^{3+} with $HO_2^{\bullet}$ from reaction 6,[57] with an organic radical $R^{\bullet}$ from reaction 7 and/or superoxide ion ($O_2^{\bullet -}$) from reaction 8.[79]

$$Fe^{3+} + HO_2^{\bullet} \rightarrow Fe^{2+} + O_2 + H^+ \quad k_2 = 2 \times 10^3\ M^{-1}\ s^{-1} \tag{6}$$

$$Fe^{3+} + R^{\bullet} \rightarrow Fe^{2+} + R^+ \tag{7}$$

$$Fe^{3+} + O_2^{\bullet -} \rightarrow Fe^{2+} + O_2 \quad k_2 = 5 \times 10^7\ M^{-1}\ s^{-1} \tag{8}$$

Few rate constants are available for reaction 7, with tertiary alkyl radicals and radicals α to −OH, −OR, or −amide N groups being the most reactive species with k_2 values of 10^7−10^8 M^{-1} s^{-1}.[57] The propagation of Fenton's reaction 1 is feasible owing to the production of $HO_2^{\bullet}$ by reaction 9[80] and $O_2^{\bullet -}$ by reaction 10,[81] as well as the attack of $^{\bullet}OH$ to saturated (RH) or aromatic (ArH) organics, which gives dehydrogenated or hydroxylated derivatives via reaction 11 or 12,[47] respectively. The hydroxylated radical formed in reaction 12 can further react with O_2 as shown in reaction 13.[57]

$$H_2O_2 + {}^{\bullet}OH \rightarrow H_2O + HO_2^{\bullet} \quad k_2 = 2.7\times10^7\ M^{-1}\ s^{-1} \tag{9}$$

$$HO_2^{\bullet} \leftrightarrows H^+ + O_2^{\bullet-} \quad pK = 4.8 \tag{10}$$

$$RH + {}^{\bullet}OH \rightarrow R^{\bullet} + H_2O \quad k_2 = 10^7 - 10^9\ M^{-1}\ s^{-1} \tag{11}$$

$$ArH + {}^{\bullet}OH \rightarrow ArHOH^{\bullet} \tag{12}$$

$$ArHOH^{\bullet} + O_2 \rightarrow ArOH + HO_2^{\bullet} \quad k_2 = 10^8 - 10^9\ M^{-1}\ s^{-1} \tag{13}$$

Note that reaction 3 and primordially reaction 9 play a scavenging role with H_2O_2 destruction and, consequently, are parasitic reactions competing with Fenton's reaction 1. Hydroxylated organics can also be produced from reaction 14 by direct hydrolysis of carbocation R^+ formed in reaction 7.

$$R^+ + H_2O \rightarrow ROH + H^+ \tag{14}$$

This reaction can be hindered if the release of a proton from a position adjacent to the positively charged carbon is favored, leading to the formation of a double bond. On the other hand, the radical $R^{\bullet}$ participates in the regeneration of Fe^{2+} by reaction 7 but also in the destruction of Fe^{2+} by reaction 15 along with its self-dimerization by reaction 16:

$$R^{\bullet} + Fe^{2+} + H^+ \rightarrow RH + Fe^{3+} \tag{15}$$

$$2R^{\bullet} \rightarrow R{-}R \tag{16}$$

The inhibition reactions 14−24[57,76,78,82–84] promote the removal of reactive radicals by competition with organic substrate and can restrict the range of several experimental parameters. For example, the existence of the parasitic reaction 17[82] has huge importance for limiting the use of a high Fe^{2+} content in the medium, which is usually lower than 1.0 mM. Worth remarking, reactions 9 and 17 promoting the consumption of $^{\bullet}OH$ by the Fenton's reagent are then major wasting reactions that decrease the oxidizing power of the Fenton system. Despite the quite high rate constant of reactions 20−24, their significance is relatively low because of the poor concentrations of radical species in the bulk, which limits their occurrence compared with other reactions involving the participation of some nonradical species.

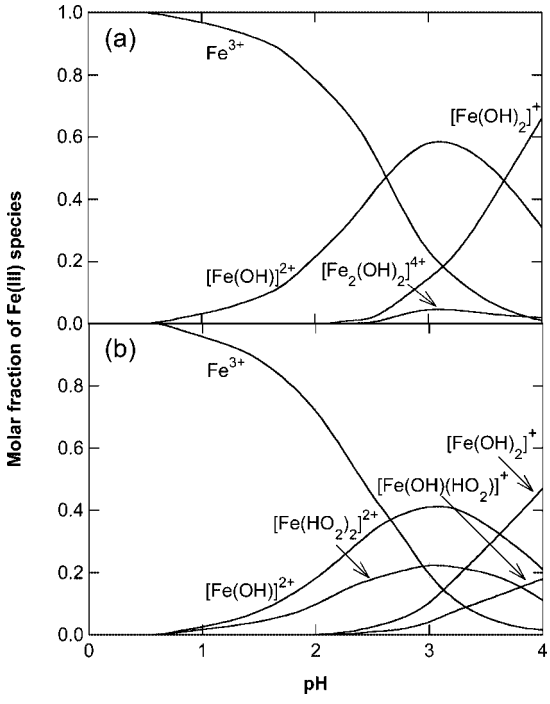

Figure 2. Speciation of soluble Fe(III) species in acidic aqueous medium with 0.1 M $NaClO_4$ at 25 °C: (a) in the absence of H_2O_2 and presence of 1 mM Fe^{3+} and (b) in the presence of 0.5 M H_2O_2 and 0.5 mM Fe^{3+}. Adapted with permission from ref 92. Copyright 1999 Elsevier.

$$Fe^{2+} + {}^{\bullet}OH \rightarrow Fe^{3+} + OH^- \quad k_2 = 3.2\times10^8\ M^{-1}\ s^{-1} \tag{17}$$

$$Fe^{2+} + HO_2^{\bullet} + H^+ \rightarrow Fe^{3+} + H_2O_2 \quad k_2 = 1.2\times10^6\ M^{-1}\ s^{-1} \tag{18}$$

$$Fe^{2+} + O_2^{\bullet-} + 2H^+ \rightarrow Fe^{3+} + H_2O_2 \quad k_2 = 1.0\times10^7\ M^{-1}\ s^{-1} \tag{19}$$

$$O_2^{\bullet-} + HO_2^{\bullet} + H^+ \rightarrow H_2O_2 + O_2 \quad k_2 = 9.7\times10^7\ M^{-1}\ s^{-1} \tag{20}$$

$$HO_2^{\bullet} + HO_2^{\bullet} \rightarrow H_2O_2 + O_2 \quad k_2 = 8.3\times10^5\ M^{-1}\ s^{-1} \tag{21}$$

$$HO_2^{\bullet} + {}^{\bullet}OH \rightarrow H_2O + O_2 \quad k_2 = 7.1\times10^9\ M^{-1}\ s^{-1} \tag{22}$$

$$O_2^{\bullet-} + {}^{\bullet}OH \rightarrow OH^- + O_2 \quad k_2 = 1.01\times10^{10}\ M^{-1}\ s^{-1} \tag{23}$$

$$^{\bullet}OH + {}^{\bullet}OH \rightarrow H_2O_2 \quad k_2 = 6.0\times10^9\ M^{-1}\ s^{-1} \tag{24}$$

Several authors have documented that the rate of the Fenton's reaction 1 is strongly dependent on the presence of radical scavengers, as in the case of inorganic ions such as chloride, sulfate, nitrate, carbonate, and hydrogencarbonate.[85] However, this behavior has not always been observed. On the basis of this apparent contradiction, some authors have argued for the formation of other oxidizing agents in the Fenton process.[86] Using electron paramagnetic resonance measurements, experimental evidence has been found for the presence of hypervalent iron complexes (e.g., ferryl or Fe(IV) ions) under certain operating conditions.[87,88] From this finding, Kremer[89] proposed the formation of a mononuclear Fe(IV) oxo complex as follows:

$$Fe^{2+} + H_2O_2 \rightarrow [Fe(OH)_2]^{2+} \rightarrow Fe^{3+} + {}^{\bullet}OH + OH^- \tag{25}$$

In contrast to hydroxyl radical, the ferryl ion $[Fe(OH)_2]^{2+}$ can only oxidize organic molecules by electron transfer. Anyway, despite being a controversial question, some kind of consensus has been found among researchers who consider that both the "classical" (i.e., based on hydroxyl radicals) and "nonclassical" (i.e., ferryl ion based) mechanisms coexist and predominate one or the other depending on the operation conditions. In this scenario, Pignatello et al.[90] demonstrated the cogeneration of both $^{\bullet}OH$ and a high-valent oxoiron complex by time-resolved laser flash photolysis spectroscopy

$$[Fe^{III}-OOH]^{2+*} \rightarrow \{Fe^{III}-O^{\bullet} \leftrightarrow Fe^{IV}=O\} + {}^{\bullet}OH \quad (26)$$

where $[Fe^{III}-OOH]^{2+*}$ represents an excited state and the overall reaction can be interpreted as an intraligand reaction. From these results, the authors proposed that ferryl formation in secondary reactions under classical Fenton conditions cannot be ruled out.

The efficiency of the Fenton's reagent is a function of various factors such as temperature, pH, H_2O_2, and catalyst concentrations, which control the regeneration ability of Fe^{2+} from Fe^{3+} produced along the process. The catalytic activity of iron species is mainly determined by the solution pH.[91] At pH 2.8 the concentration of Fe^{2+} available in the reaction medium is at its maximum, which gives rise to the highest rate of Fenton's reaction 1.[60,61] In contrast, at pH > 5.0 Fe(III) species start precipitating as $Fe(OH)_3$, thereby decreasing the quantity of catalyst in the solution and breaking the H_2O_2 into O_2 and H_2O. Figure 2a and 2b illustrate the speciation of 1 mM Fe(III) up to pH 4.0 at 0.1 M ionic strength in the absence and presence of H_2O_2, respectively, which are also typical conditions used in EF systems. $[Fe(H_2O)_6]^{3+}$ or simply Fe^{3+} is the sole species at pH 0 in both cases, but it practically disappears at pH 4.0 because it is replaced by hydroxy complexes such as $[Fe(OH)]^{2+}$, $[Fe(OH)_2]^{+}$, and $[Fe_2(OH)_2]^{4+}$ in the former case and even by hydroperoxy complexes such as $[Fe(HO_2)_2]^{+}$ and $[Fe(OH)(HO_2)]^{+}$ in the latter. At the optimum pH of 2.8, about one-half of the free Fe^{3+} is always present in the bulk. Therefore, a strict pH control is needed to operate in such conditions. Temperature is also a crucial parameter. When the temperature increases, the kinetics of the reactions is enhanced but, at the same time, the H_2O_2 decomposition to O_2 and H_2O is greatly favored. Regarding the concentration of both components of the Fenton's reagent, their action is so closely linked that usually experiments are done on the basis of the optimization of the $[Fe^{2+}]/[H_2O_2]$ ratio instead of treating them independently.

The main advantages of the Fenton process for wastewater treatment are the following:[58] (i) simple and flexible operation allowing easy implementation in existing plants, (ii) easy-to-handle chemicals, and (iii) no need for energy input. However, the following disadvantages have been emphasized:[23] (i) its relatively high cost and risks related to the storage and transportation of H_2O_2, (ii) high amounts of chemicals are spent for acidifying effluents at pH 2.0−4.0 before decontamination and/or for neutralizing treated solutions before disposal, (iii) accumulation of iron sludge that needs to be removed at the end of the treatment, and (iv) overall mineralization is not feasible by the formation of complexes of Fe(III) with generated carboxylic acids that cannot be destroyed with bulk $^{\bullet}OH$.

The amount of H_2O_2 added can be minimized by optimizing its concentration, and iron sludge can be prevented by using solid iron-containing catalysts such as zeolites, alumina, iron-modified clays, mesoporous molecular sieves, iron oxides, ion-exchange resins, and iron-exchanged Nafion membranes, which can be easily separated from treated solutions.[57,58] In current applications with actual wastewater, the Fenton method is coupled to processes such as coagulation, membrane filtration, and biological oxidation to degrade organics to a much larger extent.[92,93] Another possibility is the use of the photo-Fenton process discussed below.

2.3. Photo-Fenton Process

The pioneering study of Zepp and co-workers[94] demonstrated that $[Fe(OH)]^{2+}$ ion, the pre-eminent form of Fe(III) at pH 2.8−3.5 (see Figure 2), plays a key role when the dark Fenton process is photoassisted by UV irradiation leading to the photo-Fenton process. This procedure can utilize UVA (λ = 315−400 nm), UVB (λ = 285−315 nm), and UVC (λ < 285 nm) lights as energy source, although the intensity and wavelength of radiation has a significant influence on the destruction rate of organic pollutants. A disadvantage of this process is the excessive economical cost arising from the use of artificial light. Recent work has shown that the alternative use of sunlight (λ > 300 nm) as a free and renewable energy source in the so-called solar photo-Fenton process is also useful for wastewater remediation.[38,95] In fact, the determination of a parameter called the "environmental-economic index" (EEI) has shown that solar-driven photo-Fenton is preferable to lamp-driven photo-Fenton if both environmental and economic aspects must be satisfied in a well-balanced manner.[96]

The action of photons in the photo-Fenton process is complex. Hydroxyl radicals are produced from Fenton's reaction 1 as well, but the drawback of the large accumulation of Fe(III) species decelerating the treatment is avoided from the reductive photolysis of $[Fe(OH)]^{2+}$ according to reaction 27, thus regenerating the Fe^{2+} that catalyzes the Fenton's reaction 1 and producing additional $^{\bullet}OH$:[95,97]

$$[Fe(OH)]^{2+} + h\nu \rightarrow Fe^{2+} + {}^{\bullet}OH \quad (27)$$

The quantum efficiency for reaction 27 was determined as 0.14−0.19 at 313 nm.[98] More recently, the application of a novel method using DMSO as a $^{\bullet}OH$ probe compound has shown that the quantum yields for the photolysis of Fe(III)−hydroxy complexes, including $[Fe(OH)]^{2+}$, decrease with increasing wavelength in the range 240−380 nm.[99]

In addition, UV light can induce the photodegradation of some oxidation byproducts or their complexes with Fe(III) promoting Fe^{2+} regeneration. This is the case for the photodecarboxylation of Fe(III)−carboxylate species according to reaction 28:[100]

$$Fe(OOCR)^{2+} + h\nu \rightarrow Fe^{2+} + CO_2 + R^{\bullet} \quad (28)$$

As an example, oxalic acid forms complexes such as $Fe(C_2O_4)^{+}$, $Fe(C_2O_4)_2^{-}$, and $Fe(C_2O_4)_3^{3-}$ that absorb photons from 250 to 580 nm and whose photodecarboxylation follows reaction 29 by passing through an excitation state undergoing a ligand−metal charge transfer:[101]

$$2Fe(C_2O_4)_n^{(3-2n)} + h\nu \rightarrow 2Fe^{2+} + (2n-1)C_2O_4^{2-} + 2CO_2 \quad (29)$$

Photolysis of H_2O_2 from reactions 30 and 31 can also occur if Xe/Hg arc or low-pressure Hg lamps in the UVC region, with 90% at 253.7 nm and 10% at 184.9 nm, are used.[25] Moreover, these two radiations are useful for AOPs applications because they are usually included in the absorption spectra of many pollutants.

$$H_2O_2 + h\nu \rightarrow 2{}^{\bullet}OH \quad (30)$$

$$H_2O_2 + h\nu \rightarrow H^{\bullet} + HO_2^{\bullet} \quad (31)$$

3. H_2O_2 Electrogeneration for Water Treatment

EAOPs based on the cathodic electrogeneration of H_2O_2 are being successfully applied to the treatment of acidic

wastewater containing POPs.[26,27,48,54,102–104] The great interest for these indirect electrooxidation methods arises from the fact that reactions involved in the cathodic reduction of oxygen proceed at low potential and in homogeneous environment.[105] H_2O_2 electrosynthesis, sometimes called electroperoxidation,[104] can be performed with divided or undivided cells, which show very different behavior depending on the cathode and operational parameters chosen, as can be deduced from selected results summarized in Tables 2 and 3 for such electrolytic systems. The fundamentals of H_2O_2 electrogeneration and the characteristics of cathodes and electrolytic systems used are described in this section.

3.1. Fundamentals

H_2O_2 can be continuously supplied to an acidic contaminated aqueous solution contained in an electrolytic cell from the two-electron reduction of oxygen gas, directly injected as pure gas or bubbled air, by reaction 32 with $E° = 0.695$ V/SHE, which takes place more easily than its four-electron reduction to water from reaction 33 with $E° = 1.23$ V/SHE:[51]

$$O_{2(g)} + 2H^+ + 2e^- \rightarrow H_2O_2 \quad (32)$$

$$O_{2(g)} + 4H^+ + 4e^- \rightarrow 2H_2O \quad (33)$$

In alkaline solutions, oxygen gas is reduced to hydroperoxide ion (HO_2^-), the conjugate base of H_2O_2 ($pK_a = 11.64$),[106] via reaction 34 with $E° = -0.065$ V/SHE, which is also favored over its complete four-electron transformation into hydroxide ion by reaction 35:

$$O_{2(g)} + H_2O + 2e^- \rightarrow HO_2^- + OH^- \quad (34)$$

$$O_{2(g)} + 2H_2O + 4e^- \rightarrow 4OH^- \quad (35)$$

The mass transfer of oxygen from the gas phase to the cathode when dissolved O_2 is used is shown in Figure 3.[107] Oxygen gas is first dissolved in the aqueous phase and further transferred from the bulk to the cathodic surface, where it is reduced to hydrogen peroxide. Agladze et al.[108] proposed that O_2 reduction always takes place via reaction 34, giving HO_2^- and OH^-, responsible for the alkaline

Table 2. Selected Results Reported for the Cathodic Electrogeneration of H_2O_2 in Divided Cells

cell configuration	operation conditions[a]	$[H_2O_2]$/mg L^{-1}	current efficiency/%[b]
	three-electrode cell		
H-type reactor with glass frit separator, a Pt wire anode, and a 43 cm^2 graphite plate cathode[107]	125 (catholyte) and 50 mL (anolyte) of 0.5 M Na_2SO_4, pH 11, 25 °C; O_2 flow rate in catholyte 5 mL s^{-1}; $j = 0.5$ mA cm^{-2} up to 200 C	*c*	92
flow plant with a Nafion 417 cationic membrane, a Pt gauze anode (50 mm × 50 mm), and an RVC cathode (50 mm × 50 mm × 12 mm)[123]	2.5 L of 1 M NaOH (catholyte) pumped at 0.19 m s^{-1}, room temperature; air saturation; $E_{cat} = -0.6$ V/SCE ($I = 95$ mA)	6[d]	94
same flow plant equipped with a Nafion 450 cationic membrane[112]	2 L of 10 mM HCl + 50 mM NaCl (catholyte) pumped at 0.13 m s^{-1}, room temperature; O_2 supply; $E_{cat} = -0.6$ V/SCE up to 6000 C	0.76−1.21[e]	60
cylindrical tank with a cationic membrane, a Pt plate anode, and a 5 cm^2 GDE cathode[140]	100 mL of 1 M Na_2SO_4 (catholyte), 25 °C; O_2 supply; $E_{cat} = -0.4$ to -0.6 V vs Ag/AgCl for 5 h	600[d]	*c*
cylindrical tank with a cationic membrane, a Pt anode and a 5 cm^2 carbon-PTFE GDE (A) or graphite (B) cathode[111]	100 mL of 0.04 M Na_2SO_4/0.05 M $NaHSO_4$ (catholyte) at pH 3 and room temperature and 100 mL of 0.01 M $NaClO_4$ (anolyte); O_2 or air flow rate 130 mL min^{-1}; $E_{cat} = -0.9$ V/SCE up to 500 C	800 (A) 100 (B)	85 (A) 85 (B)
flow plant with two N424 Nafion membranes, two 150 cm^2 Ti/$(Ta_2O_5)_{0.6}(IrO_2)_{0.4}$ anodes, and an RVC plate cathode (50 mm × 150 mm × 6 mm, gap = 5 mm)[146]	3.5 L of 0.3 M K_2SO_4 (catholyte) pumped at 300 L h^{-1}, pH 2.5 or 10, 10 °C; O_2 flow rate 6 L min^{-1}; $E_{cat} = -1.6$ V/SCE for 300 min	850	65
cylindrical tank with a cationic membrane, a Pt anode, and a 5 cm^2 carbon-PTFE GDE cathode[139]	100 mL of seawater (catholyte) at pH 3 and room temperature and 100 mL of 0.01 M $NaClO_4$ (anolyte); O_2 flow rate in catholyte 130 mL min^{-1}; $E_{cat} = -0.9$ V/SCE up to 2400 C	2900	70
cylindrical tank with a porous glass diaphragm, a Pt wire anode, and a 6.15 cm^2 carbon-PTFE GDE cathode[145]	250 (catholyte) and 10 mL (anolyte) of 0.05 M Na_2SO_4, pH 7, 25 °C; air flow rate in catholyte 20 mL s^{-1}; $j = 30$ mA cm^{-2} for 60 min	8.8[d]	47 (as maximum)
	two-electrode cell		
cylindrical tank with insulating diaphragm, a 67 cm^2 Ti/RuO_2 anode, and a 177 cm^2 carbon-felt RVC cathode[102–104]	5 L of tap water (catholyte) at 20 °C; anodic O_2 or air supply; $I = 2000$ mA for 90 min	15	*c*
cylindrical tank with a cotton diaphragm and a 14 cm^2 Ti/IrO_2/RuO_2 anode and carbon-PTFE GDE cathode[141,142,144]	100 mL of 0.02 M Na_2SO_4 (catholyte), pH 7; air flow rate in the catholyte 25 mL s^{-1}; $j = 39$ mA cm^{-2} for 100 min	8.3	*c*
flow plant with a filter-press cell containing a membrane, a 100 cm^2 DSA anode and carbon-PTFE GDE cathode (gap = 6.5 mm)[108]	5 L of 0.05 M Na_2SO_4 (catholyte) pumped at 360 L h^{-1}, pH 3−13, 25−60 °C; O_2 or air flow rate 30 g h^{-1}; $I = 3000$ mA for 60 min	1000	98−100 (at 35 min)

[a] Applied current (I), current density (j), and cathodic potential (E_{cat}). [b] Calculated from eq 40. [c] Not reported. [d] Concentration in millimolar. [e] H_2O_2 electrogeneration rate in μmol s^{-1}.

Table 3. Selected Results Reported for H_2O_2 Electrogeneration in Undivided Cells

cell configuration	operation conditions[a]	$[H_2O_2]$/mg L^{-1}	current efficiency/%[b]
	three-electrode cell		
cylindrical tank with a Pt plate anode and a 5 cm^2 GDE cathode[140]	100 mL of 1 M Na_2SO_4, 25 °C; O_2 supply; E_{cat} = −0.4 to −0.6 V vs Ag/AgCl for 5 h	350[c]	*d*
cylindrical tank with a Pt anode and a rotating RVC cathode (ϕ = 11 mm) at 900 rpm[150]	130 mL of 0.3 M K_2SO_4, pH 3.5 or 10, 10 °C; O_2 content 25 mg L^{-1};E_{cat} = −1.6 V/SCE for 240 min	275	7.8
cylindrical tank with a graphite stick anode and a carbon-PTFE GDE (A), MWNT (B), or Fe-MWNT (C) cathode (2.2 cm × 5.2 cm)[115]	250 mL of 0.05 M Na_2SO_4, pH 3, 25 °C; O_2 flow rate 400 mL min^{-1}; E_{cat} = −0.85 V/SCE for 90 min	95 (A) 105 (B) 110 (C)	60 (A) 45 (B) 52 (C)
cylindrical tank with a Pt anode and a 5 cm^2 carbon-PTFE GDE cathode[139]	100 mL of seawater at pH 3 and room temperature; O_2 flow rate 130 mL min^{-1}; E_{cat} = −0.9 V/SCE up to 687 C	78	6
cylindrical tank with a Pt wire anode and a 6.15 cm^2 carbon-PTFE GDE cathode[145]	250 mL of 0.05 M Na_2SO_4, pH 7, 25 °C; air flow rate 20 mL s^{-1}; j = 30 mA cm^{-2} for 60 min	5.6[c]	30 (as maximum)
	two-electrode cell		
cylindrical tank with a 10 cm^2 Pt sheet anode and a 3.1 cm^2 carbon-PTFE GDE cathode[148]	100 mL of 0.05 M Na_2SO_4, pH 3.0, 25 °C; O_2 flow rate 20 mL min^{-1}; I = 450 mA for 300 min	73[c]	80 (15 min) 50 (120 min)
cylindrical tank with a 20 cm^2 Ti/RuO_2 mesh anode and a 20 cm^2 ACF (A) or graphite (B) cathode[122]	500 mL of 0.05 M Na_2SO_4, pH 3.0; O_2 supply; I = 360 mA for 180 min	0.6[c] (A) 0.05[c] (B)	*d* *d*
cylindrical tank with a 14 cm^2 Ti/IrO_2/RuO_2 anode and carbon-PTFE GDE cathode[141,142,144]	100 mL of 0.02 M Na_2SO_4, pH 7; air flow rate 25 mL s^{-1}; j = 39 mA cm^{-2} for 100 min	5.6	*d*
flow plant with a filter-press cell with a 20 cm^2 BDD anode and carbon-PTFE GDE cathode (gap = 1 cm)[149]	2.5 L of 0.05 M Na_2SO_4 pumped at 180 L h^{-1}, pH 3, 25 °C; O_2 overpressure 8.6 kPa; I = 3000 mA for 540 min	54[c]	*d*
cylindrical tank with a Pt gauze anode and a 3.10 cm^2 carbon-felt (A) or 4 cm^2 carbon-sponge (B) cathode[114]	125 mL of 0.05 M Na_2SO_4, pH 3.0, 25 °C; O_2 flow rate 100 mL min^{-1}; I = 100 mA for 180 min	2.70 (A) 8.05 (B)	*d* *d*

[a] Applied current (I), current density (j), and cathodic potential (E_{cat}). [b] Calculated from eq 40. [c] Concentration in millimolar. [d] Not determined.

medium detected into the pores of gas diffusion electrodes (GDEs). This means reaction 32 in usual acidic solutions could proceed via HO_2^- formation followed by protonation of this species to H_2O_2 when crossing the interface with the acidic bulk.

Hydrogen peroxide production and stability depend on factors such as cell configuration, cathode properties, and operation conditions, as can be seen in Tables 2 and 3. In both alkaline and acidic media, there are major parasitic reactions which result in a lower current efficiency. For example, electrochemical reduction at the cathode surface from reaction 36 and, to a much lesser extent, disproportion in the bulk by reaction 37 are given regardless the cell configuration:[109]

$$H_2O_2 + 2H^+ + 2e^- \rightarrow 2H_2O \quad (36)$$

$$2H_2O_2 \rightarrow O_{2(g)} + 2H_2O \quad (37)$$

When an undivided cell is utilized, H_2O_2 is also oxidized to O_2 at the anode via $HO_2^{\bullet}$ as an intermediate by the following reactions:[110]

$$H_2O_2 \rightarrow HO_2^{\bullet} + H^+ + e^- \quad (38)$$

$$HO_2^{\bullet} \rightarrow O_{2(g)} + H^+ + e^- \quad (39)$$

Consequently, the accumulation of H_2O_2 is lower than its electrogeneration. Its concentration in solution can be determined by reflectometry,[111] permanganometry,[112] iodometry,[107] cerium oxidation of H_2O_2 with ferrous orthophenanthroline as an indicator,[102] or spectrophotometric measurements based on the Ti(IV)−H_2O_2 complex,[113] iodide,[114] and

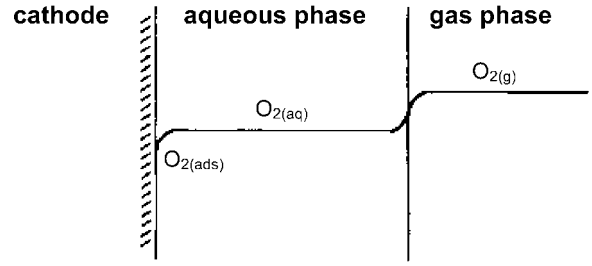

Figure 3. Scheme of the mass transfer of oxygen from the gaseous phase to the cathodic surface. Reprinted with permission from ref 107. Copyright 1993 The Electrochemical Society.

ferric−oxalate[115] methods. The current efficiency (%) for H_2O_2 accumulation is then calculated from eq 40

$$CE = \frac{nFc(H_2O_2)V}{1000M(H_2O_2)Q} \times 100 \quad (40)$$

where n represents the stoichiometric number of electrons transferred in reaction 32, F is the Faraday constant (96 487 C mol^{-1}), $c(H_2O_2)$ is the concentration of accumulated H_2O_2 (mg L^{-1}), V is the volume of the treated solution (L), 1000 is a conversion factor, $M(H_2O_2)$ is the molecular weight of H_2O_2 (34 g mol^{-1}), and Q is the charge consumed during the electrolysis.

3.2. Cathode Materials

H_2O_2 electrogeneration applied to water treatment is carried out by dissolving O_2 or air in the solution to be reduced at suitable cathode materials or by directly injecting the gas into GDEs. Especially worth noting are the pioneer

works reporting the excellent use of cathodes such as mercury,[116,117] graphite,[107,118] carbon-PTFE O_2 diffusion,[110,119] and three-dimensional electrodes such as carbon felt,[120,121] activated carbon fiber (ACF),[122] reticulated vitreous carbon (RVC),[112,123,124] carbon sponge,[114] and carbon nanotubes (NT).[115] However, the use of mercury has been disregarded owing to its potential toxicity.

Although it has long been known that carbon electrodes produce H_2O_2 from O_2 reduction, the intensive investigations in this field started in the 1970s, when Oloman and Watkinson[125,126] used trickle-bed electrochemical reactors consisting of fluidized or packed beds of graphite particles. Carbon is nontoxic, unlike mercury, and exhibits a high overpotential for H_2 evolution and low catalytic activity for H_2O_2 decomposition, along with relative good stability, conductivity, and chemical resistance. Due to the poor solubility of O_2 in aqueous solution (about 40 or 8 mg L^{-1} in contact with pure O_2 or air, respectively, at 1 atm and 25 °C),[107] GDEs and three-dimensional electrodes of high specific surface area are preferred as cathodes to supply reasonable current densities for practical applications.

GDEs have a thin and porous structure favoring the percolation of the injected gas across its pores to contact the solution at the carbon surface. These electrodes possess a large number of active surface sites leading to a very fast O_2 reduction and large accumulation of H_2O_2.[110,119] They usually incorporate PTFE that serves to bind the carbon particles into a cohesive layer and impart some hydrophobic character to the electrode. Figure 4a shows a scanning electron microscopy (SEM) image of the surface of a typical GDE.[127] The presence of PTFE (white grains) covering a given surface of the layer, which brings about enough hydrophobicity, can be observed, as well as macropores allowing the transport of reactant gas.

Three-dimensional electrodes present a high ratio of surface area to volume, combined with low cost and easy handling. They are very useful for counteracting the limitations of the low space-time yield and low normalized space velocity resulting from electrochemical processes with two-dimensional electrodes. A three-dimensional electrode can be obtained by means of a fluidized bed, packed bed, rolling tube, or porous material, the latter option being the most widespread way of preparing cathodes for water treatment. Due to the particular hydrodynamic conditions inside such electrodes, both large specific electrode areas and large numbers of the mass transfer coefficients of dissolved O_2 can be obtained.

The carbon-felt electrode has such a high specific surface that favors the fast generation of both components of the Fenton's reagent (H_2O_2 and Fe^{2+}), and then $^{\bullet}OH$ is produced from Fenton's reaction 1 in the bulk but without significant H_2O_2 accumulation.[121] ACF is a three-dimensional carbon material with a high adsorption capacity and good conductivity.[128] Its excellent mechanical integrity makes it easy to configure as a stable electrode, giving a relatively large accumulation of H_2O_2.[122] RVC is preferred for H_2O_2 production. It is a microporous, glassy carbon material presenting low density and thermal expansion, along with high thermal and electrical conductivities. It has an open-pore honeycomb structure, as shown in Figure 4b,[129] high void volume between 90 and 97% depending on the pores per inch (i.e., ppi grade), a high surface area and rigid structure, alongside many other properties carefully reviewed by Pletcher and Walsh.[130]

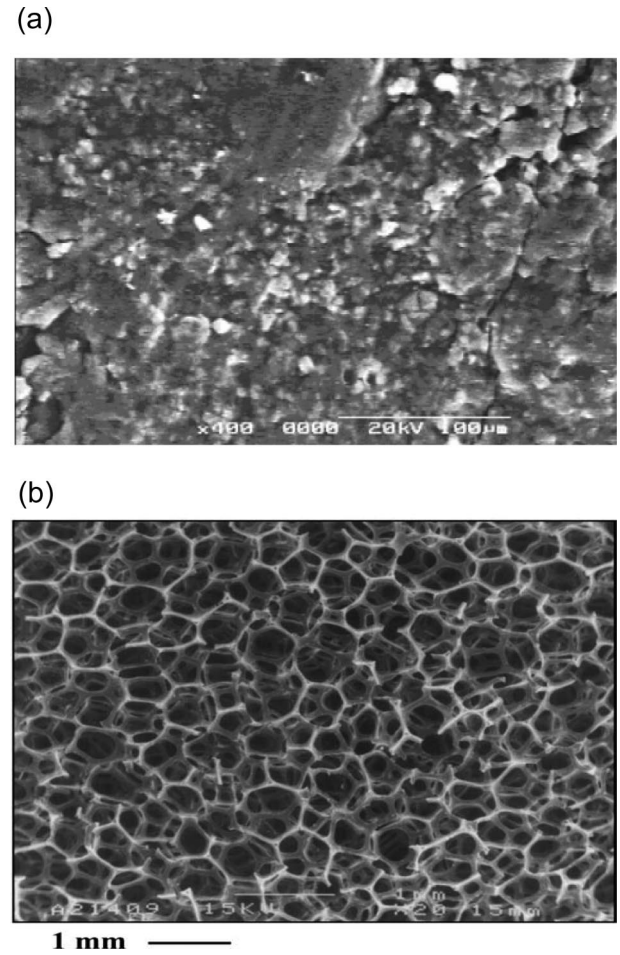

Figure 4. (a) SEM micrograph of the surface of a typical gas diffusion electrode (GDE) (magnification 400×). Reprinted with permission from ref 127. Copyright 2005 American Chemical Society. (b) SEM micrograph of a 100 ppi (nominal pores per linear inch) reticulated vitreous carbon (RVC) sample. Reprinted with permission from ref 129. Copyright 2004 Elsevier.

Novel electrode materials have recently been proposed as suitable and even more performing for carrying out electrochemical water treatment with H_2O_2 electrogeneration. It is worth noting the study of NT, mainly focused until now on their role as anode materials.[131] Factors including the closed topology, tubular structure, and functionalization ability of these materials must be carefully selected to test their long-term stability and reliability as carbon cathodes for H_2O_2 production. Fu et al.[115] prepared Fe-modified multiwalled carbon nanotubes (Fe-MWNT) from electrochemical deposition of Fe_2O_3 onto MWNT and concluded that the former electrode yields higher H_2O_2 production and better current efficiency than the latter, as can be seen in Table 3, thus being a promising material for application in the EF process. The SEM images of Figure 5 clearly illustrate that the MWNT surface is rough with many nanoscale pores, fibrosis of PTFE, and disordered nanotubes, whereas the Fe-MWNT material shows a good coverage by Fe_2O_3 grains. Energy-dispersive spectroscopy reveals that its surface contains 2.34% Fe, which appears in a granular form similar to rust.

3.3. Divided Cells

A large variety of three- and two-electrode divided electrolytic cells have been utilized for electrogenerating H_2O_2 to be applied to water remediation. The performance of these systems with

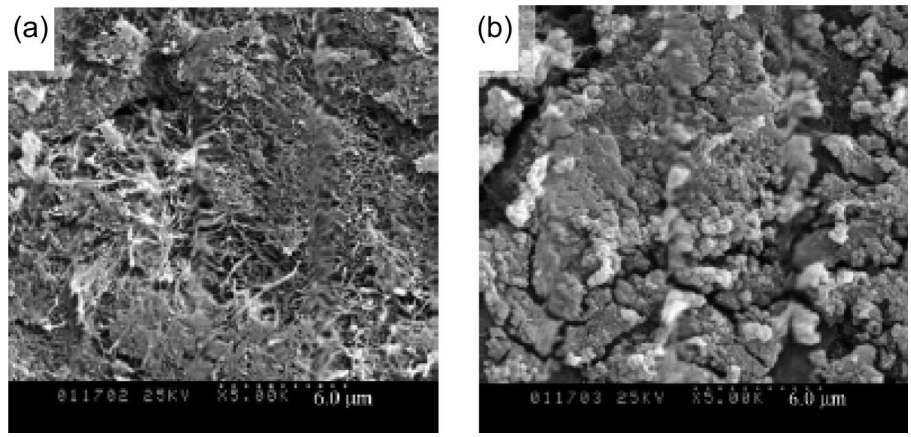

Figure 5. SEM micrographs of (a) multiwalled carbon nanotubes (MWNT) and (b) Fe-MWNT samples. Reprinted with permission from ref 115. Copyright 2007 Acta Physico-Chimica Sinica.

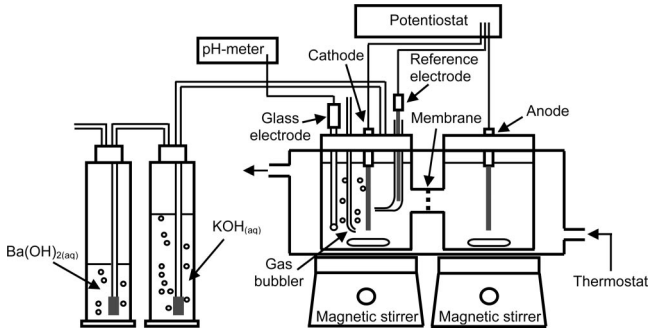

Figure 6. Sketch of an H-type divided cell and equipment used for cathodic H_2O_2 electrogeneration and organics degradation. O_2 was bubbled close to the cathode, and released CO_2 was collected and quantified. Adapted with permission from ref 118. Copyright 1986 Society Chemical Engineers, Japan.

two separate solutions, catholyte and anolyte, is determined under potentiostatic or galvanostatic conditions (see Table 2). In the former case, a constant cathodic potential (E_{cat}) against a reference electrode is submitted to the catholyte to provide a current between the anode and cathode, whereas in the latter case, a constant current (I) or current density (j) is directly supplied to the cell. Glass frits, diaphragms, and cationic membranes are typically employed as separators between the cathodic and anodic compartments. Glass frits and diaphragms prevent the mixing of cathodically produced H_2O_2, avoiding its destruction at the anode from reactions 38 and 39. The cationic membranes, usually made of Nafion, are more specific and only allow small cations such as protons to freely penetrate through it.

Original studies on the performance of a three-electrode divided cell were reported by Sudoh et al.[118,132,133] They utilized an H-type two-compartment cell such as that of Figure 6 with a graphite cathode and found a maximum current efficiency of 85% for H_2O_2 accumulation in 0.5 M Na_2SO_4 as the catholyte by applying $E_{cat} = -0.6$ V vs Ag/AgCl/KCl (satd) at pH 3.0 under O_2 sparging. They also observed a gradual increase in H_2O_2 concentration with rising consumed charge in the pH range 1.0−3.0.[118] Do and Chen[107,134,135] described similar results using the same H-type dual-compartment reactor equipped with an anodically treated graphite cathode with or without modification by metalloporphyrins. These authors found a maximum current efficiency of 92% working up to $E_{cat} = -0.39$ V vs Ag/AgCl/KCl (3 M). Thereafter, the efficiency gradually dropped with E_{cat} rising toward more negative values because of the side reaction 36 along with H_2 evolution from direct proton reduction as well as H_2O_2 decomposition via reaction 37 when the temperature is above 25 °C. A sparging O_2 rate higher than 5 mL s^{-1} was needed to keep the catholyte saturated with this gas (solubility ≈ 40 mg L^{-1}), while it was transferred from the bulk to the cathode to be reduced to H_2O_2. The same group further reported the paired electrolysis of dissolved O_2 in the catholyte and chloride ion in the anolyte, giving H_2O_2 and ClO^- ion, respectively, as oxidizing agents of formaldehyde.[136–138]

An interesting comparative study on the ability of graphite and GDE cathodes to electrogenerate H_2O_2 was reported by Da Pozzo et al.[111] These authors utilized two different three-electrode cells, one of them equipped with a Nafion 324 cationic membrane (see Figure 7a) and the other one with an agar−H_2O−$NaClO_4$ plug sintered-glass disk (see Figure 7b), for the electrolysis of 100 mL of 0.04 M Na_2SO_4 + 0.05 M $NaHSO_4$ as the catholyte. Figure 7c illustrates the continuous H_2O_2 accumulation with time at $E_{cat} = -0.9$ V/SCE in both cells, although with much greater performance, close to the ideal behavior, for the O_2-diffusion cathode in the membrane cell compared with graphite in the same cell or in the salt-bridge cell. Several electrogeneration trials were also undertaken in the membrane cell with the graphite cathode in the range from −0.6 to −1.1 V/SCE, and a maximum current efficiency of 85% was obtained at the optimum E_{cat} value of −0.6 V/SCE. The same efficiency was determined for the O_2-diffusion electrode, which was practically independent of applied charge, operating between −0.6 and −0.9 V/SCE (see Table 2). These results demonstrate that the GDEs exhibit a higher selectivity for H_2O_2 production thanks to the direct supply of O_2 to the electrode surface, thus minimizing the extent of side reactions. More recently, the same group explored the possibility of electrogenerating H_2O_2 in seawater for disinfection using the membrane cell of Figure 7a with the O_2-diffusion cathode.[139]

Other authors[108,140–145] have also reported the excellent performance of GDEs for H_2O_2 electrogeneration in different three- and two-electrode systems. For example, Agladze et al.[108] obtained current efficiencies up to 98−100% by recirculating 5 L of 0.05 M Na_2SO_4 at pH 3.0−13.0 and 25−60 °C as the catholyte through a flow plant with a two-electrode filter-press cell containing a heterogeneous MK-40 type proton-exchange membrane, a 100 cm^2 DSA anode, and a 100 cm^2 carbon-PTFE cathode fed with an O_2 or air flow rate of 30 g h^{-1} operating at 3 A and a liquid flow rate of 360 L h^{-1} for 60 min (see Table 2). However, a decrease

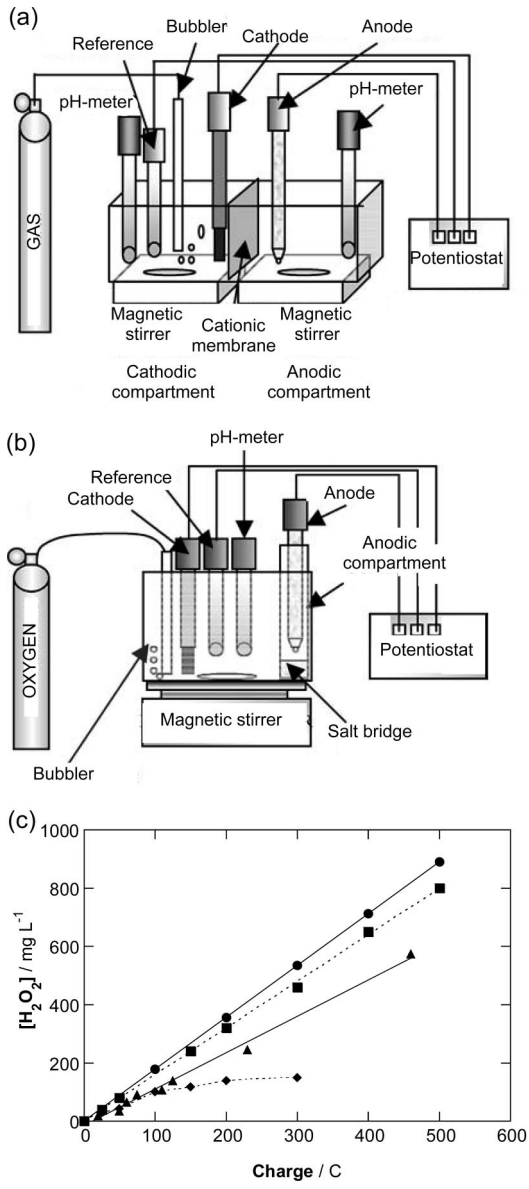

Figure 7. Schemes of bench-scale divided three-electrode cells and equipment with (a) a Nafion 324 cationic membrane and (b) an agar-H_2O-$NaClO_4$ plug sintered-glass disk, equipped with a 5 cm^2 Pt anode, a 5 cm^2 carbon-PTFE gas GDE or graphite cathode, and a SCE as reference electrode, used in the electrolysis of 100 mL of a 0.04 M Na_2SO_4/0.05 M $NaHSO_4$ buffer solution at room temperature by injecting O_2 at 130 mL min^{-1}. (c) Accumulated H_2O_2 concentration in the catholyte against charge consumed at a cathodic potential E_{cat} = −0.9 V/SCE for (●) 100% current efficiency; (■) GDE in cell a, (▲) graphite in cell b, and (◆) graphite in cell a. Adapted with permission from ref 111. Copyright 2005 Springer.

in current efficiency with increasing current, temperature, and, especially, pH was observed, reaching values as low as 13.4% at 20 A, 60 °C, and pH 3.0 and 2.7% at 5 A, 25 °C, and pH 13.0. Current efficiencies greater than 95% have also been found for a two-electrode Pt/O_2 cell containing a KCl solution of pH 3.0−3.5 as the catholyte under galvanostatic electrolysis at 80 mA.[143] In contrast, a much lower efficiency of 47% in 0.05 M Na_2SO_4 of pH 7.0 has been reported by Panizza and Cerisola[145] using a three-electrode cell with a Pt anode and an O_2-diffusion cathode fed with air (see Table 2).

Batch recirculation flow plants with three-electrode cells equipped with three-dimensional RVC cathodes have also

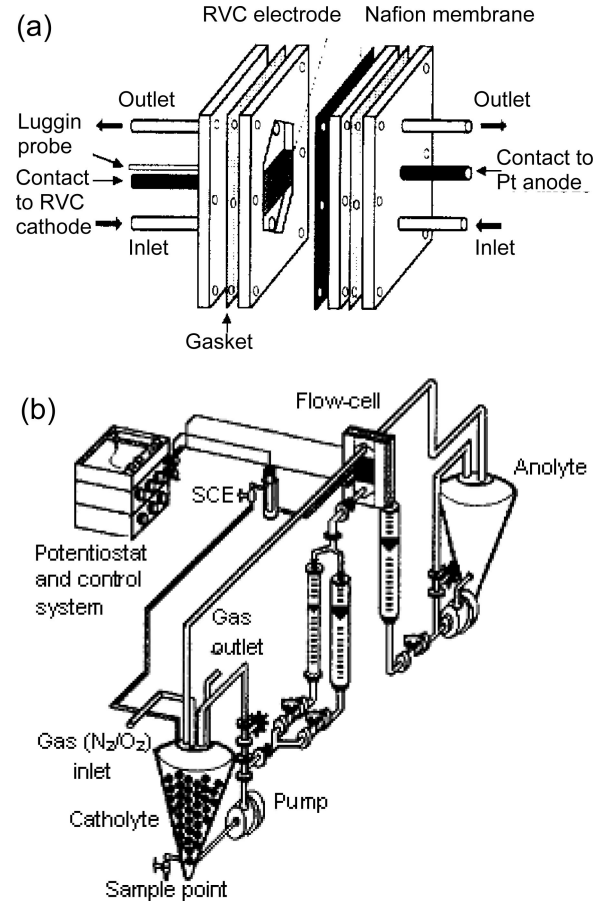

Figure 8. Sketches of (a) a divided three-electrode flow cell with an RVC cathode and (b) the experimental setup used for H_2O_2 electrogeneration in batch operation mode. Reprinted with permission from ref 112. Copyright 1998 Elsevier.

been utilized for H_2O_2 production. Figure 8 depicts the flow cell and flow circuit employed by Alvarez-Gallegos and Pletcher.[112] Maximum current efficiencies of 56−68% were obtained for 10 mM HCl and 10 mM H_2SO_4 (pH ≈ 2.0) as catholytes at E_{cat} values between −0.4 and −0.7 V/SCE, which slightly increased by adding NaCl and Na_2SO_4 as the background electrolyte, respectively. These authors also observed the fast disappearance of H_2O_2 in the presence of 1 mM Fe(II) owing to the action of Fenton's reaction 1. On the other hand, Figure 9a shows a scheme of the bench-scale divided flow reactor used by Badellino et al.,[146] which contains two parallel Ti plates coated with $(Ta_2O_5)_{0.6}(IrO_2)_{0.4}$ acting as anodes and a central stainless steel plate coated with RVC on both sides as the cathode, separated by N424 Nafion membranes, with a total area of 150 cm^2. Figure 9b and 9c illustrate that optimum conditions for the electrolysis of 3.5 L of 0.3 M K_2SO_4 at pH 10.0, room temperature, and a liquid flow rate of 300 L h^{-1} are reached operating at E_{cat} = −1.6 V/SCE and an O_2 flow rate of 6 L min^{-1}, when the solution remains saturated by this gas at 25 mg L^{-1}. In these optimized conditions, pseudo-zero-order kinetics can be observed for H_2O_2 accumulation, with an average apparent rate constant of 6.7×10^{-2} g L^{-1} m^{-2} s^{-1}. However, only a 65% current efficiency was attained due to simultaneous water formation from reaction 33 and H_2O_2 decomposition from reactions 36 and 37, respectively.

On the other hand, Liu et al.[147] reported a deeper study to clarify the effect of experimental key parameters affecting H_2O_2 accumulation during the treatment of 150 mL of 15

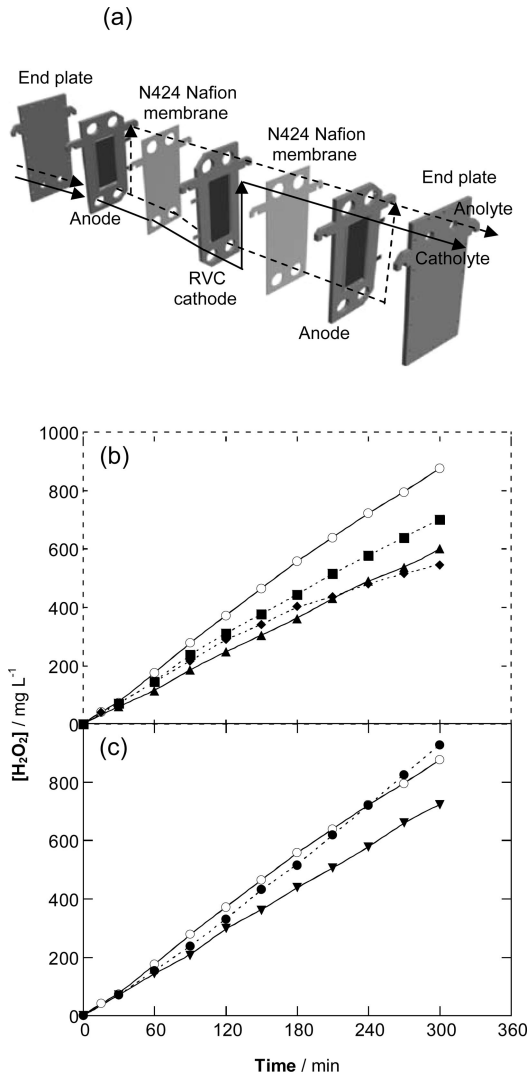

Figure 9. (a) Expanded view of a bench-scale divided flow reactor to electrogenerate H_2O_2 in batch operation mode. Two parallel Ti plates coated with $(Ta_2O_5)_{0.6}(IrO_2)_{0.4}$ acted as anodes, and a central stainless steel plate coated with RVC on both sides acted as cathode, separated by N424 Nafion membranes, with a total area of 150 cm^2. Electrolyses were performed with 3.5 L of 0.3 M K_2SO_4 at pH 10, room temperature, and liquid flow rate of 300 L h^{-1}. (b) H_2O_2 concentration profiles at E_{cat} of (○) −1.6, (■) −1.5, (▲) −1.4, and (◆) −1.7 V/SCE and O_2 flow rate of 6 L min^{-1}. (c) H_2O_2 concentration profiles at E_{cat} = −1.6 V/SCE and O_2 flow rate of (▼) 4, (○) 6, and (●) 8 L min^{-1}. Adapted with permission from ref 146. Copyright 2007 Springer.

mM phenol solutions in 0.01 M Na_2SO_4 of pH 2.5 as the catholyte of a three-electrode Pt/carbon cell equipped with a carbon rod cathode of 5 mm diameter and 80 mm length. They demonstrated that decreasing Fe^{2+} content from 1.0 to 0.05 mM, increasing j from 0.04 to 0.32 mA cm^{-2}, and growing O_2 concentration from 0.26 to 0.57 mM led to a proportionally greater H_2O_2 concentration in the medium for 90 min, exhibiting very good linear fittings to a pseudo-first-order kinetics. The removal of phenol was then accelerated as less H_2O_2 was accumulated because of the greater production of oxidant $^{\bullet}OH$ via Fenton's reaction 1.

3.4. Undivided Cells

The additional oxidation of cathodically electrogenerated H_2O_2 at the anode of three- and two-electrode undivided cells via reactions 38 and 39 causes a notable loss of accumulation

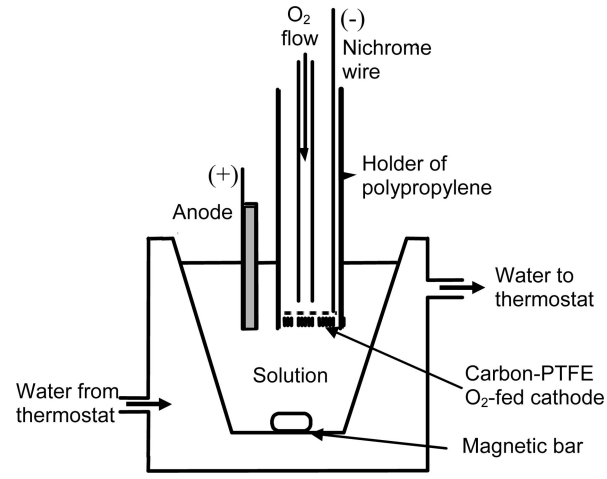

Figure 10. Scheme of a bench-scale open and stirred two-electrode undivided tank reactor utilized for H_2O_2 electrogeneration under EF and PEF conditions. The carbon-PTFE GDE cathode was directly fed with pure O_2. Adapted with permission from ref 110. Copyright 1995 The Electrochemical Society.

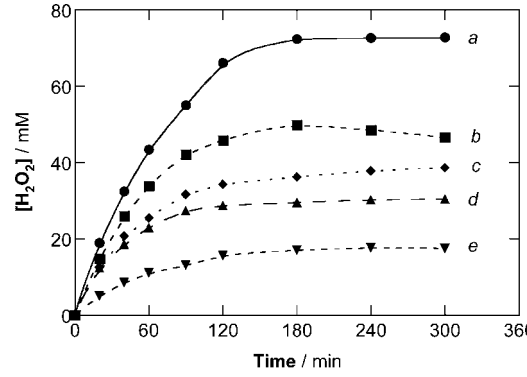

Figure 11. Evolution of the concentration of H_2O_2 accumulated during the electrolysis of 100 mL of 0.05 M Na_2SO_4 solutions of pH 3.0 at 25 °C using the Pt/O_2 cell of Figure 10: (*a*, *b*, and *e*) without Fe^{2+}; (*c* and *d*) with 1.0 mM Fe^{2+} (EF conditions), and (*d*) under a 6 W UVA irradiation (PEF conditions). Applied current: (*a*) 450, (*b*−*d*) 300, and (*e*) 100 mA. Reprinted with permission from ref 148. Copyright 2000 Elsevier.

of this compound compared with similar divided cells. This behavior can be easily deduced from comparative trials[139–142,144,145] presented in Tables 2 and 3. An advantage of using undivided cells is the lower cell voltage needed for electrolysis because the voltage penalty of the separator of divided cells is avoided. However, reactive oxygen species (ROS) and other weaker oxidants can also be produced at the anode, complicating the degradation process of POPs in EAOPs based on Fenton's reaction chemistry, as discussed below.

The characteristics of H_2O_2 accumulation in an undivided cell were first described by Brillas and co-workers,[113,148] who utilized the two-electrode cell schematized in Figure 10 containing a 10 cm^2 Pt sheet anode, a 3 cm^2 carbon-PTFE O_2-diffusion cathode, and 100 mL of a 0.05 M Na_2SO_4 solution of pH 3.0 vigorously stirred with a magnetic bar. As can be seen in Figure 11, the concentration of H_2O_2 accumulated in this Pt/O_2 cell operating under galvanostatic conditions at 25 °C always increases with time attaining a quasi-steady value after 2−3 h of electrolysis, just when its generation rate at the O_2-diffusion cathode from reaction 32 becomes equal to its decomposition rate at the Pt anode from reaction 37. The steady concentration increases linearly with rising current of 100 (curve *e*), 300 (curve *b*), and 450 mA

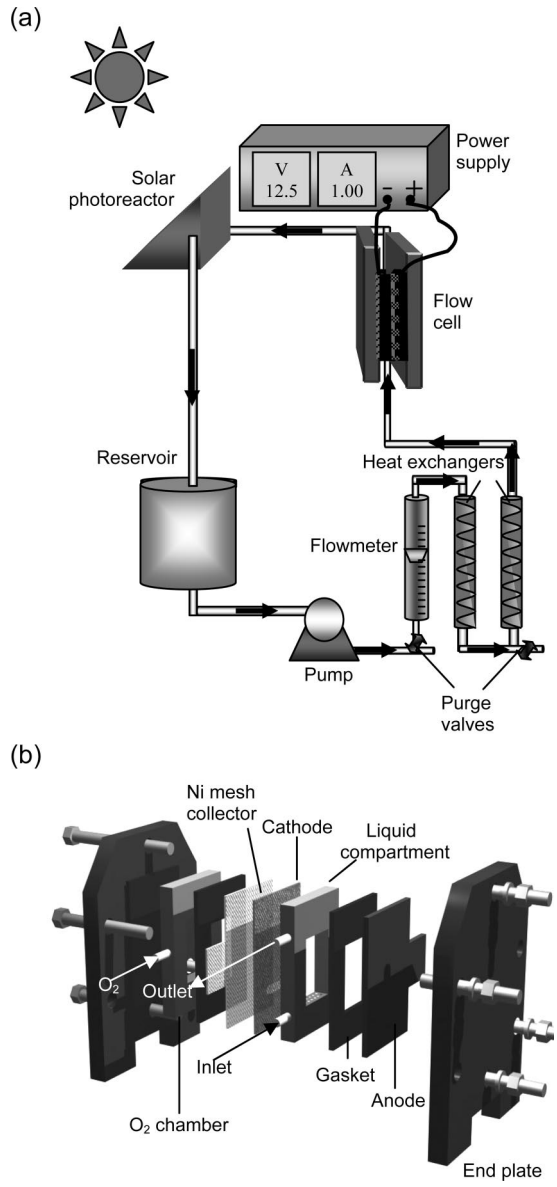

Figure 12. Sketches of (a) the batch recirculation flow plant and (b) the undivided filter-press cell with a 20 cm^2 BDD anode and a 20 cm^2 GDE cathode used for H_2O_2 electrogeneration and SPEF degradation of POPs. Reprinted with permission from ref 149. Copyright 2007 Elsevier.

(curve *a*) because of the concomitant acceleration of reactions 32 and 38. A slight decrease in the plateau corresponding to the steady-state concentration takes place in the presence of 1.0 mM Fe^{2+} (EF conditions) by H_2O_2 consumption from Fenton's reaction 1, as deduced by comparing curves *b* and *c* determined at 300 mA. The acceleration of H_2O_2 destruction under 6 W UVA illumination (PEF conditions) due to additional Fe^{2+} regeneration from the photoreduction reaction 27 is confirmed from the slight concentration decay observed by comparing curves *c* (without illumination) and *d* (with UVA light). Recently, this group has reported similar trends for H_2O_2 accumulation by electrolyzing 2.5 L of a 0.05 M Na_2SO_4 solution of pH 3.0 in the batch flow plant of Figure 12 containing a filter-press reactor with a 20 cm^2 boron-doped diamond (BDD) anode and a 20 cm^2 O_2-diffusion cathode operating at *I* between 1 and 3 A.[149] A high decay of H_2O_2 concentration was found when a solution of 100 mg L^{-1} of the herbicide mecoprop (MCPP) of pH 3.0 was treated by SPEF if the cell was coupled to a solar photoreactor of 600 mL irradiation volume (see Figure 12a) due to the acceleration of Fenton's reaction 1 by the fast consumption of $^{\bullet}OH$ to degrade the organic matter.

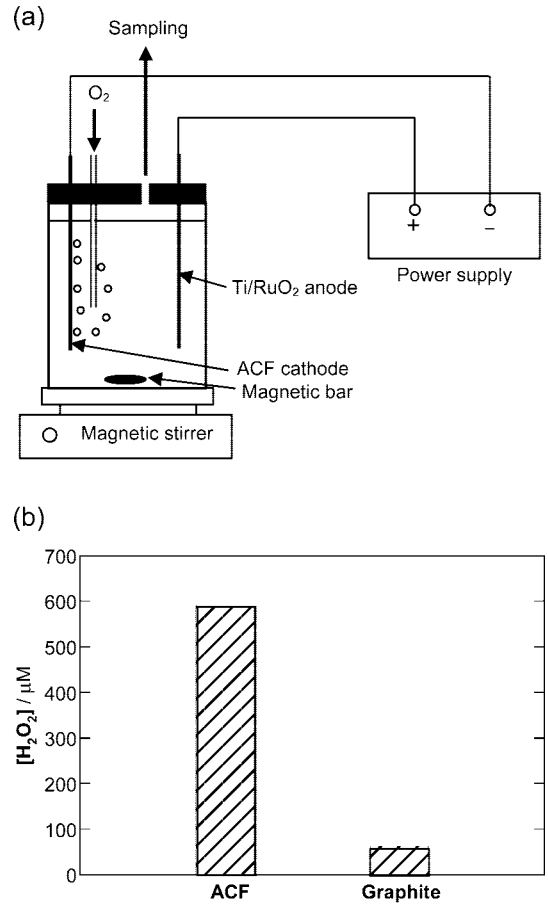

Figure 13. (a) Experimental setup of a bench-scale open and stirred two-electrode undivided tank reactor with a Ti/RuO_2 mesh anode and an activated carbon fiber (ACF) cathode, both of 20 cm^2 area, utilized for the EF treatment of POPs. (b) H_2O_2 concentration after 180 min of electrolysis of 500 mL of an O_2-saturated 0.05 M Na_2SO_4 solution of pH 3.0 at 0.36 A and room temperature using ACF or graphite as cathode. Adapted with permission from ref 122. Copyright 2005 Elsevier.

Several authors have also confirmed the profiles of H_2O_2 evolution of Figure 11 for three-electrode undivided cells (see Table 3).[115,139,140,145,150] For example, Badellino et al.[150] used a cylindrical tank reactor with a Pt anode and a rotating RVC cathode to electrolyze 130 mL of 0.3 M K_2SO_4 solution of pH 3.5 or 10.0 at 10 °C and constant E_{cat} in the range from −0.5 to −1.9 V/SCE. As in the case of a flow divided cell with the same cathode material (see Figure 9), optimum conditions were attained at $E_{cat} = -1.6$ V/SCE, although with a poor current efficiency of 7.8% for H_2O_2 accumulation at 240 min (see Table 3). H_2O_2 production decayed with increasing temperature as a result of the lower O_2 solubility in the aqueous solution, without significant pH effect.

Other studies have compared the ability of several cathodes to electrogenerate H_2O_2. Thus, Wang et al.[122] used the two-electrode tank reactor of Figure 13a with a 20 cm^2 Ti/RuO_2 mesh anode to electrolyze 500 mL of an O_2-saturated 0.05 M Na_2SO_4 solution of pH 3.0 at 0.36 A. Figure 13b shows that 600 and 52 μM H_2O_2 was accumulated in 180 min with 20 cm^2 ACF and graphite cathodes, respectively, meaning that the former is a better material because of its larger specific area and the greater number of mesopores helping O_2 diffusion. Özcan et al.[114] recently reported that a carbon

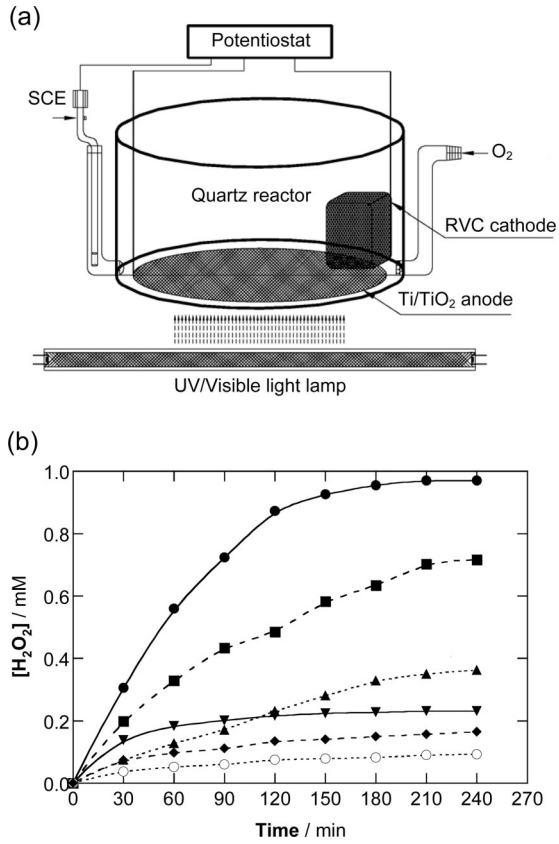

Figure 14. (a) Experimental setup of the three-electrode undivided quartz cell with 5 cm^2 electrodes utilized for H_2O_2 electrogeneration in 30 mL of an O_2-saturated 0.01 M Na_2SO_4 solution of pH 6.2 at room temperature. The Ti/TiO_2 anode was illuminated with an 8 W UVA lamp. (b) H_2O_2 concentration profiles obtained for a (●, ■, ▲) Pt/RVC and (▼, ◆, ○) TiO_2/RVC cell at (●, ▼) 1.5, (■, ◆) 1.0, and (▲, ○) 0.5 mA. Reprinted with permission from ref 151. Copyright 2006 Elsevier.

sponge cathode leads to the accumulation of a nearly three times higher concentration of H_2O_2 than a carbon-felt cathode, whose structure is quite similar to that of ACF. They also found that $I > 100$ mA was detrimental on H_2O_2 accumulation because reduction of O_2 to H_2O from reaction 33 became preferential.

Finally, novel EAOPs have been developed in recent years based on the photoelectrochemical ability of the semiconductor TiO_2. Xie and Li[151] proposed the simultaneous formation and destruction of H_2O_2 in an O_2-saturated 0.01 M Na_2SO_4 solution using the three-electrode undivided TiO_2−Ti/RVC cell of Figure 14a. In this system, H_2O_2 is electrogenerated at the RVC cathode and destroyed at the anode surface due to (i) its direct oxidation from reaction 38 and (ii) its conversion into •OH when the semiconductor anode is illuminated with a UVA light of $\lambda_{max} = 365$ nm. This energy source promotes one electron from the valence to the conduction band (e^-_{CB}) with the production of a hole (h^+) from reaction 41, and afterward a certain amount of H_2O_2 formed at the cathode can be directly transformed into •OH from reaction 42:

$$TiO_2 + h\nu \rightarrow h^+ + e^-_{CB} \quad (41)$$

$$e^-_{CB} + H_2O_2 \rightarrow {}^{\bullet}OH + OH^- \quad (42)$$

Figure 14b illustrates the existence of a much lower accumulation of H_2O_2 in the TiO_2−Ti/RVC cell in comparison with a Pt/RVC cell (without UVA illumination) for all currents tested, which is explained by its enhanced destruction in the photoelectrochemical system by reaction 42.

4. Electro-Fenton (EF) Process

EAOPs based on Fenton's reaction chemistry are emerging technologies for water remediation. Over the past decade, they have experienced a significant development showing great effectiveness for the decontamination of wastewater polluted with toxic and persistent pesticides, organic synthetic dyes, pharmaceuticals and personal care products, and a great deal of industrial pollutants. The EF process was the first method proposed among this kind of EAOPs and laid the foundation for a large variety of related processes, as summarized in Figure 1. The origins, fundamentals, and experimental characteristics of EF are thoroughly detailed in this section, whereas the peculiarities of the other related methods will be presented in subsequent sections.

The EF technology is based on the continuous electrogeneration of H_2O_2 at a suitable cathode fed with O_2 or air (see section 3), along with the addition of an iron catalyst to the treated solution to produce oxidant •OH at the bulk via Fenton's reaction 1. In an undivided cell, the process is complicated by the simultaneous destruction of pollutants with ROS, mainly oxidant •OH formed at the anode, as discussed below. The major advantages of this indirect electro-oxidation method compared with the chemical Fenton process are as follows:[33,34,121,152] (i) the on-site production of H_2O_2 that avoids the risks related to its transport, storage, and handling, (ii) the possibility of controlling degradation kinetics to allow mechanistic studies, (iii) the higher degradation rate of organic pollutants because of the continuous regeneration of Fe^{2+} at the cathode, which also minimizes sludge production, and (iv) the feasibility of overall mineralization at a relatively low cost if the operation parameters are optimized.

In EF and most related technologies, soluble Fe^{3+} can be cathodically reduced to Fe^{2+} by reaction 43, which is known as electrochemical catalysis, with $E° = 0.77$ V/SHE:[153]

$$Fe^{3+} + e^- \rightarrow Fe^{2+} \quad (43)$$

The fast regeneration of Fe^{2+} by reaction 43 accelerates the production of •OH from Fenton's reaction 1. This enhances the decontamination of organic solutions achieved with these EAOPs, which possess much greater degradation ability than similar AO and Fenton processes used separately. This behavior is illustrated in Figure 15 for the Fered−Fenton method, in which both H_2O_2 and Fe^{2+} are simultaneously added to the electrolytic cell.[154] As can be seen, AO of a landfill leachate solution of pH 3.0 with two Ti/RuO_2−IrO_2 electrodes could only remove 10% of its initial COD. In contrast, using the Fenton's reagent increases COD reduction to 34%, while the combined Fered−Fenton process has much higher oxidation power, yielding 81% COD decay under similar conditions as a result of the efficient cathodic regeneration of Fe^{2+}.

4.1. Origins

The original papers dealing with the in-situ formation of Fenton's reagent by simultaneous cathodic reduction of O_2 from reaction 32 and Fe^{3+} ions from reaction 43 were devoted to the one-step hydroxylation of some aromatics for organic electrosynthesis. However, low yields and difficulty

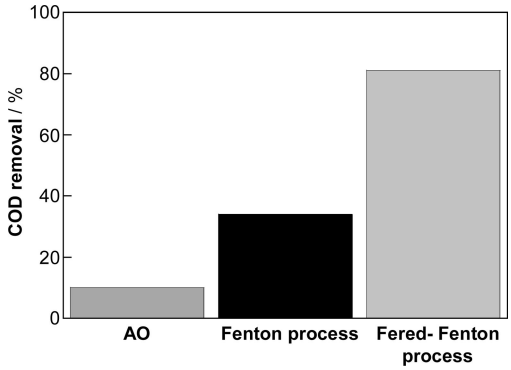

Figure 15. Percentage of COD removal obtained after 75 min of treatment of 200 mL of landfill leachate solutions ($COD_0 = 500$ mg L^{-1}) of pH 3 in a tank cell. Method: AO at 2A; Fenton process with 0.34 M H_2O_2 and 28 mM Fe^{2+}; Fered−Fenton process at 2 A with 0.34 M H_2O_2 and 28 mM Fe^{2+}. In the electrochemical treatments, the anode and cathode were Ti/RuO_2-IrO_2 of 5 cm × 11.9 cm in dimension. Adapted with permission from ref 154. Copyright 2006 Elsevier.

in stopping the reaction were common drawbacks owing to the nonselectivity of •OH. The pioneering work of Tomat and Vecchi[116] reported the transformation of benzene into phenol in H_2SO_4, with a current yield up to 60%, by using a Hg cathode at $E_{cat} = -0.35$ V/SCE. Tomat and Rigo further considered systematically the hydroxylation of toluene,[155,156] some polymethylated benzenes,[157] cyclohexane,[158] and aliphatic hydrocarbons by applying similar conditions with Fe(II) as well as with V(IV), V(III), or Cu(I) to catalyze Fenton-like reactions.[159] Fleszar and Sobkowiak[160] extended the generation of Fenton's reagent to Pb, Cu, and Ag cathodes to hydroxylate benzene and phenol in 0.1 M H_2SO_4. The study of Tzedakis et al.[117] on the oxidation of benzene in batch and continuous mode with a Hg cathode demonstrated that a higher conversion degree with yields of 70% is obtained if the phenol formed is continuously removed from the electrochemical cell during electrolysis. More recently, Oturan and co-workers reported the polyhydroxylation of salicylic[161] and benzoic[162] acids, as well as of some chlorophenoxy herbicides and other aromatic pesticides,[152] at pH 3.0 by •OH generated on a mercury cathode at $E_{cat} = -0.5$ V/SCE with the addition of Fe^{3+}.

In view of the toxicity of Hg and other metals used as cathodes, efforts have been made toward the H_2O_2 electrogeneration with environmentally friendly electrodes made of carbonaceous materials (see section 3.2). The effectiveness of these kinds of materials to oxidize organics was initially tested for electrosynthesis purposes. For example, Wellmann and Steckhan[163,164] described the direct hydroxylation of aromatic compounds such as benzene, chlorobenzene, fluorobenzene, and benzonitrile to the corresponding phenols, with yields between 20% and 80% using a graphite cathode. Similarly, Matsue et al.[165] carried out the hydroxylation of some alkylbenzenes in diluted aqueous solutions. Savinova et al.[166] reported an unexpected high selectivity for the partial oxidation of ethane to acetaldehyde and ethanol in an EF system with a carbon-PTFE GDE cathode and Fe^{2+} and/or Cu^{2+} as catalysts, which was ascribed to the efficient separation of products and •OH on the three-phase (electrode, electrolyte, and gas) boundary of the GDE. Hsiao and Nobe[167,168] proposed a batch-packed bed flow reactor for the hydroxylation of phenol and chlorobenzene at pH 3.8 without O_2 sparging, where the oxygen evolved at the Pt anode and Fe^{3+} introduced to the solution were reduced downstream at the RVC cathode to H_2O_2 and Fe^{2+}, respectively. Unfortunately, the process rate in this system was not sufficiently high for practical purposes and was probably limited by its low H_2O_2 production rate. Oturan's group also recently reported the production of monohydroxylated metabolites of the drug riluzole[120] and mono-, di-, and trihydroxylated derivatives of chlorophenoxy pesticides[153] by EF with a carbon-felt cathode at room temperature and pH 2.0.

In 1986, Sudoh et al.[118] were the first to apply the electrogenerated Fenton's reagent to wastewater treatment, considering the degradation of O_2-saturated phenol solutions with Fe^{2+} as the catalyst in the cathodic compartment of the H-type Pt/graphite cell of Figure 6 at $E_{cat} = -0.6$ V vs Ag/AgCl/KCl (satd). From this study, an increasing number of papers have been published dealing with the destruction of toxic and refractory organic pollutants in water by means of EF and related processes, being remarkable the extensive work of the groups of Brillas and Oturan using carbon-PTFE O_2-diffusion and carbon-felt cathodes, respectively. Some patents on the use of the EF method for water remediation remain available.[169,170]

4.2. Fundamentals of EF for Water Remediation

4.2.1. Cell Configuration

The EF technology utilizes three- and two-electrode divided and undivided electrolytic cells in which H_2O_2 is continuously electrogenerated at the cathode fed with O_2 or air from reaction 32. Cathode materials such as graphite, RVC, ACF, carbon felt, and GDEs are most typically employed (see section 3.2). Anode materials such as graphite, Pt, metal oxides, and BDD are usually preferred. Some divided cells used for the EF treatment of organics are given in Figures 6, 7a, 7b, and 8. Examples of undivided cells are depicted in Figures 10, 13a, and 14a. Figure 16a shows the typical undivided two-electrode cell with a high surface carbon-felt cathode used by Oturan's group[171] in its EF studies. Figure 16b presents a recirculation flow plant with an undivided two-electrode filter-press cell with a GDE cathode utilized by Brillas' group for aniline degradation.[172] Figure 17 illustrates the most usual tank reactors used for water remediation by EF, along with the main reactions taking place in the electrodes. As can be seen, Fe^{2+} is rapidly regenerated from the cathodic reduction of Fe^{3+}, except for GDEs where this reaction is very slow because O_2 reduction is predominant.[173] In addition, •OH and other ROS formed at the anode can also act as oxidants in undivided cells. The fundamentals and characteristics of the electrogeneration of Fe^{2+} and anodically formed •OH are analyzed below.

4.2.2. Cathodic Fe^{2+} Regeneration

The EF treatment of organic pollutants can be visualized in the catalytic cycle of Figure 18.[121] The simultaneous reduction of O_2 from reaction 32 and Fe^{3+} from reaction 43 allows the Fenton's reaction 1 between electrogenerated H_2O_2 and Fe^{2+} with the production of •OH and Fe^{3+}. The oxidant radical can either dehydrogenate unsaturated compounds (RH) or hydroxylate aromatic pollutants (Ar) until their overall conversion into CO_2.

This cycle indicates that apart from the knowledge about the cathodic H_2O_2 generation described in section 3, it is

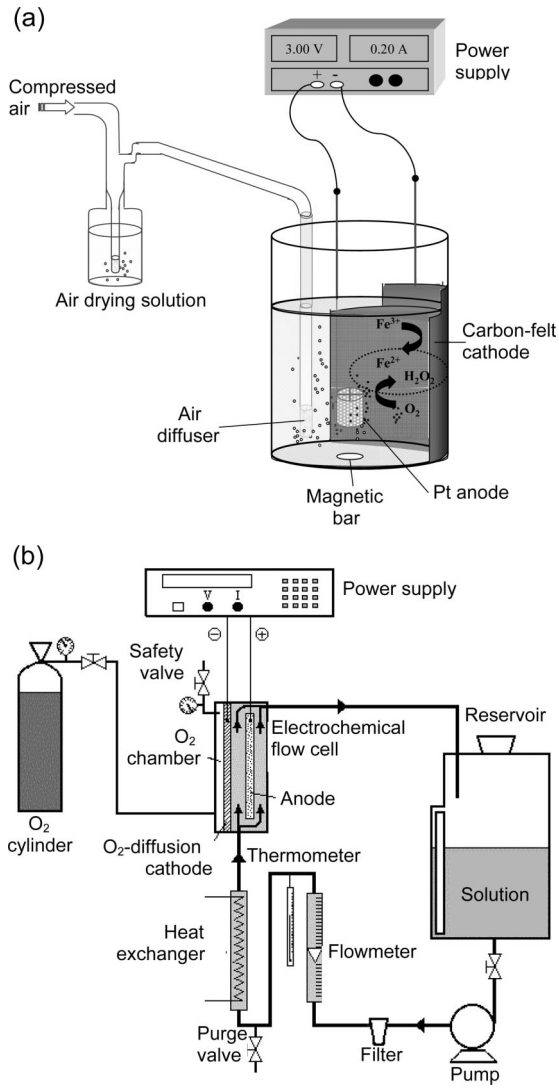

Figure 16. (a) Sketch of a bench-scale open and stirred two-electrode undivided tank reactor with a 60 cm^2 carbon-felt cathode fed with compressed air utilized for the EF treatment of organic solutions. Reprinted with permission from ref 171. Copyright 2008 Elsevier. (b) Scheme of a batch recirculation flow plant with an undivided filter-press electrochemical reactor containing a 100 cm^2 carbon-PTFE GDE fed with pure O_2 used for the EF and PC degradation of 30 L of aniline solutions in 0.05 M Na_2SO_4 at pH 3.0 and 40 °C under galvanostatic conditions. Reprinted with permission from ref 172. Copyright 2002 Elsevier.

also needed to ascertain the catalytic behavior of the Fe^{3+}/Fe^{2+} couple considering the cathodic regeneration of Fe^{2+}, which depends on factors such as electrode potential and area, pH, temperature, and catalyst content, as clarified by Qiang et al.[174] These authors established the optimal conditions to minimize the production of iron sludge in a divided graphite/graphite cell by electrogenerating Fe^{2+} in 0.05 M $NaClO_4$ solutions at a constant potential or constant current density. They found an optimum $E_{cat} = -0.1$ V/SCE for 500 mg L^{-1} Fe^{3+} in terms of current efficiency corresponding to $j = 43$ mA cm^{-2}, a linear increase in j with initial Fe^{3+} concentration, and an acceleration of Fe^{2+} regeneration with rising cathode surface area and temperature. Regeneration degrees between 75% and 98% were obtained in the pH range 1.0−2.5, rapidly decreasing at higher pH values due to Fe^{3+} hydrolysis (see Figure 2). Fe^{2+} could be produced only up to $E_{cat} = -0.8$ V/SCE since higher potentials favor H_2 evolution from reaction 44 with $E° = -0.83$ V/SHE:

$$2H_2O + 2e^- \rightarrow H_{2(g)} + 2OH^- \quad (44)$$

On the other hand, the selection of the iron source strongly relies upon the nature of the cathode. As an example, Figure 19 illustrates the evolution of Fe^{3+} and Fe^{2+} concentrations by electrolyzing solutions of Fe^{3+} for 60 min in different undivided cells.[173] Results in Figure 19a for a GDE cathode show that the starting 4.0 mM Fe^{3+} remains practically unchanged using a BDD or Pt anode, as expected if the low quantity of Fe^{2+} produced at the GDE from reaction 43 is rapidly transformed into Fe^{3+} from Fenton's reaction 1. In contrast, Figure 19b depicts that 0.2 mM Fe^{3+} is completely reduced to Fe^{2+} at a three-dimensional carbon-felt cathode, although soluble Fe^{2+} is only stable with Pt and slowly precipitates as $Fe(OH)_3$ over the cathode with BDD, because the higher cell voltage applied in the latter case increases the rate of reaction 44, producing greater amounts of OH^- near the cathode surface that enhance the iron precipitation. In these cells, the slow oxidation of Fe^{2+} at the anode is also feasible:

$$Fe^{2+} \rightarrow Fe^{3+} + e^- \quad (45)$$

These findings prove that Fe^{2+} is the preferred catalyst for GDE electrodes to accelerate the production of $^{\bullet}OH$ at the early stages of the EF process, because this ion is progressively removed from the solution. Conversely, both Fe^{3+} and Fe^{2+} ions can be utilized as alternative iron sources with three-dimensional carbonaceous materials because of the fast regeneration of Fe^{2+} that can then react largely with electrogenerated H_2O_2 to continuously yield high amounts of $^{\bullet}OH$. This possibility has been recently confirmed by Oturan et al.,[171] who found the same decay rate for malachite green with either 0.2 mM Fe^{2+} or 0.2 mM Fe^{3+} as the catalyst using an undivided Pt/carbon felt cell at 60 mA.

4.2.3. Anodic Generation of Heterogeneous Hydroxyl Radical

In an undivided cell, organics are destroyed by $^{\bullet}OH$ produced homogeneously from Fenton's reaction 1 but also by the action of heterogeneously formed hydroxyl radical ($M(^{\bullet}OH)$), which is produced at a high O_2-overvoltage anode (M) from water oxidation by reaction 46:[175–177]

$$M + H_2O \rightarrow M(^{\bullet}OH) + H^+ + e^- \quad (46)$$

The whole process is called "paired electrocatalysis" because the oxidizing agents can be formed from both the anode and the cathode reactions. It requires high oxidation power anodes, i.e., anodes with high O_2 overpotential to minimize the extent of O_2 evolution from reaction 47:

$$2M(^{\bullet}OH) \rightarrow 2M + O_2 + 2H^+ + 2e^- \quad (47)$$

The oxidative action of $M(^{\bullet}OH)$ is rather ineffective for classical electrodes such as Pt, SnO_2, PbO_2, IrO_2, or RuO_2, being much more efficient when BDD is used as the anode. It has been found that operating at a high current, within the water discharge region, reactive $BDD(^{\bullet}OH)$ is produced in much higher quantities than $Pt(^{\bullet}OH)$ and can completely mineralize aromatics and unsaturated compounds such as carboxylic acids.[176] Furthermore, the low adsorption ability of $^{\bullet}OH$ on BDD favors its dimerization to H_2O_2 by reaction 48, whereas the high oxidation power of this anode facilitates

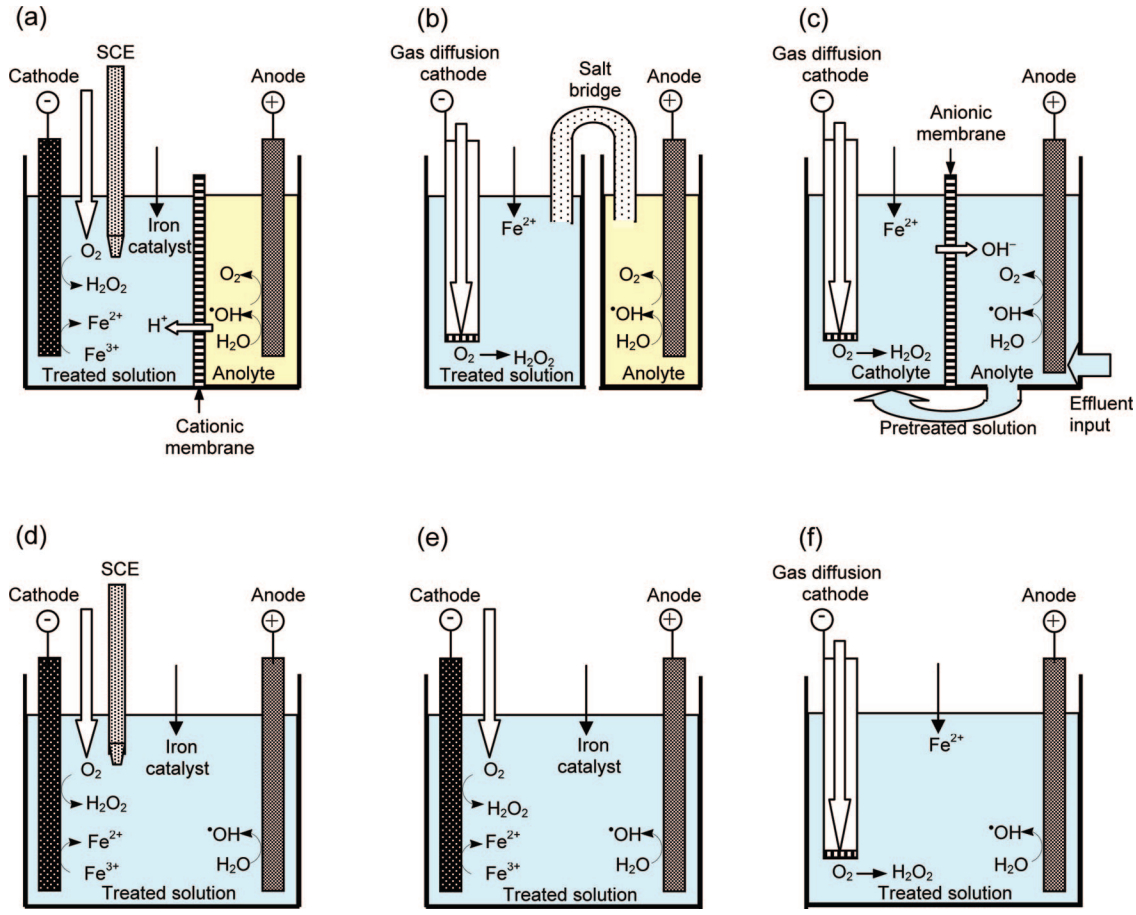

Figure 17. Schematic representation of bench-scale (a−c) divided and (d−f) undivided cells used in EF treatments of organics from wastewaters. The main reactions at the electrodes are given. H_2O_2 is electrogenerated at the cathode from O_2 or air feeding. An iron catalyst (Fe^{2+} or Fe^{3+}) or strictly Fe^{2+} is added to the solution. (a and d) Saturated calomel electrode (SCE) is the reference electrode. (b) Cationic membrane may be used instead of the salt bridge. (c) Solution pretreated in the anolyte is further degraded in the catholyte.

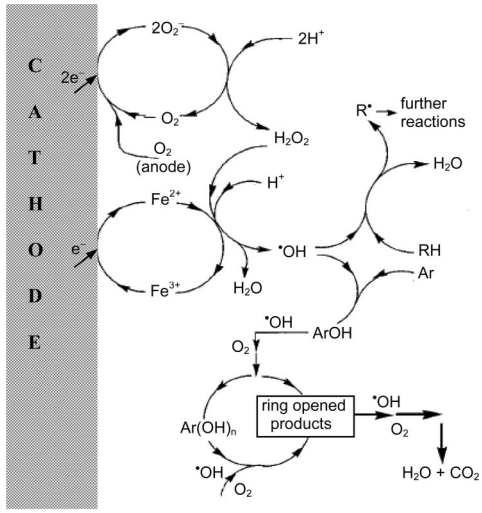

Figure 18. Schematic representation of the main reactions involved in the EF process in a divided cell. RH is an unsaturated compound that undergoes dehydrogenation, while Ar is an aromatic pollutant that is hydroxylated. Adapted with permission from ref 121. Copyright 2000 Springer.

the generation of ozone from water discharge by reaction 49 with $E° = 1.51$ V/SHE and other weaker oxidizing agents such as $S_2O_8^{2-}$ ion from oxidation of SO_4^{2-} and HSO_4^- ions from reactions 50 and 51, respectively, when sulfate medium is employed:[175,178]

$$2BDD(^{\bullet}OH) \rightarrow 2BDD + H_2O_2 \quad (48)$$

$$3H_2O \rightarrow O_{3(g)} + 6H^+ + 6e^- \quad (49)$$

$$2SO_4^{2-} \rightarrow S_2O_8^{2-} + 2e^- \quad (50)$$

$$2HSO_4^- \rightarrow S_2O_8^{2-} + 2H^+ + 2e^- \quad (51)$$

In addition, when BDD is used with chlorinated pollutants or chloride medium, the oxidant Cl_2 is also present in the bulk coming from the anodic oxidation of chloride ion.[179]

Although the EF degradation of organics in an undivided cell is mainly ascribed to their oxidation with $^{\bullet}OH$ in the bulk and M($^{\bullet}OH$) at the anode surface, parallel destruction with weaker oxidizing species such as ROS ($HO_2^{\bullet}$, H_2O_2, O_3), ferrate ion and other hypervalent iron species, $S_2O_8^{2-}$ ion, Cl_2, etc., is also possible. The effect of oxidizing species different from $^{\bullet}OH$ produced from Fenton's reaction 1 is not significant when a carbon-felt cathode is used because this reaction has a prevailing role due to the high Fe^{2+} accumulation in the medium. In contrast, the influence of the anode is very notable when the cathode is a GDE because of its poor Fe^{2+} regeneration ability. This can be deduced from Figure 20,[180] which exemplifies the comparative TOC decay against the consumed specific charge for four treatments of

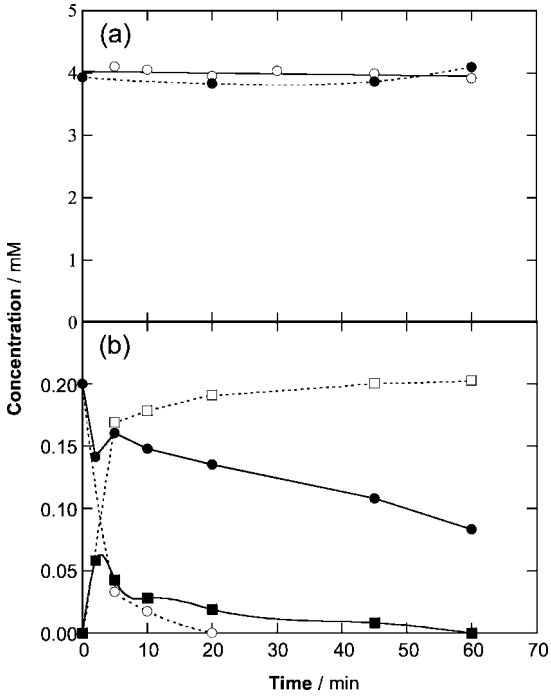

Figure 19. Time course of Fe^{3+} and Fe^{2+} concentrations during the electrolysis of 200 mL of 0.05 M Na_2SO_4 solutions at pH 3.0, 300 mA, and room temperature. Plots: (a) 4.0 mM Fe^{3+} and a 3 cm^2 O_2-diffusion cathode in the cell of Figure 10 and (b) 0.20 mM Fe^{3+}, air-saturated solutions and a 60 cm^2 carbon-felt cathode in the cell of Figure 16a. Species: (○) Fe^{3+} and (□) Fe^{2+} using a 3 cm^2 Pt anode; (●) Fe^{3+} and (■) Fe^{2+} using a 3 cm^2 BDD anode. Adapted with permission from ref 173. Copyright 2007 Elsevier.

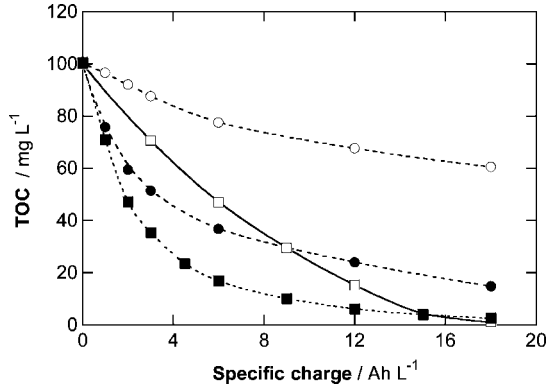

Figure 20. TOC abatement with specific charge for the degradation of 100 mL of 230 mg L^{-1} 2,4-dichlorophenoxyacetic acid (2,4-D) solutions of pH 3.0 using the cell of Figure 10 at 300 mA and 35 °C. (○) Anodic oxidation with H_2O_2 electrogeneration (AO-H_2O_2) with a 10 cm^2 Pt anode and a 3 cm^2 GDE cathode; (●) EF with a 10 cm^2 Pt anode, a 3 cm^2 GDE cathode, and 1 mM Fe^{2+}; (□) anodic oxidation (AO) with a 3 cm^2 BDD anode and a 3 cm^2 graphite cathode; (■) EF with a 3 cm^2 BDD anode, a 3 cm^2 GDE cathode, and 1 mM Fe^{2+}. Reprinted with permission from ref 180. Copyright 2004 Elsevier.

230 mg L^{-1} of the herbicide 2,4-dichlorophenoxyacetic acid (2,4-D) at 300 mA. A much higher oxidation power for AO with a BDD/graphite cell than for AO-H_2O_2 with a Pt/O_2 cell can be observed. Similarly, the EF process with a GDE cathode is much more potent with BDD than with Pt, indicating that the removal of organics with reactive BDD(•OH) is an important degradative pathway which aids fast and efficient mineralization.

The combination of both anode and cathode reactions for water treatment has also been proposed for divided cells.

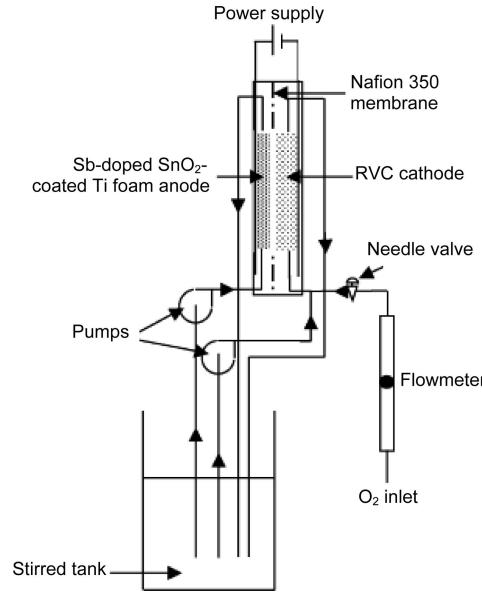

Figure 21. Hydraulic circuit and divided electrochemical flow cell equipped with an Sb-doped SnO_2-coated titanium foam anode and an RVC cathode fed with pure O_2 utilized for the degradation of 300 mL of phenol solutions in 0.25 M Na_2SO_4 by coupling AO and EF. Reprinted with permission from ref 181. Copyright 2002 Elsevier.

For example, Fockedey and Van Lierde[181] utilized the hydraulic circuit with the divided flow reactor of Figure 21 for the treatment of phenol by coupling AO and EF oxidations in the anolyte and catholyte, respectively. This procedure allowed a significant electric charge reduction of 6.3 kAh during the degradation of 1 kg phenol at 10 mA cm^{-2}, with an energy consumption of 5 kWh (kg COD)$^{-1}$. Recently, Montanaro et al.[182] considered the divided BDD/O_2 cell with an anionic membrane of Figure 17c to reduce the phosphorus content of an effluent from the manufacture of phosphorus-based flame retardants. The method consisted in the AO treatment of 100 mL of a fresh solution in the anolyte, followed by EF oxidation of this pretreated solution in the catholyte. The anionic membrane allows the passage of OH^- ions from the cathodic to the anodic compartment to maintain the catholyte pH close to 1.5, thereby avoiding iron precipitation. A sequential running saved charge and time by using both anode and cathode performances in parallel, only requiring 240 min at 10 mA cm^{-2} to decrease the phosphorus content below the limits needed.

4.3. Experimental Features

This section is devoted to analyzing the experimental characteristics of the EF process for the removal of POPs from wastewater. Current efficiency and energetic parameters are defined, and the influence of key operation parameters on the oxidation power of this method is detailed. Modeling of the reaction of POPs with homogeneously formed •OH, as well as a design methodology developed for EF optimization, are further described. Finally, the use of metallic ions rather than iron ions as catalysts in this technology is discussed.

4.3.1. Current Efficiency and Energetic Parameters

The decontamination process of organic pollutants in EF and related technologies is monitored from the abatement of the COD and/or TOC values of the treated solution. From

these data, the percentages of COD and TOC decays are calculated by eqs 52 and 53, respectively

$$\text{COD decay}(\%) = \frac{(\Delta\text{COD})_t}{\text{COD}_0} \times 100 \quad (52)$$

$$\text{TOC decay}(\%) = \frac{(\Delta\text{TOC})_t}{\text{TOC}_0} \times 100 \quad (53)$$

where $(\triangle\text{COD})_t$ and $(\triangle\text{TOC})_t$ are the corresponding removals in COD (mg O_2 L^{-1}) and TOC (mg carbon L^{-1}) at electrolysis time t and COD_0 and TOC_0 are their initial values before treatment. COD data also allow calculating efficiency parameters for assessing the efficiency of electrochemical processes in terms of the consumed electrical charge. The instantaneous current efficiency at a given electrolysis time in batch operation mode at a constant current is defined by eq 54[176]

$$\text{ICE}(\%) = \frac{(\text{COD}_t - \text{COD}_{t+\Delta t})FV_s}{8I\Delta t} \times 100 \quad (54)$$

where COD_t and $\text{COD}_{t+\Delta t}$ are the COD values (g O_2 L^{-1}) at times t and $t + \triangle t$ (s), F is the Faraday constant (96 487 C mol^{-1}), V_s is the solution volume (L), the constant 8 is the oxygen equivalent mass (g eq^{-1}), and I is the applied current (A). Similarly, the average current efficiency at time t is given by eq 55

$$\text{CE}(\%) = \frac{(\Delta\text{COD})_t FV_s}{8It} \times 100 \quad (55)$$

where $(\triangle\text{COD})_t$ is the experimental COD decay (g O_2 L^{-1}) at time t (s). When TOC data are determined for a single pollutant, the mineralization current efficiency for electrolyzed solutions at a given time t (h) is calculated from eq 56[148,149]

$$\text{MCE}(\%) = \frac{(\Delta\text{TOC})_t nFV_s}{4.32 \times 10^7 mIt} \times 100 \quad (56)$$

where $\Delta(\text{TOC})_t$ is the TOC decay (mg carbon L^{-1}), n is the number of electrons exchanged in the mineralization process of the organic compound, m is the number of carbon atoms of the molecule under study, and 4.32×10^7 is the conversion factor for units homogenization (= 3600 s h^{-1} × 12 000 mg carbon mol^{-1}).

Energy-related parameters are essential figures of merit for comparing the viability of EF and related methods between them and against other electrochemical technologies.[183] Operating at constant I, energy consumption per unit volume, unit COD mass, and unit TOC mass are obtained from eqs 57, 58, and 59, respectively[149]

$$\text{energy consumption (kWh m}^{-3}) = \frac{E_{\text{cell}}It}{V_s} \quad (57)$$

$$\text{energy consumption (kWh(g COD)}^{-1}) = \frac{E_{\text{cell}}It}{(\Delta\text{COD})_t V_s} \quad (58)$$

$$\text{energy consumption (kWh(g TOC)}^{-1}) = \frac{E_{\text{cell}}It}{(\Delta\text{TOC})_t V_s} \quad (59)$$

where E_{cell} is the average cell voltage (V), t is the electrolysis time (h), and $(\triangle\text{COD})_t$ and $(\triangle\text{TOC})_t$ are the corresponding decays in COD (mg O_2 L^{-1}) and TOC (mg carbon L^{-1}).

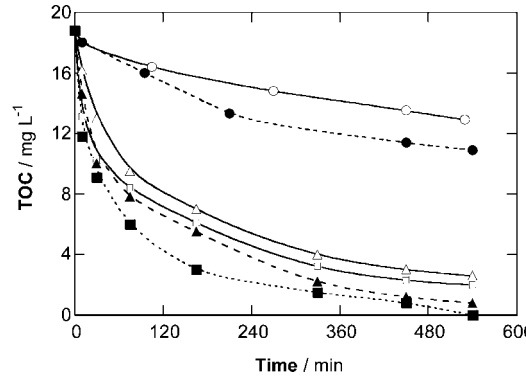

Figure 22. Effect of pH and background electrolyte on TOC removal of 150 mL of aqueous solutions of 0.2 mM of the pesticide methyl parathion with 0.1 mM Fe^{3+} by EF treatment in the undivided Pt/carbon felt cell of Figure 16a at 150 mA and room temperature. Initial pH: (○) 1.0, (□) 3.0, and (△) 4.0 in H_2SO_4 medium and (●) 1.0, (■) 3.0, and (▲) 4.0 in $HClO_4$ medium. Reprinted with permission from ref 186. Copyright 2007 Elsevier.

4.3.2. Influence of Operation Parameters

The degradation rate of organic wastewater in the EF process depends on operation parameters such as O_2 feeding, stirring rate or liquid flow rate, temperature, solution pH, electrolyte composition, applied potential or current, and iron catalyst and initial pollutant concentration. Most of these parameters are optimized in the cell used for achieving the best current efficiency and lowest energy cost. High flow rates of pure O_2 or air are normally used either to feed the GDE cathode or maintain the solution saturated with O_2 to obtain the maximum H_2O_2 production rate from reaction 32. Similarly, the solution stirring rate in tank reactors or liquid flow rate in flow cells is chosen at sufficiently high values to obtain fast homogenization of treated solutions and enhance the mass transfer of reactants toward the electrodes to yield the maximum rates of electrode reactions. Ambient temperatures are normally employed. A rise in temperature to 35−40 °C increases the mineralization rate,[184] but greater temperatures are detrimental because of the strong acceleration of chemical H_2O_2 decomposition from reaction 37.[108]

The solution pH is an important control parameter for maintaining the effectiveness of the EF process. Several authors[184–186] have reported its maximum efficiency in undivided cells with carbon-felt and GDE cathodes at pH 3.0, which is close to pH 2.8 where the maximum production of $^{\bullet}OH$ is expected from Fenton's reaction 1.[71] The nature of the inorganic acid used to adjust the solution pH can also play a significant role in the oxidation power of this technique. As an example, Figure 22 illustrates the effect of pH and the anion of the electrolyte (sulfate or perchlorate) on the degradation rate of the organophosphorus insecticide methyl parathion with 0.1 mM Fe^{3+} in the undivided Pt/carbon felt cell of Figure 16a at 150 mA.[186] A quicker TOC removal can be observed at pH 3.0 in comparison with pH 4.0 and 1.0 in both media, while perchlorate solutions are always more rapidly decontaminated. After 9 h of electrolysis, the solution TOC is reduced by approximately 100% at pH 3.0 in perchlorate medium. The mineralization rate is slightly slower at pH 4.0, where part of Fe^{3+} precipitates as

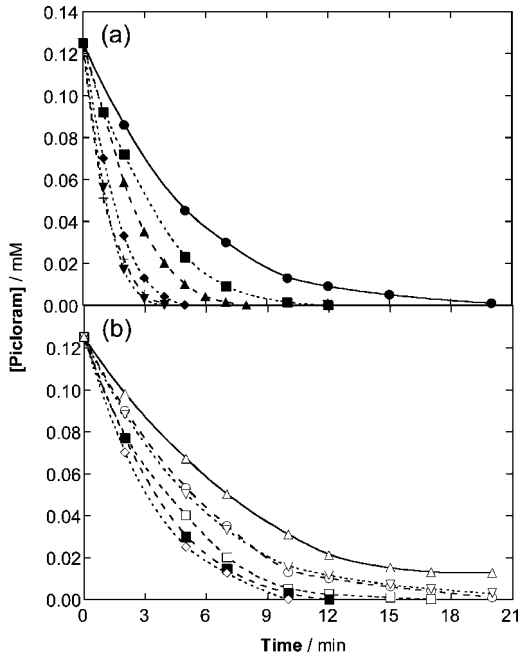

Figure 23. Effect of (a) current and (b) Fe^{3+} content on picloram concentration decay of 150 mL of 0.125 mM pesticide solutions in 0.05 M Na_2SO_4 of pH 3.0 at room temperature using an undivided Pt/carbon felt cell such as that of Figure 16a. In plot (a), 0.1 mM Fe^{3+} and current: (●) 30, (■) 60, (▲) 100, (◆) 200, (▼) 300, and (+) 500 mA. (b) Current of 60 mA and Fe^{3+} concentration: (○) 0.02, (□) 0.05, (■) 0.1, (◇) 0.2, (▽) 0.5, and (△) 1.0 mM. Reprinted with permission from ref 190. Copyright 2008 Elsevier.

$Fe(OH)_3$, and becomes almost insignificant at pH 1.0 when Fe^{2+} forms complexes with H_2O_2 and SO_4^{2-} ions. A similar trend was found for chloride media. Daneshvar et al.[187] confirmed that the removal rate of the dye Orange II in different 0.05 M electrolyte solutions with 1 mM Fe^{3+} using a three-electrode Pt/graphite felt cell operating at $E_{cat} = -0.5$ V/SCE also decreases in the sequence $ClO_4^- > Cl^- \gg SO_4^{2-}$. This was as a result of the decay in free iron ion concentration in the bulk by the formation of Fe(III) complexes with the two latter ions, along with the additional action of SO_4^{2-} ions as scavengers of $^{\bullet}OH$ in the bulk. This trend is justified by the fact that perchlorate does not form complexes with Fe(III), while about 20% or 80% of 1 mM Fe^{3+} is complexed in the presence of 0.05 M chloride or sulfate, respectively.[186] The dye Orange II was much more slowly removed with sulfate than with chloride.

Other important operation parameters are the applied potential (E_{cat}) and current in three- and two-electrode cells, respectively. In the first case, E_{cat} is usually chosen to attain the maximum H_2O_2 production rate via reaction 32 before H_2 discharge from reaction 44, and its value depends on the cathode material used (see section 3.2). This parameter, for example, has been optimized at −0.5 V/SCE for carbon felt,[120,121] graphite,[174] and graphite felt,[187] −0.9 V/SCE for carbon-PTFE GDEs,[111] −1.0 V/SCE for modified graphite felts,[188] and −1.6 V/SCE for RVC.[146] It has also been observed[187,189] that a larger cathode area favors both H_2O_2 production and Fe^{2+} regeneration, leading to a higher concentration of $^{\bullet}OH$ from Fenton's reaction 1. On the other hand, the applied current exerts a large influence on the degradation rate of POPs under galvanostatic electrolysis. As an example, Figure 23a shows the picloram (4-amino-3,5,6-trichloropyridine-2-carboxylic acid) concentration decays determined by reversed-phase high-performance liquid chromatography (HPLC) for a solution with 0.125 mM of this pesticide and 0.1 mM Fe^{3+} using the cell of Figure 16a at different currents.[190] The decay kinetics of picloram is strongly accelerated as the current increases from 30 to 500 mA. At 300 mA, for example, the pesticide disappears in only 4 min, with this time becoming gradually longer with decreasing *I*. However, very similar results are obtained for 300 and 500 mA, indicating that the system has already attained its maximum oxidation power at about 300 mA. This trend is general for POPs in all EF systems (also verified by the mineralization rate) since COD and TOC decays are significantly enhanced with increasing *I* up to a certain kinetically limiting value.

A key factor in the EF process is the concentration of Fe^{3+} or Fe^{2+} required as catalyst, which is a function of the cathode employed. For example, at pH 3.0 optimum Fe^{3+} contents of 0.1−0.2 mM are needed for carbon-felt cathodes,[190,191] whereas a greater content of 0.5−1.0 mM Fe^{2+} is optimum for carbon-PTFE GDE cathodes[184,185] because of their lower ability for Fe^{2+} regeneration (see section 4.2.2). The former experimental conditions are confirmed in Figure 23b from the picloram concentration decay with rising Fe^{3+} contents from 0.02 to 1.0 mM at 60 mA. These findings indicate that the maximum production of $^{\bullet}OH$ via Fenton's reaction 1 takes place at the optimized Fe^{3+} or Fe^{2+} contents, since at higher catalyst concentration the oxidant generation is progressively inhibited because of the greater extent at which waste reaction 17 is given. On the other hand, an increase in initial pollutant concentration always causes its slower kinetic decay and lower percentages of COD and TOC removals, which is expected if more organic matter is oxidized by similar amounts of electrogenerated oxidants.[185]

Therefore, the best experimental conditions for the EF treatment of organic wastewater are obtained operating at high O_2 or air flow rates, high stirring or liquid flow rate, temperatures up to 35−40 °C, solution pH near 3.0, and optimized Fe^{2+} or Fe^{3+} concentration to obtain the maximum $^{\bullet}OH$ production rate in the bulk. The electrolyte composition is limited to sulfate and chloride ions, since media involving perchlorate ions with lower complexing power are toxic and not environmentally viable. While E_{cat} can be optimized in three-electrode systems, the oxidation power related to the applied current in undivided two-electrode cells depends on the pollutant concentration, cell configuration, and anodes utilized, which can electrogenerate competitive strong oxidants such as BDD($^{\bullet}OH$) (see section 4.2.3). In general, lower currents and greater organic contents lead to higher current efficiency with smaller energy consumption but requiring longer times for attaining acceptable mineralization degrees. These effects will be analyzed in the environmental applications of this technique (see section 7).

4.3.3. Modeling and Experimental Design Methodology

A high number of works devoted to the degradation of synthetic solutions with pure POPs by EF and related technologies have followed their kinetics decays and the evolution of oxidation intermediates and inorganic ions released by different techniques, mainly by HPLC and ionic chromatography. In some cases, oxidation byproducts have also been identified by mass spectrometry techniques such as GC-MS. These data have allowed the study of kinetic behavior of treated pollutants and the proposal of their degradation paths.

Table 4. Absolute Second-Order Rate Constant ($k_{2,P}$) Determined from Eq 60 by the Competition Kinetics Method for the Reaction of Several Pesticides and Dyes with Homogeneous $^{\bullet}OH$ Formed During the EF Process in Sulfuric Acid Solutions at Room Temperature Using Three- and Two-Electrode Pt/Carbon Felt Cells

organic compound	C_0[a]/mM	operation conditions	current/mA	E_{cat}[b]/V vs SCE	$k_{2,P} \times 10^{-9}$/M^{-1} s^{-1}
		pesticides			
divided cell					
2,4-D[121]	1.0	150 mL, 0.01 M H_2SO_4, 1 mM Fe^{3+}		−0.50	35
imazapyr[193]	0.10	125 mL, pH 3, 0.5 mM Fe^{2+}		−0.50	5.4
undivided cell					
methyl parathion[186]	0.13	150 mL, pH 3, 0.1 mM Fe^{3+}	100		4.2
picloram[190]	0.125	150 mL, 0.05 M Na_2SO_4, pH 3, 0.2 mM Fe^{3+}	60		2.7
propham[191]	0.50	150 mL, 0.05 M Na_2SO_4, pH 3, 0.5 mM Fe^{3+}	60		2.2
pentachlorophenol[192]	0.03	125 mL, pH 3, 1 mM Fe^{2+}	50		3.6
diuron[194]	40[c]	125 mL, pH 3, 0.5 mM Fe^{3+}	100		4.8
chlortoluron[197]	0.05	150 mL, 0.05 M Na_2SO_4, pH 3, 0.1 mM Fe^{3+}	60		4.9
carbofuran[197]	0.05		60		3.2
bentazone[197]	0.05		60		2.6
imazapyr[198]	0.10	125 mL, pH 3, 0.1 mM Fe^{3+}	60		4.5
imazaquin[198]	0.10		60		5.4
		dyes			
undivided cells					
Basic Blue 9,[195] [d]	0.25	125 mL, pH 3, 0.5 mM Fe^{3+}		−0.50	2.4
Direct Red 28,[195] [e]	0.25			−0.50	5.5
Reactive Orange 70,[195] [f]	0.25			−0.50	14
Direct Orange 61,[196] [g]	0.05	500 mL, pH 3, 0.05 M Na_2SO_4, 0.1 mM Fe^{2+}	60		21
Basic Blue 20,[199] [h]	0.05	250 mL, pH 3, 0.05 M Na_2SO_4, 0.2 mM Fe^{3+}	40		1.3
Basic Green 4,[199] [i]	0.05		40		2.7
Basic Violet 3,[199] [j]	0.05		40		2.5
Food Green 3,[199] [k]	0.05		40		2.2

[a] Initial compound concentration. [b] Cathodic potential in a three-electrode cell. [c] Initial concentration in mg L^{-1}. [d] Methylene Blue. [e] Congo Red. [f] Drimarene Yellow. [g] Pyrazol Fast Orange GNL. [h] Methyl Green. [i] Malachite Green. [j] Crystal Violet. [k] Fast Green FCF.

The decay kinetics of most initial pollutants in divided and undivided cells fits well with the theoretical equation of a pseudo-first-order reaction.[121,148,184–186] This suggests a direct attack of hydroxyl radical ($^{\bullet}OH$ in the bulk and/or M($^{\bullet}OH$)) on the organic molecule by an elementary second-order reaction, which behaves as a pseudo-first-order reaction because hydroxyl radicals are continuously produced and destroyed at a similar rate to attain a steady-state concentration in the bulk and/or the vicinity of the anode. On the basis of this simple model, Oturan's group determined the absolute second-order rate constant ($k_{2,P}$) for the reaction of pollutants (P) with $^{\bullet}OH$ in the bulk from the competition kinetics method with a standard competition substrate (S), whose absolute rate constant ($k_{2,S}$) with this radical is well established.[121,186,190–199] The most widely tested substrates have been benzophenone ($k_{2,S} = 8.70 \times 10^9$ M^{-1} s^{-1})[200] and benzoic ($k_{2,S} = 4.30 \times 10^9$ M^{-1} s^{-1}),[47] 4-hydroxybenzoic ($k_{2,S} = 2.19 \times 10^9$ M^{-1} s^{-1}),[201] and salicylic ($k_{2,S} = 2.70 \times 10^{10}$ M^{-1} s^{-1})[202] acids. The EF process is performed with a solution containing equimolar concentrations of both the pollutant and substrate, and their exponential concentration decay is measured for short electrolysis times by reversed-phase HPLC, thereby making it possible to simultaneously obtain the pseudo-first-order rate constant for the pollutant ($k_{1,P}$) and competition substrate ($k_{1,S}$). The $k_{2,P}$ value is then calculated from eq 60:

$$k_{2,P} = k_{2,S} \times \frac{k_{1,P}}{k_{1,S}} \quad (60)$$

Table 4 summarizes the $k_{2,P}$ values determined for several pesticides and dyes using both divided and undivided Pt/carbon felt cells under potentiostatic or galvanostatic operation modes. As can be seen, this parameter varies between 1.3×10^9 and 3.5×10^{10} M^{-1} s^{-1} as expected for hydroxylation reactions of aromatic compounds (see reaction 12).

Recently, Liu et al.[147] proposed a more complex kinetic model considering the rates of all the main reactions involved in the EF process such as Fe^{2+} regeneration, H_2O_2 electrogeneration and decomposition, Fenton's reaction, and $^{\bullet}OH$ reactions including organics oxidation. They confirmed the validity of such a model by justifying the inverted S-shaped curves obtained for the phenol concentration decay against time in a divided three-electrode Pt/carbon cell.

On the other hand, Oturan's group proposed the optimization of operation parameters in the EF process by means of experimental design methodology.[197,203] This is based on multivariate polynomial models where the values of the independent variables are systematically modified by carrying out a minimum set of experiments, and their analysis allows predicting the most favorable operating conditions within the experimental region chosen. They used a factorial design methodology and a Doehlert matrix to, respectively, optimize the decay kinetics and mineralization rate of pollutants considering its concentration, current, and electrolysis time as operation variables in both cases. From this experimental design methodology, for example, the fastest decay kinetics of chlortoluron (3-(3-chloro-4-methylphenyl)-1,1-dimethylurea) in 0.05 M Na_2SO_4 with 0.1 mM Fe^{3+} at pH 3.0 was found for a 0.05 mM solution of this pesticide at 60 mA, disappearing in 4 min with $k_{2,P} = 4.9 \times 10^9$ M^{-1} s^{-1} (see Table 4).[197] In contrast, the maximum mineralization efficiency with TOC removal of 98% was achieved after 8 h of treatment of 0.125 mM pesticide at 300 mA.

4.3.4. Use of Other Metallic Ions as Catalysts

Little work has been reported on the alternative use of Cu^{2+}/Cu^{+},[204,205] Co^{3+}/Co^{2+},[205,206] and Mn^{3+}/Mn^{2+} couples[205]

instead of the Fe^{3+}/Fe^{2+} pair to electrogenerate $^{\bullet}OH$ in the bulk from Fenton-like reactions. Chen et al.,[206] mimicking Oturan's ideas,[192] proposed an electro-Fenton-like "electro $Co^{2+}-H_2O_2$ system" based on Fenton-like reaction 61:

$$Co^{2+} + H_2O_2 + H^+ \rightarrow Co^{3+} + {}^{\bullet}OH + H_2O \quad (61)$$

It was tested with an undivided three-electrode Pt/graphite cell, similar to that of Figure 7b, containing 50 mL of an air-saturated solution with 0.1 mM of the xanthene dye Bromopyrogallol Red with 0.1 mM Co^{2+} in 0.2 M phosphate buffer solution of pH 4.0. At $E_{cat} = -0.75$ V/SCE, the solution was completely decolorized in 10 min and the initial COD of 3320 mg L^{-1} was reduced by 96% in 30 min. They found that this system possessed about a 10 times higher oxidation ability than its comparable EF treatment with 3.0 mM Fe^{2+}. However, this Fe^{2+} concentration in EF is excessive because it favors the loss of $^{\bullet}OH$ via reaction 17. More accurately, Pimentel et al.[205] showed that the EF degradation of 330 mL of 0.33 mM phenol solutions with 0.1 mM Fe^{2+} or 0.1 mM Co^{2+} in 0.05 M Na_2SO_4 of pH 3.0 using the undivided Pt/carbon felt of Figure 16a yielded a similar TOC reduction of 80% and 78%, respectively, after 4 h of electrolysis at 100 mA. In contrast, these authors observed that Cu^{2+} concentrations as high as 10 mM were needed to obtain acceptable degradation rates of phenol. The Cu^{2+}/Cu^+ system involves the reduction of Cu^{2+} to Cu^+ with $HO_2^{\bullet}$ from reaction 62, with $k_2 = 5.0 \times 10^7$ M^{-1} s^{-1},[78] and/or with organic radicals $R^{\bullet}$ by reaction 63, followed by regeneration of Cu^{2+} due to oxidation of Cu^+ with H_2O_2 giving $^{\bullet}OH$ from the Fenton-like reaction 64 with $k_2 = 1.0 \times 10^4$ M^{-1} s^{-1}:[207]

$$Cu^{2+} + HO_2^{\bullet} \rightarrow Cu^+ + H^+ + O_2 \quad (62)$$

$$Cu^{2+} + R^{\bullet} \rightarrow Cu^+ + R^+ \quad (63)$$

$$Cu^+ + H_2O_2 \rightarrow Cu^{2+} + {}^{\bullet}OH + OH^- \quad (64)$$

Note that some authors have reported the positive cocatalytic effect of copper ions in Fenton systems as a result of the enhanced Fe^{2+} regeneration from reaction 65:[208]

$$Cu^+ + Fe^{3+} \rightarrow Cu^{2+} + Fe^{2+} \quad (65)$$

This synergistic effect has been tested in EF by Brillas' group, who found an acceleration of the degradation rate of nitrobenzene,[209] the drug paracetamol,[185] and the dye Indigo Carmine[210] when treated at pH 3.0 with 1.0 mM Fe^{2+} + 0.25 mM Cu^{2+} in relation to 1.0 mM Fe^{2+} alone with the Pt/O_2 cell of Figure 10. This improvement was related to the following: (i) production of additional $^{\bullet}OH$ via reaction 64 as well as via Fenton's reaction 1 favored by reaction 65 and (ii) easier oxidation of complexes of Cu^{2+} with some intermediates compared with the competitively formed Fe(III) complexes that are much more slowly removed.

4.4. Novel EF Systems

Some novel EF systems with H_2O_2 electrogeneration based on solid iron phases that act as mineral, supported, or immobilized catalysts have been proposed. In some cases, these systems allow extending the pH range to neutral media, thereby preventing the accumulation of iron sludge.

Sánchez-Sánchez et al.[211] studied the viability of goethite (α-FeOOH) as an iron dosage source for aniline mineralization by a modified EF process, giving rise to the so-called goethite-catalyzed EF (GEF) process. In further work,[212] the same group extended this study to other mineral iron oxides such as wustite (FeO), magnetite (Fe_3O_4), and hematite (α-Fe_2O_3) for their use in both EF and PEF processes. The percentage of TOC removed after 5 h of EF treatment of 100 mg L^{-1} aniline solutions with 1 g L^{-1} of all these solid catalysts or 0.5 mM Fe^{2+} using a Pt/GDE cell is depicted in Figure 24. As can be seen, the use of wustite and magnetite yields 62% and 58% of soluble TOC decay, respectively, which is greater than the 54% TOC decay for the EF process with Fe^{2+}, but the performance with goethite and hematite is much lower. This trend relates to the ability of the solid iron oxides to release Fe^{2+} to the bulk to react with electrogenerated H_2O_2 via Fenton's reaction 1, so that they behave as pure homogeneous catalysts that act as self-regulators of iron supply.

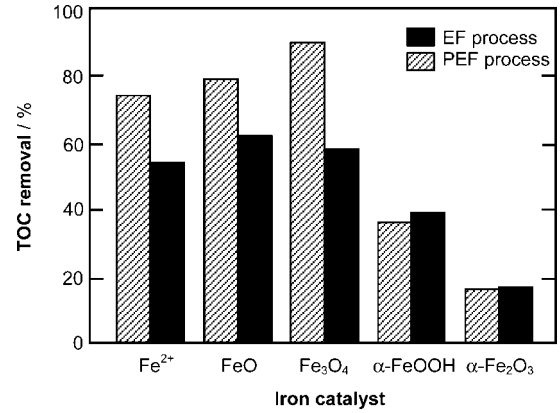

Figure 24. Comparison of TOC removal reached after 5 h of EF and PEF degradation of 250 mL of 100 mg L^{-1} aniline solutions with different catalysts in 0.2 M Na_2SO_4 of pH 3 using a Pt/GDE cell such as that of Figure 17f at 250 mA and 25 °C. The carbon-PTFE GDE cathode was fed with air at 0.5 L min^{-1}. Catalyst concentration: 0.5 mM of Fe^{2+} or 1 g L^{-1} of wustite (FeO), magnetite (Fe_3O_4), goethite (α-FeOOH), and hematite (α-Fe_2O_3). In PEF, an 8 W UVC lamp ($\lambda_{max} = 254$ nm) was used. Reprinted with permission from ref 212. Copyright 2007 The Electrochemical Society.

A Chinese group[213,214] explored a combined multiple-phase electrochemical oxidation packed bed method using porous graphite as the anode and cathode, with a $CuO-Co_2O_3-PO_4^{3-}$ modified kaolin catalyst packed near the electrodes. While H_2O_2 was produced at the cathode, the degradation of organics was interpreted as a result of the adsorption of pollutants on the porous anode catalyst, followed by their oxidation by $^{\bullet}OH$ produced from the oxidation/decomposition of H_2O and H_2O_2 at the modified kaolin. Leaching of Co^{3+} and Cu^{2+} was confirmed during electrolysis, but the possible oxidative role of their related Fenton-like reactions 61 and 64 was not considered. The same group also applied this system, but with the kaolin dispersed in the solution, to the treatment of a pulp and paper wastewater and found an excellent COD decay of 97% in 73 min at 30 mA cm^{-2}, starting from 1670 mg L^{-1} COD.[215]

Several authors have proposed the use of three-dimensional electrode reactors equipped with granular activated carbon (GAC) as a particle electrode, packed between the anode and the cathode. Under these conditions, the particles of GAC act as microelectrodes under the applied potential, favoring the generation of $^{\bullet}OH$ and increasing current efficiency. For example, Xiong et al.[216,217] tested an undivided three-phase

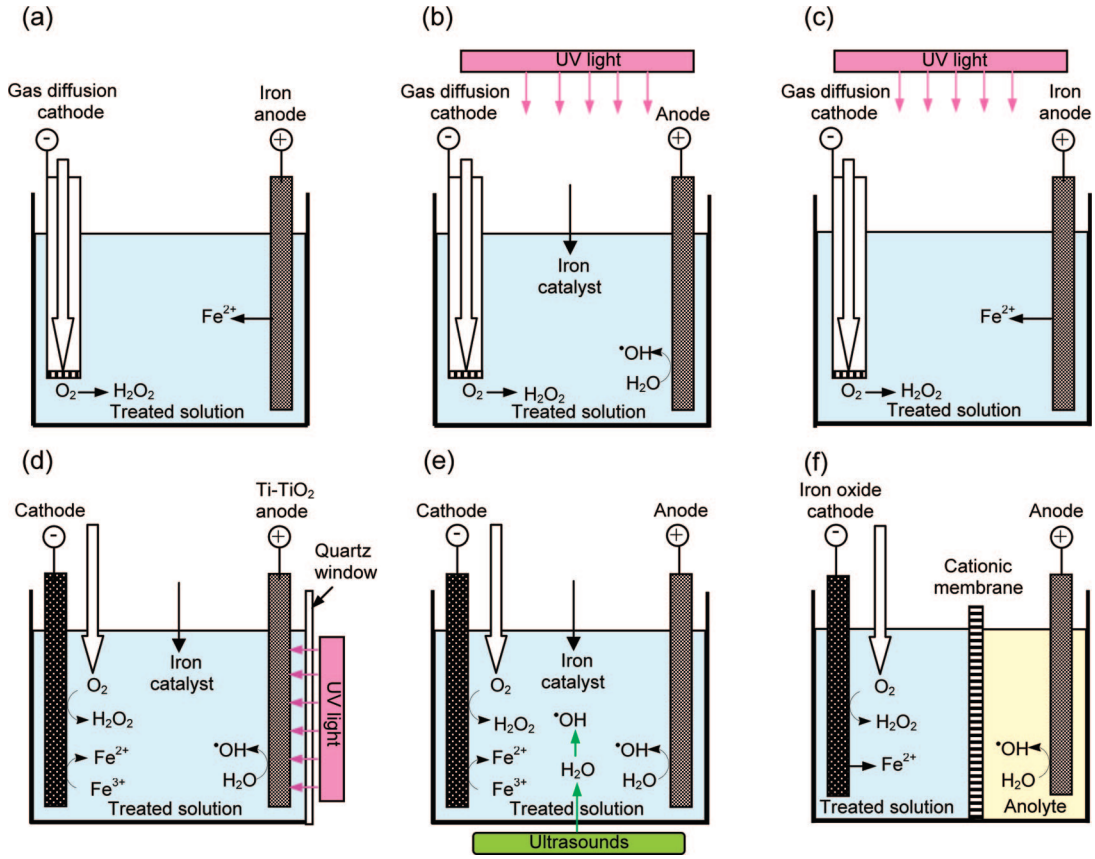

Figure 25. Schematic representation of bench-scale two-electrode tank reactors used in combined EF processes: (a) PC, (b) PEF with artificial UV irradiation or SPEF with sunlight illumination, (c) PPC, (d) PEC-EF, (e) SEF, and (f) cathodic Fe^{2+} generation. The main reactions at the electrodes are given, and H_2O_2 is generated at the cathode from O_2 or air feeding.

three-dimensional electrode tank reactor with two stainless steel electrodes and a GAC packed bed between them under an air flow rate of 5 L min^{-1} to degrade phenol and formic acid. The application of current causes the polarization of every carbon particle, which behaves as an anode on one side and a cathode on the other to produce H_2O_2. The authors employed the same system to assess the destruction of aniline in the presence of added Fe^{2+}, confirming the formation of $^{\bullet}OH$ radicals by spin trapping.[218] A decrease in COD removal efficiency with time was observed owing to the passivation of the carbon particles by a polymeric film, which could be overcome by electrolysis in the presence of a MnO_2. Recently, Xu et al.[219] also employed this system for the treatment of the dye Acid Orange 7 and found that an ACF cathode was more effective than a graphite or stainless steel cathode due to its larger surface area. For 1 L of a 300 mg L^{-1} dye solution in 3 g L^{-1} Na_2SO_4 of pH 3.0 treated with a stainless steel anode and an ACF cathode, both of 35 cm^2 apparent area, with 50 g of GAC in the interelectrode gap of 3 cm and an air flow rate of 3 L min^{-1}, 96% color and 54% TOC removals with a cost of 865 kWh (kg TOC)$^{-1}$ were reached after 60 min of electrolysis at 20 V. The influence of Fe^{2+} released from anode oxidation was also evaluated.

On the other hand, Liu et al.[220] developed an in-situ-controlled pH EF system using the H^+ and OH^- released from electrode reactions in a system composed of three consecutive two-electrode cells capable of treating 120 mL of solution each. In the first step, the initial neutral solution enters the anodic chamber of the first divided cell to decrease its pH to 3.5. In the second step, the resulting solution is treated by the EF process into the second undivided cell after dosing Fe^{2+} without a pH change. In the final step, the treated solution at pH 3.5 enters the cathodic chamber of the third divided cell to undergo EF. In this latter step the pH increases to 7.0. The performance of the system was assessed through the degradation of dimethylphtalate with a Pt anode and graphite cathode, which mainly took place during the second and third steps when a large amount of $^{\bullet}OH$ was produced in the bulk. Almost 100% dimethylphtalate decay and 60% TOC reduction were achieved after 90 min following this three-step process. This system then seems very useful for its potential application to the EF treatment of effluents with neutral pH without requiring the addition of chemicals.

5. Combined EF Processes

Different combined electrochemical technologies based on Fenton's reaction chemistry, such as PC, PEF, SPEF, PPC, PEC-EF, SEF, and cathodic generation of Fe^{2+} (see Figure 1), have been proposed to enhance the efficiency of the EF process. They aim to synergize coupling methods to minimize or even eliminate some drawbacks of the individual techniques by contribution of others.[24] The peculiarities of all these combined EF processes are described in this section.

5.1. Peroxi-Coagulation (PC) Process

The PC method was first proposed by Brillas' group.[172,221–226] It utilizes an undivided cell such as the one shown in Figure 25a, containing a sacrificial iron anode and a cathode able to generate H_2O_2 from reaction 32. Under these conditions, soluble Fe^{2+} is supplied to the solution from the oxidation

Table 5. Percentages of TOC Removal Calculated from Eq 53 and Coagulated and Mineralized TOC Obtained After 6 h of PC Treatment of 100 mL Solutions of Pesticide with a Concentration Equivalent to 100 mg L^{-1} TOC in 0.05 M Na_2SO_4 of pH 3.0 at 35 °C in an Fe/O_2 Cell at Different Current Values and Under pH Regulation[223–226]

pesticide	current/mA	% TOC removal	% coagulated TOC	% mineralized TOC
4-CPA[a]	100	91	48	43
MCPA[b]	100	92	49	43
2,4-D[c]	100	81	38	43
	300	92	45	47
	450	92	50	42
dicamba[d]	100	94	48	46
	300	94	94	0
	450	94	94	0
2,4,5-T[e]	100	93	54	39

[a] 4-Chlorophenoxyacetic acid. [b] 4-Chloro-2-methylphenoxyacetic acid. [c] 2,4-Dichlorophenoxyacetic acid. [d] 3,6-Dichloro-2-methoxybenzoic acid. [e] 2,4,5-Trichlorophenoxyacetic acid.

of the Fe anode by reaction 66, with $E° = -0.44$ V/SHE, following a faradaic behavior:

$$Fe \rightarrow Fe^{2+} + 2e^- \quad (66)$$

Thus, the Fe^{2+} generated is quickly oxidized by H_2O_2 according to Fenton's reaction 1 to yield a Fe^{3+}-saturated solution, while the excess of this ion precipitates as $Fe(OH)_3$ because of the concomitant increase in solution pH, which is continuously regulated by adding diluted H_2SO_4. All produced hydrogen peroxide is then consumed, allowing the removal of the organic matter from the wastewater by the combined action of their oxidation with •OH generated from Fenton's reaction 1 and their coagulation with the great quantity of $Fe(OH)_3$ precipitate formed. Elemental analysis confirmed the existence of both competitive removal modes by determining the percentages of coagulated TOC in the sludge and of mineralized TOC, as shown in Table 5 for the PC treatment of different pesticides for 6 h using a 10 cm^2 Fe anode and a 3 cm^2 GDE cathode fed with O_2. At 100 mA, about 40−50% of organics become coagulated or mineralized, although coagulation predominates as the current rises to 450 mA owing to the greater production of both Fe^{2+} from reaction 66 and H_2O_2 from reaction 32. In the case of dicamba, for example, all organics are retained in the $Fe(OH)_3$ from 300 mA, meaning that PC rather behaves as a phase-separation method. The current then determines the catalyst−coagulant dosage rate, which largely influences the separation process and removal efficiency.

Alvarez-Gallegos et al.[109] reported a procedure similar to PC with a divided cell. Figure 26 shows the H-type stainless steel/RVC cell used, coupled to a solar panel to feed the power supply. Fe^{2+} is released in the anolyte from stainless steel oxidation by reaction 66, and the cationic membrane allows its passage toward the catholyte to react with the H_2O_2 generated at RVC. As a result, an excess of H_2O_2 was detected in the catholyte as a function of cell voltage. For 350 mL of 0.05 M Na_2SO_4 at pH 2.0, about 20% and 10% current efficiency for H_2O_2 accumulation was found at 1.5 and 2.5 V, respectively. The oxidation ability of the system was confirmed from the total decolorization attained for a 0.1 mM solution of the dye Reactive Black 5 after 20 h of electrolysis at 2.5 V.

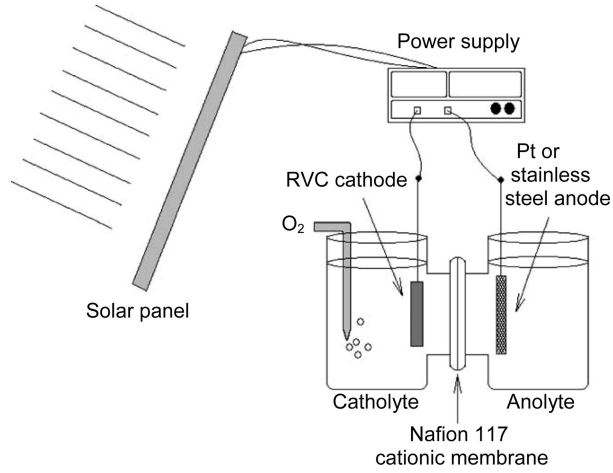

Figure 26. Scheme of the experimental setup of an H-type divided cell coupled to a solar panel (50 W, 17 V, 2.9 A) for the treatment of 350 mL of solutions of organics in 0.05 M Na_2SO_4 at pH 2 and room temperature. The anode was a Pt or stainless steel gauze of 15 mm × 15 mm, and the cathode was a three-dimensional RVC of 15 mm × 15 mm × 5 mm thick. Reproduced with permission from ref 109. Copyright 2005 Elsevier.

5.2. Photoelectro-Fenton (PEF) and Solar Photoelectro-Fenton (SPEF) Processes

The PEF method has been proposed and extensively studied by Brillas' group using undivided open Pt/O_2 and BDD/O_2 cells such as that schematized in Figure 25b.[113,148,184,185,209,210,222,227–237] In this technique, the solution is treated under EF conditions and simultaneously irradiated with UVA light to accelerate the mineralization rate of organics via photo-Fenton process (see section 2.3). The synergistic degradation action of irradiation can be associated with (i) a higher regeneration rate of Fe^{2+} and production of additional •OH from photolysis of $[Fe(OH)]^{2+}$ by photoreduction reaction 27 and (ii) the photolysis of complexes of Fe(III) with generated carboxylic acids by reaction 28.

The existence of the former reaction can be corroborated by comparing curves *c* and *d* in Figure 11. A slight decay in accumulated H_2O_2 under a 6 W UVA illumination compared with the dark can be seen, as expected if it is more quickly destroyed from the faster Fe^{2+} regeneration. However, it was found that the mineralization of pollutants was enhanced by the rapid photolysis of complexes of Fe(III) with oxidation byproducts, mainly oxalic acid by reaction 29, with the contribution of •OH induced by reaction 27 being much less significant. A similar behavior was observed when sunlight was used as a photon energy source to treat organic effluents in the recirculation flow plant of Figure 12 using the SPEF method.[149,235] Figure 27a and 27b, respectively, illustrate the concentration and TOC decays for MCPP degraded with 0.5 mM Fe^{2+} in the flow plant with a BDD/O_2 cell. The same MCPP decay rate can be observed in Figure 27a for EF (in the dark), PEF with a 160 W UVA light, and SPEF processes, indicating that the pesticide mainly reacts with •OH produced from Fenton's reaction 1 and BDD(•OH) formed from reaction 46. In contrast, Figure 27b shows a faster TOC removal in the sequence EF < PEF < SPEF, which was ascribed to the faster photodecarboxylation of Fe(III)−oxalate complexes with solar light because of its greater irradiation intensity entering into the solution. This parameter then seems crucial for assessing the processes taking place in SPEF. Recently, Brillas' group[236,237] reported that direct solar irradiation on solutions contained in small tank reactors such

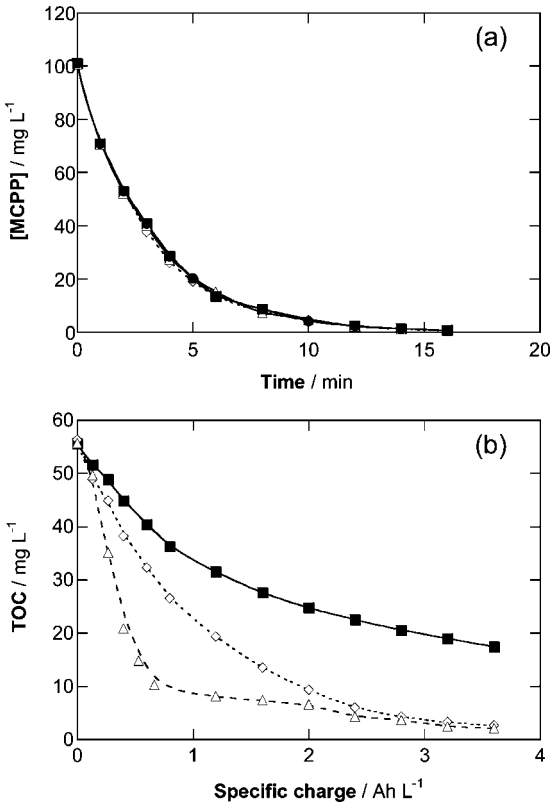

Figure 27. (a) Decay of the herbicide mecroprop (MCPP) with time and (b) TOC removal with specific charge for the degradation of 2.5 L of 100 mg L^{-1} MCPP solutions and 0.5 mM Fe^{2+} in 0.05 M Na_2SO_4 of pH 3.0 using the flow plant with a BDD/O_2 cell of Figure 12 at 50 mA cm^{-2}, 25 °C, and liquid flow of 180 L h^{-1}: (■) EF process, (◇) PEF process with a 160 W UVA lamp (λ_{max} = 360 nm), and (△) SPEF process. Adapted with permission from ref 235. Copyright 2007 Elsevier.

as that of Figure 25b accelerates the decay of organics in SPEF compared with PEF because of the higher production rate of •OH by reaction 27 resulting from of the greater photon intensity supplied to the system. In conclusion, the SPEF method is more beneficial for water remediation than PEF not only because it is a cheaper and renewable energy source but also because of its superior ability to mineralize organic pollutants.

On the other hand, Irmak et al.[238] explored the PEF process with a UVC light (λ_{max} = 254 nm) for the treatment of 300 mL of an O_2-saturated 0.6 mM 4-chloro-*o*-cresol solution with 1.8 mM Fe^{2+} in H_2SO_4 of pH 2.7 using a divided three-electrode Pt/carbon felt cell at E_{cat} = −0.55 V/SCE. After applying 141 C for 300 min, the PEF process led to overall mineralization with total release of Cl^-, which was much faster than the comparable treatment by EF that only reached 42% TOC removal. The same behavior was described by Expósito et al.[212] when testing the PEF process with an 8 W UVC light for 100 mg L^{-1} aniline solutions with the addition of Fe^{2+} or mineral iron oxides as catalysts in a Pt/O_2 cell, aiming to complete their degradation study by the EF process described in section 4.4. Figure 24 shows that the use of magnetite enhances TOC removal from 58% in the dark to 90% under illumination after 5 h of treatment. In contrast, a much lower contribution to mineralization was found for wustite and Fe^{2+} and, surprisingly, no irradiation influence on TOC decay took place for goethite and hematite. Although the different actions of these catalysts were not clearly justified, the authors suggested that the greater TOC removal achieved for magnetite was due to its photocatalytic ability. They also explained that UVC light mainly accelerates photoreduction reaction 27, while UVA light predominantly photolyzes Fe(III)−carboxylate complexes, as stated above.

5.3. Other Photoassisted Processes

The photoperoxi-coagulation (PPC) method, based on the UVA irradiation of a contaminated solution treated by PC in a tank reactor such as the one schematized in Figure 25c, has also been proposed and investigated by Brillas' group.[224,225] Unfortunately, the PPC process was practically ineffective because the TOC removal rate was similar to comparable PC treatment since UVA light is mainly absorbed (or dispersed) by the $Fe(OH)_3$ precipitate in suspension, thereby preventing the action of reactions 27 and 28.

More promising results have been obtained from electrochemically manufactured CuO_2-based composites and TiO_2 materials.[239,240] Photocatalysis with TiO_2 has been widely studied for water and wastewater treatment because of its high performance and reasonable costs.[241] In such conditions, adsorbed organics can be directly oxidized according to reaction 67, under the action of holes formed from reaction 41, or by hydroxyl radical produced in reaction 68, which involves photogenerated vacancy and adsorbed water:[242]

$$h^+ + RH_{(ads)} \rightarrow R^\bullet + H^+ \quad (67)$$

$$h^+ + H_2O \rightarrow {}^\bullet OH + H^+ \quad (68)$$

In the presence of H_2O_2, formation of •OH by reaction 42 was also suggested.[151] The major loss of efficiency in this procedure arises from the recombination of electrons promoted to the valence band with either unreacted holes from reaction 69 or adsorbed •OH from reaction 70:[243]

$$e_{CB}^- + h^+ \rightarrow TiO_2 + \text{heat} \quad (69)$$

$$e_{CB}^- + {}^\bullet OH \rightarrow OH^- \quad (70)$$

A higher efficiency of wastewater remediation can be achieved using photoelectrocatalysis (PEC), in which either a constant *j* or a constant bias anodic potential (E_{anod}) is applied to a TiO_2-based thin film anode subjected to UV illumination. Since the photoinduced electrons are continuously extracted from the anode by the external electrical circuit, parasitic reactions 69 and 70 are inhibited, and the production of holes from reaction 41 and •OH from reaction 68 is accelerated. This significantly enhances the oxidation of organics compared with traditional photocatalysis.[242−244] For example, Xie and Li used bisphenol A as an organic probe to carry out a comparative study that demonstrated the greater effectiveness of PEC compared with TiO_2 photocatalysis.[151,245,246]

A variant of PEC is the so-called photoelectrochemical electro-Fenton (PEC-EF), which is based on the synergistic oxidative action of a TiO_2 photoanode and •OH formed via Fenton's reaction 1 between cathodically generated H_2O_2 and Fe^{2+} added to the solution using, for example, a tank reactor such as that in Figure 25d.[242,243,247−249] Most research in PEC-EF has been performed with planar or annular TiO_2 photoanodes, although the use of three-dimensional TiO_2 nanotubes arrays[245] has opened the door to further research on tackling environmental challenges.

It is interesting to remark on the study made by Xie and Li[242] showing the superiority of PEC-EF for removing the

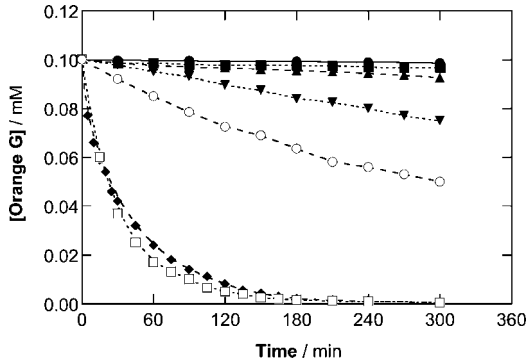

Figure 28. Orange G concentration decay for the photoassisted electrochemical oxidation of 30 mL of a 0.1 mM dye solution in 0.01 M Na_2SO_4 of pH 6.2 using the cell of Figure 14a. In PEC the bias potential of the Ti/TiO_2 anode was 0.71 V/SCE, while E_{cat} of −0.54 or −0.71 V/SCE was applied to the RVC cathode for H_2O_2 electrogeneration: (●) Direct photolysis, (■) AO with a TiO_2−Ti/Pt cell, (▲) TiO_2−Ti photocatalysis, (▼) PEC with a TiO_2−Ti/Pt cell, (○) PEC with a TiO_2−Ti/RVC cell, (◆) PEF with 17.6 mg L^{-1} Fe^{2+} at pH 3.0 with a TiO_2−Fe/RVC cell, and (□) PEC-EF with 17.2 mg L^{-1} Fe^{2+} at pH 3.0 using a TiO_2−Ti/RVC cell. Reprinted with permission from ref 242. Copyright 2006 Elsevier.

azo dye Orange G compared with AO and single photoassisted methods. Comparative trials were carried out with the quartz reactor of Figure 14a filled with 30 mL of a 0.1 mM solution of the dye using an 8 W UVA lamp as a light source. Figure 28 illustrates that Orange G is not directly photolyzed by UVA light, and at 5 h, it is slightly removed in 3% by AO with a TiO_2−Ti/Pt cell at E_{anod} = 0.71 V/SCE and in 8% by TiO_2−Ti photocatalysis, as expected if small amounts of adsorbed $^{\bullet}OH$ and holes are formed as oxidants at the TiO_2 surface. At the same time, PEC using the TiO_2−Ti/Pt cell enhances dye removal to 25% by the photogeneration of more holes by the passage of the current. The dye abatement achieved with this technique significantly improves to 50% when Pt is replaced by an RVC cathode at E_{cat} = −0.54 V/SCE because Orange G is also oxidized with H_2O_2 produced from the O_2 reduction by reaction 32. In contrast, the dye disappears completely when applying PEF to a TiO_2−Fe/RVC cell with 17 mg L^{-1} Fe^{2+}, pH 3.0, and E_{cat} = −0.71 V/SCE, and its disappearance rate even shows a slight increase in PEC-EF with a TiO_2−Ti/RVC cell, as a result of the additional formation of large amounts of $^{\bullet}OH$ from Fenton's reaction 1 and/or photoreduction reaction 27. The latter method also provided the greatest mineralization degree, reaching 74% in 5 h. A similarly strong improvement of the decolorization efficiency and TOC removal has been described by Peralta-Hernández et al.[243] for the compared treatment of 250 mL of O_2-saturated solutions with 2 mg L^{-1} of the azo dye Direct Yellow 52 in 0.05 M Na_2SO_4 with 0.25 or 0.50 mM Fe^{2+} at pH 2.0 by PEC-EF and EF in the dark using an undivided concentric annular TiO_2−Ti/graphite cloth flow cell with a central 75 mW cm^{-2} UVA light working in the batch recycle mode.

5.4. Sonoelectro-Fenton (SEF) Process

Several papers[250−253] have reported the coupling strategy between sonochemistry and different AOPs such as the Fenton process, giving rise to the concept of advanced sonochemical hybrid techniques that possess significantly greater efficacy for water remediation even though their fundamentals are yet unexplored. The well-known effect of ultrasounds applied to aqueous solutions is cavitation. This phenomenon consists in the formation, growth, and collapse of microbubbles that concentrate the acoustic energy into microreactors, leading to extreme conditions within a short time (<1 ns) and involving the pyrolysis of organics by enhancing their reactions with hydroxyl radicals produced by water decomposition from reaction 71:[252]

$$H_2O +))) \rightarrow {}^{\bullet}OH + H^{\bullet} \quad (71)$$

where [)))] denotes the ultrasonic irradiation.

A recent study by González-García et al.[254] on H_2O_2 electrosynthesis carried out in a sonoelectrochemical flow reactor with an RVC cathode demonstrated that the efficiency for H_2O_2 accumulation strongly increased from 26% to 82% when ultrasounds of 20 kHz and 750 W were applied to 3 L of a NaOH/boric acid solution of pH 10 electrolyzed at E_{cat} = −1.0 V/SCE and 21 °C for 3 h under recirculation at 70 L h^{-1}. This phenomenon was related to the continuous supply of a greater amount of O_2 toward the cathode due to the higher mass transfer regime achieved by convection. Interestingly, ultrasound-assisted H_2O_2 electrogeneration faces the two major drawbacks of O_2 electroreduction expressed in reaction 32, namely, the low solubility of this gas in water and the sluggish kinetics of O_2 reduction which leads to poor current efficiency. Despite these apparent advantages, only two papers[255,256] have reported the combined oxidative action of ultrasonic waves and EF, the so-called sonoelectro-Fenton (SEF) process, on organic pollutants in wastewater.

Abdesalam and Birkin[255] reported the sonoelectrochemical degradation of the dye Meldola Blue when using a recirculation three-electrode flow cell with a Pt gauze as an anode and an RVC cathode of 15 mm × 10 mm × 5 mm thick coupled to a piezoelectric transducer of 124 kHz and 100 V for treating 100 mL of 0.1 mM dye solutions with different Fe^{2+} concentrations in 0.05 M Na_2SO_4 at pH 2.0 and 25 °C. An apparent rate constant of 2.4×10^{-2} min^{-1} was found for the decolorization of the dye with 0.5 mM Fe^{2+} as the optimum catalyst content at E_{cat} = −0.7 V/Ag, which is twice the value determined for the comparable EF process, thus confirming the synergistic action of ultrasounds. Under these conditions, the solution COD was reduced by 61% after 100 min of sonoelectrochemical treatment. A more accurate study has recently been presented by Oturan et al.,[256] which reports for the first time the term sonoelectro-Fenton (SEF) process. An undivided Pt/carbon felt tank reactor with a ceramic piezoelectric transducer placed on its base, such as that schematized in Figure 25e, was used to carry out a comparative study on the performance of EF and SEF. The concentration decay of 250 mL of 1 mM of the herbicide 2,4-D, 0.5 mM of the herbicide 4,6-dinitro-*o*-cresol (DNOC), and 0.1 mM of the dye Azobenzene with 0.1 mM Fe^{3+} in O_2-saturated solutions with 0.05 M Na_2SO_4 at pH 3.0 was comparatively determined at 200 mA. For SEF, either a low frequency of 28 kHz or high frequency of 460 kHz was applied within an output power range from 20 to 80 W. Analogous behavior was always obtained for both frequencies. As an example, Figure 29 shows that at 28 kHz 2,4-D removal is significantly accelerated in SEF at 20 W compared with EF, but using 60 W does not promote a higher destruction rate, while a further increase to 80 W strongly inhibits the process. Similar results were found for DNOC, while no effect of ultrasounds was observed for Azobenzene, suggesting that the nature of the organic structure plays an important role in SEF. The improvement yielded by SEF at

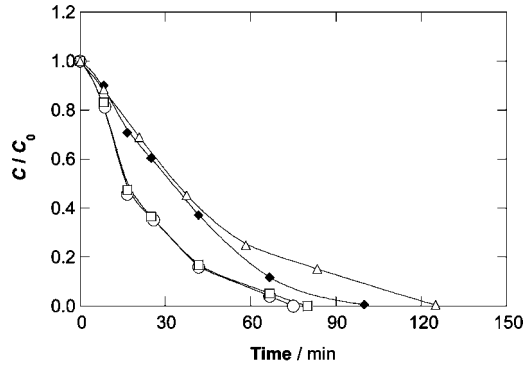

Figure 29. Normalized concentration decay of 2,4-D with electrolysis time during the treatment of 250 mL of solutions containing 1 mM of the herbicide and 0.1 mM Fe^{3+} in 0.05 M Na_2SO_4 at pH 3.0 and room temperature using the Pt/carbon felt cell of Figure 25e at 200 mA. Technique: (◆) EF process and SEF process at 28 kHz frequency and output power of (○) 20, (□) 60, and (△) 80 W. Reprinted with permission from ref 256. Copyright 2008 Elsevier.

20 W was ascribed to (i) the enhancement of the transfer of reactants Fe^{3+} and O_2 toward the cathode for the electrogeneration of Fe^{2+} and H_2O_2, as well as of the transfer of both products to the solution increasing $^{\bullet}OH$ production by Fenton's reaction 1 and accelerating the destruction process, (ii) the additional generation of $^{\bullet}OH$ by sonolysis from reaction 71, and (iii) the pyrolysis of organics due to cavitation promoted by ultrasound irradiation.

5.5. Cathodic Generation of Fe^{2+}

An interesting combined EF process has recently been proposed by Ai and co-workers[257] which uses core−shell Fe−Fe_2O_3 nanowires deposited on carbon nanotubes. The resulting Fe−Fe_2O_3−NTs composite can be used as an O_2-diffusion cathode for H_2O_2 electrogeneration from reaction 32, as commented for other NTs in section 3.2, and can slowly release Fe^{2+} to the solution by the leakage of nanowires to produce $^{\bullet}OH$ from Fenton's reaction 1. The proposed EF process with the cathodic generation of Fe^{2+} was tested in the divided two-electrode reactor exemplified in Figure 25f, where the reactions taking place in the electrodes are indicated. By applying a cell voltage between a 2 cm^2 Pt anode and a 3 cm^2 Fe−Fe_2O_3−NTs composite cathode to electrolyze 150 mL of 0.05 M Na_2SO_4 of pH 6.0 in the catholyte, electrogenerated H_2O_2 was accumulated up to 1.7×10^{-2} mM in 120 min thanks to the presence of macropores and mesopores. In the same solution, iron ions (Fe^{2+} and Fe^{3+}) achieved a steady concentration close to 25 mM after 90 min of electrolysis, as can be seen in Figure 30a. The performance of this combined EF process was ascertained by treating 1×10^{-5} M of the fluorone dye Rhodamine B under the same conditions. Figure 30b illustrates that 92% of this dye was removed in 120 min using the Fe−Fe_2O_3−NTs cathode, presenting a much better performance than comparatively prepared Fe−Fe_2O_3−graphite and Fe−Fe_2O_3−ACF cathodes. The difference was ascribed to the enhanced diffusion conditions for O_2 offered by the porous NTs. Further studies are needed to clarify whether this EF process with the cathodic generation of Fe^{2+} can be useful in practice.

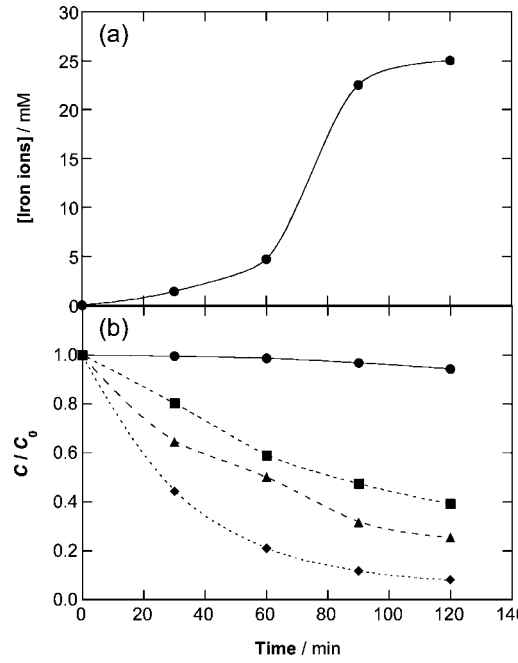

Figure 30. (a) Concentration of iron ions released during the electrolysis of 150 mL of 0.05 M Na_2SO_4 at pH 6.0 and room temperature in the catholyte of a divided Pt/Fe−Fe_2O_3−NTs cell such as that of Figure 25f by applying a cell voltage of 1.2 V. Air at a flow rate of 5 L min^{-1} was fed to the catholyte. (b) Normalized concentration decay for 1.044×10^{-5} M of Rhodamine B under the above conditions for the following cathodes: (●) carbon nanotubes (NTs), (■) Fe−Fe_2O_3−graphite, (▲) Fe−Fe_2O_3−ACF, and (◆) Fe−Fe_2O_3−NTs. Adapted with permission from ref 257. Copyright 2007 American Chemical Society.

6. EAOPs with Addition of H_2O_2 to the Solution or Its Indirect Production

This section describes the characteristics of various EAOPs based on Fenton's reaction chemistry in which the reagent H_2O_2 is not cathodically generated, unlike the EF and combined EF processes discussed so far. These methods are summarized in the classification of Figure 1. First, processes with H_2O_2 added to the solution such as Fered−Fenton, ECP, and AFT are presented. Photoassisted treatments based on the two former procedures, as well as ECP coupled to biological post-treatment (bio-ECP remediation), are subsequently discussed. Other electrochemical Fenton techniques involving the plasma-assisted Fenton process or anodic generation of H_2O_2 are finally considered.

6.1. Fered−Fenton Process

The foundations of this method were laid in the early 1990s,[258,259] which led to a patent by a Chinese group in 1997.[260] These authors investigated the process in detail for water remediation,[261–266] which predated the publication of further studies.[154,267,268] The Fered−Fenton process, also called EF-Fere, consists in the addition of either Fe^{2+} or Fe^{3+} to the initial wastewater along with the continuous injection of H_2O_2 during the treatment in an undivided electrolytic cell. Fe^{3+} is then cathodically reduced to Fe^{2+} by reaction 43, which reacts with added H_2O_2 to produce $^{\bullet}OH$ via Fenton's reaction 1. Water is also reduced to H_2 at the cathode from reaction 44 and oxidized to $^{\bullet}OH$ at the anode surface from reaction 46. All these reactions are shown in the scheme of an operative tank reactor presented in Figure

31a. Slow oxidation of small amounts of Fe^{2+} to Fe^{3+} at the anode from reaction 45 is also feasible.

The operation parameters in Fered−Fenton involve a great concentration of iron ions added at low pH and cathodic current density, which need to be optimized for each electrolytic system and treated wastewater. A total amount of H_2O_2 equivalent to 1.2 times the stoichiometric quantity required for the overall removal of COD is constantly dosed using a pump along the electrolysis. For a cell such as that of Figure 31a, a Ti rod coated with a DSA of IrO_2−RuO_2 was employed as an anode, surrounded by a cylindrical stainless steel cathode, with a ratio between the anode and the cathode areas of about 1:10.[261–265] The larger cathode area promoted the cathodic reduction of Fe^{3+} and minimized the anodic oxidation of Fe^{2+}, with the best performance for Fe^{2+} electrogeneration at pH 2.0 (without $Fe(OH)_3$ precipitation) being provided for a stainless steel cathode rather than using other materials such as Ti, Pb, and graphite. Using this cell for the degradation of 5 L of a high-strength hexamine-containing wastewater from a petrochemical industry with 17 100 mg L^{-1} COD, for example, Chou et al.[261] reported a COD decay as high as 94% by adding 380 g L^{-1} of H_2O_2 for 5 h when operating at optimum conditions of pH 2.0, 5 g L^{-1} of ferric sulfate and cathodic current density of 10 mA cm^{-2} by recirculating the effluent at a flow rate of 9 L min^{-1}. Note that the use of pH values higher than 2.5 leads to extensive precipitation of $Fe(OH)_3$ because of the continuous OH^- production at the cathode from reaction 44 with the consequent loss in performance of the system.

Kinetic modeling for the Fered−Fenton process in the above electrolytic system was reported by Anotai et al.,[264] who proposed the complex eq 72 for the initial decay rate (r_0) of aniline including all the species participating in the process

$$r_0 = 2.6\times10^{-3}[Fe^{2+}]^{0.08}[H_2O_2]^{-0.14}[\text{aniline}]^{0.46} \quad (72)$$

where aniline approaches half-order, suggesting a process controlled by the attack of $^{\bullet}OH$. In contrast, Rao et al.[267] found a pseudo-first-order removal for the dye Reactive Black 5.

More recently, the same group utilized the cell depicted in Figure 32a with double- or single-cathode configurations for the Fered−Fenton destruction of 3.5 L of 10 mM benzene sulfonic acid (BSA) with 8 mM Fe^{2+} and 166 mM H_2O_2 at pH 2.0.[266] The recently patented double-cathode configuration[269] was proven to be superior because it provides faster Fe^{2+} electrogeneration, which accelerates the mineralization rate of pollutants. Figure 32b illustrates the TOC abatement during the treatment of the above BSA solution using the latter geometry for chemical Fenton and Fered−Fenton processes at an anodic current density of 7.58 mA cm^{-2} and cathodic current density of 7.1 mA cm^{-2}. As can be seen, TOC is reduced by 46% and 64% after 480 min of Fenton and Fered−Fenton, respectively, although no significant enhancement of mineralization is attained after 240−300 min because of the formation of byproducts that cannot be oxidized with $^{\bullet}OH$. The higher performance of Fered−Fenton is then due to the continuous regeneration of Fe^{2+} at the surface of both cathodes.

Also noticeable is a variant of SEF proposed by Yasman et al.,[270] who degraded 10 mL of 1.2 mM 2,4-D and 2,4-dichlorophenol solutions in 0.5 g L^{-1} Na_2SO_4 at pH 3.0 and 25 °C using a Ni/Ni cell with a 20 kHz transducer dipped into the solution and working at 100 mA. After adding 2 mM Fe^{2+} and 30 mM H_2O_2, the overall destruction of both

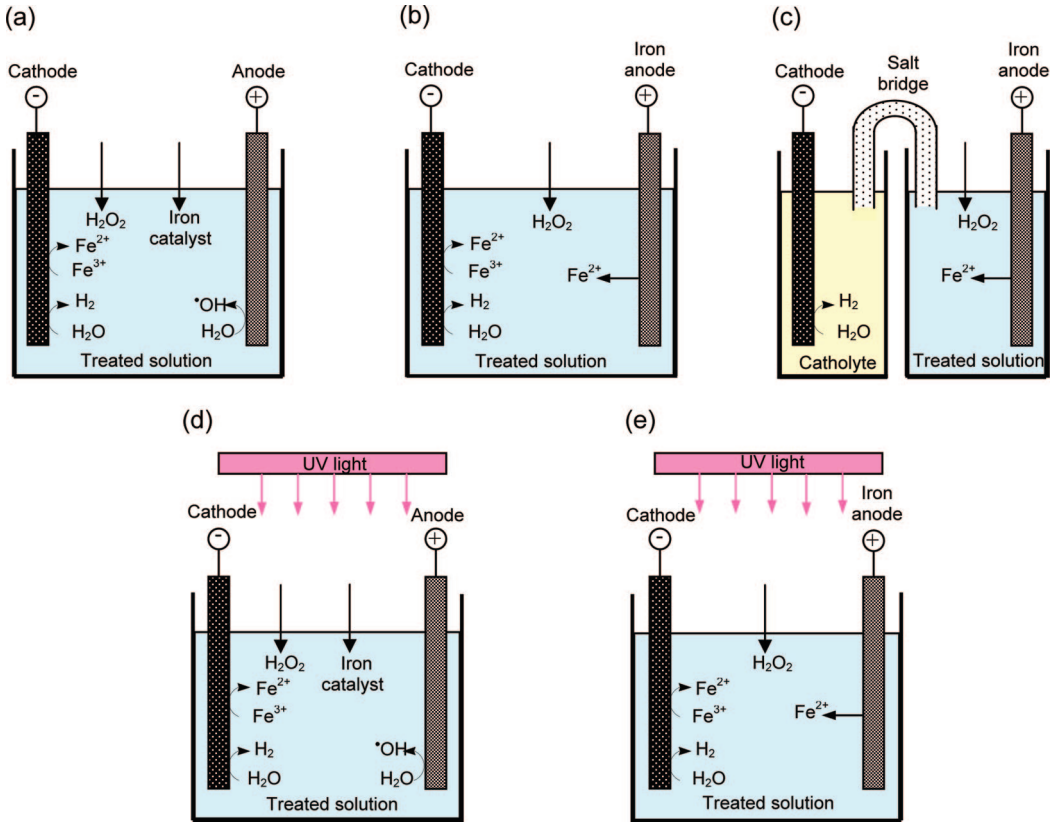

Figure 31. Schematic representation of bench-scale two-electrode cells and main reactions taking place in EAOPs with addition of H_2O_2 to the solution: (a) Fered−Fenton, (b) ECP, (c) AFT, (d) photoassisted Fered−Fenton, and (e) photoassisted ECP.

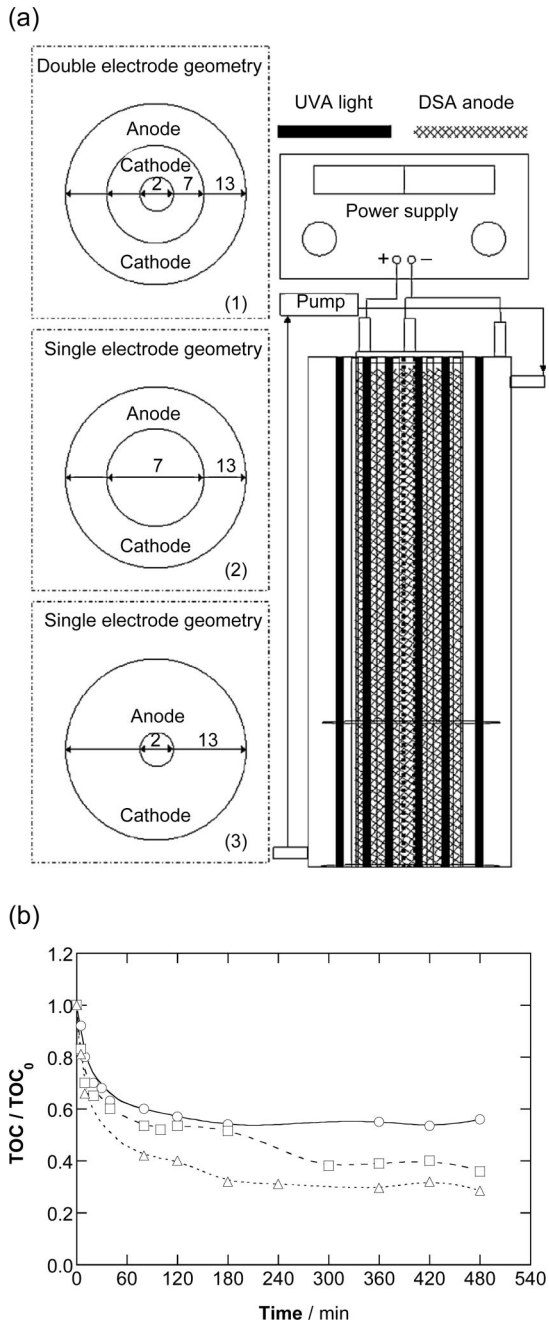

Figure 32. (a) Experimental setup of a cylindrical tank reactor used for the Fered−Fenton treatment of organics wastewaters under galvanostatic conditions. The reactor (13 cm diameter × 35 cm height) contained a Ti/IrO_2−RuO_2 anode and two or one stainless steel cathodes (diameters in cm) with the 1, 2, or 3 configuration. The solution recirculated with a pump, and in photoassisted Fered−Fenton it was illuminated with 16 UVA lamps of 3 W (λ_{max} = 360 nm). (b) Normalized TOC decay for 3.5 L of 10 mM benzene sulfonic acid (BSA) at pH 2 with addition of 8 mM Fe^{2+} and 166 mM H_2O_2 using configuration 1 of Figure 32a. Process: (○) Fenton process (without current), (□) Fered−Fenton, and (△) photoassisted Fered−Fenton by applying 7.1 mA cm^{-2} at the cathodes and 7.58 mA cm^{-2} at the anode. Adapted with permission from ref 266. Copyright 2008 Elsevier.

initial pollutants was achieved in 10 min of such treatment, while very low removal was found from the chemical Fenton process.

These results indicate that Fered−Fenton differs from the previously discussed EF in that it uses a much higher content of iron ions, which act as reactants rather than catalysts, in contrast to what was observed for EF and combined EF methods.

6.2. Electrochemical Peroxidation (ECP) Process

A large number of papers have been published on water remediation using electrolytic cells with a sacrificial iron (or steel) anode for Fe^{2+} electrogeneration from anodic dissolution by reaction 66 and an inert cathode where H_2 is produced from H_2O reduction, in which H_2O_2 is externally added to the treated solution to oxidize the organic matter with $^{\bullet}OH$ formed from Fenton's reaction 1. Although several authors have considered these processes as a kind of "electro-Fenton",[56] they should be regarded as a variant of the PC method described in section 5.1. In this context, two main technologies, electrochemical peroxidation (ECP), which is discussed in the present section, and anodic Fenton treatment (AFT), which will be analyzed in section below, have been developed. The difference between both technologies simply arises from the use of undivided or divided cells, respectively, as exemplified in the tank reactors given in Figure 31b and 31c, respectively. This allows the cathodic regeneration of Fe^{2+} from reaction 43 in ECP, a process that cannot take place in AFT. In both cases, the controlled Fe^{2+} electrogeneration can help minimize the extent of both the parasitic reaction 17 and the accumulation of iron sludge, but in most cases, coagulation with the $Fe(OH)_3$ precipitate formed depending on pH and the applied current can be an important alternative route for organics removal.

ECP is a term derived from the classic Fenton peroxidation or chemical Fenton's process.[56] Strictly speaking, the process was first proposed by Lemley's group as an electrochemical peroxide treatment,[271–273] which was tested for the degradation of synthetic solutions of several herbicides at circumneutral pH using a cell such as that of Figure 31b equipped with iron or steel electrodes under galvanostatic conditions. This team found that ECP provided greater COD removal than direct electrocoagulation and that the process improved when carrying out stepwise dosing of H_2O_2 during electrolysis instead of a single initial addition, because the controlled addition of H_2O_2 allows minimizing the waste of $^{\bullet}OH$ by reaction 9. Another key operating factor was the $[Fe^{2+}]/[H_2O_2]$ ratio utilized, which was calculated on the assumption that eq 66 for Fe dissolution verifies Faraday's law and all the Fe^{2+} thus generated reacts with H_2O_2 via Fenton's reaction 1. Figure 33a illustrates the concentration decay of a 0.14 mM solution of the herbicide atrazine at an initial pH 5.5 using thick cold-rolled steel plates as electrodes at 0.3 A under continuous dosing of H_2O_2. The fastest and total disappearance of the herbicide can be observed at a constant $[Fe^{2+}]/[H_2O_2]$ ratio of 1:5 where maximum $^{\bullet}OH$ production from Fenton's reaction 1 is attained. A lower 1:1 ratio promotes a quite poor atrazine removal due to the slow generation of the radical oxidant, whereas a higher 1:10 ratio decelerates the process probably because of the increase in the rate of the parasitic reaction 9.

Despite the previous works by Lemley and co-workers, ECP has been patented by Chiarenzelli's group,[274] who successfully applied this method to the treatment of real wastewater.[274–277] Bench- and pilot-scale experiments were made by adding H_2O_2 to effluents of pH 3.0−5.3 through supply tubes to electrolytic cells equipped with large sacrificial iron-containing electrodes such as cast iron or mild steel electrodes. AC or oscillating DC between 0.1 and 1

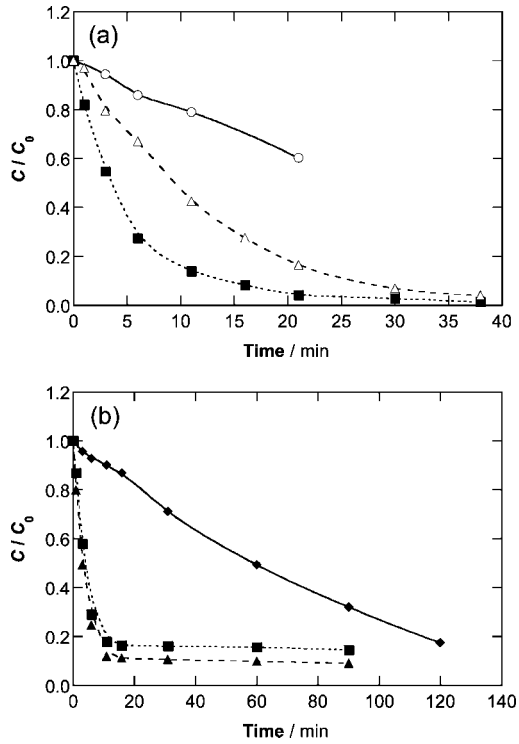

Figure 33. (a) Normalized concentration decay for atrazine during the ECP treatment of 400 mL of 0.14 mM herbicide solutions in 0.5 g L^{-1} NaCl of pH 5.5 using an undivided tank reactor such as that of Figure 31b with thick cold rolled steel plates as electrodes, 0.3 A, and room temperature under continuous dosing of 0.0018 M H_2O_2 to maintain a constant $[Fe^{2+}]/[H_2O_2]$ ratio of (○) 1:1, (■) 1:5, and (△) 1:10. (b) Normalized atrazine concentration decay for the same solution with stepwise addition of 0.025 M H_2O_2 for treatment by (◆) UVA irradiation, (▲) ECP process at 0.3 A for 5 min, and (■) photoassisted ECP process at 0.3 A for 5 min under UVA irradiation using a cell such as that of Figure 31e. Reproduced with permission from ref 273. Copyright 1998 American Chemical Society.

cycle s^{-1} current up to 15 A was applied to increase the reactive surface area of electrodes, keeping them clean and free from fouling. Excellent removal of volatile organic compounds (VOCs) and polychlorinated biphenyls (PCBs) from liquids or adsorbed soils, sediments, and sludges was obtained with minimal quantities of iron sludge formed. This group extended the ECP method to decontaminate solutions with heavy inorganic metallic ions, showing the effective removal of As, Cr, Pb, Se, and V at pH 3.5−4.6 using a cell similar to that of Figure 31b with mild steel electrodes.[278–280]

Other authors also employed the ECP process, sometimes called the EF-Feox process, for degrading synthetic[281,282] and real[283–292] wastewaters. The most relevant results obtained in these works will be presented in section 7 in a discussion about their environmental applications.

6.3. Anodic Fenton Treatment (AFT)

6.3.1. Fundamentals

AFT was introduced by Saltmiras and Lemley[293] with the aim of improving the performance of ECP. These authors proposed the use of a divided cell to avoid the negative effect of the formation of OH^- at the cathode from water reduction by reaction 44, which raises pH and is then against the optimum conditions of $^{\bullet}OH$ production from Fenton's reaction 1. This process has been extensively developed for water remediation by Lemley's group, who considered three different bench-scale electrolytic systems. The salt bridge cell schematized in Figure 31c[293–298] was utilized as a first step. An H-type two-compartment cell with an anionic or cationic membrane between the anolyte and catholyte and magnetic stirring was further explored.[299–307] Recently, a flow cell composed of two electrochemical half cells separated by an anionic membrane with continuous recirculation of the anolyte was tested.[308–310] All these systems contained an iron plate with an area of 20−30 cm^2 as an anode and a graphite rod as a cathode and were used to treat small volumes of 90−350 mL of anolyte with low contents of organic pollutants and NaCl as the background electrolyte at pH 2.0−3.0 and a constant current of 0.01−0.24 A for short time periods of 2−40 min under continuous H_2O_2 addition with a peristaltic pump. Under these conditions, no significant changes of pH were found and very low amounts of $Fe(OH)_3$ sludge were formed. In most trials, the fastest and overall removal of starting POPs and their primary byproducts was obtained with an $[Fe^{2+}]/[H_2O_2]$ ratio of 1:10, but a low degree of mineralization was usually attained according to those few works where organic carbon was monitored. The NaCl content in the catholyte and anolyte and its ratio determined the process efficiency in membrane cells because Cl^- can react with $^{\bullet}OH$, lowering the removal rate of organics. For example, based on tests using H-type cells with an anionic or cationic exchange membrane to degrade 200 mL of 0.1 mM of the carbamate insecticide carbaryl at 0.05 A for 5 min, Wang and Lemley[299] demonstrated that the anionic membrane provided a better performance than the cationic one because it prevented the loss of protons from the anolyte. The best treatment efficiency with 100% removal of carbaryl was obtained for optimal NaCl concentrations of 0.02 M in the anolyte and 0.08−0.10 M in the catholyte.

6.3.2. AFT Modeling

Lemley and co-workers proposed semiempirical kinetic modeling to describe the time course of reactants in AFT. Since Fe^{2+} and H_2O_2 are continuously injected into the anolyte, a rapid accumulation of both species with electrolysis time was always found until a steady state was reached (when their production/addition and destruction rates became equal). This behavior was justified, for example, by Kong and Lemley,[308] who elaborated a model based on the control of Fe^{2+} and H_2O_2 consumption from Fenton's reaction 1 that was successfully used in modeling the profiles of both reagents during the treatment of 90 mL of 0.1 mM carbaryl in 0.08 M NaCl as the anolyte of a flow cell with an $[Fe^{2+}]/[H_2O_2]$ delivery ratio of 1:5 at 0.02 A and liquid flow rate of 7.5 mL min^{-1} for 40 min. For a similar cell, Zhang and Lemley[309] also developed a semiempirical model with the Kintecus modeling program that showed a good fit for the evolution of Fe^{2+}, total iron species, and H_2O_2 during the degradation of 100 mL of 202.6 μM of the insecticide *N*,*N*-diethyl-3-methylbenzamide (DEET) in 0.02 M NaCl at a $[Fe^{2+}]/[H_2O_2]$ ratio between 1:5 and 1:20, 0.05 A, and liquid flow rate from 9.4 to 37.4 mL min^{-1} for 20 min. Moreover, in this study the $^{\bullet}OH$ concentration in the bulk was determined by the competition kinetics method using benzoic acid up to 25 μM as a chemical probe for a $[Fe^{2+}]/[H_2O_2]$ ratio of 1:10 at a liquid flow rate of 27.4 mL min^{-1}, assuming that both organics react with $^{\bullet}OH$ following a second-order kinetics. Figure 34 shows that $^{\bullet}OH$ evolves to a steady-state content of about 7.5×10^{-12} M, and its profile

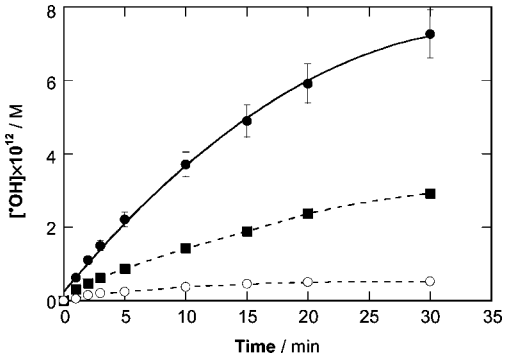

Figure 34. Concentration of hydroxyl radical accumulated in 100 mL of solutions with the insecticide *N*,*N*-diethyl-3-methylbenzamide (DEET) in 0.02 M NaCl degraded in the anolyte of a flow AFT reactor with a 20 cm^2 iron plate anode, continuous H_2O_2 addition, and a liquid flow rate of 27.4 mL min^{-1}, determined by the competition kinetics method with benzoic acid as a chemical probe. DEET concentration, current: (●) 202.6 μM, 0.05 A; (■) 501.5 μM, 0.05 A; (○) 202.6 μM, 0.01 A. The solid line represents the fitting to an exponential model, and the dotted lines fit to experimental points. Adapted with permission from refs 309 and 310. Copyright 2006 and 2007, respectively, American Chemical Society.

fits well with an exponential model established by the authors. This figure also depicts the lower •OH concentration obtained by Zhang and Lemley under comparable conditions for 501.5 and 202.6 μM of DEET at 0.05 and 0.01 A, respectively.[310] These trends indicate the greater efficiency of the flow cell when treating higher pesticide contents, producing smaller amounts of •OH if less Fe^{2+} is generated at lower applied current.

Lemley and co-workers also modeled the decay kinetics of POPs in AFT because most of them did not fit with the typical second-order reaction usually found in EF systems. They first developed the so-called inverted S-shaped model to successfully explain the removal of the herbicide 2,4-D in a salt bridge cell, which showed a low decay rate at the beginning and end of the process but a higher rate at the middle stages.[294] This model also served to predict the inverted S-shaped decay of 2,4-D in mixtures with other organics, using this compound as a competition substrate for determining a k_2 value of 8.2×10^9 M^{-1} s^{-1} for alachlor, 3.7×10^9 M^{-1} s^{-1} for atrazine, 8.4×10^9 M^{-1} s^{-1} for aldicarb, 9.6×10^9 M^{-1} s^{-1} for thymol, 2.0×10^9 M^{-1} s^{-1} for toluene, 1.6×10^9 M^{-1} s^{-1} for methanol, 3.8×10^9 M^{-1} s^{-1} for benzoic acid, and 6.0×10^9 M^{-1} s^{-1} for benzyl alcohol. The inverted S-shaped model was further validated for the AFT degradation of the pesticide diazinon,[296] as well as of various carbamate insecticides[300,301] and chloroacetanilide herbicides,[303,305] but it had to be modified to explain the influence of the interaction between Fe^{3+} and triazine and triazinone herbicides, such as metribuzin, ametryn, simetryn, prometon, terbumeton, atrazine, cyanazine, and metamitron.[302] This modified model was also suitable to fit the carbaryl decay in the presence of a surfactant owing to the formation of a complex carbaryl-surfactant-Fe(III) interfering with the kinetics.[307] A pseudo-first-order model was later proposed to describe the kinetics of herbicide decays in the presence of humic acid,[303] which was based on the blockage of Fe^{2+} by the increase in pH by the influence of this acid and its chelating properties. This vast experience in AFT modeling was very valuable for the studies recently carried out on soil remediation because it was demonstrated that 2,4-D in soil slurries follows a two-stage kinetics that evolves from a pseudo-first-order to an inverted S-shaped model as a result of the presence of •OH scavengers and the lower herbicide concentration with prolonging electrolysis time.[306]

Two other models were designed for simulating the kinetic data obtained in flow cells. A semiempirical differential equation based on hydraulic and rate parameters and solved by using a fourth-order Runge−Kutta method was proposed and validated for the decay of alachlor, carbofuran, diazinon, metalachlor, and 2,4-D.[308] Finally, the semiempirical model introduced at the beginning of this section dealing with the use of the Kintecus modeling program[309] was further developed by combining the reaction mechanism of the Fenton system with that of the organic pollutant, thereby providing kinetic profiles to justify the decay of the insecticide DEET. This Kintecus model was also positively validated for the AFT treatment of nine amide compounds under similar conditions, showing a good correlation between the experimental and the modeling data.[310]

6.4. Photocombined Processes

The combination of Fered−Fenton with simultaneous UVA illumination of the effluent has been recently patented for the electrolytic system with a double-cathode geometry and 16 UVA lamps of 3 W depicted in Figure 32a.[311] The main electrode reactions in this photoassisted Fered−Fenton are schematized in Figure 31d and are the same as in the case of Fered−Fenton (see Figure 31a). The action of UVA light is related to the fast photodecomposition of complexes of Fe(III) with final carboxylic acids from reaction 28. Ting et al.[266] reported that the photoassisted Fered−Fenton treatment of organics from wastewater with the above configuration showed a better performance than analogous treatment in the dark. As an example, Figure 32b shows that UVA light promotes the mineralization of 10 mM BSA up to 72% in 480 min, a value higher than the 64% found for Fered−Fenton. The higher oxidation of the former was ascribed to the enhanced removal of persistent Fe(III)−oxalate complexes under UVA irradiation via reaction 29. On the other hand, Huang et al.[265] used the setup with a $Ti-IrO_2-RuO_2$ anode surrounded by a cylindrical stainless steel cathode described in section 6.1, in which a 45 W UVA lamp was placed at the top to irradiate 1.5 L of a solution containing the dye Reactive Black B. About 98% mineralization removal was achieved under illumination, which was higher than 93% reported under Fered−Fenton conditions.

A limited number of papers have also explored the ECP treatment of organics photoassisted with UVA[272,273] or UVC[292] light. It was found that this photocombined method was not much more efficient than ECP because electrolyses were carried out without pH regulation (which rapidly attained values > 7.0), causing the precipitation of $Fe(OH)_3$ with coagulated organics and stopping the production of •OH from Fenton's reaction 1. Moreover, irradiation was mainly adsorbed by $Fe(OH)_3$ precipitate (as explained for PPC in section 5.3). Figure 33b illustrates that 400 mL of a 0.14 mM atrazine solution of pH 5.5 is slowly degraded by dosing 0.025 M H_2O_2 under UVA light, seeing its concentration only reduced by 83% in 120 min.[273] In contrast, when the same solution is treated by ECP or photoassisted ECP with UVA light using cells such as those of Figure 31b and 31e with steel electrodes at 0.3 A for 5 min, a very rapid herbicide removal of up to 86% and 82% in 16 min, respectively, can be observed. Under these conditions, atrazine decays at a

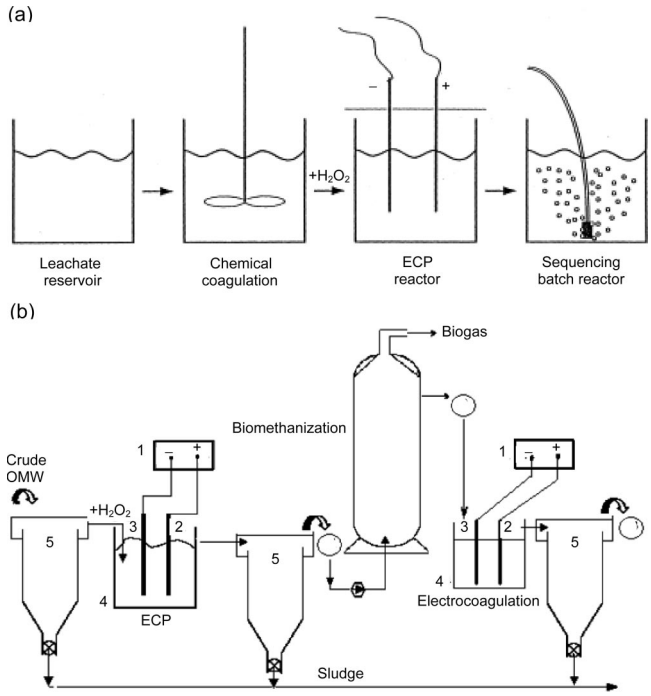

Figure 35. (a) Flow process of a chemical coagulation−ECP−biological treatment of landfill leachate. Reprinted with permission from ref 312. Copyright 2000 Elsevier. (b) Schematic representation of a bio-ECP process for the treatment of olive oil mill wastewater (OMW): (1) Power supply, (2) cast iron anode, (3) cast iron cathode, (4) electrolytic cell, and (5) sedimentation tank. Adapted with permission from ref 313.Copyright 2006 Elsevier.

similar rate in the absence and presence of UVA light, since the main oxidant is $^{\bullet}OH$ formed from Fenton's reaction 1, but over longer periods both processes become inefficient because the pH is about 7.8 and this oxidant is not generated. A more spectacular behavior has been reported by Altin[292] when treating 500 mL of a landfill leachate of 2350 mg L^{-1} COD with 3 g L^{-1} H_2O_2 at pH 3.0 by ECP and photoassisted ECP with 1.4 W m^{-2} UVC irradiation using cells with similar configurations to those of Figure 31b and 31e, respectively, containing two pairs of cast iron anodes and cathodes and applying 2.5 A. He found that the photoassisted process was the best performing one, giving 94% COD and 97% color removal in 20 min. However, these yields gradually decreased over longer time periods because of the slow dissolution of organic matter retained on the large precipitate of $Fe(OH)_3$ formed because the pH increased to values >8.0.

6.5. Bio-ECP Remediation

A greater reduction in the organic load of wastewater is feasible by coupling the ECP process with a more inexpensive biological post-treatment. However, this interesting bio-ECP remediation has only been tested for some real effluents such as landfill leachate[312] and olive oil mill wastewater (OMW).[313–315] Figure 35a shows a flow process of three steps involving chemical coagulation, the ECP process, and a sequencing batch reactor (SBR), which was designed by Lin et al.[312] as an efficient and cost-effective treatment of a leachate effluent. It contained about 2000 mg L^{-1} COD, which was initially reduced by over 50% by chemical coagulation with addition of polyaluminium chloride, while its pH decreased from 8.1 to 4.1. Further ECP degradation of 1 L of the chemically treated wastewater using 22.6 cm^2 cast iron electrodes with the addition of 500 mg L^{-1} H_2O_2 for 30 min with a power consumption of about 6 kWh gave overall decolorization and 295 mg L^{-1} residual COD at pH 5.2. Finally, SBR treatment of the resulting wastewater with activated biological sludge continuously aerated at an air flow rate of 25 L min^{-1} for 9 h led to water with less than 90 mg L^{-1} COD and enough quality to be directly discharged to a natural water body. More recently, Khoufi et al.[313,314] proposed the combination of ECP, biomethanization, and electrocoagulation processes for the overall detoxification of OMW. The lab-scale plant utilized for the treatment of 3 L of these wastewaters containing 100 g L^{-1} COD and 12 g L^{-1} polyphenols is depicted in Figure 35b, where the biogas produced from anaerobic biotreatment can be used as an energy source. The starting ECP treatment of the raw OMW at pH 4.0 was performed with 150 dm^2 iron electrodes at 1.8 A dm^{-2} and by adding 1 g L^{-1} H_2O_2 for 2 h, giving rise to the removal of 26% COD and 66% polyphenolic compounds, thus decreasing the toxicity to 67% and improving the efficiency of the subsequent anaerobic digestion. The second step, i.e., the biomethanization process, reduced the toxicity to 45% and final electrocoagulation treatment of the anaerobic digestion effluent under conditions similar to those of ECP but without the H_2O_2 addition, allowing the almost total reduction of COD and complete detoxification with removal of suspended solids and lipid content, improving the quality of the treated water for potential reuse. Worth noting, this combined process was also tested at a large scale, with a 25 000 L digester, demonstrating its technical feasibility for industrial application.

6.6. Electrochemical Fenton Methods with Indirect H_2O_2 Production

Pulsed high-voltage electrical discharge processes have been successfully applied to the destruction of some POPs on the lab scale.[316–319] This nonthermal plasma method produces a cocktail of reactive species such as high-energy electrons, $^{\bullet}OH$, $H^{\bullet}$, $O^{\bullet}$, and $O_2^{\bullet-}$, as well as long-lived active molecules such as O_3, H_2O_2, excited-state neutral molecules, and ionic species, which can oxidize organic pollutants. The addition of Fe^{2+} or Fe^{3+} to the aqueous medium strongly accelerates the degradation rate of organics because of the extra production of $^{\bullet}OH$ with generated H_2O_2 from Fenton's reaction 1.[317–319] The main disadvantage of this plasma-assisted Fenton process is the excessive energy requirement for its application at an industrial scale. To clarify the oxidation ability of the process, Grymonpré et al.[317] studied the degradation of 450 mL of 100 mg L^{-1} of phenol at pH 5.0, with the conductivity adjusted with either KCl or $FeSO_4$ at 150 μS cm^{-1}, using a stirred and thermostatted cylindrical cell equipped with five high-voltage Pt point electrodes and a ground RVC disk electrode of 8 cm diameter with injection of an O_2 flow and generation of pulsed discharge plasma with 45 kV voltage amplitude, 60 Hz pulse frequency, and 2 nF capacitance. The quickest degradation process was obtained in the presence of Fe^{2+}, with total phenol removal in 45 min and 53% TOC reduction in 60 min. Similarly, Hao et al.[319] studied the destruction of 100 mL of 100 mg L^{-1} *p*-chlorophenol solutions in 0.1 M KCl containing 0.2 mM Fe^{2+} or Fe^{3+} at pH 6.5−7.0. After 40 min of application of the pulsed discharged plasma at 14 kV and 150 Hz, they found a decay in pH up to 3.8−4.2 due to the formation of acidic byproducts and overall removal of *p*-chlorophenol, which disappeared exhibiting a pseudo-first-order constant rate of 1.6×10^{-3} s^{-1} in the absence of iron ions, increasing

to 2.5×10^{-3} s^{-1} with Fe^{3+} and 2.9×10^{-3} s^{-1} with Fe^{2+}. The enhancement of the process in the presence of Fe^{3+} was ascribed to its fast reduction to Fe^{2+}, suggesting that continuous regeneration of this ion is crucial in plasma-assisted Fenton processes for ensuring great production of oxidant •OH from Fenton's reaction 1.

A very different electrochemical Fenton process arises from the combination of anodic generation of H_2O_2 in AO with Fenton's reaction chemistry. Such a possibility was explored by Saracco et al.[320] for the treatment of 4 L of 10 mg L^{-1} of coumaric acid in 0.01 M Na_2SO_4 at pH ca. 3.0 and 25 °C as the anolyte of a divided flow cell with a 200 cm^2 Ti/Pt or a PbO_2 anode and a 200 cm^2 stainless steel cathode separated by an anionic membrane under the application of 20 mA cm^{-2} for 240 min in batch operation mode. H_2O_2 accumulation up to about 6 mM for Ti/Pt or 0.3 mM for PbO_2 was detected in the anolyte after 2 h of AO coming from the recombination of •OH by reaction 48 or hydrolysis of $S_2O_8^{2-}$, formed from reactions 50 and 51, to HSO_4^- by reaction 73:

$$S_2O_8^{2-} + 2H_2O \rightarrow 2HSO_4^- + H_2O_2 \qquad (73)$$

The half-conversion time for coumaric acid decreased from 110 to 70 min for Ti/Pt and 283 to 128 min for PbO_2 when 0.4 g L^{-1} $Fe_2(SO_4)_3$ was added to the anolyte, indicating the formation of •OH from Fenton's reaction 1 because Fe^{2+} is regenerated mainly via Fenton-like reaction 3. Unfortunately, no more data for this combined process are available to assess its viability for wastewater treatment. However, it is worth noting that some processes commented on in section 4.2.3 that combine the use of high oxidation power anodes with H_2O_2 electrogeneration may also take advantage of the anodic production of H_2O_2, although its contribution has been disregarded because of the greater accumulation of H_2O_2 from the cathode.[180]

7. Environmental Applications

EF and related electrochemical technologies are being developed to remove POPs from wastewater with the aim of preserving the aquatic environment. Table 6 summarizes the organic compounds treated in synthetic solutions by these methods. In accordance with this classification, this section will analyze the degradative behavior of pesticides, dyestuffs, PPCPs, and industrial pollutants with a special emphasis on the oxidation intermediates detected, reaction pathways proposed, and trends for the decay of initial pollutants or total organic content. The last section is devoted to detailing the main results obtained from treating real wastewater.

7.1. Pesticides

Pesticides are substances or mixtures of substances designed to prevent, destroy, repel, or mitigate pests such as weeds (herbicides), insects (insecticides), fungi (fungicides), or rodents (rodenticides). They are widely used in agricultural activities to protect crops and livestock, usually by acting as plant regulators, defoliants, or desiccants. They are also used to maintain roads and railroads networks, as well as by private individuals to upkeep their gardens or the surroundings of their places of residence.[4] Unfortunately, these toxic compounds can move from the application site into aqueous compartments, giving rise to high levels of contamination in groundwater aquifers and surface water.[4,6,33,34] In addition, organic pesticides contained in wastewater are biorefractory and cannot be easily removed by conventional oxidation methods in municipal sewage treatment plants, thus worsening the environmental situation. In this context, EAOPs based on Fenton's reaction chemistry can be an alternative for treating these kinds of effluents because they have been proven to be very effective in destroying a large variety of these POPs, even allowing the complete mineralization of their oxidation intermediates. Although preliminary work dealing with the application of these EAOPs for pesticide decontamination was started using a toxic Hg cathode aiming at H_2O_2 electrogeneration,[152] most papers have utilized environmentally friendly systems such as EF and combined EF processes with carbon-felt, RVC, or GDE cathodes as well as ECP and AFT treatments, as discussed below.

Table 6. Classification of Pure Organic Compounds Contained in Synthetic Solutions Treated by EAOPs Based on Fenton's Reaction Chemistry

type of pollutant	family or group name
	pesticides
herbicides	benzoic acids[226,230]
	carbanilates[191]
	chloroacetanilides[271,273,303,305]
	diazine[197]
	dinitroanilines[295]
	dinitrophenols[256]
	imidazolinones[193,198]
	phenoxyacetic acids[121,146,148,150,152,153,180,184,223–226,228,229,256,257,294,306]
	phenoxypropionic acids[152,153,234,235]
	picolinic acids[190,271]
	triazines[271,273,297]
	triazinones,[302,304]
	triazoles[325]
	ureas[194,197,203,322,324]
insecticides	carbamates[153,197,204,299–301,307,308]
	insect repellents[309,310]
	organochlorines[192,323]
	organophosphorus[153,186,272,296,321]
fungicides	aliphatics[204]
	dithiocarbamates[204]
rodenticides	coumarins[153]
	indandiones[153]
	dyestuffs
	acid[119,122,124,127,187,210,219,242,329–334,337,338]
	basic[114,171,195,199,206,255,258,332]
	direct[195,196,243,318]
	disperse[256]
	food color[199]
	mordant[318]
	reactive[109,195,265,267,318,335,336]
	solvent[119]
	PPCPs
	NSAIDs[161,185,231,236]
	antibiotics[173,237,343]
	blood lipid regulators derivatives[152,153,232,233]
	neuroprotectors[120,343]
	industrial pollutants
	aliphatics
	acyclic[119,123,124,159,189,293,298]
	cyclic[158,259]
	aromatics
	anilines[113,119,124,172,211,212,218,221,227,247,264,346,355]
	benzenes[116,117,124,160,162–165,167,168,209,213,214,220,266,276,277,282]
	cresols[124,149,238]
	heteroaromatic derivatives[357,358]
	methylated benzenes[155–157,165,356]
	phenols[118,119,124,143,147,167,168,181,205,222,248,249,257,268,286,288,317,319,320,345–354]

7.1.1. EF with Carbon-Felt Cathode

Oturan and co-workers extensively studied the mineralization process and oxidation intermediates of a high number of aromatic pesticides under the application of the EF process

using divided and undivided cells with a high specific surface area carbon-felt cathode surrounding the anode. As explained in previous sections, such a cathode generates H_2O_2 from reaction 32 and, at the same time, keeps an efficient Fe^{2+} concentration in the bulk from reaction 43, giving a rapid and almost complete destruction of organic pollutants with •OH produced from Fenton's reaction 1. Hydroxylation of pesticides has been widely ascertained, and their absolute second-order rate constant has been determined by the competition kinetics method, as described in section 4.3.3 and shown in Table 4.

7.1.1.1. Divided Cells. Former studies were performed with a three-electrode divided cell similar to that in Figure 17a. Electrolyses were carried out with 125−150 mL of O_2-saturated aqueous H_2SO_4 solutions with 0.5−2 mM Fe^{3+} or Fe^{2+} at pH 2.0−3.0 and $E_{cat} = -0.5$ V/SCE using a Pt anode. The first paper of Oturan[121] reported that the EF process with 1 mM Fe^{3+} yielded the rapid and almost total mineralization (>95% TOC decay) of 1 mM of the phenoxyacetic herbicide 2,4-D after consuming 2000 C, although removal of the initial pollutant only required consumption of 700 C. Reversed-phase HPLC analysis of electrolyzed solutions revealed the initial generation of hydroxylated derivatives such as 2,4-dichlorophenol, 2,4-dichlororesorcinol, 4,6-dichlororesorcinol, 2-chlorohydroquinone, and 1,2,4-trihydroxybenzene. The formation of these byproducts at the early stages of the treatment agrees with the expected nonselective attack of •OH on the aromatic ring of 2,4-D, which is accompanied by dechlorination. Similarly, these intermediates can react with •OH to give polyhydroxylated compounds and quinones, which in turn undergo the attack of the oxidant that causes the cleavage of the benzene moiety, producing short-chain carboxylic acids.

The fast decay of the initial pollutant and formation of hydroxylated derivatives was confirmed in further work[153] on the analogous treatment of a chlorophenoxyacetic herbicide such as 2,4,5-T, chlorophenoxypropionic herbicides such as MCPP, CPMP (2-(4-chlorophenoxy)-2-methylpropionic acid), and 2,4-DP (2-(2,4-dichlorophenoxy)propionic acid), the carbamate insecticide bendiocarb (2,2-dimethyl-1,3-benzodioxol-4-yl methylcarbamate), the rodenticides coumatetralyl (4-hydroxy-3-(1,2,3,4-tetrahydro-1-naphthyl)-coumarin) and chlorophacinon (2-[2-(4-chlorophenyl)-2-phenylacetyl]indan-1,3-dione), as well as the organophosphorus insecticide pirimiphos-methyl (*O*-(2-diethylamino-6-methylpyrmidin-4-yl)-*O*,*O*-dimethylphosphorothioat). For the organochlorine insecticide PCP (pentachlorophenol),[192] 82% mineralization of a saturated solution (0.03 mM) of pH 3.0 was found after consumption of 1500 C, attaining a total release of all chlorine as Cl^- at 600 C. Tetrachloro-*o*-benzoquinone and tetrachloro-*p*-benzoquinone were identified by HPLC as aromatic intermediates that disappeared along with starting PCP at 200 C. The much slower release of Cl^- suggests that dechlorination also takes place during the degradation of chlorinated aliphatic compounds formed upon cleavage of the benzenic structure of chlorinated aromatic intermediates.

The notorious effectiveness of EF was also corroborated for the imidazolinone herbicides imazapyr (2-(4-isopropyl-4-methyl-5-oxo-2-imidazolin-2-yl)nicotinic acid)[193] and imazaquin (2-(4-isopropyl-4-methyl-5-oxo-2-imidazolin-2-yl)quinoline-3-carboxylic acid[198] and three organophosphorus insecticides.[321] In the former case, the COD of a 0.1 mM imazapyr solution with 0.5 mM Fe^{2+} at pH 3.0 was rapidly reduced by 95% after consuming 300 C, while the initial herbicide disappeared at 100 C. In the latter case, treatment of 0.32 mM malathion, 0.50 mM tetraethyl-pyrophosphate, and 0.09 mM parathion ethyl solution with 2 mM Fe^{3+} in 0.01 M H_2SO_4 yielded more than 80% COD decay at 6000 C.

7.1.1.2. Undivided Cells. More recently, Oturan's group extended its research to using an undivided Pt/carbon felt cell such as that in Figure 16a under experimental conditions similar to those of the previous divided one, with optimization of the catalyst concentration.[194,322,323] Thus, for 125 mL of an O_2-saturated 40 mg L^{-1} diuron solution with 0.5 mM Fe^{3+} in H_2SO_4 of pH 3.0 at 100 mA,[194] it was found that the initial herbicide disappeared in 10 min, whereas TOC was reduced by 93% at 1000 C. Additionally, the evolution of the toxicity of diuron solutions treated by EF has recently been discussed in terms of the intermediates formed along the electrolysis.[322] More work by the same group aiming at soil remediation explored the possibility of treating soil extract solutions containing high PCP loads,[323] based on the addition of hydroxypropyl-β-cyclodextrin (HPCD) to soil wash effluents to increase by up to 3.5 times the PCP concentration during the water flush of the soil. An HPCD content of 5 mM in 125 mL of an O_2-saturated solution with 0.5 mM Fe^{3+} at pH 3.0 accelerated the decay rate of 0.15 mM PCP at 50 mA, probably due to the formation of a ternary PCP−HPCD−iron complex that is directly oxidized by •OH. The total disappearance of the pesticide and 90% COD abatement were achieved after 11 h of electrolysis. Accumulation of short-chain carboxylic acids such as monochloroacetic, dichloromaleic, acetic, formic, and oxalic acids was detected during the mineralization process.

The EF method has also shown an excellent ability to degrade aqueous solutions of commercial formulations of fungicides such as Mistel GD from Novartis Agro and Cuprofix from ELF Atochem Agri.[204] Mistel GD is a mixture containing the active principles cymoxanil and mancozeb and some additives, whereas Cuprofix contains cymoxanil, zineb, $CuSO_4$, and surfactants as additives. Reversed-phase HPLC analysis of a Mistel GD solution at 100 mA revealed the fast and complete removal of cymoxanil and mancozeb after 90 and 120 min of electrolysis, respectively. The use of either Fe^{3+} or Cu^{2+} as a catalyst (see section 4.3.4) led to practically the same decay rate, although it was slightly higher for Cu^{2+}. In contrast, the catalytic action of Fe^{2+} on H_2O_2 via Fenton's reaction 1 was more effective than Cu^+ via Fenton-like reaction 64 regarding COD reduction since 92% or 80% of mineralization was attained using Fe^{3+} or Cu^{2+} as a catalyst, respectively, after consuming 6000 C at 300 mA. The catalytic action of Cu^{2+} in EF was corroborated by electrolyzing a Cuprofix solution without Fe^{3+} addition. At 100 mA, overall removal of its principle actives zineb and cymoxanil was attained in 70 and 150 min, respectively. Cuprofix was completely mineralized in 8 h at 350 mA, although its degradation rate was slightly higher in the presence of Fe^{3+}, thereby confirming its synergistic action with Cu^{2+}.

Further research by Oturan's group focused on the optimization of EF operation parameters such as the solution pH, nature of inorganic ion of the electrolyte, concentration of catalyst, and applied current, as exemplified in Figure 22 for the organophosphorus insecticide methyl parathion[186] and in Figure 23 for the picolinic acid derivative picloram,[190] as already discussed in section 4.3.2. On the other hand, the use of factorial design methodology and the Doehlert matrix simplified the search for the best operation conditions for

the decay kinetics and mineralization rate, respectively, of the phenylurea herbicide chlortoluron.[203] It is then noteworthy that the application of optimized EF with a carbon-felt cathode allows achieving the quick destruction of the initial pollutant and high degrees of decontamination, with almost overall mineralization in many cases.

Several papers have also included the calculation of the mineralization current efficiency (MCE) from eq 56. For example, MCE values for total conversion of methyl parathion and the carbanilate herbicide propham (phenylcarbamic acid isopropyl ester) into CO_2 and inorganic ions were determined from reactions 74[186] and 75,[191] respectively:

$$C_8H_{10}NO_5PS + 22H_2O \rightarrow 8CO_2 + NO_3^- + SO_4^- + PO_4^{3-} + 54H^+ + 48e^- \quad (74)$$

$$C_{10}H_{13}NO_2 + 21H_2O \rightarrow 10CO_2 + NO_3^- + 55H^+ + 54e^- \quad (75)$$

A sharp decay in efficiency when prolonging the electrolysis time was found for the degradation of these pesticides, which is associated with the progressive formation of oxidation byproducts that are more difficult to destroy with $^{\bullet}OH$ compared with the initial pollutant.

GC-MS and HPLC analyses of electrolyzed solutions allowed the identification and quantification of aromatic and aliphatic intermediates formed during the oxidative degradation of many pesticides.[186,190,191,194,197,198,203] In addition, released inorganic ions such as Cl^-, NO_3^-, NH_4^+, SO_4^{2-}, and PO_4^{3-} were monitored by ion chromatography. Figure 36a, 36b, and 36c illustrate the evolution of aromatic compounds, carboxylic acids, and inorganic ions detected when a 0.12 mM methyl parathion solution in $HClO_4$ medium of pH 3.0 was degraded at 60 mA.[186] The persistence of all aromatic intermediates was similar to that of the initial pesticide, as shown in Figure 36a, since they react at a similar rate constant of 10^8-10^{10} M^{-1} s^{-1} with $^{\bullet}OH$,[47] being completely removed in a maximum of 50 min. In contrast, Figure 36b shows that small quantities of carboxylic acids such as glycolic, maleic, formic, and oxalic acids are present in the medium for more than 8 h of electrolysis because of their much slower reactivity with $^{\bullet}OH$. Furthermore, a very slow release of sulfate, phosphate, and nitrate ions during the mineralization process can be seen in Figure 36c, suggesting that these ions are lost from both aromatic and aliphatic byproducts. After 540 min of treatment, the release of sulfate (100%) and phosphate (94%) ions is almost quantitative but only 82% of the theoretically expected nitrate ion is accumulated, probably due to its partial reduction to NH_4^+ at the cathode or the simultaneous production of volatile NO_x.

The general reaction sequence proposed for methyl parathion mineralization is shown in Figure 37. The initial attack of $^{\bullet}OH$ on the pesticide gives methyl paraoxon with a loss of sulfate ion. Subsequent breakage of the lateral chain of this product by hydroxylation via the C(4)−O bond leads to dimethylphosphate, which is destroyed releasing phosphate ion, and 4-nitrophenol, which is oxidized to 4-nitrocatechol or hydroquinone with the loss of nitrate ion. Hydroquinone is then transformed into *p*-benzoquinone. A further attack by $^{\bullet}OH$ on 4-nitrocatechol and *p*-benzoquinone opens the benzenic ring to give aliphatic compounds that evolve into carboxylic acids such as maleic and glycolic, which are eventually oxidized into oxalic acid. This acid, along with another ultimate acid such as formic, is finally converted into CO_2. Note that the O_2 bubbled into the solution in EF systems based on the use of high specific surface area carbon cathodes, such as the latter,[190,205] is sometimes proposed as an additional oxidizing agent. This seems plausible because $O_2^{\bullet-}$ can be readily formed in this kind of radical-based system, leading to the generation of the oxidant $HO_2^{\bullet}$ from the equilibrium reaction 10.

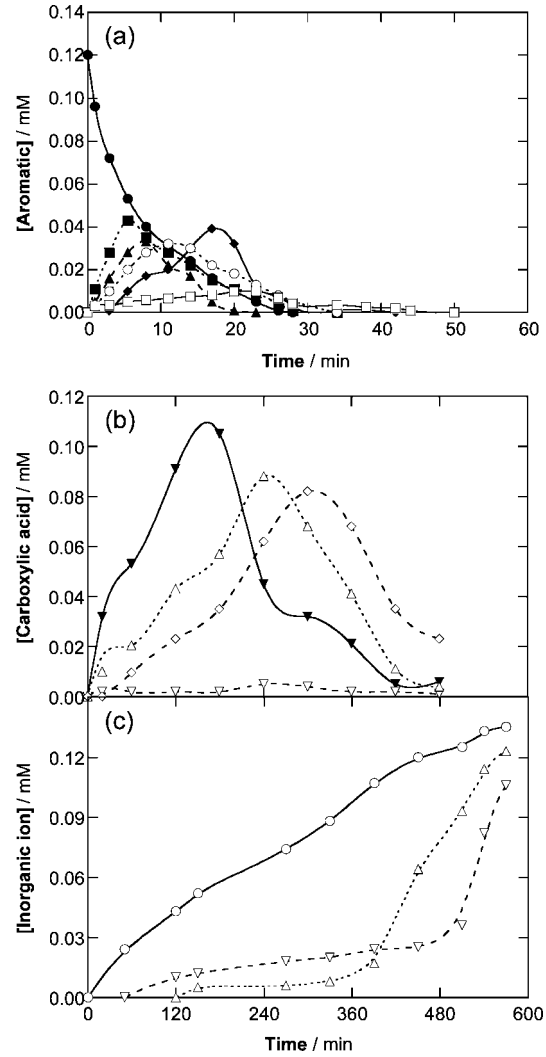

Figure 36. Evolution of the concentration of organic pollutants and inorganic ions detected during the EF process of 150 mL of a 0.12 mM methyl parathion solution with 0.1 mM Fe^{3+} in $HClO_4$ medium of pH 3.0 using the Pt/carbon felt cell of Figure 16a at 60 mA: (a) (●) methyl parathion, (■) methyl paraoxon, (▲) 4-nitrophenol, (◆) 4-nitrocatechol, (○) hydroquinone, and (□) *p*-benzoquinone; (b) (▼) glycolic, (▽) maleic, (△) formic, and (◇) oxalic acids; (c) (○) sulfate, (▽) nitrate, and (△) phosphate ions. Reprinted with permission from ref 186. Copyright 2007 Elsevier.

7.1.2. EF with Reticulated Vitreous Carbon Cathode

The degradation of 2,4-D in a three-electrode undivided Pt/RVC tank reactor such as that of Figure 17a has been studied by Badellino et al.[150] Solutions of 130 mL of 100 mg L^{-1} of the herbicide in 0.3 M K_2SO_4 at pH 3.5 and 10 °C were electrolyzed at $E_{at} = -1.6$ V/SCE by AO-H_2O_2, EF with 1 mM Fe^{2+}, and PEF with 1 mM Fe^{2+} under a 8 W UVC irradiation of the solution, always maintaining a content of 25 mg L^{-1} of dissolved O_2. The faster 2,4-D decay was found in the latter method owing to the photolytic action of

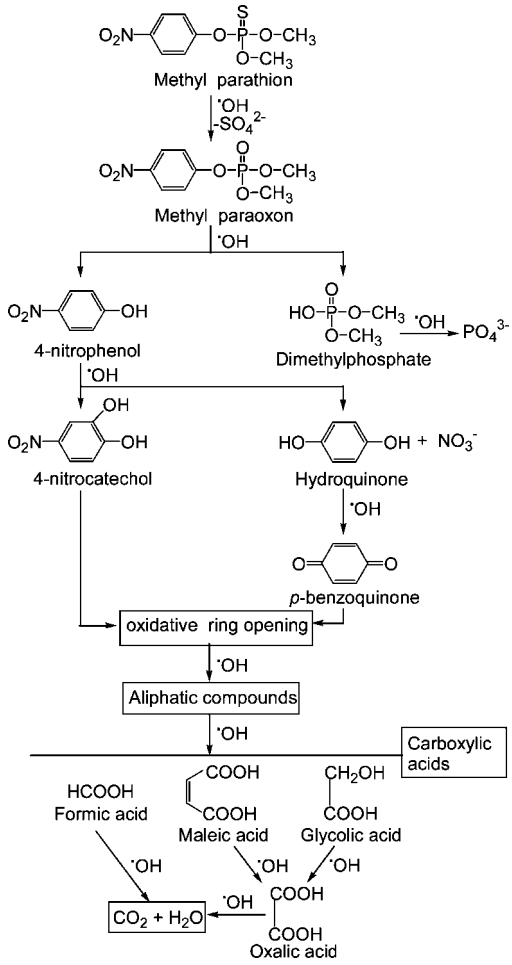

Figure 37. Proposed reaction sequence for methyl parathion mineralization by hydroxyl radical following EF process in a Pt/carbon felt cell. Reprinted with permission from ref 186. Copyright 2007 Elsevier.

UVC light, but illumination did not enhance the degradation process of the intermediates, giving a similar 67−69% mineralization after 90% herbicide removal by EF and PEF, respectively, much higher values than the 58% obtained for AO-H_2O_2. The EF process was then more viable since it needed a lower energy consumption of 0.05 kWh (g TOC)$^{-1}$ compared with 0.98 kWh (g TOC)$^{-1}$ for PEF. Hydroxylated derivatives such as 4-dichlorophenol, 2,4-dichlororesorcinol, 4,6-dichlororesorcinol, and 2-chlorophenol were identified in all cases. The same authors extended the above treatments to using the flow cell of Figure 9a at a liquid flow rate of 300 L h^{-1}.[146] They confirmed the increase of the oxidation power of EAOPs tested in the sequence AO-H_2O_2 < EF < PEF, achieving 95% TOC reduction in 300 min using the PEF method and only 64% mineralization using the EF method.

Recently, Losito et al.[324] reported the EF degradation of 50 mL of 5 mg L^{-1} of phenylurea herbicides such as isoproturon (3-(4-isopropylphenyl)-1,1-dimethylurea), chlortoluron, and chloroxuron (*N*-[4-(4-chlorophenoxy)phenyl]-*N*,*N*-dimethylurea) in H_2SO_4 medium of pH 3.0 with 0.017−0.024 mM Fe^{3+} (1:1 [substrate]:[Fe^{3+}]) at $E_{cat} = -0.5$ V vs Ag/AgCl. Isoproturon was removed in 60 min, but the other two chlorinated pesticides were more refractory and remained for 180 min. HPLC coupled to electrospray ionization tandem mass spectrometry revealed the generation of different byproducts related to the existence of single and multiple hydroxylation steps with the substitution of H, alkyl groups, or Cl, depending on the herbicide, as well as the demethylation of the dimethylamino moiety, eventually followed by hydroxylation.

7.1.3. EF and Combined EF Processes with Gas Diffusion Electrode

Brillas' group investigated the degradative behavior of several common herbicides with undivided two-electrode cells containing a carbon-PTFE GDE as the cathode and different anode materials such as Pt, BDD, and Fe. The cathode was fed with pure O_2 and led to large amount of H_2O_2 from reaction 32 (see Figure 11) but low Fe^{2+} regeneration (see section 4.3.2). The anode was shown to exert a clear influence on the efficacy of the process.

7.1.3.1. Pt/O_2 Cell. The undivided Pt/O_2 cells of Figures 10 and 25b were used to degrade chlorophenoxy acid herbicides such as 2,4-D,[148] 4-CPA (4-chlorophenoxyacetic acid),[184] 2,4,5-T,[228] and MCPA (4-chloro-2-methylphenoxyacetic acid)[229] and the chlorobenzoic acid herbicide dicamba (3,6-dichloro-2-methoxybenzoic acid)[230] using the AO-H_2O_2, EF, and PEF processes. Electrolyses of 100 mL of contaminated solutions in 0.05 M Na_2SO_4 were performed in the pH range 2.0−6.0 at a constant current between 100 and 450 mA and temperature of 25.0 or 35.0 °C. The EF and PEF methods were made by adding 0.2−2 mM $FeSO_4$ to the starting solutions, while the latter method became operative by illuminating the solution with a 6 W UVA light of $\lambda_{max} = 360$ nm. The cathode was always fed with pure O_2 at a flow rate of 12−20 mL min^{-1}.

As an example, Figure 38a shows the comparative TOC removal for 266 mg L^{-1} of 2,4,5-T with 1 mM Fe^{2+} at pH 3.0, 100 mA, and 35.0 °C using the above-mentioned treatments. AO in a similar Pt/graphite cell gives a slightly lower TOC decay than AO-H_2O_2, indicating that Pt(•OH) formed at the anode surface by reaction 46 starting from a potential of 1.2 V/SCE is more powerful than electrogenerated H_2O_2. The oxidation power of the studied EAOPs increases in the sequence AO-H_2O_2 < EF < PEF, which agrees with the results reported by Badellino et al.[146] The higher mineralization rate of EF compared with AO-H_2O_2 can be ascribed to the quicker reaction of organics with •OH produced from Fenton's reaction 1 than with Pt(•OH) (see section 4.2.3). However, EF is only effective for approximately 120 min because at longer electrolysis times the accumulated byproducts are hardly attacked by •OH to give a maximum of 60% TOC removal in 360 min. Therefore, the performance of EF with GDE is less significant than in previous EF systems with a carbon-felt cathode, which promotes almost overall degradation of the initial pollutant and its oxidation byproducts. On the other hand, in systems with GDEs, total mineralization can also be easily achieved by PEF, as a result of the fast photodecomposition of complexes of Fe(III) with byproducts.

Table 7 summarizes the percentages of TOC removal after 1 and 3 h of electrolysis of solutions with 100 mg L^{-1} TOC of 4-CPA, MCPA, 2,4-D, and 2,4,5-T at pH 3.0 and 100 mA. The relative oxidation power of EAOPs tested with Pt for the treatment of all herbicides is in accordance to that exposed above, attaining 16−28%, 53−65%, and 90−99% mineralization after 3 h of electrolysis by AO-H_2O_2, EF, and PEF, respectively. Table 7 also shows the MCE values calculated from eq 56, assuming that their conversion into carbon dioxide and chloride ion verifies reaction 76 for

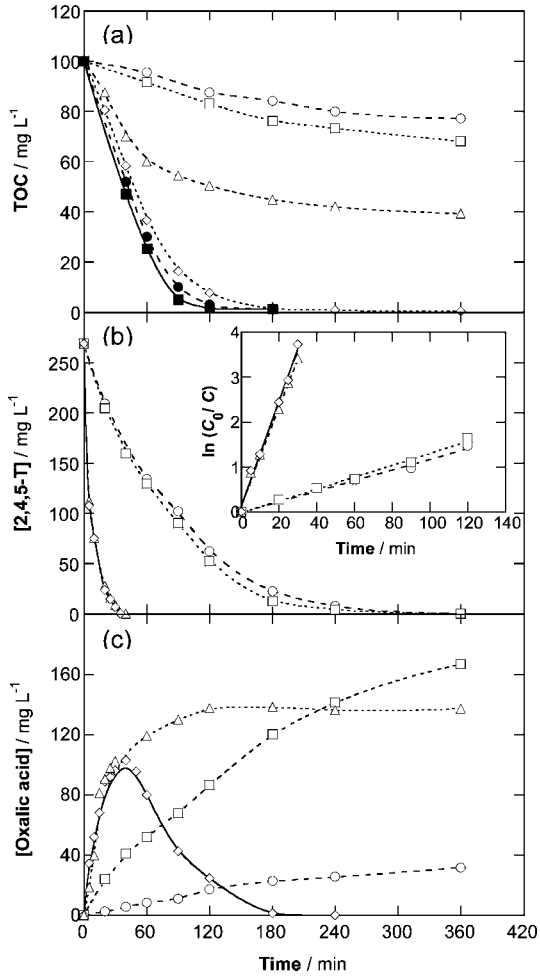

Figure 38. (a) TOC removal, (b) herbicide concentration decay, and (c) evolution of oxalic acid with electrolysis time for the degradation of 100 mL of 266 mg $L^{-1}$of 2,4,5-T in 0.05 M Na_2SO_4 at pH 3.0 and 35.0 °C: (○) AO in a Pt/graphite cell at 100 mA, (□) AO-H_2O_2 in the Pt/O_2 cell of Figure 10 at 100 mA, (△) EF with 1 mM Fe^{2+} in the same cell at 100 mA, and PEF with 1 mM Fe^{2+} and 6 W UVA irradiation in a Pt/O_2 cell such as that of Figure 25b at (◇) 100, (●) 300, and (■) 450 mA. Adapted with permission from ref 228. Copyright 2003 Elsevier.

4-CPA,[184] reaction 77 for MCPA,[229] reaction 78 for 2,4-D,[148] and reaction 79 for 2,4,5-T:[228]

$$C_8H_7ClO_3 + 13H_2O \rightarrow 8CO_2 + Cl^- + 33H^+ + 32e^- \quad (76)$$

$$C_9H_9ClO_3 + 15H_2O \rightarrow 9CO_2 + Cl^- + 39H^+ + 38e^- \quad (77)$$

$$C_8H_6Cl_2O_3 + 13H_2O \rightarrow 8CO_2 + 2Cl^- + 32H^+ + 30e^- \quad (78)$$

$$C_8H_5Cl_3O_3 + 13H_2O \rightarrow 8CO_2 + 3Cl^- + 31H^+ + 28e^- \quad (79)$$

The efficiency decreases with increasing time owing to the progressive decrease of organic content that, moreover, is more difficult to oxidize with •OH.

Optimum operative conditions for EF and PEF treatments were found working at pH 3.0−4.0, where maximum •OH production from Fenton's reaction 1 takes place, and at 0.5−1.0 mM Fe^{2+}. An increase in the current caused quicker TOC decay in all EAOPs (see Figure 38a) by the concomitant production of more Pt(•OH) and/or homogeneously formed •OH because more H_2O_2 is accumulated in the bulk (see Figure 11). Nevertheless, the MCE values gradually decreased at a higher current because of the great increase in the rate of parasitic reactions 9, 17, and 47, which contribute to •OH wasting, and reaction 49. In contrast, higher efficiency was obtained with rising initial herbicide content as a result of the larger extent of reactions involving the destruction of organics with hydroxyl radical and the concomitant decay in the rate of previous nonoxidizing parasitic reactions.

The decay kinetics for initial pollutants was monitored by reversed-phase HPLC. As illustrated in Figure 38b for 2,4,5-T,[228] herbicide concentration is reduced very slowly in AO and AO-H_2O_2 for 360 min, in agreement with the low oxidation ability of electrogenerated Pt(•OH). In contrast, total destruction is achieved only after 40 min and at a similar rate by both EF and PEF because of the production of a higher quantity of •OH generated from Fenton's reaction 1, without significant participation from the photoreduction reaction 27. The concentration decay agreed with the kinetics equation and was related to a pseudo-first-order reaction (see inset of Figure 38b). The corresponding rate constants (k_1) for the aforementioned herbicides are summarized in Table 7, being about 2 orders of magnitude higher for EF and PEF than for AO-H_2O_2.

GC-MS and HPLC analyses of treated solutions revealed the formation of aromatic intermediates such as (i) hydroquinone and *p*-benzoquinone for 4-CPA,[184] (ii) 4-chloro-*o*-cresol, methylhydroquinone, and methyl-*p*-benzoquinone for MCPA,[229] (iii) 2,4-dichlorophenol, 4,6-dichlororesorcinol, chlorohydroquinone, and chloro-*p*-benzoquinone for 2,4-D,[148] and (iv) 2,4,5-trichlorophenol, 2,5-dichlorohydroquinone, 4,6-dichlororesorcinol, and 2,5-dihydroxy-*p*-benzoquinone for 2,4,5-T,[228] which persisted while the initial herbicide was being removed. A high number of short-chain carboxylic acids coming from the cleavage of the benzene rings and release of aliphatic lateral chains were always identified by ion-exclusion HPLC. The most relevant behavior was observed for oxalic acid, which was accumulated in AO, AO-H_2O_2, and EF but rapidly destroyed in PEF (see Figure 38c). These trends indicate that oxalic acid and its complexes with Fe(III) are hardly oxidized by hydroxyl radical, whereas the rapid photodecarboxylation of Fe(III)−oxalate complexes from reaction 29 accounts for the total mineralization achieved in PEF, thus explaining its higher oxidation power. The authors reported the total release of initial chlorine as Cl^-. From the results obtained for 2,4,5-T degradation they also proposed the reaction sequence of Figure 39, which is representative of the pathway followed by other herbicides.[228] Initial breakage of the lateral chain via the C(1)−O bond gives 2,4,5-trichlorophenol and glycolic acid. The phenolic derivative is then hydroxylated in the C(4) and C(5) positions, yielding 2,5-dichlorohydroquinone and 4,6-dichlororesorcinol, respectively, with a loss of Cl^-. Subsequent hydroxylation with total dechlorination of the latter two diols leads to 2,5-dihydroxy-*p*-benzoquinone, which undergoes cleavage of its benzenic ring to produce a mixture of malic, maleic, and fumaric acids, which are oxidized to oxalic acid. Simultaneously, the dehydrogenation of glycolic acid followed by the hydroxylation of the resulting glyoxylic acid may also lead to oxalic acid. Parallel oxidation of both glycolic and glyoxylic acids produces formic acid, which is transformed into CO_2. Oxalic acid is slowly mineralized to

Table 7. Percentage of TOC Removal Calculated from Eq 53, Mineralization Current Efficiency (MCE) Calculated from Eq 56, and Pseudo-First-Order Rate Constant (k_1) Determined for the Degradation of 100 mL of Solutions with 100 mg L^{-1} TOC of Chlorophenoxyacetic Acid Herbicides in 0.05 M Na_2SO_4 of pH 3.0 by Different EAOPs at 100 mA Using a Carbon-PTFE GDE Fed with O_2 as Cathode[148,180,224,226]

				after 1 h of treatment		after 3 h of treatment		
method	anode	herbicide	T/°C	% TOC removal	MCE	% TOC removal	MCE	k_1/min^{-1}
AO-H_2O_2	Pt	4-CPA	35	18	16	28	8.3	4.9×10^{-3}
		MCPA	35	9.6	8.9	22	7.0	5.9×10^{-3}
		2,4-D	25	4.7	3.9	16	4.4	7.9×10^{-3}
		2,4,5-T	35	4.8	3.7	21	5.4	1.3×10^{-2}
AO-H_2O_2	BDD	4-CPA	35	25	22	54	16	5.4×10^{-3}
		MCPA	35	24	23	58	18	7.0×10^{-3}
		2,4-D	35	27	22	57	16	7.1×10^{-3}
		2,4,5-T	35	20	16	59	15	6.6×10^{-3}
EF[a]	Pt	4-CPA	35	48	42	60	18	0.12
		MCPA	35	41	39	65	20	0.12
		2,4-D	25	35	29	57	16	0.18
		2,4,5-T	35	38	30	53	14	0.11
EF[a]	BDD	4-CPA	35	37	33	75	22	0.27
		MCPA	35	49	47	76	24	0.14
		2,4-D	35	50	42	78	22	0.31
		2,4,5-T	35	49	38	80	21	0.24
PEF[b]	Pt	4-CPA	35	78	70	98	29	0.16
		MCPA	35	66	62	91	29	0.14
		2,4-D	25	52	44	90	25	0.23
		2,4,5-T	35	64	50	99	26	0.12
PC	Fe	4-CPA	35	74	66	86	26	0.14
		MCPA	35	68	64	85	27	0.17
		2,4-D	25	56	47	76	21	0.19
		2,4,5-T	35	59	46	84	22	0.16

[a] Catalyst: 1 mM Fe^{2+}. [b] Catalyst: 1 mM Fe^{2+} and UVA light.

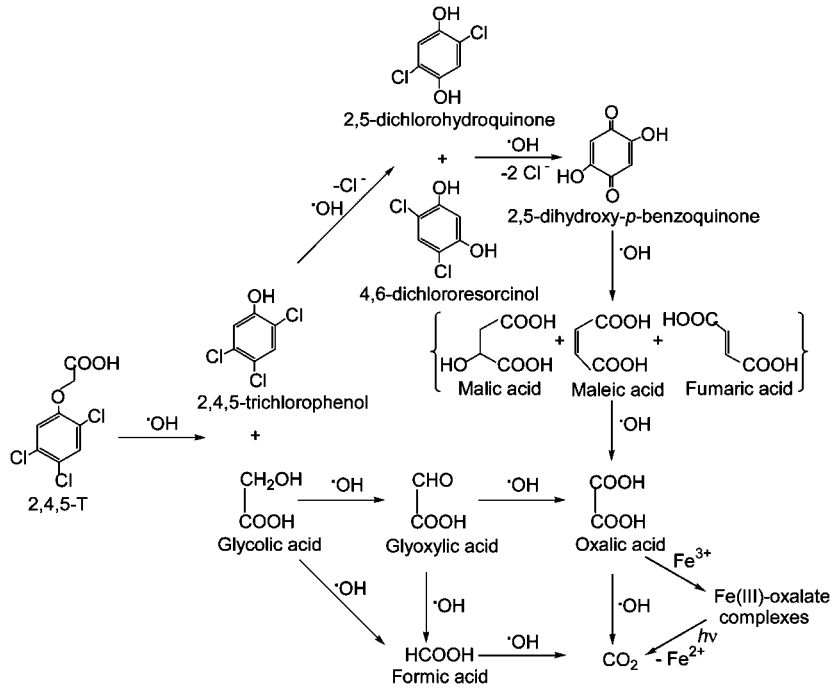

Figure 39. Proposed reaction sequence for 2,4,5-T degradation in acidic aqueous medium by EF and PEF using a Pt/O_2 cell. Adapted with permission from ref 228. Copyright 2003 Elsevier.

CO_2 by AO-H_2O_2, whereas it forms Fe(III) complexes in the EAOPs with iron ions. Such complexes are slowly destroyed in EF and quickly photolyzed, with a loss of Fe^{2+}, in PEF.

EF degradation of 100 mg L^{-1} TOC of the triazole herbicide amitrole (3-amino-1,2,4-triazole) was further studied by Da Pozzo et al.[325] with 1 mM Fe^{2+} at pH 3.0 in the Pt/O_2 cell of Figure 10. Unlike the partial mineralization by EF reported for the previous herbicides, complete destruction of amitrole and its intermediates was achieved because of the absence of oxalic acid as a final byproduct. Low accumulation was observed for released NO_3^- and NH_4^+ ions, as expected if volatile *N*-products can be formed and lost during the process.

7.1.3.2. BDD/O_2 Cell. The AO-H_2O_2 and EF treatments of 100 mg L^{-1} TOC of 4-CPA, MCPA, 2,4-D, and 2,4,5-T at pH 3.0 and 100 mA were studied in the undivided BDD/O_2 cell of Figure 10 under conditions similar to those of the previous Pt/O_2 cell.[180] Figure 20 illustrates that 2,4-D can be completely mineralized by both methods with BDD,

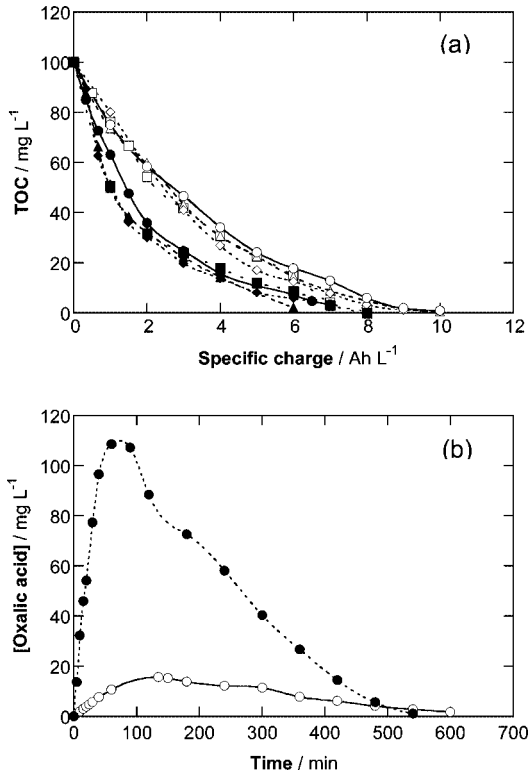

Figure 40. (a) TOC abatement with consumed specific charge for the degradation of 100 mL of (○, ●) 194 mg L^{-1} 4-CPA, (□, ■) 200 mg L^{-1} MCPA, (△, ▲) 230 mg L^{-1} 2,4-D, and (◇, ◆) 266 mg L^{-1} 2,4,5-T solutions in 0.05 M Na_2SO_4 of pH 3.0 using the BDD/O_2 cell of Figure 10 at 100 mA and 35.0 °C: (○, □, △, ◇) AO-H_2O_2 and (●, ■, ▲, ◆) EF with 1 mM Fe^{2+}. (b) Time course of oxalic acid concentration during treatment of the above 4-CPA solution. Reprinted with permission from ref 180. Copyright 2004 Elsevier.

which are much more potent than the analogous procedures with Pt owing to the higher oxidation power of BDD(•OH) compared with Pt(•OH) (see section 4.2.3). Figure 40a depicts that all herbicide solutions are degraded at a similar rate in each EAOP with BDD, attaining total mineralization after 9−10 h (specific charge 9−10 Ah L^{-1}) of AO-H_2O_2 and 6−8 h (specific charge 6−8 Ah L^{-1}) of EF with 1 mM Fe^{2+}. Therefore, both methods with BDD are much more efficient than the homologous ones with Pt, as can be observed from the MCE values in Table 7. However, this behavior cannot be related to the faster reaction of aromatics with reactive BDD(•OH) because initial herbicides decayed with a similar k_1 value for each method with Pt or BDD (see Table 7). These findings also confirm the quicker reaction of these herbicides with •OH in the bulk rather than at the Pt or on the BDD surface.

Analysis of generated carboxylic acids in the above trials revealed the accumulation of final oxalic acid. Figure 40b shows the evolution of this acid during 4-CPA treatment.[180] The persistence of Fe(III)−oxalate complexes in EF with BDD is not related to their oxidation with •OH in the bulk because they are stable in EF with Pt (see Figure 39c) and, hence, are slowly mineralized by reaction with BDD(•OH). The slow destruction of such complexes at the BDD accounts for the long time needed for the total decontamination of herbicides by EF with BDD. This occurs at similar times to those needed using AO-H_2O_2, in which less acid is accumulated (see Figure 40b) because it is practically removed at the same rate as it is produced. It was also found that the Cl^- released in all treatments with BDD was slowly oxidized to Cl_2.

The great oxidation power of EAOPs with BDD was recently corroborated from the degradation of the phenoxypropionic herbicide 2,4-DP in the electrolytic cell of Figure 25b.[237] It was observed again that overall mineralization was attained in EF with 1 mM Fe^{2+} because the great production of •OH in the bulk from Fenton's reaction 1 rapidly destroyed the aromatic compounds, whereas the high generation of reactive BDD(•OH) favored the destruction of final carboxylic acids. Also in this case UVA irradiation in PEF had little effect on the degradation rate of pollutants. Chlorohydroquinone and chloro-*p*-benzoquinone were detected as primary aromatic intermediates, further on being oxidized to maleic, fumaric, malic, lactic, pyruvic, acetic, formic, and oxalic acids.

A further study focused on clarifying the viability of the SPEF method with BDD using the flow plant schematized in Figure 12 to degrade MCPP.[235] Figure 27b shows that the degradation of 2.5 L of 100 mg L^{-1} of MCPP with 0.5 mM Fe^{2+} of pH 3.0 at 50 mA cm^{-2} and 25 °C is much faster for SPEF than for EF or PEF with UVA irradiation. In the SPEF process, however, TOC is very slowly removed after being reduced by 82% at 100 min (0.67 Ah L^{-1}), attaining 96% mineralization at 9 h (3.6 Ah L^{-1}) with a 46 kWh m^{-3} energy cost. Its efficiency, calculated from eq 56, increased strongly with rising herbicide content up to 0.64 g L^{-1} and reached values as high as 337% in the early stages of this treatment, thereby confirming the quick photolysis of Fe(III) complexes. Kinetics and HPLC measurements revealed the fast reaction of MCPP with •OH to yield 4-chloro-*o*-cresol, 2-methylhydroquinone, and 2-methyl-*p*-benzoquinone as primary intermediates. Oxalic and acetic acids were detected as the most persistent final products. It was concluded that overall mineralization is reached because Fe(III)−oxalate complexes are rapidly photodecomposed by sunlight, while Fe(III)−acetate complexes are slowly but progressively oxidized by BDD(•OH).

7.1.3.3. Fe/O_2 Cell. Acidic solutions containing 4-CPA, MCPA, 2,4-D, 2,4,5-T, and dicamba have also been treated by PC and PPC in Fe/O_2 cells such as those in Figure 25a and 25c, respectively, under conditions similar to those used with Pt and BDD anodes.[223−226] In PC, the sacrificial Fe anode was quantitatively oxidized to Fe^{2+} by reaction 66 and large amounts of $Fe(OH)_3$ precipitate were formed. According to Table 7, 76−86% TOC removal and 21−27% MCE were achieved after 3 h of electrolysis for 100 mg L^{-1} TOC of all chlorophenoxyacetic herbicides degraded by PC at 100 mA. These values are higher than those determined for EF with Pt and BDD but lower than those obtained for PEF with Pt. All these compounds also underwent a pseudo-first-order decay kinetics in PC, giving k_1 values quite similar to those found for the other EAOPs with Pt and BDD (see Table 7), as expected if the main oxidant is •OH produced from Fenton's reaction 1. The same intermediates were detected using EF, PEF, and PC, suggesting that the radical mechanism initiated by •OH presents some features applicable to a variety of organic compounds. The faster decay of soluble TOC by PC compared with EF was ascribed to the dual contribution of the mineralization process and coagulation of intermediates with the $Fe(OH)_3$ sludge formed, as explained in section 5.1. Increasing the current accelerated TOC abatement with a predominance of coagulation (see

Table 5) because the faster generation of •OH favored the formation of intermediates and a larger proportion of them were retained by the greater quantity of $Fe(OH)_3$ precipitate produced. Low contents of oxalic acid were detected after 6 h of electrolysis at 100 mA, indicating the existence of slow coagulation of their Fe(III) complexes. The percentage of Cl^- detected in the final electrolyzed solutions was 86% for 4-CPA, 76% for MCPA, 100% for 2,4-D and dicamba, and 90% for 2,4,5-T.[226] This fact was explained by the destruction of most chlorinated derivatives with a concomitant loss of Cl^-, whereas the resulting organic products were prone to coagulation with the iron sludge.

7.1.4. ECP and AFT Treatments

Former studies of Lemley's group on ECP[271–273] assessed the oxidation power of this method to remove various herbicides including alachlor, metolachlor, atrazine, cyanazine, picloram, malathion, and methyl parathion. Galvanostatic electrolyses were performed with a stirred tank reactor such as that in Figure 31b, containing iron or steel plates as electrodes to anodically generate Fe^{2+} from reaction 66 for treating 400 mL of the contaminated solution in 0.5 g L^{-1} NaCl at circumneutral pH between 5.0 and 6.5. In their first work,[271] 10 mL of 30%(v/v) H_2O_2 was added to the initial solution and a current of 0.3 A was applied for a short time period from 5 to 20 min, aiming for the electrogeneration of 100 to 400 mg L^{-1} Fe^{2+}. Reversed-phase HPLC analyses of electrolyzed solutions revealed faster herbicide decay for 200 mg L^{-1} Fe^{2+} in all cases, attaining almost total removal of 30 mg L^{-1} of alachlor and picloram as well as 70 mg L^{-1} of metolachlor but only removing 86% and 50% of 30 mg L^{-1} of atrazine and cyanazine, respectively. A pseudo-first-order decay reaction was only verified for picloram, with $k_1 = 4.7\ h^{-1}$. Overall removal of malathion and methyl parathion under the same conditions was further reported by Roe and Lemley.[272] Later, Pratap and Lemley[273] investigated more extensively the particularities of ECP treatment with metolachlor and atrazine solutions to show that stepwise dosing of H_2O_2 and keeping a constant $[Fe^{2+}]/[H_2O_2]$ ratio of 1:5 enhanced the removal of both herbicides up to their total abatement (see Figure 33a) and that solution irradiation with UVA light did not improve their decay rate (see Figure 33b). Deethyldeisopropylatrazine, deethylatrazine, and 2-hydroxyatrazine were detected by HPLC as primary intermediates of atrazine, so it could be concluded that *N*-dealkylation and hydroxylation with dechlorination constituted its main initial degradation steps.

Following the above ECP studies, Lemley and coworkers[294–297,299–310] reported the fast decay of a vast number of herbicides and insecticides by means of AFT using the salt bridge cell schematized in Figure 31c, an H-type two-compartment cell with an anionic membrane or a flow cell composed of two electrochemical half cells separated by an anionic membrane. The characteristics of these AFT systems with continuous H_2O_2 addition, along with a description of several models proposed by these authors to explain the evolution of H_2O_2, Fe^{2+}, total iron ions and •OH species, and the decay kinetics of pesticides, were detailed in section 6.3. In these studies, operation conditions were optimized to attain the most rapid disappearance of pesticides, but their mineralization process was almost disregarded.

When Salmiras and Lemley[297] studied the degradation of 100 mL of 0.14 mM atrazine solutions in 0.5 g L^{-1} NaCl of pH 5.5 as the anolyte of a salt bridge cell with a 20 cm^2 iron anode at 0.12 A and at an optimized $[Fe^{2+}]/[H_2O_2]$ ratio of 1:5, they found that the herbicide decayed following a pseudo-first-order reaction with $k_1 = 1.95\ min^{-1}$, which was completely removed in about 3 min, i.e., about 10 times faster than similar ECP treatment (see Figure 33a). This enhancement was accounted for by the greatest production of •OH from Fenton's reaction 1 in AFT, because the anolyte rapidly reached a favorable pH of about 2.5 instead of about 6.5 obtained by ECP. From HPLC analysis, seven primary dealkylated and/or hydroxylated derivatives were identified from atrazine oxidation. The reaction pathway proposed for the formation of such products in Figure 41 shows that *N*-dealkylation followed by hydroxylation with dechlorination (solid arrows) is the preferred degradative route of atrazine in AFT. The existence of a hydroxylation step from the attack of generated •OH on pesticides was further confirmed using an H-type two-compartment cell with an anionic membrane containing 0.02 M NaCl as the optimized concentration in the anolyte. For the carbamate insecticide carbaryl (1-naphthyl *N*-methylcarbamate),[299,301,307] the hydroxylated intermediate 1-naphthol and its oxidation product 1,4-naphthoquinone, along with (phthalic acid-*O*-)yl *N*-methylcarbamate coming from the partial breakdown of its naphthalene ring, were detected by GC-MS. Similarly, Wang and Lemley[301] reported the generation of several hydroxylated derivatives from other carbamate insecticides: (i) 2,3-dihydro-2,2-dimethylbenzofuran-7-ol, 2-hydro-3-hydroxyl-2,2-dimethylbenzofuran-7-ol, and 2-hydro-3-oxo-2,2-dimethylbenzofuran-7-ol for carbofuran (2,3-dihydro-2,2-dimethylbenzofuran-7-yl methylcarbamate), (ii) 2-(1,3-dioxolan-2-yl)phenol, (2-hydroxylethyl)salicylate, and 2-hydroxyl benzaldehyde for dioxacarb (2-(1,3-dioxolan-2-yl)phenyl methylcarbamate), (iii) 2,2-dimethyl-1,3-benzodixol-4-ol for bendiocarb, (iv) 3-isopropyl-5-hydroxyl benzaldehyde and 3-methyl-5-(2-hydroxy-2-propyl)phenol for promecarb (3-isopropyl-5-methylphenyl methylcarbamate), and (v) 2-(1-methylpropyl)phenol and 2-acetyl phenol for fenobucarb (2-(1-methylpropyl)phenyl methylcarbamate). Several hydroxylated

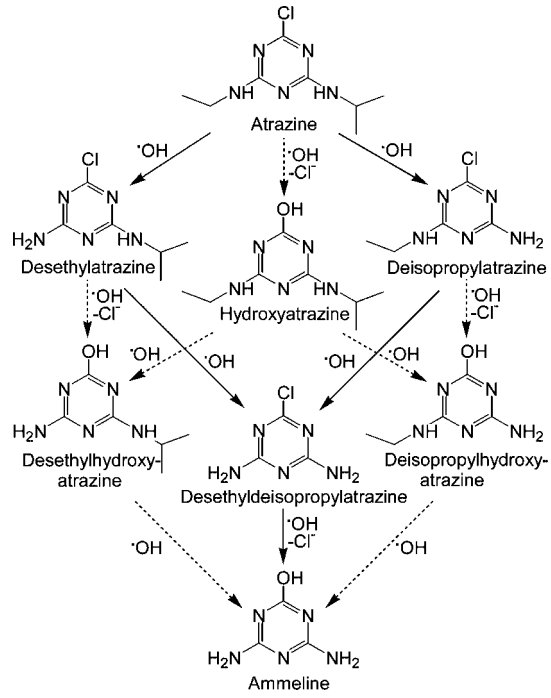

Figure 41. Proposed reaction pathway for the initial AFT degradation of atrazine. Adapted with permission from ref 297. Copyright 2002 Elsevier.

intermediates were also found for chloroacetanilide herbicides such as acetochlor, alachlor, butachlor, metolachlor, and propachlor,[305] whereas deamination derivatives were mainly detected for the triazinone herbicide metribuzin.[304]

COD and five-day biological oxygen demand (BOD_5) were determined by Lemley and co-workers for the AFT treatment of some pesticides in the membrane cell. For example, when 200 mL of 0.2 mM carbofuran with 0.02 M NaCl was degraded with an $[Fe^{2+}]/[H_2O_2]$ ratio of 1:10 at 50 mA,[300] it was found that the pesticide was completely removed in 9 min with a COD reduction of 71%, increasing the BOD_5/COD ratio from 0.04 to 0.63 and making the resulting wastewater suitable for biodegradation. For the similar treatment of 0.16 mM solutions of metolachlor,[305] the BOD_5/COD ratio increased progressively to 0.30 and 0.58 in 10 and 20 min, respectively, while overall removal of the initial pesticide was attained in 5 min, indicating that biodegradability is feasible after 10 min of electrolysis when primary intermediates are transformed into less recalcitrant byproducts. These findings prove that AFT could be used as a good EAOP for detoxifying organic wastewater before biological post-treatment.

Finally, an interesting contribution of Lemley's group is referred to the potential application of AFT for soil remediation following an ex-situ approach, which reduces the environmental impact of pH adjustment.[303,306] The herbicides 2,4-D and alachlor were satisfactorily treated under experimental conditions that simulated a more realistic complex system with the presence of humic acid as the •OH scavenger, which modifies the mechanisms and kinetics of processes based on Fenton's reaction chemistry.

7.2. Dyestuffs

Around 10 000 different synthetic organic dyes, with 7×10^5 tons produced yearly, are extensively used worldwide in many fields of up-to-date technology including various branches of the textile industry, leather tanning industry, paper production, food technology, agricultural research, and light-harvesting arrays, as well as in hair colorings.[326] The majority of dyestuffs consumed at an industrial scale are azo (−N═N−) derivatives, although anthraquinone, indigoid, arylmethane, and xanthene compounds are frequently utilized.[327] Apart from its common name, each dye also receives a color index (C. I.) name, which consists of the name of a general property of the product, followed by its color name and order number. The former name can be Acid (i.e., negatively charged), Basic (i.e., positively charged), Reactive (i.e., anionic dye used in the textile industry), Mordant (i.e., a metallic ion is required for showing their color or staining selectivity), Disperse (i.e., nonionic dye used in aqueous dispersion), and so on. Dyestuffs treated by EAOPs based on Fenton's reaction chemistry are listed in Table 6 according to this nomenclature.

Synthetic dyes possess properties such as resistance to abrasion, photolytic stability, and resistance to chemical and bacterial attack, which make them remain unaltered for long periods. Their presence in water causes phenomena such as eutrophication, underoxygenation, color, and odor alteration, as well as persistence and long-term bioaccumulation. The large release of dyeing wastewaters into the environment, mainly from the textile industry, is then a dramatic source of aesthetical pollution and perturbation of aquatic life, and this represents a major concern because dyestuffs cannot be destroyed by conventional treatments.[325,326] AOPs are more powerful treatments because they effectively decolorize these pollutants, although they usually do not remove COD utterly.[328] Recent work on EAOPs has shown an efficient oxidation of dyestuffs from synthetic wastewater using the EF and related electrochemical methods, even providing total mineralization.

7.2.1. EF Process

Many authors have reported the beneficial use of EF for degrading dyestuffs. The first paper regarding such application was published by Alvarez-Gallegos and Pletcher,[124] who studied the decolorization and mineralization of 1.8 L of the azo dye Amaranth (C. I. Acid Red 27) in 0.05 M Na_2SO_4 with 1 mM Fe^{2+} at pH 2.0 using the divided three-electrode Pt/RVC flow cell in Figure 8, with a cathode of 50 mm × 50 mm × 12 mm, at $E_{cat} = -0.7$ V/SCE, room temperature, and a liquid flow rate of 0.13 m s^{-1}. For a 0.33 mM solution, complete color removal was achieved after the consumption of 3000 C with an energy cost of 1.4 kWh m^{-3}, whereas more than 95% COD was reduced by imposing 6120 C. Harrington and Pletcher[119] used the same system to degrade Acid Red 27 as well as the azo dyes Methyl Orange (C. I. Acid Orange 52) and Fat Brown RR (C.I. Solvent Brown 1). Zhang et al.[329,330] recently developed a novel carbonaceous cathode for its application in EF treatment to destroy Acid Red 27. Total dye decay and 83% TOC removal were found after 120 min for 200 mL of an O_2-saturated solution of 85 mg L^{-1} of the dye in 0.1 M Na_2SO_4 degraded in an undivided three-electrode cell similar to that in Figure 17d with a Pt anode and a 10.5 cm^2 polypyrrole/anthraquinonedisulfonate composite film-modified graphite cathode operating at optimal conditions of 2 mM Fe^{2+}, pH 3.0, and $E_{cat} = -0.65$ V/SCE.

Better insight into the degradative behavior of dyes has been reported by Oturan's group. Former studies for the azo dyes Acid Orange 52, Methyl Red (C. I. Acid Red 2), and the arylmethane Malachite Green (C. I. Basic Green 4)[331,332] using a divided Pt/carbon felt cell similar to that in Figure 17a showed a good performance for achieving almost overall COD removal of 110 mL of 0.5 mM solutions of dyes, following a pseudo-first-order decay, in H_2SO_4 medium of pH = 2.0 in the presence of 0.5 mM Fe^{3+} at $E_{cat} = -0.5$ V/SCE. Later, this group[171,195,196,199] utilized the undivided tank reactor of Figure 16a, equipped with a small 4.5−5.5 cm^2 Pt sheet or cylinder as an anode, centered in the cell, and surrounded by a larger 60 cm^2 carbon-felt cathode. A strong inhibition for the oxidation process of 500 mL of air-saturated 1.0 mM Direct Orange 61 solutions in 0.05 M Na_2SO_4 of pH 3.0 was found with increasing Fe^{2+} concentration in the above two-electrode cell because of the concomitant loss in •OH from the larger extent of the parasitic reaction 17.[196] This trend can be observed in Figure 42a since a Fe^{2+} concentration of 0.1, 0.2, and 0.5 mM causes decreasing TOC decay of 96%, 63%, and 55%, respectively, after 480 min of electrolysis at 100 mA. Figure 42b shows the fastest decay found for 0.05 mM Direct Orange 61 with the most favorable 0.1 mM Fe^{2+} operating at 60 mA, attaining total removal in 50 min. The inset of this figure illustrates that the dye reacts with •OH in the bulk following a pseudo-first-order kinetics with $k_1 = 5.0 \times 10^{-3}$ s^{-1}. This corresponds to a k_2 value of 2.1×10^{10} M^{-1} s^{-1} (see Table 4), as determined by the competition kinetics method, which determines a steady-state •OH concentration of 2.4×10^{-13} M. The quickest degradation of this dye was obtained for 0.53 mM at 250 mA,

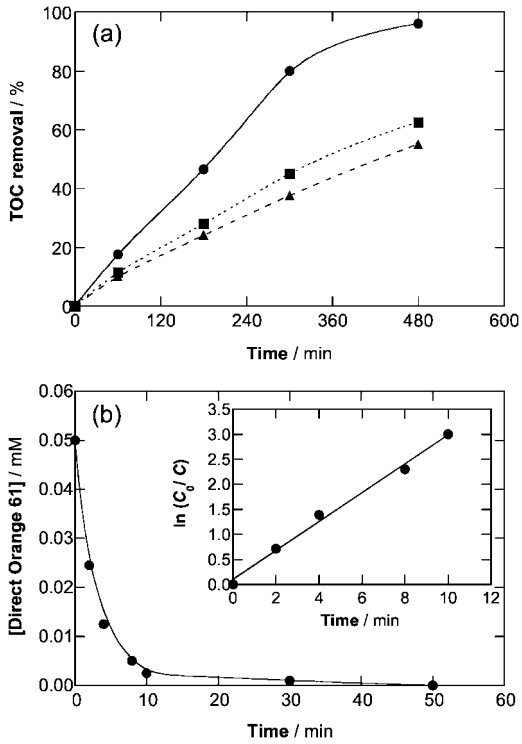

Figure 42. (a) Influence of Fe^{2+} concentration on TOC removal for 500 mL of 1.0 mM of Direct Orange 61 in 0.05 M Na_2SO_4 of pH 3.0 treated by EF with the undivided cell of Figure 16a with a 5.5 cm^2 Pt sheet as anode and a 60 cm^2 carbon felt cathode at 100 mA. Initial Fe^{2+} content: (●) 0.1, (■) 0.2, and (▲) 0.5 mM. (b) Dye concentration decay for a 0.050 mM solution with 0.1 mM Fe^{2+} at 60 mA. The inset gives its kinetic analysis as a pseudo-first-order reaction. Adapted with permission from ref 196. Copyright 2007 Elsevier.

reaching 98% TOC removal in 360 min. Similar decay kinetics but with lower k_2 values (see Table 4) were obtained for Reactive Orange 70, Direct Red 28, and Basic Blue 9 under comparable conditions in a three-electrode cell.[195] For the EF treatment of 250 mL of 0.5 mM Malachite Green with 0.2 mM Fe^{3+} or Fe^{2+} as catalyst at pH 3.0, total color removal was achieved in 22 min and overall mineralization in 540 min working at 200 mA.[171] The decay of this dye followed pseudo-first-order kinetics, and its k_1 value increased from 1.7×10^{-3} to 4.0×10^{-3} s^{-1} when the applied current varied from 60 to 200 mA, as expected by the faster production of •OH from Fenton's reaction 1 as a result of the enhancement of the H_2O_2 electrogeneration rate from reaction 32. Thorough analysis of treated solutions allowed detecting aromatic intermediates such as 4-dimethylaminobenzophenone, 4-aminophenol, benzoic acid, 4-aminobenzoic acid, 4-nitrocatechol, and quinones, which are oxidized to final carboxylic acids such as oxalic, maleic, fumaric, glycolic, and formic acids, with the release of NO_3^-, NO_2^-, and NH_4^+ ions. Thus, the authors concluded that the degradation proceed via various parallel pathways initiated by primary splitting of the triaryl structure upon attack of •OH. Sirés et al.[199] also described an analogous degradative behavior, with similar oxidation pathways, for other arylmethane dyes such as Methyl Green (C. I. Basic Blue 20), Crystal Violet (C. I. Basic Violet 3), and Fast Green FCF (C. I. Food Green 3). The k_2 values for these three dyestuffs and Malachite Green were quite similar, varying between 1.31×10^{-9} and 2.65×10^{-9} M^{-1} s^{-1} in the order Methyl Green < Fast Green FCF < Crystal Violet < Malachite Green, as expected if all of them undergo a similar attack of •OH but with a clear effect of the number and complexity of the substituents. The ICE calculated from eq 54 for the EF treatment of these arylmethanes decreased dramatically from an initial value of about 50% to close to zero by the end of treatment. As observed during the first stages of the process, COD depletion fitted well with a pseudo-first-order kinetics due to the main fast reaction of all the aromatic intermediates with •OH, whereas at long electrolysis times it was much slower owing to the formation of less reactive intermediates, mainly carboxylic acids as specified above. On the other hand, Oturan and co-workers[114] reported a faster and more efficient mineralization during the treatment of 125 mL solutions of 0.2 mM Melacryl Blue (C.I. Basic Blue 3) in 0.1 M $NaNO_3$ with 0.1 mM Fe^{3+} at pH 3.0 and 15 °C under the application of 100 mA, when the cathode of a cell similar to that in Figure 16a was a three-dimensional carbon sponge sized 18 cm^2 instead of a carbon-felt cathode with the same apparent surface area because of its greater ability to electrogenerate H_2O_2 (see section 3.4). Using the system with the carbon sponge cathode a 92% TOC removal was obtained after 480 min, with decreasing MCE values from 35% at 30 min to 7.2% by the end of electrolysis. In contrast, only 51% TOC decay and MCE values from 9.1% to 4.2% were obtained for the carbon-felt cathode.

Similar effects of operation parameters on the EF degradation of dyestuffs have been described by other authors. When Wang et al.[122] electrolyzed 500 mL of O_2-saturated solutions with 200 mg L^{-1} of the azo dye Acid Red 14 in 0.05 M Na_2SO_4 with 1 mM Fe^{2+} at pH 3.0 using the undivided RuO_2/ACF cell in Figure 13a at 500 mA for 6 h, total decolorization and 73% TOC removal were achieved. TOC decay gradually increased with increasing both the current from 120 to 500 mA and the Fe^{2+} concentration to 1 mM, but mineralization was decelerated at greater Fe^{2+} contents due to the higher consumption of •OH from reaction 17. Zhou et al.[333,334] discussed the EF process of 100 mL of Methyl Red solutions with an undivided three-electrode Pt/graphite-PTFE cell such as that in Figure 17d with electrodes of 1 cm^2 area. Under optimum conditions of 0.1 M Na_2SO_4, 0.2 mM Fe^{2+}, pH 3.0, and $E_{cat} = -0.55$ V/SCE, a 20 mg L^{-1} solution became colorless in 20 min, whereas at a higher concentration of 100 mg L^{-1} only 74% color removal was attained. This partial dye removal confirms the much lower oxidation power of EF with two-dimensional cathodes compared with systems equipped with three-dimensional cathodes, such as those used by Guivarch et al.[331] for the treatment of the same dye. Section 4.3.2 explained the interesting result of Daneshvar et al.,[187] who showed a clear influence of the anion of the electrolyte on the color removal of 0.02 mM Orange II (C. I. Acid Orange 7) solutions in 0.050 M $NaClO_4$, Na_2SO_4, or NaCl with 0.1 mM Fe^{3+} at pH 3.0 and $E_{cat} = -0.50$ V/SCE using a Pt/carbon felt cell such as that in Figure 17d. The same authors also reported that the performance of a carbon-felt cathode could be varied as a function of the O_2 flow rate. They also paid attention to the aromatic byproducts formed, suggesting that dissociation of the azo bond with the formation of sulfanilic acid occurs as a first step upon attack of •OH.

The interesting research of Shen et al. is especially noteworthy.[127] They used a two-chamber cell connected with a K_2SO_4 bridge to perform a "dual electrode oxidation", a concept also explored by other authors for water treatment,[182] simultaneously involving H_2O_2 electrogeneration for EF degradation in the cathodic chamber with a Pt-carbon GDE

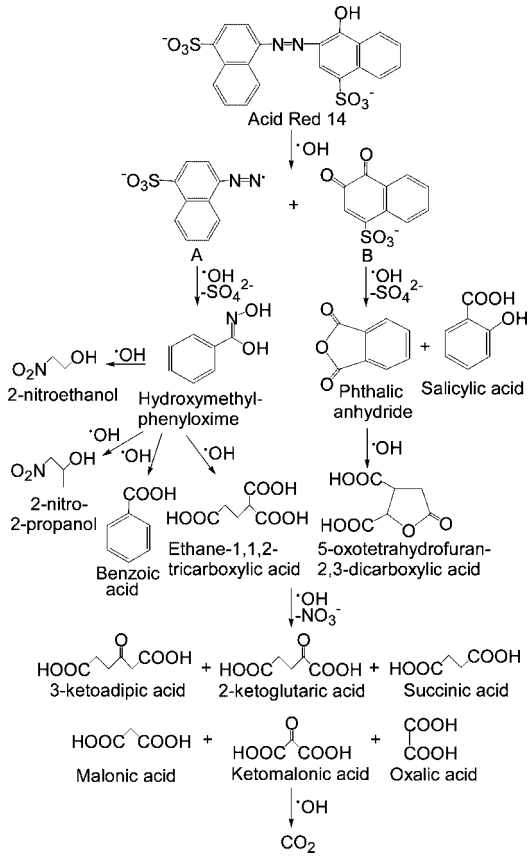

Figure 43. Proposed reaction sequence for the degradation of the azo dye Acid Red 14 by the EF process. Adapted with permission from ref 127. Copyright 2005 American Chemical Society.

cathode fed with air and AO in the anodic chamber with a graphite anode. The performance of the system was tested for the treatment of 500 mL of 60 mg L^{-1} of the azo dye Acid Red 14 in 0.05 M Na_2SO_4 at pH 3.0 in both chambers, with addition of 50 mM Fe^{2+} to the catholyte. After 80 min of electrolysis at 58 mA, the EF process yielded 66% COD removal, a value higher than the 56% obtained by AO. Twenty intermediates including esters, acids, and nitrogenated compounds were detected by GC-MS during the EF treatment. From these results, they proposed the reaction sequence depicted in Figure 43 considering •OH the main oxidant. The −OH group of Acid Red 14 is initially oxidized to =O while its C−N=N− bond is broken, yielding the undetected intermediates A and B, which are converted into hydroxymehyl-phenyloxime, phthalic anhydride, and salicylic acid with the release of SO_4^{2-}. Hydroxymethyl-phenyloxime then evolves to 2-nitroethanol, 2-nitro-2-propanol, benzoic acid, and ethane-1,1,2-tricarboxylic acid, whereas phthalic anhydride is degraded to 5-oxotetrahydrofuran-2,3-dicarboxylic acid. Further oxidation of these byproducts, with release of the NO_3^- from nitrocompounds, gives short-chain linear carboxylic acids such as 3-ketoadipic, 2-ketoglutaric, succinic, malonic, ketomalonic, and oxalic acids, which are finally mineralized to CO_2.

7.2.2. PEF Process

Fewer papers have dealt with the PEF treatment of acidic dyestuffs solutions. However, in all of them the superiority of this method in relation to analogous EF process has been well demonstrated.

Kusvuran et al.[335,336] reported the comparative EF and PEF degradation of azo dyes Reactive Red 120 and Reactive Black 5 using a bench-scale divided three-electrode cell equipped with a Pt gauze anode and a 15 cm^2 carbon-felt cathode. Both methods were tested with 250 mL of O_2-saturated solutions containing from 20 to 100 mg L^{-1} of each dye and a 3-fold mM Fe^{2+} content at pH 3.0 as a catholyte. H_2O_2 was generated at $E_{cat} = -0.55$ V/SCE, and a UVC lamp of $\lambda_{max} = 254$ nm was employed to irradiate the solution. The decolorization process in EF verified a pseudo-first-order kinetics with a decreasing rate as dye content increased because the same quantity of oxidant •OH is produced from Fenton's reaction 1 at the working potential. After 30 min of EF, total decolorization was found for 20 mg L^{-1} of both dyes, but only about 80−85% color removal was obtained for 100 mg L^{-1}. The PEF process always provided quicker decolorization, mainly by the additional generation of •OH in the bulk by reactions 27 and 30. However, a very poor TOC removal close to 20% was found for 100 mg L^{-1} of both dyes after 3 h of EF, only raising to ca. 29% using PEF. Such a low mineralization degree completely disagrees with many results reported by various groups (see results in Table 7 for pesticides). Toxicity measurements showed that solutions degraded for 90 min by EF and PEF were sufficiently detoxified to be disposed safely into the environment.

Peralta-Hernández et al.[337] described a much more efficient PEF process for the treatment of a solution of 400 mL with 50 mg L^{-1} of the azo dye Orange II with 0.2 mM Fe^{2+} in 0.05 M Na_2SO_4 at pH 3.0 using a concentric annular undivided graphite cloth/graphite cloth flow reactor with a 164 cm^2 cathode area operating in batch mode at 300 mA cm^{-2} and a liquid flow rate of 100 mL min^{-1}. The effluent was irradiated with a central 75 mW cm^{-2} UVA lamp of $\lambda_{max} = 360$ nm under O_2 bubbling for H_2O_2 electrogeneration. Complete decolorization in less than 5 min and 80% TOC removal in 1 h were obtained by PEF as a result of the great production of •OH from Fenton's reaction 1 and photoreduction reaction 27. A similar decolorization rate, but a smaller 63% TOC decay, was found for the comparable EF treatment. A significantly better performance of PEF was also reported by Wang et al.[338] following their EF study on Acid Red 14 mentioned above.[122] To apply this process, they modified the undivided RuO_2/ACF cell in Figure 13a by introducing an 11 W UVC lamp positioned in a hollow quartz tube between the electrodes. A reduction of about 94% TOC was found after 6 h of PEF treatment of 450 mL of an O_2-saturated solution containing 200 mg L^{-1} of dye in 0.05 M Na_2SO_4 with 1 mM Fe^{2+} of pH 3.0, which is a value much greater than the 73% TOC decay obtained for the similar EF treatment at 500 mA.[122]

On the other hand, Flox et al.[210] investigated more exhaustively the peculiarities of the PEF process using a GDE and Fe^{2+} and Cu^{2+} as cocatalysts. These authors performed the EF and PEF treatments of 100 mL of acidic aqueous solutions containing 220 mg L^{-1} of Indigo Carmine (C. I. Acid Blue 64) at pH 3.0 with the Pt/O_2 and BDD/O_2 cells of Figures 10 and 25e, with electrodes of a 3 cm^2 area, at 100 mA and 35.0 °C. The EF process with a Pt anode and 1.0 mM Fe^{2+} provided poor mineralization because only 49% TOC removal was attained in 540 min. In contrast, 91% of TOC was reduced by EF with a BDD anode at the same time, reaching total mineralization with the loss of NH_4^+ in 780 min. Reversed-phase HPLC analyses of treated solutions

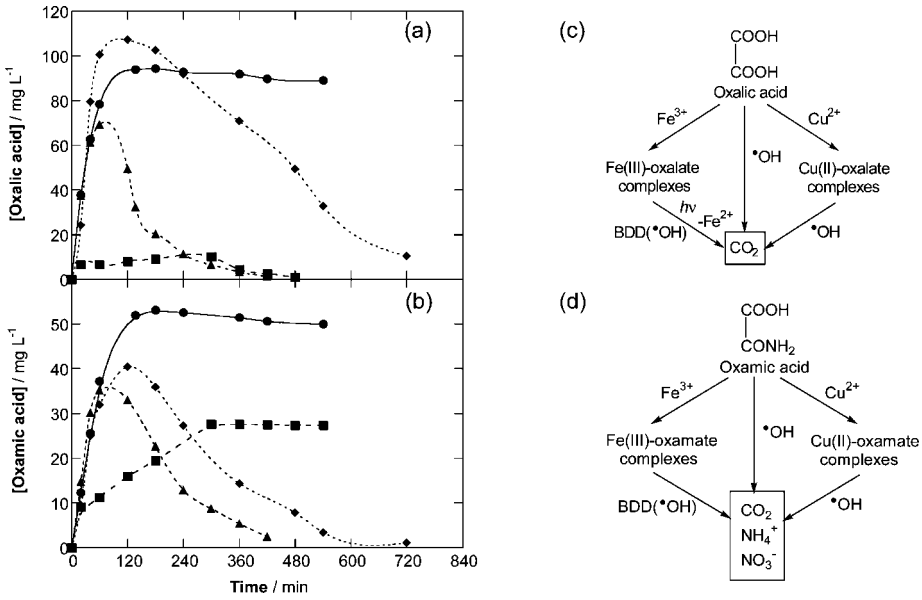

Figure 44. Time course of the concentration of (a) oxalic and (b) oxamic acids during the degradation of 100 mL of 220 mg L^{-1} Indigo Carmine solutions in 0.05 M Na_2SO_4 at pH 3.0, 33 mA cm^{-2}, and 35.0 °C using the Pt/O_2 or BDD/cell of Figure 10 or 25e with 3 cm^2 electrodes. Process: (●) EF with Pt and 1.0 mM Fe^{2+}, (■) PEF with Pt, 1.0 mM Fe^{2+}, and a 6 W UVA light; (◆) EF with BDD and 1.0 mM Fe^{2+}; (▲) PEF with Pt and 1.0 mM Fe^{2+} + 0.25 mM Cu^{2+}. Proposed pathways for the mineralization of (c) oxalic and (d) oxamic acids. Reprinted with permission from ref 210. Copyright 2006 Elsevier.

showed that Indigo Carmine followed a pseudo-zero-order reaction kinetics, disappearing at the same time as its aromatic derivatives isatin 5-sulfonic acid, indigo, and isatin, mainly by reaction with the •OH produced from Fenton's reaction 1. Ion-exclusion HPLC detected the persistent oxalic and oxamic acids, which are present in the medium in the form of Fe(III)−oxalate and Fe(III)−oxamate complexes. Figure 44a and 44b shows that both complexes undergo a slow reaction with •OH generated from Fenton's reaction 1 and Pt(•OH) generated from reaction 46 in EF with Pt, although they are completely destroyed with BDD(•OH) in EF with BDD, in agreement with the great oxidation power of the latter radical. When the solution was irradiated with a 6 W UVA lamp to apply PEF with Pt, the TOC abatement attained 84% in 540 min and Fe(III)−oxalate complexes disappeared in 480 min (see Figure 44a) but Fe(III)−oxamate complexes were not destroyed and attained a steady concentration (see Figure 44b). The highest mineralization power of PEF compared with EF was ascribed to the quick photolysis of Fe(III)−oxalate complexes under UVA irradiation from reaction 29 involving Fe^{2+} regeneration.[101] Cu^{2+} was then added as a cocatalyst to try to produce an additional quantity of •OH from Fenton-like reaction 64. Surprisingly, it was found that PEF with Pt and 1.0 mM Fe^{2+} + 0.25 mM Cu^{2+} yielded almost total mineralization (>97% TOC reduction) in about 450 min owing to a faster and total destruction of both oxalic and oxamic acids (see Figure 44a and 44b). The synergistic effect of Fe^{2+} and Cu^{2+} in this method was explained by the following: (i) photolysis of Fe(III)−oxalate complexes and (ii) simultaneous reaction of competitively formed Cu(II)−oxalate and Cu(II)−oxamate complexes[339] with •OH in the bulk. On the basis of these results, the different reaction pathways of Figure 44c and 44d were proposed to describe the mineralization of oxalic and oxamic acids, respectively, in the situations tested.

7.2.3. Other EAOPs Based on Fenton's Reaction Chemistry

In previous sections, we explained the good performances of various technologies for the degradation of synthetic wastewater. For example, Bromopyrogallol Red was successfully treated by EF with Co^{2+} as a catalyst,[206] Orange II by EF with an ACF cathode and GAC microelectrodes,[219] Remazol Black B (C. I. Reactive Black 5) by PC,[109] Orange G (C. I. Acid Orange 10)[242] and Direct Yellow 52[243] by PEC-EF, Meldola Blue (C. I. Basic Blue 9) by SEF,[255] and Rhodamine B (C. I. Basic Violet 10) by cathodic generation of Fe^{2+} ions.[257] The Fered−Fenton method explained in section 6.1 has also been used for this purpose. For the treatment of the azo dye Reactive Black 5, Rao et al.[267] managed to remove more than 92% COD in 15 min for an optimized $[Fe^{2+}]/[H_2O_2]$ ratio, where the degradation was about seven times faster than that provided by the traditional Fenton process. Similarly, Huang et al.[265] reported about 93% mineralization of the same azo dye, even starting from concentrated solutions of up to 10 000 mg L^{-1} COD. In the latter case, analysis of solutions with 200 mg L^{-1} Fe^{2+} of pH 2.0 treated in an undivided DSA/stainless steel flow cell at 2.8 mA cm^{-2} for 3 h under continuous H_2O_2 dosage up to 27 000 mg L^{-1} showed a rapid mineralization of generated formic acid, whereas the ultimate oxalic acid was destroyed very slowly because of the formation of persistent Fe(III)−oxalate complexes, as also reported for the EF and PC treatment of various pollutants with a GDE as a cathode.[148,184,210,228–230] Evidence of the positive action of plasma-assisted Fenton to destroy dyestuffs has been reported by Koprinavac et al.[318] They studied the degradation of 1 L of 20 mg L^{-1} solutions of the azo dyes Mordant Yellow 10, Direct Orange 39, Reactive Red 45, and Reactive Blue 137 containing 0.5 mM Fe^{2+} and 2.5 mM H_2O_2 at natural pH for 60 min. While the chemical Fenton process provided a maximum of 93% color removal and 37% mineralization, with Direct Orange 39 the most prone to such degradation,

application of the pulsed discharged plasma at 45 kV and 60 Hz gave overall decolorization described by surprisingly large second-order rate constant values in the range from 1.3×10^8 to 8.4×10^{10} M^{-1} min^{-1}, along with 98% mineralization for all dyes. In contrast, the use of the corona discharge without Fenton's reagent was very inefficient, only promoting a 26% color decay without significant mineralization.

7.3. Pharmaceuticals and Personal Care Products (PPCPs)

Over the past decade, human and veterinary PPCPs have received increasing attention as POPs in waters. These emerging pollutants are continuously introduced in the aquatic environment at ng−μg L^{-1} levels by several routes including emission from production sites, direct disposal of overplus drugs in households and hospitals, excretion after drug administration to humans and animals, and water treatments in fish farms.[1–3] The possible interactions of PPCPs with living beings in the environment are not well documented, although available data indicate that some drugs can alter the endocrine system of fish as well as exert toxic effects on algae and invertebrates and favor the development of multiresistant strains of microorganisms.[340] Conventional sewage treatment plants provide very inefficient destruction of PPCPs because they are usually resistant to biodegradation, which means the use of oxidation technologies is needed to ensure their removal from the environment.

Chemical oxidants such as Cl_2, ClO_2, and O_3 can react with drugs and their metabolites but are unable to promote their total mineralization.[42,341] Several AOPs have been employed to remove PPCPs released into wastewaters from drug manufacturing.[42] For example, the chemical Fenton process was successfully applied to an extremely polluted pharmaceutical wastewater to significantly reduce its initial COD of 362 000 mg L^{-1}.[342] Unfortunately, few papers have reported the degradation of these compounds by EAOPs based on Fenton's reaction chemistry (see Table 6).

Preliminary studies by Oturan and co-workers in this field described the formation of hydroxylated derivatives of the neuroprotector riluzole[120,343] in EF with a carbon-felt cathode. Recent research by Brillas' group has corroborated the great mineralization degree attained in electrolytic systems with GDE for the treatment of aromatic PPCPs. First works were focused on exploring the effect of Cu^{2+} as a cocatalyst in the EF and PEF treatments of paracetamol (*N*-(4-hydroxyphenyl)acetamide), a common antipyretic/analgesic compound classified as a nonsteroidal anti-inflammatory drug (NSAID), using the Pt/O_2 cells of Figures 10 and 25e.[185,231] Solutions of 100 mL containing up to 1 g L^{-1} of this drug in 0.05 M Na_2SO_4 of pH 3.0 were electrolyzed at a constant current between 100 and 450 mA at 35 °C for 6 h. At 100 mA, the oxidation power of the catalyzed systems increased in the sequence 1 mM $Cu^{2+} \leq$ 1 mM Cu^{2+} + UVA light < 1 mM $Fe^{2+} \ll$ 1 mM Fe^{2+} + 1 mM $Cu^{2+} \approx$ 1 mM Fe^{2+} + UVA light < 1 mM Fe^{2+} + 1 mM Cu^{2+} + UVA light. The poor degradation achieved in the presence of 1 mM Cu^{2+}, with and without UVA light, was ascribed to the low production of Pt(•OH) by reaction 32 and •OH by reaction 64 under the action of the Cu^{2+}/Cu^{+} system. In EF with 1 mM Fe^{2+} less than 70% mineralization was obtained because of the formation of stable complexes of Fe(III) with oxalic and oxamic acids that cannot be attacked by •OH formed from Fenton's reaction 1. These species are photolyzed by UVA light in PEF, giving almost total mineralization.

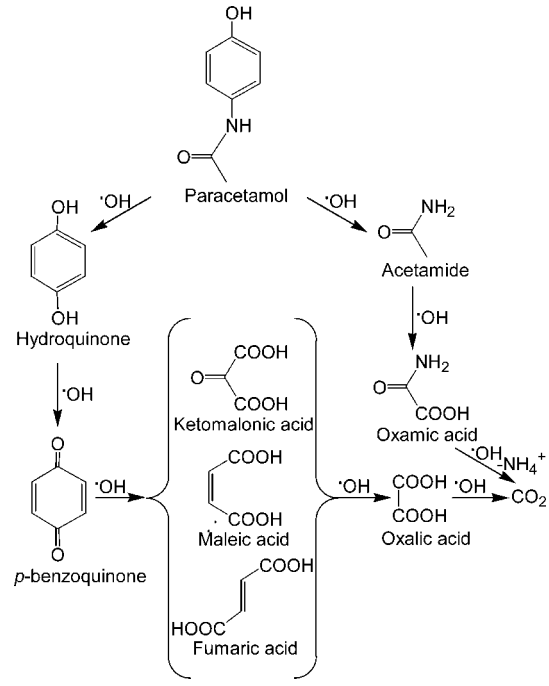

Figure 45. Proposed reaction sequence for paracetamol degradation in acid aqueous medium by EAOPs based on Fenton's reaction chemistry. Adapted with permission from ref 185. Copyright 2006 The Electrochemical Society.

Complete decontamination was also feasible with 1 mM Fe^{2+} and 1 mM Cu^{2+} because •OH can destroy the Cu(II) complexes generated. The synergistic effect of all catalysts promoted the quickest destruction using 1 mM Fe^{2+} and 1 mM Cu^{2+} under UVA irradiation. The MCE values calculated for this procedure increased with rising pollutant concentration and decreasing current. Initial nitrogen was mainly transformed into NH_4^+ ions during all treatments. From the identification of intermediates by GC-MS and HPLC, the reaction sequence of Figure 45 was proposed. The initial hydroxylation of paracetamol produces hydroquinone with a release of acetamide, which is converted into oxamic acid. Simultaneous opening of the benzenic ring of *p*-benzoquinone coming from hydroquinone degradation leads to oxalic acid via oxidation of generated carboxylic acids such as ketomalonic, maleic, and fumaric. The removal of final oxalic and oxamic acids was strongly affected by the action of catalysts, similar to what was proposed for the treatment of the dye Indigo Carmine in Figure 44c and 44d, respectively.[210] Figure 46 shows that the use of Cu^{2+} alone promotes a small accumulation of Cu(II)−oxalate and Cu(II)−oxamate complexes as a result of the slow degradation of pollutants. When only Fe^{2+} was added, Fe(III)−oxalate and Fe(III)−oxamate complexes could not be efficiently mineralized by •OH, thus limiting the oxidation ability of EF. The efficient photodecomposition of Fe(III)−oxalate complexes, along with slow but progressive photolysis of Fe(III)−oxamate ones, explains the faster mineralization in PEF. By using Fe^{2+} and Cu^{2+}, Fe(III)−oxalate, Fe(III)−oxamate, Cu(II)−oxalate, and Cu(II)−oxamate complexes are produced, but uniquely Cu(II) complexes are destroyed. The quickest and total mineralization of paracetamol with Fe^{2+} + Cu^{2+} + UVA light is then due to the oxidation of Cu(II)−oxalate and Cu(II)−oxamate complexes with •OH in parallel to the photodegradation of their Fe(III) complexes by UVA light.

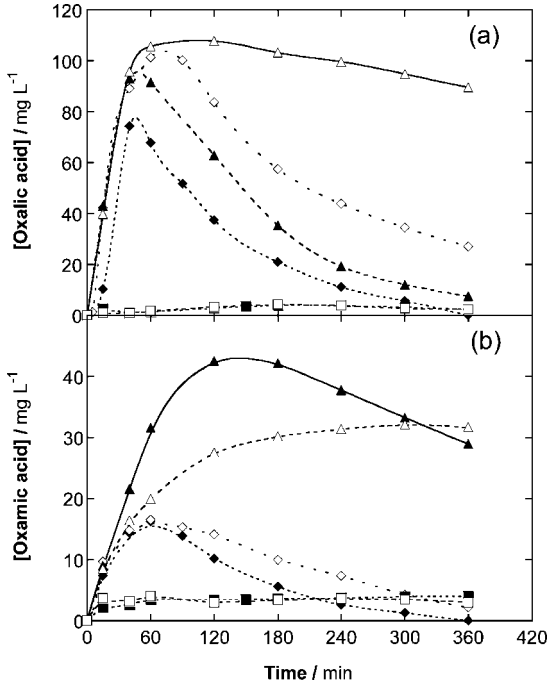

Figure 46. Evolution of (a) oxalic and (b) oxamic acids during the degradation of 100 mL of 157 mg L^{-1} paracetamol solutions in 0.05 M Na_2SO_4 at pH 3.0, 100 mA cm^{-2}, and 35.0 °C using the same Pt/O_2 cell of Figure 44. Catalyst: (□) 1 mM Cu^{2+}, (■) 1 mM Cu^{2+} + 6 W UVA light, (△) 1 mM Fe^{2+}, (▲) 1 mM Fe^{2+} + UVA light, (◇) 1 mM Fe^{2+} + 1 mM Cu^{2+}, and (◆) 1 mM Fe^{2+} + 1 mM Cu^{2+} + UVA light. Adapted with permission from ref 185. Copyright 2006 The Electrochemical Society.

Further work of Brillas' group tested the AO-H_2O_2, EF, and PEF treatments of the blood lipid regulator metabolite clofibric acid (2-(4-chlorophenoxy)-2-methylpropionic acid),[232,233] the NSAID salicylic acid (2-hydroxybenzoic acid),[236] and the biocide chloroxylenol (4-chloro-3,5-dimethylphenol)[237] in undivided Pt/O_2 and BDD/O_2 cells. Figure 47a illustrates the comparative TOC abatement found for 100 mL of 179 mg L^{-1} clofibric at pH 3.0, 100 mA cm^{-2}, and 35.0 °C for several treatments in cells with a 3 cm^2 electrode area. As can be seen, overall mineralization for AO-H_2O_2 with a BDD anode is achieved at a similar rate in the absence and presence of UVA light after consumption of 18 Ah L^{-1} in 6 h, indicating the high reactivity of BDD(•OH) generated from reaction 32 without a significant contribution from the photolysis of intermediates. In contrast, only about 40% of mineralization was promoted by analogous degradations with AO-H_2O_2 with Pt (data not shown), as expected from the lower oxidizing power of Pt(•OH). The superiority of BDD compared with Pt as an anode was also confirmed in EF and PEF with 1.0 mM Fe^{2+} as a catalyst. Figure 47a shows much faster TOC removal for these methods than for AO-H_2O_2 because of the quickest reaction of pollutants with •OH produced from Fenton's reaction 1 in EF along with the photodecomposition of Fe(III)−oxalate complexes in PEF. The solution is then completely mineralized either after 6 h (18 Ah L^{-1}) of EF with BDD and PEF with Pt or after 4 h (12 Ah L^{-1}) of PEF with BDD. The relative oxidation ability of Pt(•OH) and BDD(•OH) and homogeneously formed •OH can be observed in Figure 47b and 47c, which presents the clofibric acid decay and its pseudo-first-order kinetic analysis for the above treatments. The average k_1 value in AO-H_2O_2 raised from (1.70 ± 0.13) × 10^{-4} to (4.70 ± 0.10) × 10^{-4} s^{-1} when Pt was replaced by BDD, whereas a similar and much higher average k_1 value

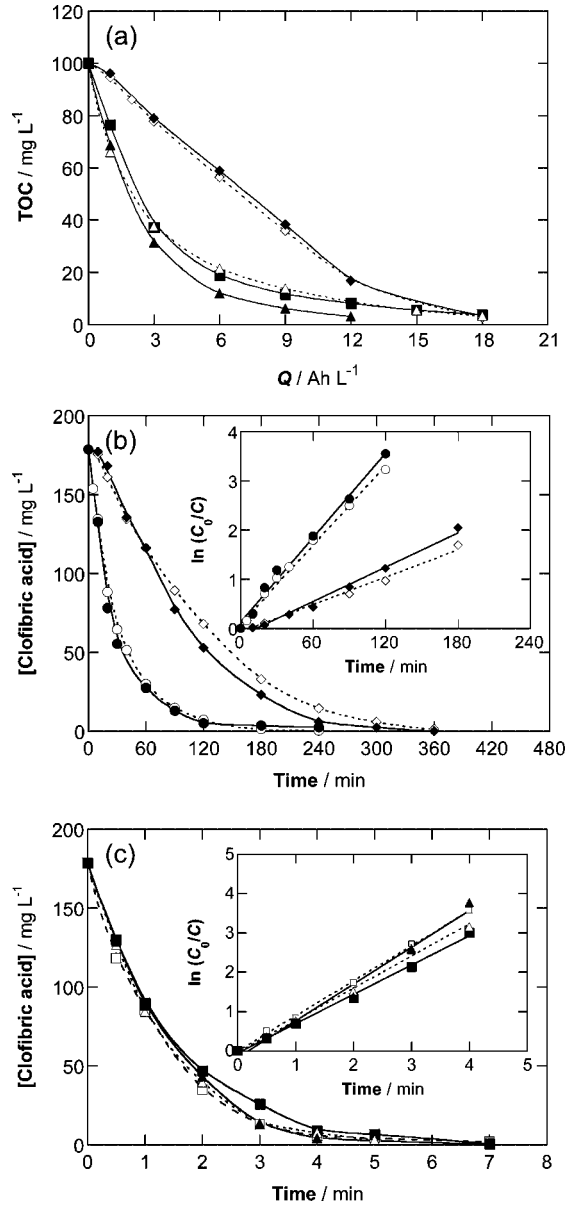

Figure 47. (a) TOC removal and (b and c) clofibric acid concentration decay with the corresponding kinetic analysis (inset) for the degradation of 100 mL of 179 mg L^{-1} of this product in 0.05 M Na_2SO_4 at pH 3.0, 100 mA cm^{-2}, and 35.0 °C using the same cells of Figure 44: (○) AO-H_2O_2 with Pt, (●) AO-H_2O_2 with Pt and 6 W UVA light, (◇) AO-H_2O_2 with BDD, (◆) AO-H_2O_2 with BDD and UVA light, (□) EF with Pt and 1.0 mM Fe^{2+}, (■) PEF with Pt and 1.0 mM Fe^{2+}, (△) EF with BDD and 1.0 mM Fe^{2+}, and (▲) PEF with BDD and 1.0 mM Fe^{2+}. Reprinted with permission from refs 232 and 233. Copyright 2007 Elsevier.

of (1.35 ± 0.10) × 10^{-2} s^{-1} was obtained for all EF and PEF treatments, thus confirming the highest reactivity of •OH formed in the bulk. Similar trends for TOC and pollutant concentration decays were found for salicylic acid and chloroxylenol. For all compounds, an increase in MCE calculated from eq 56 was seen when increasing initial concentration or decreasing current density, as expected from the minimization of parasitic reactions 9, 17, and 47. A similar behavior has been reported for the degradation of chlorophenoxy herbicides by the same EAOPs with GDE (see section 7.1.3). The comparative SPEF treatment of salicylic acid with Pt and BDD was also carried out,[256] showing a much faster TOC decay compared with PEF owing to (i) the additional production of •OH from photore-

duction reaction 27 and (ii) the quicker photolysis of Fe(III)−oxalate complexes with the greater UVA energy supplied by solar irradiation. Analysis of the treated solutions by GC-MS and HPLC allowed detecting intermediates such as (i) 4-chlorophenol, 4-chlorocatechol, hydroquinone, and *p*-benzoquinone and 2-hydroxyisobutyric, tartronic, maleic, fumaric, formic, and oxalic acids for clofibric acid, (ii) 2,3-dihydroxybenzoic, 2,5-dihydroxybenzoic, 2,6-dihydroxybenzoic, α-ketoglutaric, glycolic, glyoxylic, maleic, fumaric, malic, tartronic, and oxalic acids for salicylic acid, and (iii) 2,6-dimethylhydroquinone, 2,6-dimethyl-*p*-benzoquinone, and 3,5-dimethyl-2-hydroxy-*p*-benzoquinone and maleic, malonic, pyruvic, acetic, and oxalic acids for chloroxylenol. Hydroxylation followed by the generation of carboxylic acids is then the main degradative route of these aromatic PPCPs, as stated above for paracetamol (see Figure 45).

In a collaboration between Brillas and Oturan's groups, the EF degradation of the antimicrobials chlorophene (*o*-benzyl-*p*-chlorophenol),[173] triclocarban (*N*-(4-chlorophenyl)-*N*′-(3,4-dichlorophenyl)urea),[344] and triclosan (2,4,4′-trichloro-2′-hydroxydiphenyl ether)[344] was comparatively assessed using the undivided cells of Figures 10 and 16a, containing a Pt or BDD anode and an O_2-diffusion or carbon-felt cathode with Fe^{3+} as a catalyst. In the cells with GDE, H_2O_2 was largely accumulated but Fe^{3+} content remained unchanged, so that pollutant decay was enhanced by increasing the initial Fe^{3+} concentration because this promoted faster Fe^{2+} regeneration at the cathode with greater $^{\bullet}OH$ production from Fenton's reaction 1. In contrast, when the carbon-felt cathode was used H_2O_2 was electrogenerated in a relatively small extent, whereas Fe^{2+} was largely accumulated as a result of the quick Fe^{3+} cathodic reduction, requiring a Fe^{3+} concentration as low as 0.2 mM to obtain the maximum $^{\bullet}OH$ generation rate. Under these conditions, k_2 values of 1.00×10^{10} and 5.49×10^9 M^{-1} s^{-1} were obtained for the decay reactions of chlorophene and triclosan, respectively. Poor mineralization degree was found for the Pt/O_2 cell because of the difficult oxidation of final Fe(III)−oxalate with $^{\bullet}OH$. These complexes were completely destroyed using a BDD anode at a high current thanks to the large amount of BDD($^{\bullet}OH$) generated on its surface. Complete mineralization was also achieved in both the Pt/carbon felt and BDD/carbon felt cells with 0.2 mM Fe^{3+} owing to the efficient oxidation of Fe(II)−oxalate complexes with $^{\bullet}OH$ in the bulk. The highest oxidation power regarding total mineralization was attained for the BDD/carbon felt cell at a high current by the additional destruction of Fe(II)−oxalate complexes with BDD($^{\bullet}OH$). The overall release of Cl^- was confirmed for all treatments. Electrolyses in hydroorganic medium were found to be an interesting alternative for the study of the reaction pathway of low water-soluble pollutants. Thus, primary intermediates such as 2,4-dichlorophenol, 4-chlorocatechol, chlorohydroquinone, and chloro-*p*-benzoquinone were identified for triclosan, whereas urea, hydroquinone, chlorohydroquinone, 1-chloro-4-nitrobenzene, and 1,2-dichloro-4-nitrobenzene were reported for triclocarban.

7.4. Industrial Pollutants

Different EAOPs based on Fenton's reaction chemistry have been applied to the remediation of many synthetic wastewaters containing industrial chemicals including phenol and phenolic compounds, anilines, benzene derivatives, aliphatics, and so on (see Table 6). The main purpose of most of these studies was to demonstrate the viability of such technologies, usually paying less attention to the detection of intermediates involved in the degradation process.

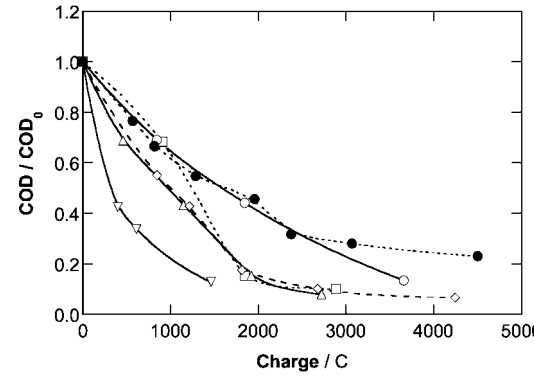

Figure 48. Normalized COD as a function of charge for the EF treatment of 1 L of 0.33 mM of different industrial pollutants with 1 mM Fe^{2+} in 0.05 M Na_2SO_4 at pH 2 as catholyte in the three-electrode flow system of Figure 8 with an RVC cathode of 50 mm × 50 mm × 12 mm at $E_{cat} = -0.7$ V/SCE and a linear flow rate of 0.13 m s^{-1}: (●) Phenol, (○) hydroquinone, (□) *p*-benzoquinone, (△) catechol, (◇) cresol, and (▽) aniline. Adapted with permission from ref 124. Copyright 1999 Elsevier.

7.4.1. Phenol and Phenolic Compounds

Phenol and phenolic compounds are widely used in the manufacture of antioxidants, biocides, disinfectants, pesticides, polymeric resins, dyes, pulp, paper, pharmaceuticals, and other synthetic materials. Therefore, such contaminants are commonly found in industrial wastewater streams from oil refineries, petrochemical and coal conversion plants, and chemical industries in general.[9,10] Ozonation, chlorination, and AOPs such as the chemical Fenton's reagent have proven useful for the remediation of effluents containing high concentrations of these pollutants.[13,14,17]

The degradation of phenol has been carried out by EF[118,119,124,147,181,205,345,346] as well by the plasma-assisted Fenton process.[317] Sudoh et al.[118] treated 170 mL of O_2-saturated phenol solutions with Fe^{2+} in the cathodic compartment of the H-type Pt/graphite cell of Figure 6 at $E_{cat} = -0.6$ V vs Ag/AgCl/KCl (satd). The current efficiency decreased from about 145 to 60% with an increasing consumed charge of 260−2600 mg L^{-1} COD at pH 3.0, with an optimum Fe^{2+} content of 2 mM for 2.5 mM phenol. Current efficiencies greater than 100% at the beginning of the process were related to additional degradation with O_2 along with $^{\bullet}OH$. Hydroquinone, cathecol, *p*-benzoquinone, muconic acid, and maleic acid were identified as intermediates. Alvarez-Gallegos and Pletcher[124] used the divided three-electrode cell in Figure 8 with an RVC cathode to degrade 1 L of O_2-saturated 0.05 M Na_2SO_4 solutions containing 0.33 mM phenol and 1 mM Fe^{2+} at pH 2.0 and $E_{cat} = -0.7$ V/SCE. As seen in Figure 48, this phenol solution is slowly mineralized, with its COD reduced by 77% after consumption of 4500 C. For comparison, Figure 48 also shows that other benzene derivatives such as hydroquinone, cresol, catechol, *p*-benzoquinone, and aniline are more easily degraded and to a larger extent by EF under comparable conditions, with a current efficiency > 50%. Similarly, a 10 mM solution of oxalic acid, which is the most important recalcitrant intermediate of those aromatics, reached 94% mineralization after imposing 8500 C for 330 min, with efficiency close to 40%. Harrington and Pletcher[119] further examined the mineralization of 80 mL of aqueous 0.05 M Na_2SO_4 solutions with

0.5−3 mM phenol and 1 mM Fe^{2+} in the pH range 1.0−3.0 using a small divided cell with a 2.3 cm^2 carbon-PTFE O_2-fed cathode working at E_{cat} from −0.4 to −1.4 V/SCE. The highest current efficiencies of 60−70% with 90% COD removal were found at pH 2.0, without significant influence of the applied E_{cat}. An energy cost < 14 kWh m^{-3} was estimated at these optimum conditions assuming a cell voltage of 5 V. The authors obtained similar results for the treatment of aniline, acetic acid, and formaldehyde. Fockedey and Van Lierde[181] used the flow cell in Figure 21 to degrade 300 mL of effluents containing up to 3 g L^{-1} phenol and 0.25 M Na_2SO_4. The best operative conditions were found at pH 3.0 with 50 mg L^{-1} Fe^{2+} and 20 mg L^{-1} of dissolved O_2, yielding an energy cost of 2.68 Ah (g COD)$^{-1}$ and a current efficiency of about 125% (note that the maximum efficiency taking advantage of both coupled anode and cathode oxidations is 200%). An undivided cylindrical flow configuration was employed by Wu et al.[345] for the treatment of phenol using a β-PbO_2 anode modified with fluorine resin and a Ni−Cr−Ti alloy cathode. Since this cathode could produce a certain amount of H_2O_2 under air sparging, the addition of 0.5 mM Fe^{2+} to 550 mL of 100 mg L^{-1} phenol in 10 g L^{-1} K_2SO_4 at pH 3.0 and 25 °C promoted the formation of $^{\bullet}OH$ by Fenton's reaction 1, which removed all initial contaminant in 60 min with 12% ICE operating at 1.5 A. Agladze et al.[346] recently reported the degradation of 1 L of synthetic solutions with 282 mg L^{-1} phenol, 178 mg L^{-1} 4-chlorophenol, and 1000 mg L^{-1} aniline in 1 g L^{-1} Na_2SO_4 and 1 mM Fe^{2+} at pH 3.0 and 20 °C using an undivided filter-press Electrocell AB cell equipped with a 100 cm^2 Ti/IrO_2−SnO_2 anode and a 100 cm^2 GDE cathode fed with pure O_2 operating in the batch recycle mode at 5 A and a liquid flow rate of 60 L h^{-1}. About 90% COD reduction with 22 kWh m^{-3} energy cost was determined for phenol and 4-chlorophenol after 30 min of treatment, whereas 92% COD removal was achieved for aniline after 120 min. Following its study with different catalysts performed on the EF process of phenol with the Pt/carbon felt of Figure 16a, Pimentel et al.[205] showed the overall TOC abatement in only 60 min when treating 150 mL of 1.0 mM phenol with 0.1 mM Fe^{3+} at pH 3.0 and 300 mA. A k_2 value of $(2.62 \pm 0.23) \times 10^9$ M^{-1} s^{-1} was determined for its reaction with $^{\bullet}OH$ formed in the bulk. The main intermediates identified by HPLC were catechol, hydroquinone, *p*-benzoquinone, and carboxylic acids such as maleic, fumaric, succinic, glyoxylic, oxalic, and formic acids.

The mineralization of 2-chlorophenol,[347] 4-chlorophenol,[222,319,346,348,349] and 2,4-dichlorophenol[248,249,257,348,349] has been explored by different technologies. Apart from the studies described previously for 4-chlorophenol by EF[346] and plasma-assisted Fenton,[319] it is noticeable in the work of Brillas and co-workers[222] on the comparative treatment of 100 mL of 178 mg L^{-1} of this compound in 0.05 M Na_2SO_4 with 1 mM Fe^{2+} at pH 3.0 by AO-H_2O_2, EF, PEF, and PC in a Pt/O_2 cell using the same methodology as described in section 7.1.3 for chlorophenoxy herbicides. In all cases, the hydroxylated derivative 4-chloro-1,2-dihydroxybenzene was detected as an intermediate, which was further oxidized to maleic, fumaric, and oxalic acids with the loss of Cl^-. At 100 mA, AO-H_2O_2 only yielded 24% TOC decay in 360 min, as expected by the low oxidation power of Pt($^{\bullet}OH$) generated from reaction 46, while EF promoted 92% mineralization over the same electrolysis time due to the more efficient attack of $^{\bullet}OH$ formed from Fenton's reaction 1, and PEF gave overall decontamination in about 240 min as a result of photodecarboxylation of Fe(III)−oxalate complexes via reaction 29. The latter method was also much more efficient than the PC process, which became effective only for 120 min, whereupon ca. 15% of the initial TOC remained in solution. Another interesting study conducted by a Chinese group[348,349] on the EF process of chlorophenols reported a decreasing decay rate in the sequence 2,4-dichlorophenol > 2,4,6-trichlorophenol > pentachlorophenol > 4-chlorophenol for treatment of 200 mL of pollutant in 0.14 M Na_2SO_4 with 3.8 mg L^{-1} Fe^{2+} at pH 2.5 using an undivided three-electrode Pt/graphite cell at $E_{cat} = -0.55$ V/SCE. From GC-MS analysis of dechlorinated products, a double-degradative route was proposed involving either cathodic reduction or direct hydroxylation in the bulk by reaction with $^{\bullet}OH$. In the case of 2,4-dichlorophenol, for example, formation of 2-chlorophenol and 4-chlorophenol as intermediates was related to its cathodic reductive dechlorination, while that of 2-chlorocatechol and 2-chlorohydroquinone was associated with hydroxylation followed by dechlorination. Recent work[248,249] on the PEC-EF treatment of 50 mL of 15 mg L^{-1} 2,4-dichlorophenol in 0.02 M Na_2SO_4 at pH 5.8 using a Ti/TiO_2 photoanode illuminated with an 8 W UVA lamp combined with a sacrificial Fe anode, along with a graphite cathode, demonstrated a 93% abatement of this pollutant with 78% mineralization in 60 min by applying a constant current of 3.2 mA. The combined process was much more efficient than the comparable PEC and EF processes alone, in agreement with the synergistic oxidative action of photoinduced holes formed from reaction 41 and $^{\bullet}OH$ produced from reactions 1 and 68.

Oturan and co-workers reported interesting results for 4-nitrophenol[350] and 2-nitrophenol.[351] The use of a divided three-electrode Pt/carbon felt cell similar to that in Figure 17a at $E_{cat} = -0.5$ V/SCE yielded the total disappearance of 4 mM 4-nitrophenol in 125 mL of an O_2-saturated solution of pH 2.0 with 0.5 mM Fe^{3+} after consumption of 1000 C and 95% COD removal for a 1 mM solution at 800 C. 4-Nitrocatechol, 4-nitropyrogallol, hydroquinone, *p*-benzoquinone, and 1,2,4-trihydroxybenzene were detected as hydroxylated intermediates, along with maleic, fumaric, and oxalic acids as major generated carboxylic acids. Further treatment of 250 mL of 0.2 mM 2-nitrophenol in 0.05 M Na_2SO_4 with 0.1 mM Fe^{3+} at pH 3.0 with the undivided Pt/carbon felt cell of Figure 16a at 300 mA confirmed overall mineralization after 8 h of electrolysis with the formation of analogous hydroxylated aromatics and carboxylic acids, along with the release of NH_4^+ and NO_3^- ions. The competition method yielded k_2 values of $(1.2 \pm 0.2) \times 10^{10}$ and 3.4×10^9 M^{-1} s^{-1} for the corresponding oxidation reaction of 4-nitrophenol and 2-nitrophenol with $^{\bullet}OH$, in good agreement with the value of 3.8×10^9 M^{-1} s^{-1} determined for 4-nitrophenol hydroxylation by pulse radiolysis at pH 7.0.[47] Furthermore, Yuan et al.[352] explored the degradation of 200 mL of solutions containing several nitrophenols in 25 g L^{-1} Na_2SO_4 of pH 3.0 by EF with 0.5 mM Fe^{2+} and by AO using a Pt/graphite cell, at 50 mA in both cases. The EF process gave a faster decay of all compounds in the sequence 4-nitrophenol > 2-nitrophenol > 2,4-dinitrophenol > 3-nitrophenol > phenol. Evidence for the cathodic reduction of 4-nitrophenol was found in cyclic voltammograms recorded in acetic buffer of pH 4.7 on graphite, as shown in Figure 49a, since they displayed an irreversible peak for the reduction of 4-nitrophenol to 4-nitrosophenol at −1.0 V/SCE,

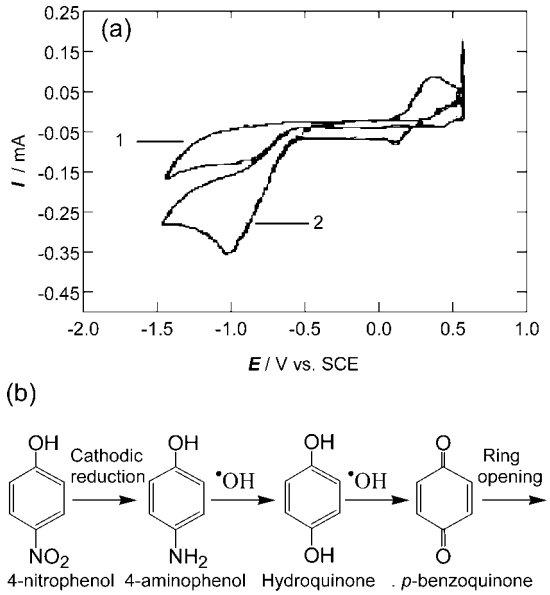

Figure 49. (a) Cyclic voltammogram recorded for the reduction of 3.2 mM 4-nitrophenol in a 25 mM acetic buffer of pH 4.7 on a graphite electrode between 0.6 and −1.5 V. (1) Acetic buffer electrolyte at 50 mV s^{-1}, and (2) 4-nitrophenol solution at 150 mV s^{-1}. (b) Proposed reaction sequence for the initial degradation of 4-nitrophenol by EF. Adapted with permission from ref 352. Copyright 2006 Elsevier.

followed by two coupled peaks at 0.30 and 0.18 V/SCE related to the equilibrium between 4-nitrosophenol and 4-aminophenol. Since no significant amounts of released NO_3^- and NO_2^- ions were detected after 13% mineralization of 3.6 mM 4-nitrophenol, they proposed the reaction pathway of Figure 49b, involving its initial cathodic reduction to 4-aminophenol, followed by oxidation of this intermediate to hydroquinone and *p*-benzoquinone with •OH formed from Fenton's reaction 1. In contrast, the predominance of hydroxylation over cathodic reduction was suggested for low 4-nitrophenol content of up to 0.2 mM, as proposed by Oturan's group. On the other hand, the Fered−Fenton treatment of 4-nitrophenol in H_2SO_4 of pH 5.0−6.0 has also been investigated by Zhang et al.[268] using a cylindrical cell of 16 cm in height equipped with a central Ti road coated with RuO_2−TiO_2 of 1.5 cm diameter, surrounded by a stainless steel cathode of 8 cm diameter. Ninety three percent COD reduction for 2.8 L of 200 mg L^{-1} solutions was obtained under an optimized $[Fe^{2+}]/[H_2O_2]$ ratio of 1:10 with the continuous addition of H_2O_2 up to 18.25 mM for 60 min, operating at 1 A and an effluent flow rate of 45 L h^{-1}.

Oturan's group also examined the EF behavior of bisphenol A (2,2-bis-(4-hydroxyphenyl)propane)[353] and vanillic acid (4-hydroxy-3-methoxybenzoic acid).[354] A divided three-electrode Pt/carbon felt cell was utilized to comparatively degrade 200 mL of O_2-saturated solutions of 0.7 mM bisphenol A in 0.01 M HCl with different contents of Fe^{2+} or Cu^{2+} as catalyst at $E_{cat} = -0.55$ V/SCE. For 1 mM Fe^{2+} or 1 mM Cu^{2+}, the same k_2 value of 1.0×10^{10} M^{-1} s^{-1} was determined for the reaction of this compound with •OH produced from reaction 1 or 64, respectively, but the degradation process with Fe^{2+} was more efficient with the charge consumed, attaining 82% mineralization after applying 10 000 C. GC-MS and HPLC analysis of electrolyzed solutions allowed proposing the initial production of *ortho*- and *meta*-monohydroxylated derivatives of bisphenol A, which are oxidized to a dihydroxylated product. Further degradation of this latter product leads to aromatic intermediates such as phenol, hydroquinone, catechol, resorcinol, and *p*-benzoquinone, subsequently transformed into carboxylic acids such as ketomalonic, maleic, acetic, and formic acids. In the case of vanillic acid, 100 mL of a solution with 0.45 mM of this pollutant and 0.5 mM Fe^{3+} in H_2SO_4 of pH 3.0 was electrolyzed in the undivided cell of Figure 16a at 200 mA. Vanillic acid followed a pseudo-first-order decay reaction, disappearing after consuming 200 C, whereas all solution COD was removed after imposing a much greater charge of 6000 C.

The ability of the SPEF process to rapidly mineralize aromatic industrial pollutants was assessed by Flox et al.[149] for *o*-, *m*-, and *p*-cresol. They employed the flow plant of Figure 12a containing the BDD/O_2 cell of Figure 12b, with electrodes of 20 cm^2 area, coupled to a solar photoreactor for the comparative EF and SPEF treatments of 2.5 L of solutions with up to 1024 mg L^{-1} of each cresol in 0.05 M Na_2SO_4 at 25−100 mA cm^{-2}, 30 °C, and a liquid flow rate of 180 L h^{-1}. Under optimized conditions of 0.25 mM Fe^{2+} and pH 3.0, the initial TOC of 128 mg L^{-1} of all cresols was reduced by 98% in 180 min using SPEF but only by 54% in EF. Similar to the SPEF treatment of the pesticide MCPP discussed above,[235] the synergistic action of sunlight producing more •OH via the photoreduction reaction 27 and fast photolysis of Fe(III)−oxalate complexes explained why MCE values were as high as 480% after 2 h of SPEF. For 25 mA cm^{-2}, solutions with 128 mg L^{-1} TOC of all cresols were totally decontaminated in about 240 min with an energy cost as low as 68 kWh (kg TOC)$^{-1}$ or 6.6 kWh per m^3 of treated solution. HPLC analysis allowed establishing that initial hydroxylation of *o*-cresol and *m*-cresol gives 2-methyl-*p*-benzoquinone via 2-methylhydroquinone, whereas dihydroxylation of *p*-cresol leads to 5-methyl-2-hydroxy-*p*-benzoquinone. These aromatic byproducts are then converted into oxalic and acetic acids as the most persistent final products. SPEF has a much better performance than the PEF process with UVC light reported by Irmak et al.[238] for the destruction of 300 mL of an O_2-saturated 0.6 mM 4-chloro-*o*-cresol solution with 1.8 mM Fe^{2+} in H_2SO_4 of pH 2.7, as detailed in section 5.2.

Boye and co-workers investigated the degradative behavior of polyhydroxy compounds such as gallic acid (3,4,5-trihydroxybenzoic acid)[143] and its derivative gallotannic acid,[286] one of the most important components of tannin wastewater. They treated 200 mL of solutions containing up to 6 mM gallic acid in 2.0 g L^{-1} KCl of pH 3.0 at 80 mA and room temperature. The EF method with 1 mM Fe^{2+} in an undivided Pt/O_2 cell promoted 70% TOC removal in 4 h, whereas the comparable PEF with UVA light led to 90% mineralization. This behavior was explained by the expected production of stable Fe(III)−oxalate complexes that can only be photodecarboxylated under UVA irradiation. In contrast, the electrocoagulation method using an Fe/Pt cell yielded 95% decontamination in 2 h because of the quick precipitation of complexes between gallic acid and Fe(III). This precipitation process, along with the parallel mineralization of gallic acid and its reaction intermediates with •OH and coagulation with $Fe(OH)_3$, explains that overall decontamination can be reached in less than 2 h by PC in an Fe/O_2 cell. Therefore, PC can be much more effective than EF and PEF for wastewater remediation when insoluble complexes of Fe(III) with pollutants are formed. On the basis of these features, the same experimental conditions were used to treat

2 g L^{-1} of gallotannic acid by electrocoagulation and PC.[286] Complete removal favored by the precipitation of its Fe(III) complexes was obtained for both treatments, although soluble COD decayed more efficiently in the PC process due to the quicker generation of Fe^{3+} from Fenton's reaction 1.

Evidence for the fast removal of phenolic compounds by ECP was reported by Martins et al.[288] for nonylphenol polyethoxylate, a common constituent of textile wastewater. A 95% removal of this compound was found after as little as 5 min of electrolysis of 600 mL of a 40 mg L^{-1} solution in 2.8 g L^{-1} NaCl at pH 5.0 and 60 °C in a stirred tank reaction with two 24 cm^2 Fe electrodes after the addition of 40 mg L^{-1} H_2O_2 by applying 1 A. This behavior was ascribed to the combined action of oxidation with $^{\bullet}OH$ produced from Fenton's reaction 1 and coagulation with the $Fe(OH)_3$ sludge generated, because comparable electrocoagulation treatment only yielded a 46% decay of the pollutant. Nevertheless, very stable intermediates were formed, as suggested by the unchanged H_2O_2 content after times longer than 5 min.

7.4.2. Anilines

Aniline and its derivatives are highly toxic because they react easily in the blood to convert hemoglobin into methahemoglobin, thereby preventing oxygen uptake. These aromatic amines are produced as byproduct or wastes in the dye, petroleum, pulp and paper, coal, perfume, and rubber industries.[17,23]

The degradation of aniline has been examined by several EAOPs based on Fenton's reaction chemistry, as explained in section 7.4.1 for EF with RVC[124] and GDE[119,346] cathodes as well as in sections 4.4 and 5.2 for EF and PEF with GDE cathodes and several mineral iron oxides as catalyst.[211,212] Anotai et al.[264] analyzed the kinetics for aniline decay during the treatment of 5 L of 0.005−0.05 M solutions of this pollutant in $HClO_4$ of pH 2.0 by the Fered−Fenton using a stirred reactor containing a Ti/Pt or DSA anode and a stainless steel cathode. Trials performed at a constant current of 4 A, with initial Fe^{2+} concentration from 0.005 to 0.05 M and the stepwise addition of H_2O_2 to reach a total content between 0.004 and 0.018 M, allowed establishing the complex kinetic eq 72, approaching to a one-half order for aniline. The total disappearance of 0.01 M aniline with 0.011 M Fe^{2+} and 0.030 M H_2O_2 was observed after 40 min of electrolysis, but its mineralization process was much slower since COD and TOC were only reduced by 57% and 49%, respectively, in 120 min. Phenol, nitrobenzene, and oxalic acid were the main intermediates accumulated in the bulk during this treatment.

Brillas' group initiated its research on EAOPs by studying the AO-H_2O_2, EF, PEF, and PC treatments of 100 mL of aniline solutions in 0.05 M Na_2SO_4 of pH 3.0. The cell in Figure 10 with a 10 cm^2 Pt foil anode and a 3 cm^2 carbon-PTFE O_2-diffusion cathode was used for AO-H_2O_2 and EF trials,[113,227] while a 6 W UVA light was employed as the energy source for PEF[113,227] taking the cell configuration of Figure 25b, and a 10 cm^2 iron foil anode was utilized for PC[221] with the configuration of Figure 25a. In all processes, nitrobenzene and *p*-benzoquinone were detected as aromatic intermediates, but only maleic and fumaric acids were identified as carboxylic acids produced from their degradation. It was proposed that nitrobenzene originated from the selective reaction of the amino group of aniline with $HO_2^{\bullet}$ formed from the anodic oxidation of generated H_2O_2 by reaction 38, while *p*-benzoquinone came from the $^{\bullet}OH$ attack on the C(4) position of aniline that yielded *p*-benzoquinonimine, followed by its hydroxylation with loss of NH_4^+. The release of about 80% of initial N as NH_4^+ in all methods indicated the predominance of the latter path, since the former only promoted the loss of 11% of N as NO_3^-. According to the behavior described in section 7.1.3 for chlorophenoxy herbicides, an increasing TOC reduction of 23%, 68%, and 92% was determined for 100 mg L^{-1} aniline after 6 h of AO-H_2O_2, EF with 1 mM Fe^{2+}, and PEF with 1 mM Fe^{2+}, respectively, operating at 100 mA and 25 °C. The mineralization degree increased with the rising current, and total decontamination was feasible using PEF at 450 mA in 6 h. The PC process was much more efficient since it removed 70% and 95% of soluble TOC in only 30 min at 100 and 450 mA, respectively, with 42% and 65% TOC retained in the $Fe(OH)_3$ sludge formed. When 1000 mg L^{-1} aniline was treated at 450 mA for 120 min, 91% decontamination was obtained by PC as a result of the large coagulation of 70% TOC in the $Fe(OH)_3$ precipitate, whereas only 44% and 47% mineralization was reached by the corresponding EF and PEF processes with 1 mM Fe^{2+}. On the basis of these findings, Brillas and Casado[172] further considered the degradation of 30 L of 1000 mg L^{-1} aniline solutions in 0.05 M Na_2SO_4 of pH 3.0 at 40 °C using the lab-scale plant in Figure 16b with an Electrocell AB cell equipped with 100 cm^2 electrodes operating in the batch recycle mode. The EF process with 1 mM Fe^{2+} in a Pt/O_2 cell gave a violet insoluble polymer, so soluble TOC was rapidly reduced by 61% in 2 h at 20 A, but it slightly decreased over longer time periods. As expected, the PC process in an Fe/O_2 cell was much more effective with >95% TOC decay in 4 h at the same current. Treatment efficiencies as high as 700% and 900% were calculated from eq 56 after 30 min of EF and PC, respectively, as expected if a large proportion of intermediates are separated from the solution as insoluble polymers or retained in the $Fe(OH)_3$ flocs. The energy consumption for total decontamination after 4 h of PC at 20 A was ca. 60 kWh m^{-3}, whereas about 70 kWh m^{-3} was needed to attain only 65% degradation by EF under the same conditions. Comparative AO-H_2O_2 in the Pt/O_2 cell only led to 18% mineralization in 6 h with a high energy cost of 502 kWh m^{-3}, showing that this process is useless in practice.

On the other hand, the degradative behavior of 4-chloroaniline was studied by Meinero and Zerbinati,[355] who carried out comparative AO-H_2O_2 and EF treatments of solutions of 200 mL containing 100 mg L^{-1} of this compound in 0.05 M Na_2SO_4 at pH 3.0 and 20 °C with a Pt/carbon cloth cell at $E_{cat} = -1$ V vs Ag/AgCl under air sparging. Overall disappearance of 4-chloroaniline with only 65% COD decay was obtained after 420 min of the former treatment. In contrast, the more potent EF process with 1 mM Fe^{2+} allowed its total removal in only 60 min, although 13% of initial COD was resistant to oxidation after 150 min of electrolysis. At that moment, the energy cost was 300 kWh $(kg\ TOC)^{-1}$.

7.4.3. Other Benzenic and Heteroaromatic Derivatives

The degradation of nitrobenzene, a well-known toxic POP in industrial wastewater, was studied by Brillas' group, who considered the synergistic catalytic action of Fe^{2+} and Cu^{2+} in EF and PEF with GDE.[209] The relative oxidation power of these methods to mineralize 100 mg L^{-1} nitrobenzene solutions in 0.05 M Na_2SO_4 at pH 3.0 and 25 °C in the Pt/O_2 cell of Figure 10 was the same as that already discussed

for the analogous treatments of the dye Indigo Carmine[210] (see section 7.2.2) and the pharmaceutical paracetamol[185,231] (see section 7.3). For example, EF with 1 mM Fe^{2+} only promoted 53% TOC decay in 360 min at 100 mA, while the combined use of 1 mM Fe^{2+} and 1 mM Cu^{2+} upgraded the organic destruction to 88% mineralization. The same trend was observed for the most potent PEF technique, which required 360 min for overall mineralization with 1 mM Fe^{2+} and only 240 min when 1 mM Cu^{2+} was added to the medium. The nitrobenzene decay always followed a pseudo-first-order reaction. Aromatic products such as 2-nitrophenol, 3-nitrophenol, 4-nitrophenol, and 4-nitrocatechol and generated carboxylic acids such as maleic, fumaric, and oxalic acids were identified by HPLC. In accordance to the reaction path in Figure 44c, this change in oxidation ability of methods tested could be related to the formation of stable Fe(III)−oxalate complexes in EF with 1 mM Fe^{2+}, which are photolyzed by UVA irradiation in PEF, and competitive Cu(II)−oxalate complexes in EF and PEF with 1 mM Fe^{2+} and 1 mM Cu^{2+} that can be quickly removed with $^{\bullet}OH$. Note that only NO_3^- was released during all nitrobenzene treatments, which contrasted with the EF destruction of 4-nitrophenol with carbon felt[350] or graphite[352] in which partial or total conversion of NO_3^- into NH_4^+ was observed owing to its significant cathodic reduction (see Figure 49b). Such a disagreement can be accounted for by the much greater H_2O_2 production at the GDE cathode, which inhibits the possible reduction of nitrogenated organics and NO_3^-.

Chen and Liang[356] applied the EF technique to decontaminate spent acid wastewater from the toluene nitration process containing 74.5% H_2SO_4, 2.7% HNO_3, 21.9% H_2O, as well as 0.9% TOC corresponding to 78.1% of 2,4-dinitrotoluene, 17.8% of 2,6-dinitrotoluene, 0.8% of 2,3-dinitrotoluene, 1.3% of 3,4-dinitrotoluene, and 2.0% of 2,4,6-trinitrotoluene. A stirred undivided Pt/Pt tank reactor with 4 cm^2 electrodes such as that in Figure 13a was employed to electrolyze 200 mL of pure sulfuric acid solutions or wastewater. The complete mineralization of the spent acid wastewater was achieved operating with 100 mg L^{-1} Fe^{2+} at a cell voltage of 6 V, 70 °C, and an O_2 flow rate of 120 mL min^{-1} for 720 min. Under these conditions, continuous H_2O_2 accumulation to 23 mg L^{-1} at 90 min was determined for pure 74% H_2SO_4, thereby ensuring that $^{\bullet}OH$ formed from Fenton's reaction 1 was the main oxidant of organics. GC-MS spectra of samples from the treated wastewater allowed proposing the reaction path in Figure 50, where gradual denitration of 2,4,6-dinitrotoluene yields 2,4- and 2,6-dinitrotoluenes in the first step, 2-nitrotoluene in the second step, and toluene as a first denitrated byproduct. Further oxidation of the methyl group of toluene leads to benzaldehyde and benzoic acid, whose cleavage gives CO_2 and H_2O as final products. All initial N was accumulated as NO_3^-.

The oxidation ability of several novel EF treatments introduced in section 4.4 has been evaluated by degrading the anionic surfactant sodium dodecylbenzene sulfonate[213,214] and dimethylphtalate.[220] The treatment of 150 mL of 750 mg L^{-1} of the former pollutant in 0.25 M Na_2SO_4 was performed in a stirred tank reactor containing 19.2 cm^2 porous graphite as the anode and cathode, with a $CuO-Co_2O_3-PO_4^{3-}$ modified kaolin catalyst packed between the electrodes. COD decayed more rapidly starting from pH 3.0−5.0 than in neutral and alkaline media and was reduced by 94% in 60 min working at 50 mA cm^{-2}. The oxidation of organics at the anode, combined with the action of $^{\bullet}OH$ formed at the catalyst surface from the decomposition of H_2O_2 generated at the cathode from the reduction of O_2 released at the anode, was suggested.

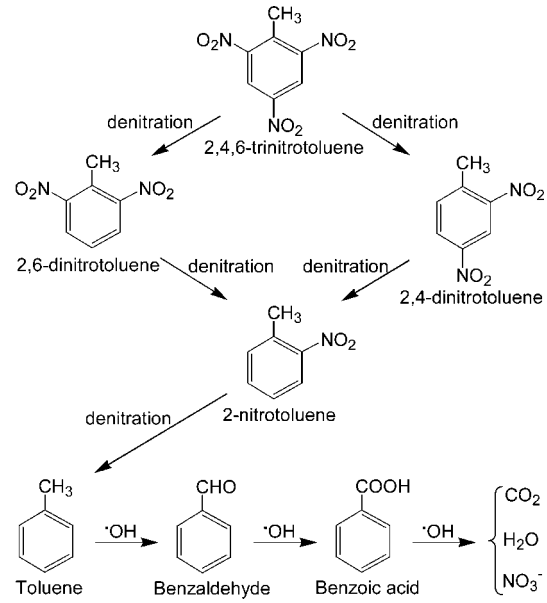

Figure 50. Proposed reaction sequence for 2,4,6-trinitrotoluene mineralization in spent acid wastewaters by EF treatment. Adapted with permission from ref 356. Copyright 2008 Elsevier.

It is here worth reminding that less significant degradation was reported for BSA using Fered−Fenton and photoassisted Fered−Fenton[266] (see Figure 32b), as described in sections 6.1 and 6.4, respectively. In contrast, the efficient destruction of PCBs[276,277] and hexachlorobenzene[282] by ECP has been reported.

The treatment of some heteroaromatic derivatives has also been discussed in the literature. Yuan and co-workers,[357,358] following their work on chlorophenols discussed above, examined the EF degradation of nitrogen−heterocyclic compounds using the same Pt/graphite cell. They found that the decay rate decreased in the sequence quinoline ≈ isoquinoline > indole ≫ pyridine, obtaining a significant correlation between the natural logarithm of their pseudo-first-order rate constant and the energy of the lowest unoccupied molecular orbital (E_{LUMO}) from quantitative structure−activity relationship analysis. The predominant degradation of indole involved its partial dimerization along with its oxidation to oxindole and isatin as a result of the combined attack of $^{\bullet}OH$ formed from Fenton's reaction 1 and direct oxidation at the Pt anode. However, only 38% TOC removal was achieved.

7.4.4. Aliphatics

Ponce de León and Pletcher[123] degraded 2.5 L of O_2-saturated formaldehyde solutions as the catholyte of a flow divided cell similar to that in Figure 8a at $E_{cat} = -0.6$ V/SCE under the batch recycling mode. TOC analysis of the electrolyzed solutions confirmed complete mineralization under EF conditions. The greatest current efficiency of 24% was found for the removal of 75% of 12 mg L^{-1} formaldehyde with 0.5 mM $FeCl_2$ at pH 3.0 after 2000 s of treatment. The addition of 10 mM NaCl or 10 mM HCl to this solution caused a slower degradation, probably due to the formation of more iron−chloride complexes. Formic acid was detected as the main oxidation intermediate of formaldehyde.

Carboxylic acids are common pollutants released during the manufacture of polymer products, the finishing and dyeing of textiles, and the synthesis of soaps and pharmaceuticals and even from the cleaning processes of nuclear power plants. Furthermore, whatever the pollutant degraded or the cathode used, prolonged oxidation weakens the bonds and makes these compounds prone to oxidative ring-opening reactions that lead to the formation of short-chain carboxylic acids, as largely discussed in this review for all the environmental applications. Apart from the destruction of oxalic and acetic acids by EF with RVC[124] and GDE[119] cathodes, respectively, described in section 7.4.1, an extensive study of 11 carboxylic acids including formic, glyoxylic, oxalic, acetic, pyruvic, glycolic, malonic, maleic, fumaric, succinic, and malic acids was reported by Oturan's group[189] using the EF methodology with the Pt/carbon felt cell in Figure 16a. Single-compound solutions containing 200 mL of 0.5 mM of each acid with 0.1 mM Fe^{2+} in 75 mM KCl of pH 3.0 were electrolyzed at 60 mA to determine their decay kinetics and detect their acid intermediates, whereas mixtures with 0.1 and 0.2 mM of all acids were treated at 300 mA to analyze their mineralization degree. All individual compounds disappeared in 40−240 min by EF, except acetic acid which only reduced by 60% in 480 min owing to its very slow reaction with $^{\bullet}OH$, as also observed by other authors.[235] From the competition kinetics method using benzoic or oxalic acid as a competition substrate, a k_2 value similar to that determined by means of other technologies was obtained for all acids, calculating a constant production of $^{\bullet}OH$ close to 10^{-12} M. A specific charge of 14 and 24 Ah L^{-1} was consumed for achieving >95% TOC removal for starting mixtures with 0.1 or 0.2 mM of each acid, respectively. Some degradation pathways were proposed for their complete mineralization, and careful attention was paid to the mechanisms involved, which were based on five basic reactions with $^{\bullet}OH$ including (i) H-atom abstraction, (ii) O_2 fixation, (iii) decarboxylation, (iv) $HO_2^{\bullet}$ release, and (v) H_2O_2 loss.

Ethylene thiourea is a known carcinogenic product and a common impurity exhibiting a concentration of up to 10% in waste from the degradation of the fungicide family of ethylenebisdithiocarbamates. Saltmiras and Lemley[293] studied the destruction of 100 mL of 0.2 mM of this pollutant by three methods: (i) chemical Fenton's reagent with 3.7 mg L^{-1} Fe^{2+} and 37 mg L^{-1} H_2O_2, (ii) ECP with an undivided cell similar to that in Figure 31b at 0.06 A, and (iii) AFT of the anolyte of the salt bridge cell schematized in Figure 31c at 0.12 A. The ECP treatment used 20 cm^2 stainless steel electrodes, whereas a similar anode and a graphite cathode were utilized in AFT treatment. In both processes, the solution containing 0.34 mM NaCl was continuously dosed with H_2O_2 to reach an optimum $[Fe^{2+}]/[H_2O_2]$ ratio of 1:10. While ethylene thiourea disappeared in 30 s by chemical Fenton, it showed a similar zero-order decay for ECP and AFT with total removal in about 90 s. Ethylene urea and 2-imidazolin-2-yl sulfonic acid were identified by HPLC as the main intermediates in all cases, although they were more rapidly destroyed in less than 10 min by AFT than by the other two techniques. This work demonstrated the potential use of AFT for water remediation, which has been extensively developed by Lemley's group, as explained in section 6.3. The effectiveness of this technique was recently tested by degrading methyl *tert*-butyl ether (MTBE),[298] a common fuel oxygenate, using the aforementioned divided salt bridge cell. An optimized $[Fe^{2+}]/[H_2O_2]$ ratio of 1:5 was determined for the electrolysis of 100 mL of a 0.89 mM solution of this pollutant in NaCl of pH 6.5 at 0.12 A. Under these conditions, MTBE disappeared in 4 min following a pseudo-first-order decay with $k_1 = 1.24$ min^{-1}, while its breakdown products detected by HPLC, namely, acetone, *t*-butyl formate, *t*-butanol, methyl acetate, acetic acid, and formic acid, were completely removed in 32 min. From these findings, it was proposed that the initial H-atom abstraction by $^{\bullet}OH$ produced carbon-centered radicals, which underwent reactions such as α,β-scission within the radical, combination with O_2, oxidation by Fe^{3+}, and reduction by Fe^{2+} before generating the final products.

7.5. Real Wastewaters

Some studies have shown the viability of EAOPs based on Fenton's reaction chemistry for the treatment of real wastewaters from different sites. A peculiarity of these wastewaters is the high load of organic matter related to a complex mixture of a large variety of contaminants such as polyphenols, organic acids, sulfur compounds, lignins, fatty acids, and so on.[359] For example, OMW is released with a pH between 3.0 and 5.9 and an organic charge as high as 220 g L^{-1} COD at a BOD_5/COD ratio between 0.2 and 0.4, containing up to 80 g L^{-1} of polyphenols and 20 g L^{-1} of total suspended solids (TSS).[287] The removal of such a wide range of highly concentrated compounds is quite complicated and relies on a strategy of coupling various methods to obtain efficient detoxification for its use at an industrial scale, as detailed for bio-ECP remediation in section 6.4.

Table 8 summarizes the effluent characteristics, operation conditions, and relevant results (percentage of decolorization, percentage of COD removal, and energy consumption among others) determined for several OMW[286,313,354] as well as tannery,[286,289] textile,[288,360] petrochemical,[261,284,291] specific industrial[182,188,262,263,285,290,361] and municipal[362] wastewater, and landfill leachates[154,292,312,363] using EF, PC, Fered−Fenton, ECP, and photoassisted ECP processes. Excellent decolorization and mineralization degrees were attained in most treatments, although sparse information is available about energy costs since only two very divergent values of 3.6 and 530 kWh (kg TOC)$^{-1}$ have been reported, corresponding to the ECP degradation of a tannery[289] and alcohol distillery[290] wastewater, respectively. Note that the BOD_5/COD ratio increases progressively when treatment time is prolonged. This suggests an enhancement of the biodegradability of most resulting wastewaters, which could be further detoxified by a biological post-treatment.

The electrolysis time represents a key operation parameter needing to be optimized in all these EAOPs. This has been clearly demonstrated by Panizza and Cerisola[188] for the EF degradation of industrial wastewater collected from the regeneration of ion-exchange resin towers. Figure 51a shows the kinetic analysis for COD decay of such solutions at pH 4.0 using an undivided three-electrode cell such as that in Figure 17d with a Pt wire anode and a graphite-felt cathode at $E_{cat} = -1$ V/SCE. The mineralization rate increases with iron concentration up to 3 mM Fe^{2+} but decelerates at higher Fe^{2+} concentrations because of the wasting effect of reaction 9. Two different slopes in the $\ln(COD/COD_0)$ vs time plots of Figure 51a can always be observed, which are associated with the expected transition from the predominant oxidation of aromatics at the early stages of the process to the destruction of low amounts of difficult to oxidize intermedi-

Table 8. Selected Results Reported for the Treatment of Real Wastewaters by Means of EAOPs Based on Fenton's Reaction Chemistry

effluent	wastewater characteristics[a]	technology	operation conditions[b]	main results[c]
olive oil mill wastewater from processing plant in Turkey[287]	45 000 mg L^{-1} COD; σ = 6.9 mS cm^{-1}	ECP	undivided iron tank with iron stirrer; 300 mL solution; 2.3% H_2O_2; j = 30 mA cm^{-2}; 20 °C	72% COD removal and 100% turbidity removal in 3 h
olive oil mill wastewater from processing plant in Tunisia[313]	112 500 mg L^{-1} COD; 19 250 mg L^{-1} BOD_5; 59 000 mg L^{-1} TSS; 11 750 mg L^{-1} TP; pH 5.4	ECP	undivided tank; 3 L solution; cast iron plates; 1000 mg L^{-1} H_2O_2; pH 4; j = 75 mA cm^{-2}; prior decantation and ultrafiltration	final water: 36 000 mg L^{-1} COD; 15 500 mg L^{-1} BOD_5; 36 000 mg L^{-1} TSS; 4200 mg L^{-1} TP; pH 7.6
olive oil mill wastewater from processing plant in Tunisia[354]	92 000 mg L^{-1} COD; σ = 12.4 mS cm^{-1}; pH 4.85	EF	undivided tank; 100 mL 50-fold diluted solution; carbon-felt cathode, Pt anode; 0.5 mM Fe^{2+}; compressed air; pH 3; I = 200 mA	decolorization in about 7 h; mineralization in 9 h
tannery wastewater from vegetal tanning in Italy[286]	100 000 mg L^{-1} COD; 32 000 mg L^{-1} TOC; 0.1% TSS; σ = 12 mS cm^{-1}	ECP	undivided tank; Pt cathode, iron anode; 400 mL solution; 2 M H_2O_2; pH 3; I = 1500 mA	80% COD removal in 7.5 h
tannery wastewater from vegetable tanning processes in Turkey[289]	2810 mg L^{-1} COD; 910 mg L^{-1} BOD_5; 1520 mg L^{-1} TSS; 6400 mg L^{-1} Cl^-; σ = 19.95 mS cm^{-1}; pH 7.2	ECP	undivided tank; 400 mL solution; 2 iron electrodes; 1670 mg L^{-1} H_2O_2; pH 3; 1.2−15 W; 20−30 °C	70% COD removal in 10 min; EC = 3.6 kWh (kg COD)$^{-1}$
textile wastewater from a plant in Brazil[288]	1136 mg L^{-1} COD; 80 mg L^{-1} TSS; σ = 3.7 mS cm^{-1}; pH 8.1	ECP	undivided tank; 500 mL solution; 2 iron electrodes; 40 mg L^{-1} H_2O_2; pH 3; I = 1000 mA	55% COD removal and 95% NP9EO removal in 30 min
textile wastewater from dyeing plant in Taiwan[360]	2942 mg L^{-1} COD; 238 mg L^{-1} Cl^-; ADMI color = 1094	EF	divided flow plant with cationic membrane; graphite rings cathodes, Pt anode; 20 mM Fe^{2+}; 0.3 L O_2 min^{-1}; pH 3; j = 6.8 mA cm^{-2}	71% color removal in 150 min
hexamine-containing wastewater from a petrochemical industry[261]	17 100 mg L^{-1} COD; 3680 mg L^{-1} hexamine; 52 mg L^{-1} TSS; σ = 9.7 mS cm^{-1}; pH 8.5	Fered−Fenton	undivided tank; 5 L solution; steel cathode, Ti/RuO_2−IrO_2 anode; 5000 mg L^{-1} Fe^{3+}; 380 000 mg L^{-1} H_2O_2; I constant	94% COD removal in 5 h
petrochemical wastewater from a petroleum storage in the United States[284]	>1000 ppb VOCs; 2−8 ppb MTBE	ECP	PVC pipe as reactor and liquid pumping at 38 L min^{-1}; 10 iron plates; pH 4.0−5.3; I = 30 000 mA (alternating current)	<1 ppb VOCs after an extended period of time
petrochemical wastewater from a plant in Taiwan[291]	200−255 mg L^{-1} COD after a biotreatment	ECP	undivided tank; stainless steel electrodes; 600 mg L^{-1} H_2O_2; pH 3.5; I = 600 mA	>80% COD removal in 3 h
industrial wastewater from flame retardant industry[182]	20 mg L^{-1} TOC; *P*-compounds; 800 mg L^{-1} Cl^-; σ = 8 mS cm^{-1}; pH 6.8	EF	membrane-divided tank; 100 mL solution each side; GDE cathode, BDD anode; 150 mg L^{-1} Fe^{2+}; air flow; pH 1.5; j = 1 mA cm^{-2}	*P*-compounds below the limits required in 240 min
industrial wastewater from regeneration of ion-exchange resin towers[188]	1361 mg L^{-1} COD; 297 mg L^{-1} NS acids; 173 mg L^{-1} AS acids; 16.5 mg L^{-1} phenol; σ = 7.4 mS cm^{-1}	EF	undivided tank; 200 mL solution; graphite-felt cathode, Pt anode, SCE as reference; 3 mM Fe^{2+}; O_2; pH 4; E_{cat} = −1 V/SCE; 35 °C	87% COD removal in 5 h
PVC-stabilizer wastewater[262]	11 000 mg L^{-1} COD; 7500 mg L^{-1} Pb; pH 7.2	Fered−Fenton	undivided tank; 5−10 L solution; steel cathode, Ti/RuO_2−IrO_2 anode; 2000 mg L^{-1} Fe^{3+}; 56 000 mg L^{-1} H_2O_2; pH 2; j = 65−200 mA cm^{-2}	98% COD removal in contrast to 36% by chemical Fenton in 6 h

Table 8. Continued

effluent	wastewater characteristics[a]	technology	operation conditions[b]	main results[c]
industrial wastewater from electroless nickel plating[263]	30 000 mg L^{-1} COD; 3000 mg L^{-1} Ni; pH 5	Fered−Fenton	undivided tank; 5−10 L solution; steel cathode, Ti/RuO_2-IrO_2 anode; 5000 mg L^{-1} Fe^{3+}; 380 000 mg L^{-1} H_2O_2; pH 2; j = 16 mA cm^{-2}	93% COD removal in 5 h in contrast to 62% by chemical Fenton; 99.9% Ni removal
industrial wastewater[285]	3400 mg L^{-1} COD; Pt/Co color = 3750	ECP	undivided tank; 5 L solution; 14 carbon steel electrodes; 1 mL 30% v/v H_2O_2; pH 3; I = 5 A	86% color removal and 78% COD removal in 25 min
alcohol distillery wastewater from a plant in Turkey[290]	4985 mg L^{-1} COD; 1507 mg L^{-1} TOC; 375 mg L^{-1} TSS; σ = 2.09 mS cm^{-1}; pH 5.15	ECP	undivided tank; 1 L solution; 6 iron electrodes; 60000 mg L^{-1} H_2O_2; pH 4; j = 60 mA cm^{-2}	93% COD removal and 89% TOC removal in 240 min; EC = 0.53 kWh (g COD)$^{-1}$
industrial wastewater[361]	142−148 mg L^{-1} COD; morpholine, NS acids; σ = 4−6 mS cm^{-1}; pH 12	EF	undivided (A) or membrane divided (B) flow plant; GDE cathode, Ti/IrO_2-SnO_2 anode; Fe^{2+}; 0.5 L O_2 min^{-1}; pH 3; j = 50 mA cm^{-2}	50 mg L^{-1} COD in (A) and 36 mg L^{-1} COD in (B) reached at 5 min
municipal wastewater from a university in Mexico[362]	328 mg L^{-1} COD; 39.3 turbidity units; σ = 1135 mS cm^{-1}; pH 8.3	PC	undivided tank; 1.8 L solution; graphite cathode, iron anode; air; pH 3.5; I = 1 A	100% color removal, 70% COD removal, and 92% turbidity removal in 60 min
landfill leachate from a landfill site in China[154,363]	5000 mg L^{-1} COD; 650 mg L^{-1} ammonia-nitrogen; pH 6.4	Fered−Fenton	undivided tank; 200 mL solution; Ti/RuO_2-IrO_2 electrodes; 38 mM Fe^{2+}; 340 mM H_2O_2; pH 3; I = 1−3 A	75 and 88% COD removal at 2 and 2.5 A, respectively, in 75 min
landfill leachate from solid waste in Turkey[292]	2350 mg L^{-1} COD; 915 mg L^{-1} BOD_5; 10.25 mg L^{-1} PO_4^{3-}; σ = 10.51 mS cm^{-1}; pH 8.36	photoassisted ECP	undivided tank; 500 mL solution; 4 cast iron electrodes; 3000 mg L^{-1} H_2O_2; pH 3; I = 2.5 A	97% color removal, 94% COD removal, and 96% phosphate removal in 20 min
landfill leachate from landfill site in Taiwan[312]	2000 mg L^{-1} COD; pH 6.5−9.5	ECP	undivided tank; 1 L solution; cast iron electrodes; 500−1500 mg L^{-1} H_2O_2; pH 4	67% COD removal in 30 min

[a] Conductivity (σ), five-day biological oxygen demand (BOD_5), total suspended solids (TSS), total polyphenols (TP), naphthalene−sulfonic (NS) acids, anthraquinone−sulfonic (AS) acids. [b] Applied current (I), current density (j), and cathodic potential (E_{cat}). [c] Energy consumption (EC), nonylphenol ethoxylate (NP9EO).

ates, such as generated carboxylic acids, at long electrolysis times. This trend is confirmed in Figure 51b by the dramatic drop in ICE from 47% at 45 min to less than 0.1% at 720 min. According to this behavior, an optimum time of 300 min was found for treating this wastewater solution with 3 mM Fe^{2+}. At that moment, just before the beginning of the second kinetic region with a much lower mineralization rate, 87% COD had already been removed. Such a well-differenced behavior in the COD decay caused by the transformation of the reaction intermediates has recently been confirmed by Sirés et al.[199] for the treatment of the dye Basic Green 4.

Inspection of Table 8 reveals that the application of EAOPs with the direct addition of H_2O_2 such as Fered−Fenton and ECP is preferred for real wastewater. The faster production of $^{\bullet}OH$ by Fenton's reaction 1 at the beginning of these treatments compared with the EF process, due to the presence of a higher quantity of H_2O_2 along with the additional separation of pollutants and TSS via coagulation with the $Fe(OH)_3$ precipitate formed, promotes a rapid decontamination of effluents with a very high organic charge. The EF process, which only leads to mineralization of pollutants, is rather useful for degrading less contaminated wastewater or avoiding the mere transference of pollutants from the aqueous to the solid phase.

8. Ongoing Research and Perspectives

Like other AOPs, EAOPs are designed to treat small volumes of toxic and persistent organic xenobiotics from the source to avoid their release into the natural water streams, because the treatment of these latter aqueous effluents becomes technically and economically difficult or even impossible once the environmentally dangerous POPs are diluted in large volumes.

As we exposed in this review, currently the theoretical fundamentals and basic applications of EF and most related technologies are well established and several laboratory bench reactors have been designed and successfully applied to the treatment of a huge variety of POPs. The next major commitment is to address the successful development of pilot plants capable of treating larger volumes, allowing thereafter the use of these methods at an industrial level. Aiming the scale up of the EAOPs presented above and betting on more effective and clean processes, suitable systems for removing organic pollutants from wastewater should be improved with some requirements from the following three standpoints. (i) Environmental: Allowing the continuous in-situ electrogeneration of H_2O_2 and catalytic regeneration of Fe^{2+} to avoid the handling of chemical H_2O_2, its transport and storage, as

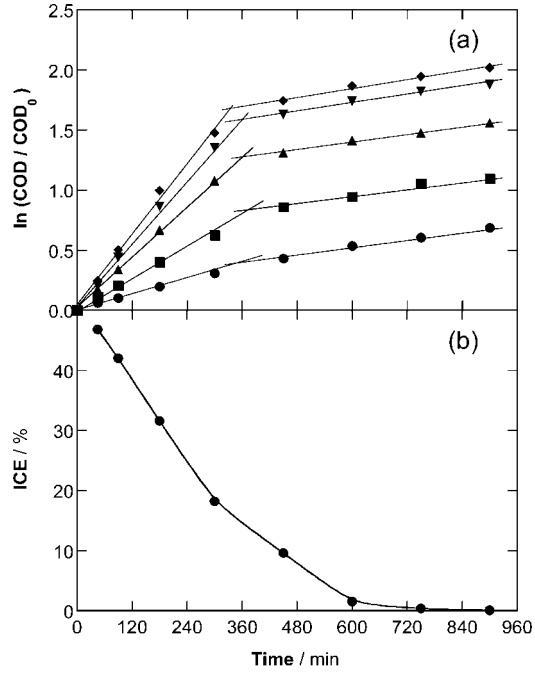

Figure 51. (a) Kinetic analysis for the pseudo-first-order COD removal during the treatment of 200 mL of O_2-saturated industrial wastewaters mainly containing naphthalene− and antraquinone− sulfonic acids at pH 4 by EF using an undivided three-electrode cell similar to that of Figure 17d with a 3 cm^2 Pt wire anode and a 15 cm^2 graphite-felt cathode at $E_{cat} = -1$ V/SCE and 35 °C. Fe^{2+} concentration: (●) 0, (■) 1, (▲) 2, (◆) 3, and (▼) 4 mM. (b) Instantaneous current efficiency determined for the trial with 3 mM Fe^{2+}. Adapted with permission from ref 188. Copyright 2001 Elsevier.

well as the formation of sludge thanks to the controlled production of a small concentration of iron ions. (ii) Technological: Some challenges to enhance the performance and efficiency of future reactors include the combination of high surface area three-dimensional cathodes such as RVC, carbon felt, carbon fiber, or carbon nanotubes and GDEs to enhance both the continuous Fe^{2+} regeneration and H_2O_2 production, respectively, the use of novel advanced materials to develop new and high-performing anodes such as oxide nanotubes including TiO_2 for photoelectrocatalytic applications, as well as electrodeposited coatings of pure, doped, and composite materials with enhanced electrocatalytic properties, the development of more efficient multiple-phase oxidation[213,214] and three-dimensional electrode reactors[218] to overcome the problems of mass transfer limitations inherent to electrode kinetics, and sunlight-assisted degradation for the destruction of persistent metallic complexes. (iii) Economical: Sunlight-driven systems based on solar panels and photovoltaic energy as a cheap source of electrical power.

An interesting research line, mainly concerning the economical and technological aspects, could be based on the coupling of EAOPs to biological post-treatment. As can be seen in Figures 20, 22, 27, 38, 40, 42, and 47, the mineralization of organics is faster at the beginning of all electrochemical treatments. On the other hand, it is well known that they lead to the increase in the BOD_5/COD ratio and, therefore, the biodegradability of the effluent.[92,305] Generally, at a mineralization degree of about 40%, the initial POPs are already transformed into carboxylic acids that are biodegradable. The use of EAOPs during a short time as pretreatment, followed by a biological post-treatment, could then provide a significant savings of electrical energy on the overall decontamination process.

It would also be interesting to explore the use of EAOPs as an alternative to ex-situ soil remediation, landfill, or incineration of concentrates from nondegradative physical treatments such as reversed osmosis or nanofiltration. There are no data available on the treatment of liquid concentrates of organic pollutants from physical treatments by EF or related techniques. Nevertheless, the feasibility of ex-situ soil treatment was shown by EF treatment of soil washing water obtained by enhanced water solubilization of organics thanks to the flushing properties of cyclodextrin.[323] More studies should be undertaken to confirm these preliminary results to develop appropriate technologies.

Finally, research should also pay attention to the great contribution that analytical techniques such as solid-phase extraction (SPE), HPLC-MS, GC-MS, or toxicity testing can make to establishing an integrated water treatment considering both the optimized experimental setup and the elucidation of the reaction pathways and biodegradability enhancement. Modeling of EAOPs including all these parameters could then be used to predict the behavior and performance of such treatments in different reactors and select the best procedures for their real application.

The potential expansion of electrochemical processes into these areas are undoubtedly optimistic because significant progress has been evidenced from the development of novel electrodes and membranes and the amelioration of the reactor setup. These developments have increased experience at a semi-industrial level and, consequently, spread the relevance and status of the electrochemical approach as a plausible and reliable alternative that has overcome the usual reluctance to electrochemistry.

9. Concluding Remarks

The ideas presented in this manuscript provide a holistic view on the progress of all electrochemical technologies based on Fenton's reaction chemistry with the aim of drawing more attention to these emerging processes, which exhibit tantalizing particularities, and promoting further research and innovation on sustainable wastewater treatment processes. The information has been revised with the utmost care and presented with accuracy and completeness. The ultimate challenge was to offer a view on the development of all advances achieved since the very beginning and convey their great performance to the scientific and business communities. Electrochemistry-based treatments are particularly appealing because of the vast number of experimental parameters, electrode materials, and cell configurations; a very dynamic scientific community continues to place electrochemistry at the leading edge of research on water remediation.

Certainly, progressive water scarcity and pollution is an unavoidable threat that must be counteracted because the welfare of living beings and the whole planet is at stake. According to the World Health Organization, 80% of diseases affecting the world population are directly associated with polluted water and more than 2.5 million people die annually from consuming contaminated water. Therefore, the efficient protection of surface and groundwater resources should be based on the treatment of wastewater before its release into the natural environment. In this scenario, the need to develop more effective, ecological, and economical water treatment technologies has made available growing

numbers of alternatives. Low cost and easy handling may be major determining factors, especially in developing countries.

EF and related EAOPs have been developed to provide alternative clean and effective technologies to be applied when conventional processes become ineffective, as is the case for wastewater containing refractory POPs. This review offers a genuine critical and complete insight into the intense research activity performed on all these technologies and published in a high and increasing number of papers over recent years. After exposing the theoretical bases of the Fenton's reaction chemistry and clarifying the particularities of the large variety of EAOPs based on it, the most interesting environmental applications for treating synthetic solutions and real wastewaters containing pollutants such as pesticides, dyestuffs, PPCPs, and industrial compounds have been extensively discussed. The noticeable ability of these electrochemical techniques for the effective destruction of these contaminants has been demonstrated. Unlike other reviews on water remediation, these data have been accompanied by interesting findings on destruction kinetics, byproducts identification, and reaction pathways involving the pollutants under study.

Many of the electrochemical technologies discussed in this review are potent enough to decontaminate wastewaters containing a large variety of organic pollutants in a wide range of experimental conditions. All of them are suitable for destroying the initial pollutant, and most can even completely mineralize the solutions treated. Therefore, these processes can be an effective, a simple, and a versatile alternative to lower performing methods. Although EF and PEF processes are perharps the most ecological and effective EAOPs, they present some drawbacks that complicate their setup such as the need to operate at pH ca. 3.0 and the continuous supply of O_2. Since wastewaters usually contain the required catalytic amounts of Fe^{2+} and/or Cu^{2+} ions and compressed air can be bubbled instead of pure O_2, EF and PEF treatments with acceptable efficiency can be suitable methods to degrade both the parent compounds and their aromatic intermediates within relatively short treatment times, just producing ultimate carboxylic acids and releasing inorganic ions. Coupling with biological treatments can be easy and effective if total mineralization is not required, as shown for bio-ECP.

Four basic types of EAOPs based on Fenton's reaction chemistry, EF, Fered−Fenton, ECP, and AFT, have been by far the most applied processes. The search for coupled processes has brought new technologies such as PC, SPEF, SEF, and PEC-EF, showing enhanced results. The synergistic combination of EF with high O_2-overvoltage anodes such as BDD and solar irradiation in SPEF must be emphasized because it promotes the combined action of hydroxyl radicals formed in the bulk and on the anode surface as well as the photodecarboxylation of hardly oxidizable complexes formed between Fe(III) and final carboxylic acids such as oxalic.

Finally, we think that this review constitutes a reference document in the field of EAOPs based on Fenton's reaction chemistry and will help those inquiring about different aspects of environmentally friendly water treatment technologies as well as helping researchers launch new ideas and technological devices and applications.

10. Acknowledgments

The authors are very grateful for the contribution of Dr. C. Flox to the preparation of the cover artwork. Dr. I. Sirés acknowledges funding from a Beatriu de Pinós postdoctoral grant and support from the Comissionat per a Universitats i Recerca del Departament d'Innovació, Universitats i Empresa (Generalitat de Catalunya). Financial support from MEC (Ministerio de Educación y Ciencia, Spain) under project CTQ2007-60708/BQU, cofunded by FEDER, is also acknowledged.

11. References

(1) Daughton, C. G. *Environ. Impact Assess. Rev.* **2004**, *24*, 711.
(2) Daughton, C. G.; Jones-Lepp, T. L. *Pharmaceuticals and Personal Care Products in the Environment. Scientific and Regulatory Issues*; ACS Symposium Series: Washington, DC, 2001.
(3) Kümmerer, K. *Pharmaceuticals in the Environment. Sources, Fate and Risks*; Springer-Verlag: Berlin, Germany, 2001.
(4) Albrechtsen, H.-J.; Mills, M. S.; Aamand, J.; Bjerg, P. L. *Pest. Manag. Sci.* **2001**, *57*, 341.
(5) Ternes, T. A.; Meisenheimer, M.; McDowell, D.; Sacher, F.; Brauch, H.-J.; Haist-Gulde, B.; Preuss, G.; Wilme, U.; Zulei-Seibert, N. *Environ. Sci. Technol.* **2002**, *36*, 3855.
(6) Gerecke, A. C.; Scharer, M.; Singer, H. P.; Müller, S. R.; Schwarzenbach, R. P.; Sagesser, M.; Ochsenbein, U.; Popow, G. *Chemosphere* **2002**, *48*, 307.
(7) Bound, J. P.; Voulvoulis, N. *Chemosphere* **2004**, *56*, 1143.
(8) Carballa, M.; Omil, F.; Lema, J. M.; Llompart, M.; García-Jares, C.; Rodríguez, I.; Gómez, M.; Ternes, T. *Water Res.* **2004**, *38*, 2918.
(9) Ródenas-Torralba, E.; Morales-Rubio, A.; de la Guardia, M. *Anal. Bioanal. Chem.* **2005**, *383*, 138.
(10) Wu, Y.; Lerner, D. N.; Banwart, S. A.; Thornton, S. F.; Pickup, R. W. *J. Environ. Qual.* **2006**, *35*, 2021.
(11) Khetan, S. K.; Collins, T. J. *Chem. Rev.* **2007**, *107*, 2319.
(12) Cheremisinoff, P. N. *Handbook of Water and Wastewater Treatment Technology*; Marcel Dekker Inc.: New York, 1994.
(13) Henze, M.; Harremoës, P.; la Cour Jansen, J.; Arvin, E. *Wastewater Treatment: Biological and Chemical Processes*, 3rd ed.; Springer-Verlag: Berlin, Germany, 2002.
(14) Tchobanoglous, G.; Burton, F. L.; Stensel, H. D. *Wastewater Engineering: Treatment and Reuse*, 4th ed.;Metcalf and Eddy Inc., Ed.; McGraw-Hill: New York, 2003.
(15) Genders, J. D.; Weinberg, N. L. *Electrochemistry for a Cleaner Environment*; The Electrosynthesis Co. Inc.: East Amherst, New York, 1992.
(16) Pletcher, D.; Walsh, F. C. *Industrial Electrochemistry*, 2nd ed.; Blackie Academic and Professional: London, 1993.
(17) Rajeshwar, K.; Ibanez, J. G. *Environmental Electrochemistry: Fundamentals and Application in Pollution Abatement*; Academic Press: San Diego, CA, 1997.
(18) Simonsson, D. *Chem. Soc. Rev.* **1997**, *26*, 181.
(19) Chen, G. *Sep. Purif. Technol.* **2004**, *38*, 11.
(20) Glaze, W. H.; Kang, J. W.; Chapin, D. H. *Ozone Sci. Eng.* **1987**, *9*, 335.
(21) Glaze, W. H. *Chem Oxid.* **1994**, *2*, 44.
(22) Andreozzi, R.; Caprio, V.; Insola, A.; Marotta, R. *Catal. Today* **1999**, *53*, 51.
(23) Tarr, M. A. *Chemical Degradation Methods for Wastes and Pollutants: Environmental and Industrial Applications*; Marcel Dekker Inc.: New York, 2003.
(24) Gogate, P. R.; Pandit, A. B. *Adv. Environ. Res.* **2004**, *8*, 501.
(25) Parsons, S. *Advanced Oxidation Processes for Water and Wastewater Treatment*; IWA Publishing: London, 2004.
(26) Brillas, E.; Arias, C.; Cabot, P. L.; Centellas, F.; Garrido, J. A.; Rodríguez, R. M. *Port. Electrochim. Acta* **2006**, *24*, 159.
(27) Garrido, J. A.; Brillas, E.; Cabot, P. L.; Centellas, F.; Arias, C.; Rodríguez, R. M. *Port. Electrochim. Acta* **2007**, *25*, 19.
(28) Laine, D. F.; Cheng, I. F. *Microchem. J.* **2007**, *85*, 183.
(29) Martínez-Huitle, C. A.; Ferro, S. *Chem. Soc. Rev.* **2006**, *35*, 1324.
(30) Panizza, M.; Cerisola, G. *Adv. Chem. Res.* **2007**, *2*, 1.
(31) Brillas, E.; Garrido, J. A.; Rodríguez, R. M.; Arias, C.; Cabot, P. L.; Centellas, F. *Port. Electrochim. Acta* **2008**, *26*, 15.
(32) Jiang, C. C.; Zhang, J. F. *J. Zhejiang Univ. Sci. A* **2007**, *8*, 1118.
(33) Oturan, M. A.; Brillas, E. *Port. Electrochim. Acta* **2007**, *25*, 1.
(34) Brillas, E.; Oturan, M. A. In *Pesticides: Impacts Environmentaux, Gestion et Traitements*; Oturan, M. A., Mouchel, J. M., Eds.; Presses de l'École Nationale des Ponts et Chaussées: Paris, France, 2007; pp 61−73.

(35) Pera-Titus, M.; García-Molina, V.; Baños, M. A.; Giménez, J.; Esplugas, S. *Appl. Catal. B: Environ.* **2004**, *47*, 219.
(36) Sharma, V. K. *Water Sci. Technol.* **2007**, *55*, 225.
(37) Sharma, V. K.; Li, X. Z.; Graham, N.; Doong, R. A. *J. Water Supply Res. Technol.: Aqua* **2008**, *57*, 419.
(38) Malato, S.; Blanco, J.; Alarcón, D. C.; Maldonado, M. I.; Fernández-Ibáñez, P.; Gernjak, W. *Catal. Today* **2007**, *122*, 137.
(39) Fujishima, A.; Zhang, X.; Tryk, D. A. *Int. J. Hydrogen Energy* **2007**, *32*, 2664.
(40) Ikehata, K.; El-Din, M. G. *Ozone Sci. Eng.* **2004**, *26*, 327.
(41) Ikehata, K.; El-Din, M. G. *Ozone Sci. Eng.* **2005**, *27*, 83.
(42) Ikehata, K.; Naghashkar, N. M.; El-Din, M. G. *Ozone Sci. Eng.* **2006**, *28*, 353.
(43) Ikehata, K.; El-Din, M. G. *J. Environ. Eng. Sci.* **2006**, *5*, 81.
(44) Andreottola, G.; Ferrarese, E. *J. Environ. Sci. Health A* **2008**, *43*, 1361.
(45) Janzen, E. G.; Kotake, Y.; Hinton, R. D. *Free Radic. Biol. Med.* **1992**, *12*, 169.
(46) Von Sonntag, C. *Water Sci. Technol.* **2008**, *58*, 1015.
(47) Buxton, G. U.; Greenstock, C. L.; Helman, W. P. *J. Phys. Chem. Ref. Data* **1988**, *17*, 513.
(48) Pletcher, D. *Acta Chem. Scand.* **1999**, *53*, 745.
(49) Thénard, L. J. *Ann. Chim. Phys.* **1818**, *8*, 306.
(50) In *Ullman's Encyclopedia of Industrial Chemistry*, 5th ed.; Elvers, B., Hawkins, S., Ravenscroft, M., Schulz, G., Eds.; VCH: Weinheim, Germany, 1989; Vol. A13; p 460.
(51) Foller, P. C.; Bombard, R. T. *J. Appl. Electrochem.* **1995**, *25*, 613.
(52) Riedl, H.-J.; Pfleiderer, G. U.S. Patent 2215883, 1940; *Chem. Abstr.* **1941**, *35*,5297.
(53) Campos-Martin, J. M.; Blanco-Brieva, G.; Fierro, J. L. G. *Angew. Chem., Int. Ed.* **2006**, *45*, 6962.
(54) Plant, L.; Jeff, M. *Chem. Eng.* **1994**; EE-16.
(55) Merli, C.; Petrucci, E.; Da Pozzo, A.; Pernetti, M. *Ann. Chim.* **2003**, *93*, 761.
(56) Neyens, E.; Baeyens, J. *J. Hazard. Mater. B* **2003**, *98*, 33.
(57) Pignatello, J. J.; Oliveros, E.; MacKay, A. *Crit. Rev. Environ. Sci. Technol.* **2006**, *36*, 1.
(58) Bautista, P.; Mohedano, A. F.; Casas, J. A.; Zazo, J. A.; Rodriguez, J. J. *J. Chem. Technol. Biotechnol.* **2008**, *83*, 1323.
(59) Fenton, H. J. H. *Chem. News* **1876**, *33*, 190.
(60) Fenton, H. J. H. *J. Chem. Soc.* **1894**, *65*, 899.
(61) Manchot, W. *Liebigs Ann. Chem.* **1901**, *314*, 177.
(62) Haber, F.; Weiss, J. *Naturwissenschaften* **1932**, *51*, 948.
(63) Haber, F.; Weiss, J. *Proc. R. Soc. London A* **1934**, *147*, 332.
(64) Merz, J. H. W.; Waters, A. *Discuss. Faraday Soc.* **1947**, *2*, 179.
(65) Barb, W. G.; Baxendale, J. H.; George, P.; Hargrave, K. R. *Trans. Faraday Soc.* **1951**, *47*, 462.
(66) Barb, W. G.; Baxendale, J. H.; George, P.; Hargrave, K. R. *Trans. Faraday Soc.* **1951**, *47*, 591.
(67) Walling, C. *Acc. Chem. Res.* **1975**, *8*, 125.
(68) Prousek, J. *Chem. Listy* **1995**, *89*, 11.
(69) Brown, R. F.; Jamison, S. E.; Pandit, K.; Pinkus, J.; White, G. R.; Braendlin, H. P. *J. Org. Chem.* **1964**, *29*, 146.
(70) Metelitsa, D. I. *Russ. Chem. Rev.* **1971**, *40*, 563.
(71) Sun, Y.; Pignatello, J. J. *Environ. Sci. Technol.* **1993**, *27*, 304.
(72) Sun, Y.; Pignatello, J. J. *J. Agric. Food Chem.* **1993**, *41*, 308.
(73) Gallard, H.; De Laat, J.; Legube, B. *New J. Chem.* **1998**, *22*, 263.
(74) Walling, C. *Acc. Chem. Res.* **1998**, *31*, 155.
(75) Lindsey, M. E.; Tarr, M. A. *Chemosphere* **2000**, *41*, 409.
(76) Rush, J. D.; Bielski, B. H. J. *J. Phys. Chem.* **1985**, *89*, 5062.
(77) De Laat, J.; Gallard, H. *Environ. Sci. Technol.* **1999**, *33*, 2726.
(78) Bielski, B. H. J.; Cabelli, D. E.; Arudi, R. L.; Ross, A. B. *J. Phys. Chem. Ref. Data* **1985**, *14*, 1041.
(79) Rothschild, W. G.; Allen, A. O. *Radiat. Res.* **1958**, *8*, 101.
(80) Christensen, H.; Sehested, K.; Corfitzen, H. *J. Phys. Chem.* **1982**, *86*, 1588.
(81) Bielski, B. H. J.; Chan, P. C. *J. Biol. Chem.* **1974**, *250*, 318.
(82) Stuglik, Z.; Zagorski, Z. P. *Radiat. Phys. Chem.* **1981**, *17*, 229.
(83) Jayson, G. G.; Keene, J. P.; Stirling, D. A.; Swallow, A. J. *Trans. Faraday Soc.* **1969**, *65*, 2453.
(84) Sehested, K.; Rasmussen, O. L.; Fricke, H. *J. Phys. Chem.* **1968**, *72*, 626.
(85) De Laat, J.; Le, G. T.; Legube, B. *Chemosphere* **2004**, *55*, 715.
(86) Ensing, B.; Buda, F.; Blöchl, P. E.; Baerends, E. J. *Phys. Chem. Chem. Phys.* **2002**, *4*, 3619.
(87) Bossmann, S. H.; Oliveros, E.; Göb, S.; Siegwart, S.; Dahlen, E. P.; Payawan, L., Jr.; Straub, M.; Wörner, M.; Braun, A. M. *J. Phys. Chem. A* **1998**, *102*, 5542.
(88) Yamazaki, I.; Piette, L. H. *J. Am. Chem. Soc.* **1991**, *113*, 7588.
(89) Kremer, M. L. *Phys. Chem. Chem. Phys.* **1999**, *1*, 3595.
(90) Pignatello, J. J.; Liu, D.; Huston, P. *Environ. Sci. Technol.* **1999**, *33*, 1832.
(91) Gallard, H.; De Laat, J.; Legube, B. *Water Res.* **1999**, *33*, 2929.
(92) Mantzavinos, D.; Psillakis, E. *J. Chem. Technol. Biotechnol.* **2004**, *79*, 431.
(93) Lucas, M. S.; Dias, A. A.; Sampaio, A.; Amaral, C.; Peres, J. A. *Water Res.* **2007**, *41*, 1103.
(94) Zepp, R. G.; Faust, B. C.; Hoigné, J. *Environ. Sci. Technol.* **1992**, *26*, 313.
(95) Oller, I.; Malato, S.; Sánchez-Pérez, J. A.; Gernjak, W.; Maldonado, M. I.; Pérez-Estrada, L. A.; Pulgarin, C. *Catal. Today* **2007**, *122*, 150.
(96) Muñoz, I.; Malato, S.; Rodríguez, A.; Domènech, X. *J. Adv. Oxid. Technol.* **2008**, *11*, 270.
(97) Pignatello, J. J. *Environ. Sci. Technol.* **1992**, *26*, 944.
(98) Faust, B. C.; Hoigné, J. *Atmos. Environ. A* **1990**, *24*, 79.
(99) Lee, C.; Yoon, J. *Chemosphere* **2004**, *57*, 1449.
(100) Zuo, Y.; Hoigné, J. *Environ. Sci. Technol.* **1992**, *26*, 1014.
(101) Safarzadeh-Amiri, A.; Bolton, J. R.; Cater, S. R. *J. Adv. Oxid. Technol.* **1996**, *1*, 18.
(102) Drogui, P.; Elmaleh, S.; Rumeau, M.; Bernard, C.; Rambaud, A. *J. Membr. Sci.* **2001**, *186*, 123.
(103) Drogui, P.; Elmaleh, S.; Rumeau, M.; Bernard, C.; Rambaud, A. *J. Appl. Electrochem.* **2001**, *31*, 877.
(104) Drogui, P.; Elmaleh, S.; Rumeau, M.; Bernard, C.; Rambaud, A. *Water Res.* **2001**, *35*, 3235.
(105) Kornienko, V. L.; Kolyagin, G. A. *Russ. J. Electrochem.* **2003**, *39*, 1308.
(106) Brillas, E.; Maestro, A.; Moratalla, M.; Casado, J. *J. Appl. Electrochem.* **1997**, *27*, 83.
(107) Do, J.-S.; Chen, C.-P. *J. Electrochem. Soc.* **1993**, *140*, 1632.
(108) Agladze, G. R.; Tsurtsumia, G. S.; Jung, B.-I.; Kim, J.-S.; Gorelishvili, G. *J. Appl. Electrochem.* **2007**, *37*, 375.
(109) Alvarez Gallegos, A.; Vergara García, Y.; Zamudio, A. *Sol. Energy Mater. Sol. Cells* **2005**, *88*, 157.
(110) Brillas, E.; Bastida, R. M.; Llosa, E.; Casado, J. *J. Electrochem. Soc.* **1995**, *142*, 1733.
(111) Da Pozzo, A.; Di Palma, L.; Merli, C.; Petrucci, E. *J. Appl. Electrochem.* **2005**, *35*, 413.
(112) Alvarez-Gallegos, A.; Pletcher, D. *Electrochim. Acta* **1998**, *44*, 853.
(113) Brillas, E.; Mur, E.; Casado, J. *J. Electrochem. Soc.* **1996**, *143*, L49.
(114) Özcan, A.; Şahin, Y.; Savaş Koparal, A.; Oturan, M. A. *J. Electroanal. Chem.* **2008**, *616*, 71.
(115) Fu, J.; Zhang, X.; Lei, L. *Acta Phys. Chim. Sin.* **2007**, *23*, 1157.
(116) Tomat, R.; Vecchi, E. *J. Appl. Electrochem.* **1971**, *1*, 185.
(117) Tzedakis, T.; Savall, A.; Clifton, M. J. *J. Appl. Electrochem.* **1989**, *19*, 911.
(118) Sudoh, M.; Kodera, T.; Sakai, K.; Zhang, J. Q.; Koide, K. *J. Chem. Eng. Jpn.* **1986**, *19*, 513.
(119) Harrington, T.; Pletcher, D. *J. Electrochem. Soc.* **1999**, *146*, 2983.
(120) Oturan, M. A.; Pinson, J.; Oturan, N.; Deprez, D. *New J. Chem.* **1999**, *23*, 793.
(121) Oturan, M. A. *J. Appl. Electrochem.* **2000**, *30*, 475.
(122) Wang, A.; Qu, J.; Ru, J.; Liu, H.; Ge, J. *Dyes Pigm.* **2005**, *65*, 227.
(123) Ponce de Leon, C.; Pletcher, D. *J. Appl. Electrochem.* **1995**, *25*, 307.
(124) Alverez-Gallegos, A.; Pletcher, D. *Electrochim. Acta* **1999**, *44*, 2483.
(125) Oloman, C.; Watkinson, A. P. *Can. J. Chem. Eng.* **1975**, *53*, 268.
(126) Oloman, C.; Watkinson, A. P. *J. Appl. Electrochem.* **1979**, *9*, 117.
(127) Shen, Z.; Yang, J.; Hu, X.; Lei, Y.; Ji, X.; Jia, J.; Wang, W. *Environ. Sci. Technol.* **2005**, *39*, 1819.
(128) Jia, J. P.; Yang, J.; Liao, J.; Wang, W. H.; Wang, Z. J. *Water Res.* **1999**, *33*, 881.
(129) Friedrich, J. M.; Ponce-de-León, C.; Reade, G. W.; Walsh, F. C. *J. Electroanal. Chem.* **2004**, *561*, 203.
(130) Pletcher, D.; Walsh, F. C. In *Electrochemical Technology for a Cleaner Environment*; Genders, J. D., Weinberg, N. L., Eds.; The Electrosynthesis Co: Lancaster, New York, 1992; p 51.
(131) Fang, J. H.; Wen, Y.; Shi, L. Y.; Cao, W. M. *J. Inorg. Mater.* **2006**, *21*, 1351.
(132) Sudoh, M.; Kitaguchi, H.; Koide, K. *J. Chem. Eng. Jpn.* **1985**, *18*, 364.
(133) Sudoh, M.; Kitaguchi, H.; Koide, K. *J. Chem. Eng. Jpn.* **1985**, *18*, 409.
(134) Do, J.-S.; Chen, C.-P. *J. Appl. Electrochem.* **1994**, *24*, 936.
(135) Do, J.-S.; Chen, C.-P. *Ind. Eng. Chem. Res.* **1994**, *33*, 387.
(136) Do, J.-S.; Yeh, W.-C. *J. Appl. Electrochem.* **1996**, *26*, 673.
(137) Do, J.-S.; Yeh, W.-C.; Chao, I.-Y. *Ind. Eng. Chem. Res.* **1997**, *36*, 349.
(138) Do, J.-S.; Yeh, W.-C. *J. Appl. Electrochem.* **1998**, *28*, 703.
(139) Da Pozzo, A.; Petrucci, E.; Merli, C. *J. Appl. Electrochem.* **2008**, *38*, 997.
(140) Kornienko, G. V.; Chaenko, N. V.; Vasil'eva, I. S.; Kornienko, V. L. *Russ. J. Electrochem.* **2004**, *40*, 148.
(141) Wang, H.; Yu, X.; Wu, L.; Wang, Q.; Sun, D. *Russ. J. Electrochem.* **2005**, *41*, 719.
(142) Wang, H.; Yu, X. J.; Sun, D. Z. *Chin. Chem. Lett.* **2005**, *16*, 1129.

(143) Boye, B.; Brillas, E.; Buso, A.; Farnia, G.; Flox, C.; Giomo, M.; Sandonà, G. *Electrochim. Acta* **2006**, *52*, 256.
(144) Wang, H.; Wang, J. *Appl. Catal. B: Environ.* **2007**, *77*, 58.
(145) Panizza, M.; Cerisola, G. *Electrochim. Acta* **2008**, *54*, 876.
(146) Badellino, C.; Rodrigues, C. A.; Bertazzoli, R. *J. Appl. Electrochem.* **2007**, *37*, 451.
(147) Liu, H.; Li, X. Z.; Leng, Y. J.; Wang, C. *Water Res.* **2007**, *41*, 1161.
(148) Brillas, E.; Calpe, J. C.; Casado, J. *Water Res.* **2000**, *34*, 2253.
(149) Flox, C.; Cabot, P. L.; Centellas, F.; Garrido, J. A.; Rodríguez, R. M.; Arias, C.; Brillas, E. *Appl. Catal. B: Environ.* **2007**, *75*, 17.
(150) Badellino, C.; Rodrigues, C. A.; Bertazzoli, R. *J. Hazard. Mater. B* **2006**, *137*, 856.
(151) Xie, Y.-B.; Li, X.-Z. *J. Hazard. Mater. B* **2006**, *138*, 526.
(152) Oturan, M. A.; Aaron, J. J.; Oturan, N.; Pinson, J. *Pestic. Sci.* **1999**, *55*, 558.
(153) Aaron, J. J.; Oturan, M. A. *Turk. J. Chem.* **2001**, *25*, 509.
(154) Zhang, H.; Zhang, D.; Zhou, J. *J. Hazard. Mater. B* **2006**, *135*, 106.
(155) Tomat, R.; Rigo, A. *J. Appl. Electrochem.* **1976**, *6*, 257.
(156) Tomat, R.; Rigo, A. *J. Appl. Electrochem.* **1984**, *14*, 1.
(157) Tomat, R.; Rigo, A. *J. Appl. Electrochem.* **1979**, *9*, 301.
(158) Tomat, R.; Rigo, A. *J. Appl. Electrochem.* **1980**, *10*, 549.
(159) Tomat, R.; Rigo, A. *J. Appl. Electrochem.* **1985**, *15*, 167.
(160) Fleszar, B.; Sobkowiak, A. *Electrochim. Acta* **1983**, *28*, 1315.
(161) Oturan, M. A.; Pinson, J.; Deprez, D.; Terlain, B. *New J. Chem.* **1992**, *16*, 705.
(162) Oturan, M. A.; Pinson, J. *J. Phys. Chem.* **1995**, *99*, 13948.
(163) Steckhan, E.; Wellmann, J. *Angew. Chem.* **1976**, *88*, 306.
(164) Wellmann, J.; Steckhan, E. *Chem. Ber.* **1977**, *110*, 3561.
(165) Matsue, T.; Fujihira, M.; Osa, T. *J. Electrochem. Soc.* **1981**, *128*, 2565.
(166) Savinova, E. R.; Kuzmin, A. O.; Frusteri, F.; Parmaliana, A.; Parmon, V. N. *Stud. Surf. Sci. Catal.* **1998**, *119*, 429.
(167) Hsiao, Y. L.; Nobe, K. *J. Appl. Electrochem.* **1993**, *23*, 943.
(168) Hsiao, Y. L.; Nobe, K. *Chem. Eng. Commun.* **1993**, *126*, 97.
(169) Clifford, A. L.; Dong, D. F.; Mumby, T. A.; Rogers, D. J. U.S. Patent 5702587A, 1997; *Chem. Abstr.* **1998**, *128*, 106183.
(170) Casado, J.; Brillas, E.; Bastida, R. M.; Vandermeiren, M. U.S. Patent 6224744B1, 2001; *Chem. Abstr.* **2001**, *134*, 315511.
(171) Oturan, M. A.; Guivarch, E.; Oturan, N.; Sirés, I. *Appl. Catal. B: Environ.* **2008**, *82*, 244.
(172) Brillas, E.; Casado, J. *Chemosphere* **2002**, *47*, 241.
(173) Sirés, I.; Garrido, J. A.; Rodríguez, R. M.; Brillas, E.; Oturan, N.; Oturan, M. A. *Appl. Catal. B: Environ.* **2007**, *72*, 382.
(174) Qiang, Z.; Chang, J.-H.; Huang, C.-P. *Water Res.* **2003**, *37*, 1308.
(175) Panizza, M.; Michaud, P. A.; Cerisola, G.; Comninellis, Ch. *J. Electroanal. Chem.* **2001**, *507*, 206.
(176) Panizza, M.; Cerisola, G. *Electrochim. Acta* **2005**, *51*, 191.
(177) Flox, C.; Cabot, P. L.; Centellas, F.; Garrido, J. A.; Rodríguez, R. M.; Arias, C.; Brillas, E. *Chemosphere* **2006**, *64*, 892.
(178) Weiss, E.; Groenen-Serrano, K.; Savall, A. *J. Appl. Electrochem.* **2008**, *38*, 329.
(179) Ferro, S.; De Battisti, A.; Duo, I.; Comninellis, C.; Haenni, W.; Perret, A. *J. Electrochem. Soc.* **2000**, *147*, 2614.
(180) Brillas, E.; Boye, B.; Sirés, I.; Garrido, J. A.; Rodríguez, R. M.; Arias, C.; Cabot, P. L.; Comninellis, C. *Electrochim. Acta* **2004**, *49*, 4487.
(181) Fockedey, E.; Van Lierde, A. *Water Res.* **2002**, *36*, 4169.
(182) Montanaro, D.; Petrucci, E.; Merli, C. *J. Appl. Electrochem.* **2008**, *38*, 947.
(183) Bolton, J. R.; Bircher, K. G.; Tumas, W.; Tolman, C. A. *Pure Appl. Chem.* **2001**, *73*, 627.
(184) Boye, B.; Dieng, M. M.; Brillas, E. *Environ. Sci. Technol.* **2002**, *36*, 3030.
(185) Sirés, I.; Garrido, J. A.; Rodríguez, R. M.; Cabot, P. L.; Centellas, F.; Arias, C.; Brillas, E. *J. Electrochem. Soc.* **2006**, *153*, D1.
(186) Diagne, M.; Oturan, N.; Oturan, M. A. *Chemosphere* **2007**, *66*, 841.
(187) Daneshvar, N.; Aber, S.; Vatanpour, V.; Rasoulifard, M. H. *J. Electroanal. Chem.* **2008**, *615*, 165.
(188) Panizza, M.; Cerisola, G. *Water Res.* **2001**, *35*, 3987.
(189) Oturan, M. A.; Pimentel, M.; Oturan, N.; Sirés, I. *Electrochim. Acta* **2008**, *54*, 173.
(190) Özcan, A.; Şahin, Y.; Savaş Koparal, A.; Oturan, M. A. *J. Hazard. Mater.* **2008**, *153*, 718.
(191) Özcan, A.; Şahin, Y.; Oturan, M. A. *Chemosphere* **2008**, *73*, 737.
(192) Oturan, M. A.; Oturan, N.; Lahitte, C.; Trevin, S. *J. Electroanal. Chem.* **2001**, *507*, 96.
(193) Kaichouh, G.; Oturan, N.; Oturan, M. A.; El Kacemi, K.; El Hourch, A. *Environ. Chem. Lett.* **2004**, *2*, 31.
(194) Edelahi, M. C.; Oturan, N.; Oturan, M. A.; Padellec, Y.; Bermond, A.; El Kacemi, K. *Environ. Chem. Lett.* **2004**, *1*, 233.
(195) Lahkimi, A.; Oturan, M. A.; Oturan, N.; Chaouch, M. *Environ. Chem. Lett.* **2007**, *5*, 35.
(196) Hammami, S.; Oturan, N.; Bellakhal, N.; Dachraoui, M.; Oturan, M. A. *J. Electroanal. Chem.* **2007**, *610*, 75.
(197) Kesraoui Abdessalem, A.; Oturan, N.; Bellakhal, N.; Dachraoui, M.; Oturan, M. A. *J. Adv. Oxid. Technol.* **2008**, *11*, 276.
(198) Kaichouh, G.; Oturan, N.; Oturan, M. A.; El Hourch, A.; El Kacemi, K. *Environ. Technol.* **2008**, *29*, 489.
(199) Sirés, I.; Guivarch, E.; Oturan, N.; Oturan, M. A. *Chemosphere* **2008**, *72*, 592.
(200) Land, E. J. *Proc. R. Soc. London A* **1968**, *305*, 457.
(201) Beltran De Heredia, J.; Torregrosa, J.; Dominguez, J. R.; Peres, J. A. *Chemosphere* **2001**, *45*, 85.
(202) Amphlett, C. B.; Adams, G. E.; Michael, B. D. *Adv. Chem. Ser.* **1968**, *81*, 231.
(203) Kesraoui Abdessalem, A.; Oturan, N.; Bellakhal, N.; Dachraoui, M.; Oturan, M. A. *Appl. Catal. B: Environ.* **2007**, *78*, 334.
(204) Oturan, N.; Oturan, M. A. *Agron. Sustain. Dev.* **2005**, *25*, 267.
(205) Pimentel, M.; Oturan, N.; Dezotti, M.; Oturan, M. A. *Appl. Catal. B: Environ.* **2008**, *83*, 140.
(206) Chen, J.; Liu, M.; Zhang, J.; Xian, Y.; Jin, L. *Chemosphere* **2003**, *53*, 1131.
(207) Sharma, V. K.; Millero, F. J. *Environ. Sci. Technol.* **1988**, *22*, 768.
(208) Gallard, H.; De Laat, J.; Legube, B. *Rev. Sci. Eau* **1999**, *12*, 713.
(209) Brillas, E.; Baños, M. A.; Camps, S.; Arias, C.; Cabot, P. L.; Garrido, J. A.; Rodríguez, R. M. *New J. Chem.* **2004**, *28*, 314.
(210) Flox, C.; Ammar, S.; Arias, C.; Brillas, E.; Vargas-Zavala, A. V.; Abdelhedi, R. *Appl. Catal. B: Environ.* **2006**, *67*, 93.
(211) Sánchez-Sánchez, C. M.; Expósito, E.; Casado, J.; Montiel, V. *Electrochem. Commun.* **2007**, *9*, 19.
(212) Expósito, E.; Sánchez-Sánchez, C. M.; Montiel, V. *J. Electrochem. Soc.* **2007**, *154*, E116.
(213) Gu, L.; Wang, B.; Ma, H.; Kong, W. *J. Chem. Technol. Biotechnol.* **2006**, *81*, 1697.
(214) Gu, L.; Wang, B.; Ma, H.; Kong, W. *J. Hazard. Mater. B.* **2006**, *137*, 842.
(215) Wang, B.; Gu, L.; Ma, H. *J. Hazard. Mater.* **2007**, *143*, 198.
(216) Xiong, Y.; He, C.; Karlsson, H. T.; Zhu, X. *Chemosphere* **2003**, *50*, 131.
(217) Xiong, Y.; He, C.; An, T.; Zhu, X.; Karlsson, H. T. *Water Air Soil Pollut.* **2003**, *144*, 67.
(218) He, C.; Xiong, Y.; Shu, D.; Zhu, X. *Bull. Electrochem.* **2002**, *18*, 535.
(219) Xu, L.; Zhao, H.; Shi, S.; Zhang, G.; Ni, J. *Dyes Pigm.* **2008**, *77*, 158.
(220) Liu, H.; Wang, C.; Li, X.; Xuan, X.; Jiang, C.; Cui, H. *Environ. Sci. Technol.* **2007**, *41*, 2937.
(221) Brillas, E.; Sauleda, R.; Casado, J. *J. Electrochem. Soc.* **1997**, *144*, 2374.
(222) Brillas, E.; Sauleda, R.; Casado, J. *J. Electrochem. Soc.* **1998**, *145*, 759.
(223) Boye, B.; Dieng, M. M.; Brillas, E. *Electrochim. Acta* **2003**, *48*, 781.
(224) Boye, B.; Brillas, E.; Dieng, M. M. *J. Electroanal. Chem.* **2003**, *540*, 25.
(225) Brillas, E.; Boye, B.; Dieng, M. M. *J. Electrochem. Soc.* **2003**, *150*, E148.
(226) Brillas, E.; Boye, B.; Baños, M. A.; Calpe, J. C.; Garrido, J. A. *Chemosphere* **2003**, *51*, 227.
(227) Brillas, E.; Mur, E.; Sauleda, R.; Sànchez, L.; Peral, J.; Domènech, X.; Casado, J. *Appl. Catal. B: Environ.* **1998**, *16*, 31.
(228) Boye, B.; Dieng, M. M.; Brillas, E. *J. Electroanal. Chem.* **2003**, *557*, 135.
(229) Brillas, E.; Boye, B.; Dieng, M. M. *J. Electrochem. Soc.* **2003**, *150*, E583.
(230) Brillas, E.; Baños, M. A.; Garrido, J. A. *Electrochim. Acta* **2003**, *48*, 1697.
(231) Sirés, I.; Arias, C.; Cabot, P. L.; Centellas, F.; Rodríguez, R. M.; Garrido, J. A.; Brillas, E. *Environ. Chem.* **2004**, *1*, 26.
(232) Sirés, I.; Centellas, F.; Garrido, J. A.; Rodríguez, R. M.; Arias, C.; Cabot, P. L.; Brillas, E. *Appl. Catal. B: Environ.* **2007**, *72*, 373.
(233) Sirés, I.; Arias, C.; Cabot, P. L.; Centellas, F.; Garrido, J. A.; Rodríguez, R. M.; Brillas, E. *Chemosphere* **2007**, *66*, 1660.
(234) Brillas, E.; Baños, M. A.; Skoumal, M.; Cabot, P. L.; Garrido, J. A.; Rodríguez, R. M. *Chemosphere* **2007**, *68*, 199.
(235) Flox, C.; Garrido, J. A.; Rodríguez, R. M.; Cabot, P. L.; Centellas, F.; Arias, C.; Brillas, E. *Catal. Today* **2007**, *129*, 29.
(236) Guinea, E.; Arias, C.; Cabot, P. L.; Garrido, J. A.; Rodríguez, R. M.; Centellas, F.; Brillas, E. *Water Res.* **2008**, *42*, 499.
(237) Skoumal, M.; Arias, C.; Cabot, P. L.; Centellas, F.; Garrido, J. A.; Rodríguez, R. M.; Brillas, E. *Chemosphere* **2008**, *71*, 1718.
(238) Irmak, S.; Yavuz, H. I.; Erbatur, O. *Appl. Catal. B: Environ.* **2005**, *63*, 243.
(239) Zhang, L.; Li, J.; Chen, Z.; Tang, Y.; Yu, Y. *Appl. Catal. A: Gen.* **2006**, *299*, 292.
(240) Zhang, Y.-G.; Ma, L.-L.; Li, J.-L.; Yu, Y. *Environ. Sci. Technol.* **2007**, *41*, 6264.
(241) Chen, X.; Mao, S. S. *Chem. Rev.* **2007**, *107*, 2891.

(242) Xie, Y. B.; Li, X. Z. *Mater. Chem. Phys.* **2006**, *95*, 39.
(243) Peralta-Hernández, J. M.; Meas-Vong, Y.; Rodríguez, F. J.; Chapman, T. W.; Maldonado, M. I.; Godínez, L. A. *Water Res.* **2006**, *40*, 1754.
(244) Li, X. Z.; Liu, H. S. *Environ. Sci. Technol.* **2005**, *39*, 4614.
(245) Xie, Y. *Electrochim. Acta* **2006**, *51*, 3399.
(246) Xie, Y. B.; Li, X. Z. *J. Appl. Electrochem.* **2006**, *36*, 663.
(247) Leng, W. H.; Zhu, W. C.; Ni, J.; Zhang, Z.; Zhang, J. Q.; Cao, C. N. *Appl. Catal. A: Gen.* **2006**, *300*, 24.
(248) Li, X. Z.; Zhao, B. X.; Wang, P. *J. Hazard. Mater.* **2007**, *147*, 281.
(249) Zhao, B. X.; Li, X. Z.; Wang, P. *Photochem. Photobiol.* **2007**, *83*, 642.
(250) Joseph, J. M.; Destaillats, H.; Hung, H.-M.; Hoffmann, M. R. *J. Phys. Chem. A* **2000**, *104*, 301.
(251) Minero, C.; Lucchiari, M.; Vione, D.; Maurino, V. *Environ. Sci. Technol.* **2005**, *39*, 8936.
(252) Adewuyi, Y. G. *Environ. Sci. Technol.* **2005**, *39*, 3409.
(253) Gogate, P. R. *Ultrason. Sonochem.* **2008**, *15*, 1.
(254) González-García, J.; Banks, C. E.; Šljukić, B.; Compton, R. G. *Ultrason. Sonochem.* **2007**, *14*, 405.
(255) Abdelsalam, M. E.; Birkin, P. R. *Phys. Chem. Chem. Phys.* **2002**, *4*, 5340.
(256) Oturan, M. A.; Sirés, I.; Oturan, N.; Pérocheau, S.; Laborde, J.-L.; Trévin, S. *J. Electroanal. Chem.* **2008**, *624*, 329.
(257) Ai, Z.; Mei, T.; Liu, J.; Li, J.; Jia, F.; Zhang, L.; Qiu, J. *J. Phys. Chem. C* **2007**, *111*, 14799.
(258) Gnann, M.; Gregor, C. H.; Schelle, S. WO Patent 9308129A1, 1993; *Chem. Abstr.* **1993**, *119*, 167125.
(259) Takiyama, M. M. K.; Chu, C.-S.; Huang, Y.-C.; Huang, C. P.; Huang, H. S. In *Hazardous and Industrial Wastes: Proceedings of the 26th Mid-Atlantic Industrial Waste Conference*; Huang, C. P., Ed.; Technomic Publishing: Lancaster, PA, 1994; pp 178−185.
(260) Huang, Y.-H.; Huang, G.-H.; Lee, S. N.; Lin, S. M. ROC Patent 088151, 1997.
(261) Chou, S.; Huang, Y.-H.; Lee, S.-N.; Huang, G.-H.; Huang, C. *Water Res.* **1999**, *33*, 751.
(262) Huang, Y.-H.; Chou, C.-C.; Huang, G.-H.; Chou, S. S. *Water Sci. Technol.* **2001**, *43*, 17.
(263) Chang, P.-H.; Huang, Y.-H.; Hsueh, C.-L.; Lu, M.-C.; Huang, G.-H. *Water Sci. Technol.* **2004**, *49*, 213.
(264) Anotai, J.; Lu, M.-C.; Chewpreecha, P. *Water Res.* **2006**, *40*, 1841.
(265) Huang, Y.-H.; Huang, Y.-F.; Chang, P.-S.; Chen, C.-Y. *J. Hazard. Mater.* **2008**, *154*, 655.
(266) Ting, W.-P.; Lu, M.-C.; Huang, Y.-H. *J. Hazard. Mater.* **2008**, *156*, 421.
(267) Rao, N. N.; Bose, G.; Khare, P.; Kaul, S. N. *J. Environ. Eng.* **2006**, *132*, 367.
(268) Zhang, H.; Fei, C.; Zhang, D.; Tang, F. *J. Hazard. Mater.* **2007**, *145*, 227.
(269) Ting, W.-P.; Huang, Y.-H.; Lu, M.-C. ROC Patent 316259, 2007.
(270) Yasman, Y.; Bulatov, V.; Gridin, V. V.; Agur, S.; Galil, N.; Armon, R.; Schechter, I. *Ultrason. Sonochem.* **2004**, *11*, 365.
(271) Pratap, K.; Lemley, A. T. *J. Agric. Food Chem.* **1994**, *42*, 209.
(272) Roe, B. A.; Lemley, A. T. *J. Environ. Sci. Health B* **1997**, *32*, 261.
(273) Pratap, K.; Lemley, A. T. *J. Agric. Food Chem.* **1998**, *46*, 3285.
(274) Scrudato, R. J.; Chiarenzelli, J. R. U.S. Patent 6045707A, 2000; *Chem. Abstr.* **2000**, *132*:212473.
(275) Chiarenzelli, J.; Falanga, L.; Wunderlich, M. *Remediation* **2000**, *10*, 3.
(276) Arienzo, M.; Chiarenzelli, J.; Scrudato, R.; Pagano, J.; Falanga, L.; Connor, B. *Chemosphere* **2001**, *44*, 1339.
(277) Chiarenzelli, J. R.; Scrudato, R. J.; Wunderlich, M. L.; Pagano, J. J. *Chemosphere* **2001**, *45*, 1159.
(278) Arienzo, M.; Chiarenzelli, J.; Scrudato, R. *Fresenius Environ. Bull.* **2001**, *10*, 731.
(279) Arienzo, M.; Chiarenzelli, J.; Scrudato, R. *J. Hazard. Mater. B* **2001**, *87*, 187.
(280) Arienzo, M.; Adamo, P.; Chiarenzelli, J.; Bianco, M. R.; De Martino, A. *Chemosphere* **2002**, *48*, 1009.
(281) Li, C.-W.; Chen, Y.-M.; Chiou, Y.-C.; Liu, C.-K. *J. Hazard. Mater.* **2007**, *144*, 570.
(282) Xie, Q.; Lu, N.; Wang, L.; Lu, X. *Fresenius Environ. Bull.* **2005**, *14*, 894.
(283) Huang, Y.-H.; Chou, S.; Perng, M.-G.; Huang, G.-H.; Cheng, S.-S. *Water Sci. Technol.* **1999**, *39*, 145.
(284) Healy, W. P.; Fina, F. L., III. *Remediation* **2000**, *11*, 17.
(285) Barrera-Díaz, C.; Ureña-Nuñez, F.; Campos, E.; Palomar-Pardavé, M.; Romero-Romo, M. *Radiat. Phys. Chem.* **2003**, *67*, 657.
(286) Boye, B.; Farnia, G.; Sandonà, G.; Buso, A.; Giomo, M. *J. Appl. Electrochem.* **2005**, *35*, 369.
(287) TezcanÜn, Ü.; Uğur, S.; Koparal, A. S.; Bakir Öğütveren, Ü. *Sep. Purif. Technol.* **2006**, *52*, 136.
(288) Martins, A. F.; Wilde, M. L.; Vasconcelos, T. G.; Henriques, D. M. *Sep. Purif. Technol.* **2006**, *50*, 249.
(289) Kurt, U.; Apaydin, O.; Gonullu, M. T. *J. Hazard. Mater.* **2007**, *143*, 33.
(290) Yavuz, Y. *Sep. Purif. Technol.* **2007**, *53*, 135.
(291) Ting, W.-P.; Huang, Y.-H.; Lu, M.-C. *React. Kinet. Catal. Lett.* **2007**, *92*, 41.
(292) Altin, A. *Sep. Purif. Technol.* **2008**, *61*, 391.
(293) Saltmiras, D. A.; Lemley, A. T. *J. Agric. Food Chem.* **2000**, *48*, 6149.
(294) Wang, Q.; Lemley, A. T. *Environ. Sci. Technol.* **2001**, *35*, 4509.
(295) Saltmiras, D. A.; Lemley, A. T. *J. Environ. Sci. Health A* **2001**, *36*, 261.
(296) Wang, Q.; Lemley, A. T. *Water Res.* **2002**, *36*, 3237.
(297) Saltmiras, D. A.; Lemley, A. T. *Water Res.* **2002**, *36*, 5113.
(298) Hong, S.; Zhang, H.; Duttweiler, C. M.; Lemley, A. T. *J. Hazard. Mater.* **2007**, *144*, 29.
(299) Wang, Q.; Lemley, A. T. *J. Agric. Food Chem.* **2002**, *50*, 2331.
(300) Wang, Q.; Lemley, A. T. *J. Hazard. Mater. B* **2003**, *98*, 241.
(301) Wang, Q.; Lemley, A. T. *J. Agric. Food Chem.* **2003**, *51*, 5382.
(302) Wang, Q.; Scherer, E. M.; Lemley, A. T. *Environ. Sci. Technol.* **2004**, *38*, 1221.
(303) Wang, Q.; Lemley, A. T. *J. Environ. Qual.* **2004**, *33*, 2343.
(304) Scherer, E. M.; Wang, Q.-Q.; Hay, A. G.; Lemley, A. T. *Arch. Environ. Contam. Toxicol.* **2004**, *47*, 154.
(305) Friedman, C. L.; Lemley, A. T.; Hay, A. *J. Agric. Food Chem.* **2006**, *54*, 2640.
(306) Kong, L.; Lemley, A. T. *J. Agric. Food Chem.* **2006**, *54*, 3941.
(307) Kong, L.; Lemley, A. T. *Water Res.* **2007**, *41*, 2794.
(308) Kong, L.; Lemley, A. T. *J. Agric. Food Chem.* **2006**, *54*, 10061.
(309) Zhang, H.; Lemley, A. T. *Environ. Sci. Technol.* **2006**, *40*, 4488.
(310) Zhang, H.; Lemley, A. T. *J. Agric. Food Chem.* **2007**, *55*, 4073.
(311) Lu, M.-C.; Ting, W.-P.; Huang, Y.-H. ROC Patent 323472, 2007.
(312) Lin, S. H.; Chang, C. C. *Water Res.* **2000**, *34*, 4243.
(313) Khoufi, S.; Aloui, F.; Sayadi, S. *Water Res.* **2006**, *40*, 2007.
(314) Khoufi, S.; Feki, F.; Aloui, F.; Sayadi, S. *Water Sci. Technol.* **2007**, *55*, 67.
(315) Abid, N.; Chamkha, M.; Godon, J. J.; Sayadi, S. *Environ. Technol.* **2007**, *28*, 751.
(316) Sugiarto, A. T.; Ohshima, T.; Sato, M. *Thin Solid Films* **2002**, *407*, 174.
(317) Grymonpré, D. R.; Finney, W. C.; Clark, R. J.; Locke, B. R. *Ind. Eng. Chem. Res.* **2004**, *43*, 1975.
(318) Koprivanac, N.; Kušić, H.; Vujević, D.; Peternel, I.; Locke, B. R. *J. Hazard. Mater. B* **2005**, *117*, 113.
(319) Hao, X.; Zhou, M.; Xin, Q.; Lei, L. *Chemosphere* **2007**, *66*, 2185.
(320) Saracco, G.; Solarino, S.; Specchia, V.; Maja, M. *Chem. Eng. Sci.* **2001**, *56*, 1571.
(321) Guivarch, E.; Oturan, N.; Oturan, M. A. *Environ. Chem. Lett.* **2003**, *1*, 165.
(322) Oturan, N.; Trajkovska, S.; Oturan, M. A.; Couderchet, M.; Aaron, J. J. *Chemosphere* **2008**, *73*, 1550.
(323) Hanna, K.; Chiron, S.; Oturan, M. A. *Water Res.* **2005**, *39*, 2763.
(324) Losito, I.; Amorisco, A.; Palmisano, F. *Appl. Catal. B: Environ.* **2008**, *79*, 224.
(325) Da Pozzo, A.; Merli, C.; Sirés, I.; Garrido, J. A.; Rodríguez, R. M.; Brillas, E. *Environ. Chem. Lett.* **2005**, *3*, 7.
(326) Robinson, T.; McMullan, G.; Marchant, R.; Nigam, P. *Bioresour. Technol.* **2001**, *77*, 247.
(327) Forgacs, E.; Cserhati, T.; Oros, G. *Environ. Int.* **2004**, *30*, 953.
(328) Lidia, S.; Claudia, J.; Santosh, N. K. *Water Res.* **2001**, *35*, 2129.
(329) Zhang, G.; Yang, F.; Gao, M.; Liu, L. *J. Phy. Chem. C* **2008**, *112*, 8957.
(330) Zhang, G.; Yang, F.; Gao, M.; Fang, X; Liu, L. *Electrochim. Acta* **2008**, *53*, 5155.
(331) Guivarch, E.; Trevin, S.; Lahitte, C.; Oturan, M. A. *Environ. Chem. Lett.* **2003**, *1*, 38.
(332) Guivarch, E.; Oturan, M. A. *Acta Chim.* **2004**, *277*−*278*, 65.
(333) Zhou, M.; Yu, Q.; Lei, L.; Barton, G. *Sep. Purif. Technol.* **2007**, *57*, 380.
(334) Zhou, M.; Yu, Q.; Lei, L. *Dyes Pigm.* **2008**, *77*, 129.
(335) Kusvuran, E.; Gulnaz, O.; Irmak, S.; Atanur, O. M.; Yavuz, H. I.; Erbatur, O. *J. Hazard. Mater. B* **2004**, *109*, 85.
(336) Kusvuran, E.; Irmak, S.; Yavuz, H. I.; Samil, A.; Erbatur, O. *J. Hazard. Mater. B* **2005**, *119*, 109.
(337) Peralta-Hernández, J. M.; Meas-Vong, Y.; Rodríguez, F. J.; Chapman, T. W.; Maldonado, M. I.; Godínez, L. A. *Dyes Pigm.* **2008**, *76*, 656.
(338) Wang, A.; Qu, J.; Liu, H.; Ru, J. *Appl. Catal. B: Environ.* **2008**, *84*, 393.
(339) Novosad, J.; Messimeri, A. C.; Papadimitriou, C. D.; Veltsistas, P.; Woolins, D. *Transition Met. Chem.* **2000**, *25*, 664.
(340) Balcioğlu, A. I.; Ötker, M. *Chemosphere* **2003**, *50*, 85.
(341) Sharma, V. K. *Chemosphere* **2008**, *73*, 1379.
(342) San Sebastián, N.; Fíguls, J.; Font, X.; Sánchez, A. *J. Hazard. Mater. B* **2003**, *101*, 315.

(343) Oturan, M. A.; Pinson, J.; Traikia, M.; Deprez, D. *Perkin Trans. 2* **1999**, *3*, 619.
(344) Sirés, I.; Oturan, N.; Oturan, M. A.; Rodríguez, R. M.; Garrido, J. A.; Brillas, E. *Electrochim. Acta* **2007**, *52*, 5493.
(345) Wu, Z.; Zhou, M.; Wang, D. *Chemosphere* **2002**, *48*, 1089.
(346) Agladze, G. R.; Tsurtsumia, G. S.; Jung, B.-I.; Kim, J.-S.; Gorelishvili, G. *J. Appl. Electrochem.* **2007**, *37*, 385.
(347) Sankara Narayanan, T. S. N.; Magesh, G.; Rajendran, N. *Fresenius Environ. Bull.* **2003**, *12*, 776.
(348) Yuan, S.; Lu, X. *J. Hazard. Mater. B* **2005**, *118*, 85.
(349) Wu, G.; Yuan, S.; Ai, Z.; Xie, Q.; Li, X.; Lu, X. *Fresenius Environ. Bull.* **2005**, *14*, 703.
(350) Oturan, M.; Peiroten, J.; Chartrin, P.; Acher, A. J. *Environ. Sci. Technol.* **2000**, *34*, 3474.
(351) Ammar, S.; Oturan, N.; Oturan, M. A. *J. Environ. Eng. Manage.* **2007**, *17*, 89.
(352) Yuan, S.; Tian, M.; Cui, Y.; Lin, L.; Lu, X. *J. Hazard. Mater. B* **2006**, *137*, 573.
(353) Gözmen, B.; Oturan, M. A.; Oturan, N.; Erbatur, O. *Environ. Sci. Technol.* **2003**, *37*, 3716.
(354) Bellakhal, N.; Oturan, M. A.; Oturan, N.; Dachraoui, M. *Environ. Chem.* **2006**, *3*, 345.
(355) Meinero, S.; Zerbinati, O. *Chemosphere* **2006**, *64*, 386.
(356) Chen, W.-S.; Liang, J.-S. *Chemosphere* **2008**, *72*, 601.
(357) Yuan, S.; Huang, Y.; Ren, D.; Lu, X. *Water Environ. Res.* **2007**, *79*, 759.
(358) Wu, G.; Yuan, S.; Huang, Y.; Lu, X. *J. Huazhong Univ. Sci. Technol. (Nat. Sci.)* **2007**, *35*, 126.
(359) Lacorte, S.; Latorre, A.; Barceló, D.; Rigol, A.; Malmqvist, A.; Welander, T. *Trends Anal. Chem.* **2003**, *23*, 725.
(360) Wang, C.-T.; Hu, J.-L.; Chou, W.-L.; Kuo, Y.-M. *J. Hazard. Mater.* **2008**, *152*, 601.
(361) Agladze, G. R.; Tsurtsumia, G. S.; Jung, B.-I.; Kim, J.-S.; Gorelishvili, G. *J. Appl. Electrochem.* **2007**, *37*, 985.
(362) Durán Moreno, A.; Frontana-Uribe, B. A.; Ramírez Zamora, R. M. *Water Sci. Technol.* **2004**, *50*, 83.
(363) Zhang, H.; Cheng, Z.; Zhang, D. *Fresenius Environ. Bull.* **2007**, *16*, 1216.

CR900136G